Reactive monolayers for surface gradients and biomolecular patterned interfaces

Carlo Nicosia

REACTIVE MONOLAYERS FOR SURFACE GRADIENTS AND BIOMOLECULAR PATTERNED INTERFACES

Carlo Nicosia

Members of the committee:

Chairman:	Prof. dr. G. van der Steenhoven	(University of Twente)
Promotor:	Prof. dr. ir. J. Huskens	(University of Twente)
Members:	Prof. E. Dalcanale	(University of Parma)
	Prof. dr. ir. D. N. Reinhoudt	(University of Twente)
	Prof. dr. G. J. Vancso	(University of Twente)
	Prof. dr. V. Subramaniam	(University of Twente)
	Prof. dr. J.J.L.M. Cornelissen	(University of Twente)

The research described in this thesis was performed within the laboratories of the Molecular Nanofabrication (MnF) group, the Mesa$^+$ Institute for Nanotechnology and the Department of Science and Technology of the University of Twente. This research was supported by the Council for Chemical Sciences of the Netherlands Organization for Scientific Research (NWO-CW, Vici grant 700.58.443).

Reactive Monolayers for Surface Gradients and Biomolecular Patterned Surfaces

ISBN: 978-90-365-0019-7
DOI: 10.3990/1.9789036500197
Cover art: Susanna Nicosia
Printed by: CPI-Wöhrmann Print Service – Zutphen (The Netherlands)

REACTIVE MONOLAYERS FOR SURFACE GRADIENTS AND BIOMOLECULAR PATTERNED INTERFACES

PROEFSCHRIFT

ter verkrijging van
de graad van doctor aan de Universiteit Twente
op gezag van de rector magnificus,
Prof. Dr. H. Brinksma,
volgens besluit van het College voor Promoties
in het openbaar te verdedigen
op donderdag 19 september 2013 om 16.45 uur

door

Carlo Nicosia
geboren op 26 juni 1983
te Guastalla, Italië

Dit proefschrift is goedgekeurd door:

Promotor: Prof. dr. ir. Jurriaan Huskens

“Little by little, one travels far” — John R. R. Tolkien

This thesis is dedicated to all my family.

Table of Contents

Chapter 1

"If you are capable of hearing, listen." — Ronald E. Capps, Off Magazine Street.

General Introduction

"Nanoscience" is the science that studies objects which size is on the nanometer scale (1-100 nm). The main driving forces behind the nanotechnology revolution are the new physical properties of materials at the nanoscale. The central challenge in nanotechnology still remains the fabrication and visualization of nanosystem. There are two approaches to the fabrication of nanosystems: top-down, which is based on the miniaturization of structures and devices using new or existing lithography techniques, and bottom-up, in which, complex systems are built from the smallest building blocks: atoms and molecules. The bottom-up approach offers many opportunities to build nanostructures with new types of functions that have revolutionized the fields of materials science,[1-6] medicine,[7-12] electronics,[13] and photonics.[14]

Self-assembly is the core concept of the bottom-up paradigm offering a route for assembling building blocks into larger, functional ensembles with nanoscale precision. Self-assembled monolayers (SAMs), formed on the surface of solid materials, are of high interest as they connect the nanoscale (SAM) with the macroscale (solid). This allows for the direct harnessing of properties of the SAM.[15] Monolayers formed on gold[3,16] and silicon oxide[17,18] are the most studied and characterized SAMs to date, and they provide a convenient, flexible, simple and robust strategy to fabricate functional surfaces.

The terminal groups of the building blocks of SAMs allow the tuning of the interfacial surface properties in terms of chemical reactivity, conductivity, wettability, adhesion, friction, corrosion resistance and (bio)compatibility. Moreover, many different organic reactions have been explored to modify the terminal groups of SAMs in order to tailor the surface properties of substrates.[19-21] The research described in this thesis aims at developing of functional and reactive SAMs for two main purposes: the fabrication of biologically active platforms by the simultaneous immobilization and detection of bioactive ligands and proteins (Chapters 3-4), and the development and application of micron-scale surface chemical gradients by means of solution gradients of electrochemically generated catalytic species (Chapters 5-8).

Chapter 2 provides a literature overview of chemical reactions employed for the modification of SAMs and the formation of microarrays and surface gradients. Specific attention is focused on recent examples of "click" reactions that allow high-yielding, efficient and selective interfacial modifications.

Chapter 3 describes the development of a thiol-sensitive fluorogenic reactive platform that allows to report the immobilization of thiols by fluorescent signaling using an orthogonally modified coumarin. This system has been employed to investigate co-localization in a supramolecular system and the retention of bioactivity of immobilized peptides for cell adhesion and differentiation.

In the work described in Chapter 4, the system introduced in Chapter 3 has been employed for the fabrication of protein arrays. The fluorogenic platform has allowed the orthogonal immobilization of visible fluorescent proteins via covalent bond formation or non-covalent assembly. Selective immobilization has been proven by co-localization of the fluorescence of the immobilized proteins and the fluorogenic group.

Chapter 5 illustrates a method for the investigation of the reactivity of interfacial reactions in space and time. To this end, electrochemically derived concentration gradients of a catalyst (Cu(I)) in solution have been employed to make micron-scale surface gradients of an alkyne-terminated dye on an azide-terminated monolayer on the area between arrayed microelectrodes on glass. With this system, the kinetics of the ligand-free, surface-confined copper(I)-catalyzed azide-alkyne 1,3-dipolar cycloaddition (CuAAC) has been studied.

Chapter 6 describes the fabrication of micron-scale surface chemical gradients with a tailored shape using the system described in Chapter 5. The reaction conditions of the CuAAC have been tuned to control the steepness and the ligand density of the surface gradients. Moreover, this method has been exploited to fabricate bi-component and biomolecular gradients and to pattern surface gradients on external azide-functionalized substrates.

Chapter 7 describes the development of a platform for the optical sensing of micron-scale pH gradients. The pH-sensitive alkyne-modified *N*-methylpiperazine naphthalimide has been immobilized on an azide monolayer on glass. To investigate the effect of the ligand density, the pK_a of the pH-sensitive dye has been determined for both homogeneous, dense surface patterns and surface gradients. This system has been employed to visualize and analyze micron-scale pH gradients at the solid/liquid interface induced by the electrolysis of water.

Chapter 8 describes the combination of a multivalent host-guest system and micron-scale surface gradients to investigate the multivalent assembly of receptor-functionalized nanoparticles on ligand-terminated monolayers. A surface gradient of the fluorogenic platform, described in Chapter 3, has been employed to simultaneously immobilize and analyze the surface density variation of adamantyl ligand units. Co-localization of the adamantyl-terminated surface gradient and fluorescently labelled β-cyclodextrin-functionalized nanoparticles has allowed the investigation of the non-linear and superselective adsorption of nanoparticles as a function of the surface density of ligand.

1.1 References

(1) Schlögl, R.; Abd Hamid, S. B. *Angew. Chem. Int. Ed.* 2004, *43*, 1628.
(2) Daniel, M. C.; Astruc, D. *Chem.Rev.* 2004, *104*, 293.
(3) Love, J. C.; Estroff, L. A.; Kriebel, J. K.; Nuzzo, R. G.; Whitesides, G. M. *Chem. Rev.* 2005, *105*, 1103.
(4) Lieber, C. M. *MRS Bull.* 2003, *28*, 486.
(5) Descalzo, A. B.; Martinez-Manez, R.; Sancenon, R.; Hoffmann, K.; Rurack, K. *Angew. Chem. Int. Ed.* 2006, *45*, 5924.
(6) Ariga, K.; Ito, H.; Hill, J. P.; Tsukube, H. *Chem. Soc. Rev.* 2012, *41*, 5800.
(7) Boisselier, E.; Astruc, D. *Chem. Soc. Rev.* 2009, *38*, 1759.
(8) Giljohann, D. A.; Mirkin, C. A. *Nature* 2009, *462*, 461.
(9) Moghimi, S. M.; Hunter, A. C.; Murray, J. C. *FASEB J.* 2005, *19*, 311.
(10) Peer, D.; Karp, J. M.; Hong, S.; FaroKhzad, O. C.; Margalit, R.; Langer, R. *Nat. Nanotechnol.* 2007, *2*, 751.
(11) Riehemann, K.; Schneider, S. W.; Luger, T. A.; Godin, B.; Ferrari, M.; Fuchs, H. *Angew. Chem. Int. Ed.* 2009, *48*, 872.
(12) Wagner, V.; Dullaart, A.; Bock, A.-K.; Zweck, A. *Nat. Biotechnol.* 2006, *24*, 1211.
(13) Lu, W.; Lieber, C. M. *Nat. Mater.* 2007, *6*, 841.
(14) Sgobba, V.; Guldi, D. M. *Chem. Soc. Rev.* 2009, *38*, 165.
(15) Ulman, A. *Chem. Rev.* 1996, *96*, 1533.
(16) Nuzzo, R. G.; Allara, D. L. *J. Am. Chem. Soc.* 1983, *105*, 4481.
(17) Onclin, S.; Ravoo, B. J.; Reinhoudt, D. N. *Angew. Chem. Int. Ed.* 2005, *44*, 6282.
(18) Sagiv, J. *J. Am. Chem. Soc.* 1980, *102*, 92.
(19) Tao, N. J. *Nat. Nanotechnol.* 2006, *1*, 173.
(20) Shipway, A. N.; Willner, I. *Acc. Chem. Res.* 2001, *34*, 421.
(21) Jonkheijm, P.; Weinrich, D.; Schroeder, H.; Niemeyer, C. M.; Waldmann, H. *Angew. Chem. Int. Ed.* 2008, *47*, 9618.
(22) Chechik, V.; Crooks, R. M.; Stirling, C. J. M. *Adv. Mat.* 2000, *12*, 1161.
(23) Haensch, C.; Hoeppener, S.; Schubert, U. S. *Chem. Soc. Rev.* 2010, *39*, 2323.
(24) Sullivan, T. P.; Huck, W. T. S. *Eur. J. Org. Chem.* 2003, *17*.

Chapter 2

"There is nothing like looking, if you want to find something. You certainly usually find something, if you look, but it is not always quite the something you were after."
— John. R. R. Tolkien, The Hobbit.

Reactive self-assembled monolayers: from surface functionalization to gradient formation

In this chapter the progress of the development of surface chemical reactions for the modification of self-assembled monolayers (SAMs) is discussed as well as the fabrication of surface chemical gradients. Various chemical reactions can be carried out on SAMs to introduce new functionalities. Highly efficient and selective "click" reactions, have largely contributed to the development and implementation of surface chemical reactions in the fields of biotechnology, drug discovery, materials science, polymer synthesis, and surface science. Besides full homogeneous functionalization, SAMs can be modified to exhibit a gradual variation of physicochemical properties in space. Numerous methods are available for the fabrication of surface chemical gradients and the recent combination with surface-confined chemical reactions has made the preparation of exceptionally versatile interfaces accessible.

*Part of this chapter has been published in: C. Nicosia and J. Huskens, *Mater. Horiz,*. 2013, accepted.

2.1 Introduction

In 1959 the physicist Richard Feynman delivered a vision of exciting new technological discoveries based on the fabrication of materials and devices at the atomic/molecular scale that we call today nanotechnologies.[1] The interesting size range where nanotechnology operates is typically from 100 nm down to the atomic level. In this range the properties of materials are different from their bulk properties due to the higher surface area and the prevalence of quantum effects.[2] These new properties of nanomaterials are conveniently employed for a wide range of fields ranging from catalysis, optics, electronics and informatics, to bio-nanotechnology and nanomedicine.[3] In the 1980's nanoscience discoveries experienced an impressive propulsion with the invention of the scanning tunnelling microscope (STM) and the atomic force microscope (AFM) allowing the imaging of surfaces with atomic resolution.

Self-assembled monolayers (SAMs) are two-dimensional nanomaterials formed spontaneously by the highly ordered assembly of the molecular constituents onto the surface of a variety of solids.[4, 5] SAMs, formed by adsorption of a one-molecule-thick layer on the surface, are excellent systems to study interfacial reactions. The exponential growth in SAM research is justified by the multi-disciplinarity of the field that gathers chemists, physicists, biologists and engineers.

The two most common families of SAMs are alkylsilanes on oxide surfaces,[6-9] and sulfur-containing molecules on gold[5, 10-12] (Scheme 2.1). Because of their ease of preparation, the spontaneous formation of a densely packed monolayer, and the conductivity of the substrate, ω-functionalized thiols (or disulfide or sulfide) monolayers on gold have been extensively studied. On the other hand, organosilane monolayers on SiO_2 (silicon or glass) can be readily integrated in silicon technology. Owing to their covalent nature, organosilane monolayers, are chemically and physically stable allowin their further functionalization.

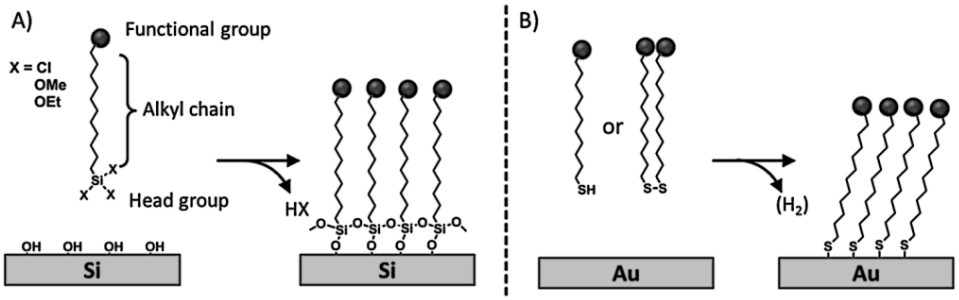

Scheme 2.1 Formation of functional silane/SiO_2 (A) and thiol-gold (B) monolayers.

The mechanism of formation of SAMs of sulfur-containing molecules on gold and organosilanes on SiO_2 has been extensively described elsewhere.[4,5,7,8] Interfacial reactions are versatile and essential modification schemes to control the surface composition and density of monolayers. The terminal groups of the building blocks of SAMs allow the fine-tuning of the interfacial surface properties in terms of chemical reactivity, conductivity, wettability, adhesion, friction, corrosion resistance and (bio)compatibility.[13] The introduction of components with different functional end groups in the monolayers can be performed through two different routes: (i) the adsorption of pre-functionalized molecules or (ii) the modification of the monolayer after formation. While the former route requires the complete synthesis of the molecular constituent of the monolayer, the latter method, based on a stepwise process, offers intrinsic advantages: (i) it enables the incorporation of groups that are not compatible with the synthesis of the building block (e.g. silane or thiol groups); (ii) it does not affect the order of the underlying monolayer; (iii) it allows the quick preparation of multiple samples; (iv) it employs ordinary synthetic procedures; (v) it requires a low amount of reagents.[5] On the other hand, since purification of the functionalized monolayer is impossible, high-yielding, efficient, selective and clean reactions are essential.

Haensch and coworkers recently described, in their critical review,[9] the chemical modification of silane-based monolayers involving nucleophilic substitution and Huisgen 1,3-dipolar cycloaddition of organic azides and acetylenes. Sullivan and Huck illustrated nucleophilic substitutions, esterification, acylation, and nucleophilic addition on thiols/Au and silanes/SiO_2 surfaces functionalized with terminal amines, hydroxyls, carboxylic acids, aldehydes, and halogens.[14] Jonkheijm and coworkers outlined, in their comprehensive review,[15] strategies for the fabrication of reactive interfaces for the fabrication of biochips. Numerous reactions are available to modify the surface chemistry of SAMs[9,14,16] (*e.g.* nucleophilic substitutions,[17-19] esterification,[20] amidation,[21-23] *etc.*).

In the last decade a lot of efforts were focused on the implementation of methods to obtain selective, efficient, robust, quantitative, simple and rapid surface transformations to reduce the formation of by-products, avoiding the need of purification and allowing easy surface analysis. Click chemistry encompasses all these properties. The click reaction approach delivered by Sharpless and coworkers in 2001,[24,25] is based on implementing highly efficient and selective reactions that reach quantitative conversion under mild conditions, essential qualities for the development of surface and materials sciences.[26-31]

Microcontact printing (μCP), scanning probe, UV and e-beam lithographies, so called "top-down" methods, are commonly employed to generate patterns of SAMs with sizes

ranging from tens of nanometers to millimeters. Microcontact printing, in particular, was introduced by Whitesides and coworkers as a fast, flexible, simple and inexpensive way to replicate patterns generated via photolithography.[32-34] In the conventional μCP, a microstructured elastomeric poly(dimethylsiloxane) (PDMS) stamp was employed to transfer molecules of the "ink" (e.g. thiols) to the surface of the substrate (e.g. gold) by conformal contact. Patterns of alkanethiols on gold were conveniently used as etch-protecting layer for the fabrication of microstructures with potential application in microelectronics.

Soon after its development, μCP evolved as a powerful tool to pattern functional reactive monolayers by means of the local chemical reaction between an ink transferred by the stamp and the functional groups introduced on the substrate. This process is called "reactive μCP" or microcontact chemistry[35-37] (Scheme 2.2).

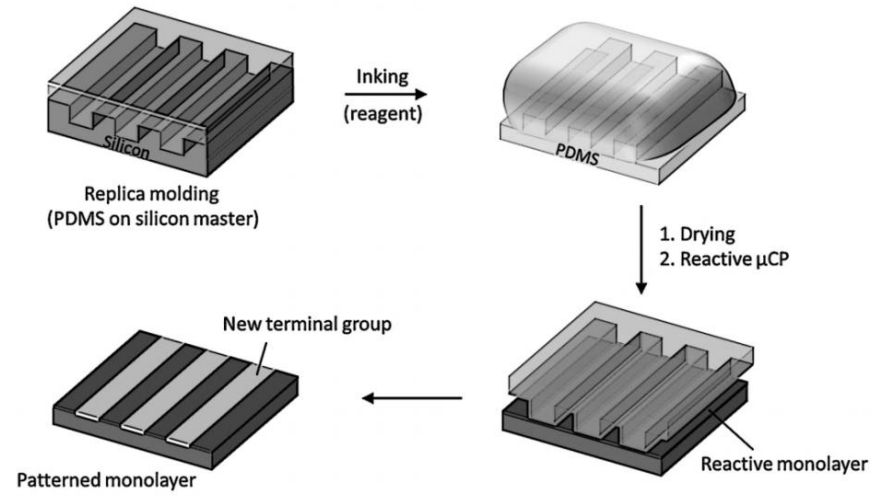

Scheme 2.2. Reactive microcontact printing: stamping of a reagent onto a reactive monolayer yields a patterned monolayer on a substrate.

Surface gradients are surfaces with a gradual variation of at least one physicochemical property in space that may evolve in time. Surface chemical gradients (Scheme 2.3) have allowed for the gradual modulation of interfacial properties and have been employed to generate smart materials and to investigate surface-driven transport phenomena like the motion of water droplets on a wettability gradient,[38] or the study of biological processes, for example the directed migration (haptotaxis) and polarization of cells on biomolecular gradients.[39] Moreover, surface gradients integrate a wide range of properties in a single sample thus providing a valuable tool for the fast high-throughput analysis of several parameters. This also circumvent often encountered problems with reproducibility and

tedious analysis of multiple samples. Two general methods are commonly employed for the development of surface chemical gradients: (i) the controlled adsorption/desorption of SAMs on gold or silicon and (ii) the chemical post-modification of SAMs.[39-42]

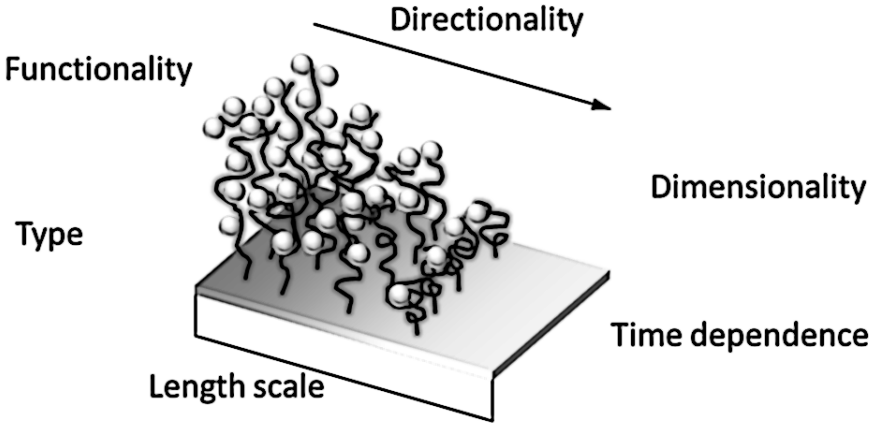

Scheme 2.3. Surface chemical gradients attributes. Adapted from Ref. 39.

In the first part of this chapter the reactivity of SAMs and the covalent modifications that have been carried out on monolayers by means of "click chemistry" from solution and by soft lithography are described. In the second part the fabrication of surface chemical gradients exploiting the assembly/disassembly of SAMs and very recent strategies based on "click"-based chemical modifications of terminal functional groups of SAMs are illustrated.

2.2 Chemical transformation of monolayers

Both thiols on gold and organosilanes on silicon or glass produce robust dense monolayers and have been used for subsequent modification using chemical reactions. A common modification of the surface properties is obtained via modular stepwise selective functionalization of pre-formed reactive SAMs.

Below are described the main recent examples in which reactive monolayers are employed in combination with click chemistry, either by reaction in solution or by soft lithography (*e.g.* μCP). In particular, the most attractive and common click reactions were considered: the azide-alkyne cycloaddition, the Michael addition, the thiol-ene reaction, the Diels-Alder cycloaddition, and the imine and oxime formation (Scheme 2.4).

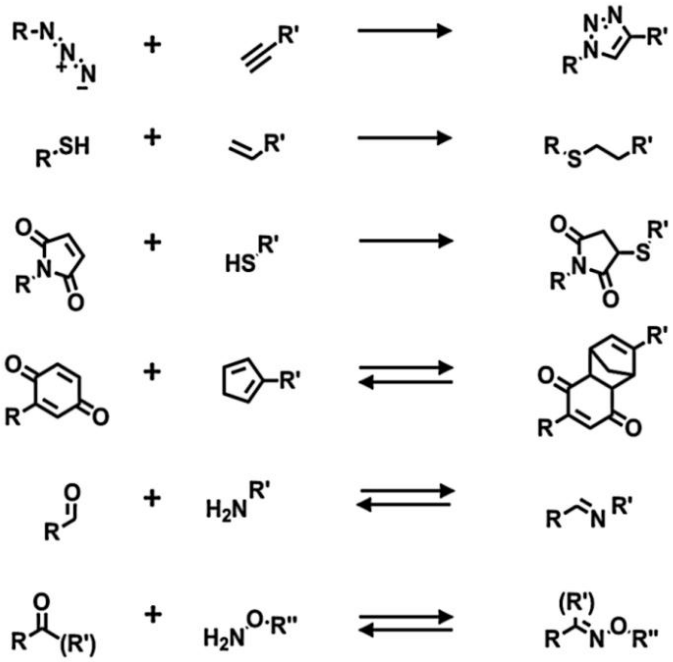

Scheme 2.4. Modification of terminal groups of monolayers by means of surface-confined reactions. Examples of "click" reactions employed for monolayers modification, from the top to the bottom: Huisgen 1,3-cycloaddition, thiol-ene reaction, Michael addition, Diels-Alder cycloaddition, and imine and oxime formation.

2.2.1 Azide-alkyne cycloaddition

The Huisgen reaction is a [3+2] cycloaddition that occurs between an organic azide (1,3-dipolar molecule) and an alkyne (dipolarophile). Owing to the kinetic stability of alkynes and azides, the reaction usually requires elevated temperature and long reaction times with the formation of a 1:1 mixture of 1,4- and 1,5-regioisomers. This reaction has obtained substantial attention only after the introduction of the Cu(I)-catalyzed azide-alkyne cycloaddition (CuAAC or "click" chemistry),[24,43,44] providing regioselectivity towards the 1,4-regioisomer and an extraordinary enhancement of reactivity (increase in reaction rate up to 10^7 times) under mild reaction conditions.[45,46] Cu(I) can be provided to the reaction mixture by means of different methods: (i) the most common approach is by chemical reduction of Cu(II) salts (usually Cu(II) sulfate pentahydrate in the presence of an excess of sodium ascorbate);[24] (ii) by direct addition of a Cu(I) salt;[47] (iii) by comproportionation of Cu(II) salts with copper metal;[43] or (iv) by electrochemical reduction of a Cu(II) salt.[48] Furthermore, although CuAAC works effectively under "ligand-free" conditions, a further acceleration of the reaction has been observed upon addition of certain chelates (e.g. amine triazoles), allowing a drastic reduction of the amount of loaded

catalyst.[49] The numerous examples in the literature confirm that a wide variety of reaction conditions can be successfully employed in the CuAAC.

The use of the CuAAC reaction has found particular value in the selective and efficient modification of SAMs. In two early reports, Collman and coworkers employed CuAAC to functionalize azide monolayers on gold electrodes (prepared mixing azidoundecanethiol with decanethiol as diluent) with alkyne-modified ferrocene in solution.[50-52] The reaction, in terms of azide consumption, was monitored via infrared (IR) and X-ray photoelectron spectroscopies (XPS), while the extent of formation of triazole was assessed via electrochemistry, exploiting the redox-active ferrocene substituents. Furthermore, using the same building blocks, they demonstrated the selective functionalization of independently addressed microelectrodes controlling the CuAAC via electrochemical activation/deactivation of a copper(II) complex (Scheme 2.5).[52] These experiments demonstrated the potential of CuAAC for the electrochemically driven local functionalization of monolayers on metals.

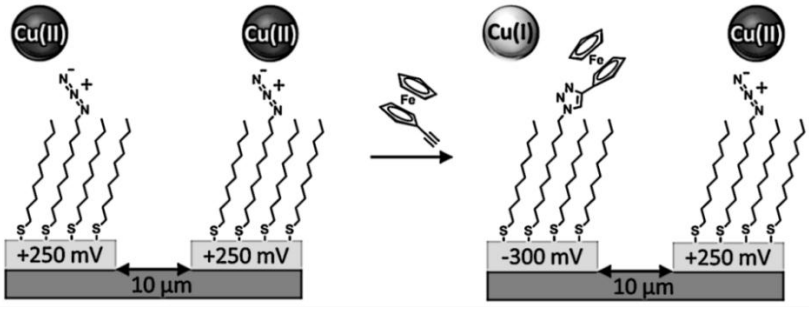

Scheme 2.5. Selective functionalization of independently addressed microelectrodes by electrochemical activation and deactivation of a copper catalyst for the CuAAC reaction. Adapted from Ref. 52.

Electrochemically driven CuAAC via scanning electrochemical microscopy (SECM) was presented by Ku *et al.* as a method to anchor small molecules to an insulating substrate.[53] Appling a gold ultra microelectrode (UME) close to an azido-terminated monolayer on glass, the Cu(I) active catalyst was locally generated via electrochemical reduction of a Cu(II) salt and employed for the patterning of an alkyne-functionalized fluorescent molecule via click reaction. This approach demonstrates how the surface patterning capability of SECM can be further extended.

Also alkyne-functionalized SAMs have been used as a platform for click modification. Lee *et al.* explored the reactivity of ethynyl-terminated SAMs on gold towards "click" chemistry using an extensive surface characterization: IR and XP spectroscopies, ellipsometry, and contact angle goniometry were employed to demonstrate that also ethynyl-terminated SAMs are useful for the introduction of functional groups on surfaces

via CuAAC.[54] Chaikof and coworkers prepared alkyne-terminated monolayers by the Diels-Alder reaction of an α,ω-poly(ethylene glycol) (PEG) linker with alkyne and cyclopentadiene terminal groups on a N-(ε-maleimidocaproyl)-functionalized glass slide.[55] This platform was employed to immobilize, by CuAAC, a wide range of azide-containing biomolecules (biotin, carbohydrates and proteins).

Soft lithographic techniques were employed in combination with "click" chemistry for the spatially resolved functionalization of monolayers. Ravoo and coworkers demonstrated the fast formation of triazo induced via microcontact printing of an alkyne-inked PDMS stamp onto an azide-functionalized monolayer on glass.[56] Surprisingly the reaction proceeded without Cu(I) catalysis, presumably owing to the high local alkyne concentration. Further studies established that the addition of Cu(I) or the use of Cu(0)-coated PDMS stamps improve the efficiency and surface density (Scheme 2.6).[57,58] "Click" chemistry by μCP was conveniently employed by Bertozzi and co-workers[58] and Ravoo *et al.*[59] to pattern microarrays of carbohydrates on azide monolayers as probes for glycan-binding receptors, antibodies, and enzymes.

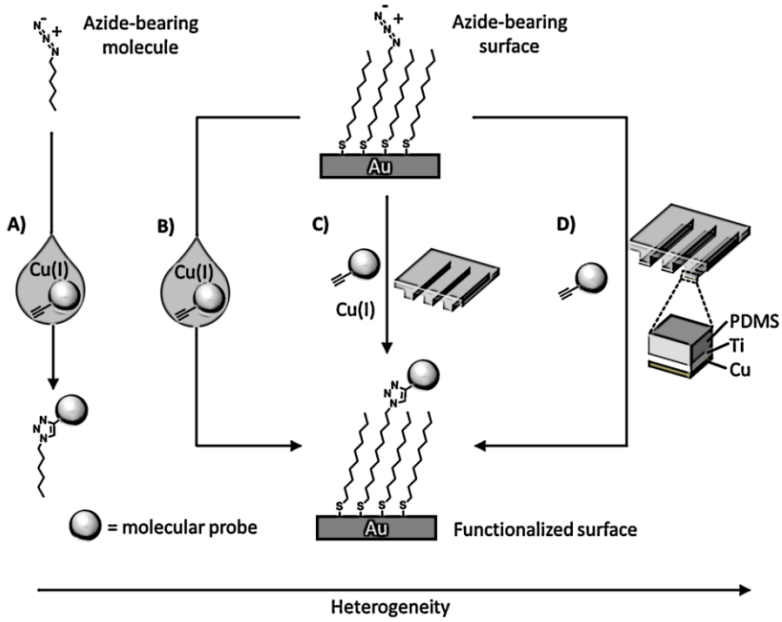

Scheme 2.6. Various routes to achieve the Cu(I)-catalyzed azide–alkyne coupling (CuAAC) in different environments: A) solution: a solution reaction where azide, alkyne, and catalyst participate in a homogeneous reaction; B) solution–surface: a heterogeneous reaction where dissolved alkyne and catalyst react with a surface bound azide; C) reagent-stamping: a heterogeneous reaction where the alkyne and catalyst are brought into contact with a surface-bound azide in the condensed phase; D) StampCat: a heterogeneous reaction where immobilized copper catalyzes the reaction of an alkyne with a surface bound azide in the condensed phase. Adapted from Ref. 57.

Nanometer-scale patterning was obtained by Paxton *et al.* by a constructive scanning probe lithography method using copper-coated atomic force microscopy tips to catalyze the CuAAC between small alkyne molecules in solution and azide-terminated monolayers on silicon surfaces.[60] The click reaction occurred only in the areas where the Cu-coated tip was brought in contact with the monolayer.

A rapid reaction under mild conditions has been also obtained in a Cu-free system by means of strained dipolarophiles such as cyclo-octynes[61] and dibenzocyclo-octynes.[62] Recently a Cu-free click chemistry[63, 64] (strain-promoted azide–alkyne cycloaddition, SPAAC) was introduced as a surface immobilization strategy ideal for biological applications due to the elimination of copper salts that are potentially cytotoxic, in combination with the high retention of activity in comparison with CuAAC.[65] Orski and coworkers employed the Cu-free click chemistry using a photoactive protected strained cyclo-octyne to achieve the selective spatial immobilization of azide-functionalized fluorescent dyes.[66] A silicon wafer was functionalized with poly(*N*-hydroxysuccidimide 4-vinyl benzoate) brushes for the coupling of a cyclopropenone-masked dibenzocyclooctynes (Scheme 2.7). UV irradiation promoted the fast decarbonylation of the cyclopropenone to the alkyne that became available for the Cu-free click chemistry with azide-modified fluorescent molecules. By means of UV irradiation in the presence of a shadow mask they fabricated multicomponent surfaces with spatially resolved chemical functionalities.

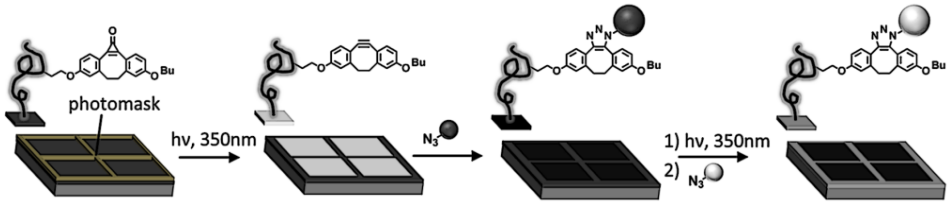

Scheme 2.7. Stepwise photodecarbonylation of cyclopropenone-masked dibenzocyclooctynes for the local immobilization of azide-functionalized dyes via Cu-free click chemistry. Adapted from Ref. 66.

Furthermore, µCP and SPAAC were employed by Ravoo and coworkers for a fast and efficient modification of azide monolayers on glass for the immobilization of multiple biomolecules on the same substrate.[67] In this work they showed the orthogonality of SPAAC with other interfacial click reactions (e.g. nitrile oxide–alkene/alkyne cycloadditions) for the fabrication of protein microarrays.

2.2.2 Michael addition and thiol-ene reactions

The two most common thiol click reactions are the base-catalyzed Michael addition reaction and the radical-mediated thiol-ene reaction. The thiolate anion and the thiyl

radical are highly reactive species leading to extremely rapid conjugation reactions with maleimides and alkenes (or alkynes), respectively.

Using thiols as reactive building blocks for the functionalization and/or patterning of surfaces has a unique biological benefit. Cysteine (Cys) is the only naturally occurring amino acid containing a thiol group in its side chain, and its relative abundance in proteins is small (less than 1%). Cys residues can be introduced in a protein through site-specific mutation of, for example, Ser or Ala residues, preferably in a remote solvent-accessible part of the protein. Gaub and coworkers genetically modified an enzyme to carry an accessible C-terminal cysteine residue, which was then shown to selectively bind to a maleimide-functionalized surface.[68]

Among other advantages, complex and diverse biologically active arrays can be prepared using large numbers of cysteine-functionalized peptides generated in solid-phase schemes. Owing to the high yield and excellent selectivity for immobilization of the maleimide-thiol reaction, Mrksich *et al.* reported that SAMs presenting a maleimide functional group can be conveniently used for the preparation of biochips upon reaction with thiol-modified biologically active ligands (e.g. peptides and carbohydrates, Scheme 2.8).[69] An interesting application was developed by Magnusson and coworkers for the fabrication of surfaces with specific effects on cell behavior.[70] In particular they used a maleimide-functionalized SAM to immobilize a Cys-modified peptide that triggers cellular chemotaxis and a calcium-dependent oxidative metabolism.

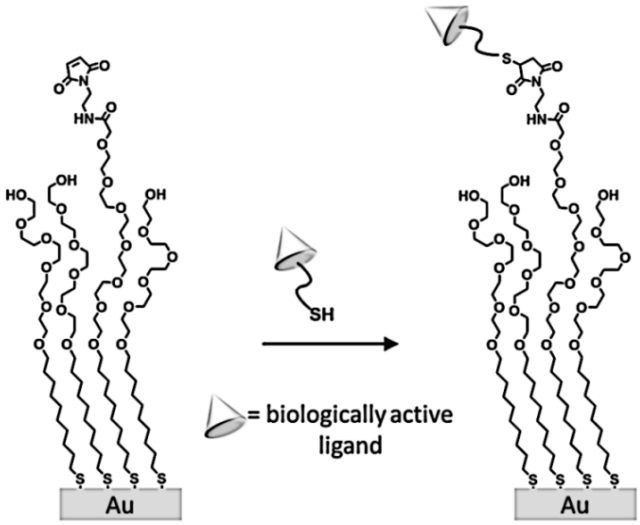

Scheme 2.8. Structure of a self-assembled monolayer used to immobilize thiol-terminated ligands. Adapted from Ref. 69.

Jonkheijm *et al.* employed the thiol–ene reaction to pattern proteins onto a surface using the biotin/streptavidin (SAv) approach.[71] An alkene-modified biotin was patterned on a thiol-modified silicon surface either upon exposure to UV light at 365 nm through a micro-featured photomask, or at 411 nm by means of laser-assisted nanopatterning. The biotin-functionalized surfaces were incubated with Cy5-labeled SAv yielding fluorescently visible protein patterns employed in a SAv sandwich approach, to immobilize bioactive enzymes. In a similar approach, Escorihuela and coworkers used UV-promoted thiol-ene coupling for the fabrication of DNA microarrays and the implementation of hybridization assays on silicon.[72] The selective attachment of DNA occurred through a multistep process including the preparation of a thiol-functionalized silicon slide, the UV-promoted thiol-ene coupling of an alkene-modified biotin and the subsequent immobilization of SAv and biotinylated DNA. A photochemical μCP method was employed by Ravoo and coworkers to pattern bioactive thiols on alkene- or alkyne-terminated SAMs on silicon oxide (Scheme 2.9).[73] An oxidized PDMS stamp was incubated in a diluted solution of thiol and a radical initiator (α,α-dimethoxy-α-phenylacetophenone, Irgacure 651), dried and brought in conformal contact with the functionalized substrate. Successful immobilization was achieved upon short time (5-600 s) UV irradiation at 365 nm. This technique, in combination with orthogonal contact chemistry for amide and triazole formation, was employed by the same group for the fabrication of multifunctional platforms for the immobilization of biomolecules in microarrays.[74]

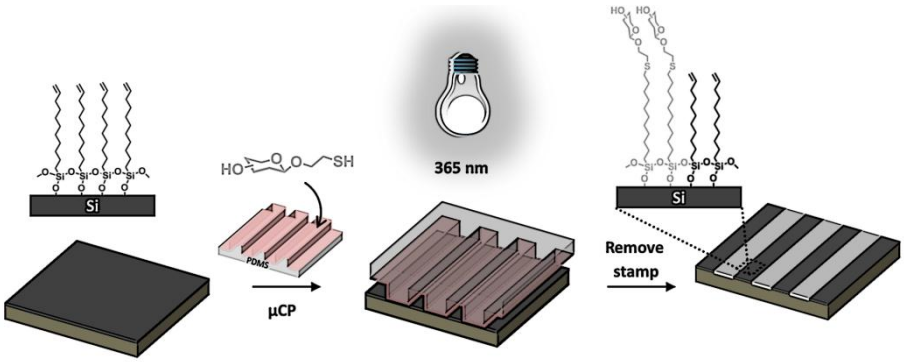

Scheme 2.9. Schematic illustration of photochemical μCP by thiol–ene chemistry: an oxidized PDMS stamp inked with a thiol and a radical initiator is placed on an alkene-terminated SAM and irradiated with UV light (365 nm). Immobilization of the thiol occurs exclusively in the area of contact. Adapted from Ref. 73.

2.2.3 Diels-Alder reaction

The Diels-Alder (D-A) reaction is a reversible [4+2] cycloaddition occurring between a conjugated diene (in the *cis* configuration) and an electron-deficient dienophile. The

reaction is orthogonal, efficient, atom conservative, it does not require a catalyst and it is insensitive to the reaction conditions (e.g. solvent, air).

The pioneers to investigate the D-A reaction for the immobilization of biologically active molecules on SAMs were Yousaf and Mrksich.[75] Hydroxyl and hydroquinone mixed SAMs on gold were prepared and the D-A reaction with cyclopentadiene-modified ligands was electrochemically modulated via oxidation of the hydroquinone to the active quinone. The D-A reaction between the quinone monolayer and a cyclopentadiene-modified biotin in solution was monitored via cyclic voltammetry, observing a loss in current due to the cycloaddition (the quinone reagent is electrochemically active while the product is not). Furthermore they used the association of biotin/streptavidin as a model system for the D-A-mediated immobilization of proteins. In this work and in follow-up studies they demonstrated that the interfacial reaction occurs following a pseudo-first-order rate law (with excess of cyclopentadiene in solution) that strongly depends on the nature of the microenvironment surrounding the quinone moieties in the monolayer.[76-78] Moreover, exploiting the local electrochemical activation of the hydroquinone groups, this reactive monolayer was conveniently and elegantly employed to direct the selective stepwise attachment and micronscale patterning of two different cell types[79], to stimulate cell migration[80] (Figure 2.1) and to fabricate peptide chips to quantify the enzymatic activity of protein kinase.[81]

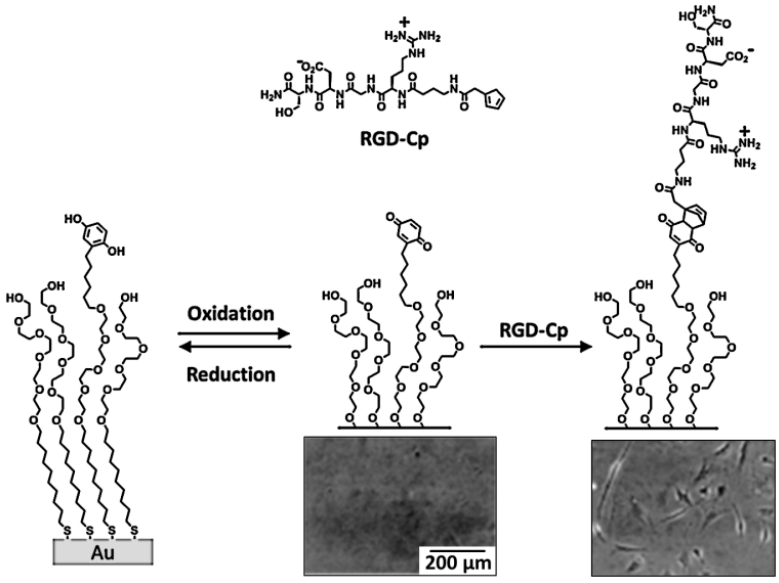

Figure 2.1. Strategy for the design of a substrate that can be electrically switched to turn on cell adhesion. Adapted from Ref. 80. © 2001 Wiley-VCH Verlag GmbH, Weinheim, Germany.

Mrksich and coworkers introduced a variation of the system for the photopatterned immobilization of ligands.[82] The hydroquinone unit was equipped with a nitroveratryloxycarbonyl (NVOC) group resulting in a photoactive monolayer. Upon UV irradiation through a microfiche mask or using the light through an optical microscope, the hydroquinone was locally deprotected and extended for the subsequent electrochemical oxidation to quinone and the D-A-mediated immobilization of cyclopentadiene-modified ligands.

More recently, Ravoo *et al.* performed the D-A reaction via reactive μCP.[83] Cyclopentadiene- or furan-modified carbohydrates were immobilized on maleimide-functionalized glass and silicon substrates by means of a fast cycloaddition locally induced via μCP. Microarrays containing up to three different carbohydrates were prepared using this method and the binding of lectins was assessed.

Photochemically activated D-A reactions were recently developed for the spatially controlled cycloaddition on SAMs.[84,85] Barner-Kowollik *et al.* achieved spatial control by immobilization of the photoactive component and subsequent direct UV activation (Figure 2.2).[84] The strategy is based on the immobilization of a triethoxysilane-functionalized *o*-methylphenyl aldehyde on a silicon substrate. This molecule was photoisomerizated to the photoenol that undergoes a fast D-A reaction in the presence of a dienophile (e.g. maleimide) (Figure 2.2). A selective local surface-confined reaction was confirmed by the photopatterning of a small-molecule ATRP initiator (Figure 2.2B), a polymer, and a peptide.

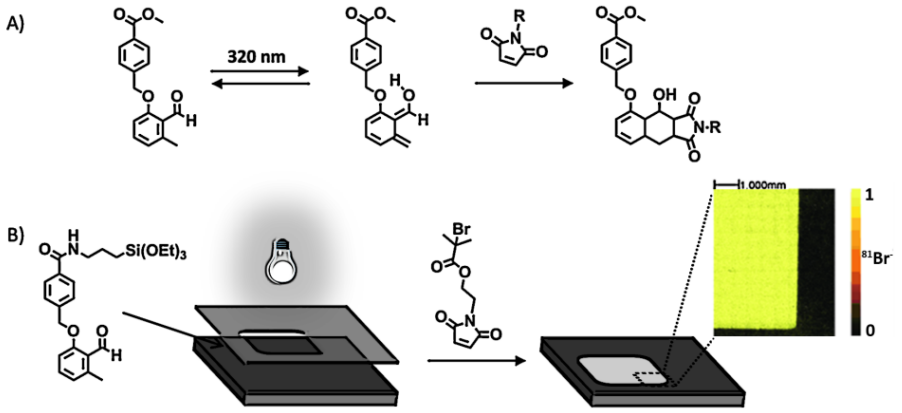

Figure 2.2. A) Photoinduced isomerization of a 2-formyl-3-methylphenoxy (FMP) derivative and subsequent Diels–Alder [4+2] cycloaddition with a dienophile. B) Structure of the FMP-functionalized monolayer and representation of the phototriggered Diels–Alder surface grafting of a bromine-containing maleimide derivative through a shadow mask. The insert shows a ToF-SIMS image of the patterned silicon wafers. Adapted from Ref. 84. © 2012 Wiley-VCH Verlag GmbH, Weinheim, Germany.

Arumugam and Popik employed a photochemically inert surface and a light-sensitive compound in solution to perform an hetero-D-A addition of 2-napthoquinone-3-methides (*o*NQMs) to a vinyl ether-functionalized substrate (Figure 2.3).[85] Irradiation of a 3-(hydroxymethyl)-2-naphthol (*o*NQM precursor) resulted in efficient and fast dehydration to *o*NQM that underwent a fast and quantitative D-A cycloaddition with vinyl groups on the surface. The facile D-A reaction combined with the short lifetime of the photoactivated species allowed the spatial control of surface derivatization. The interface reaction was visualized by the immobilization of a biotin-modified *o*NQM and subsequent co-localization of avidin-FITC (Figure 2.3B).

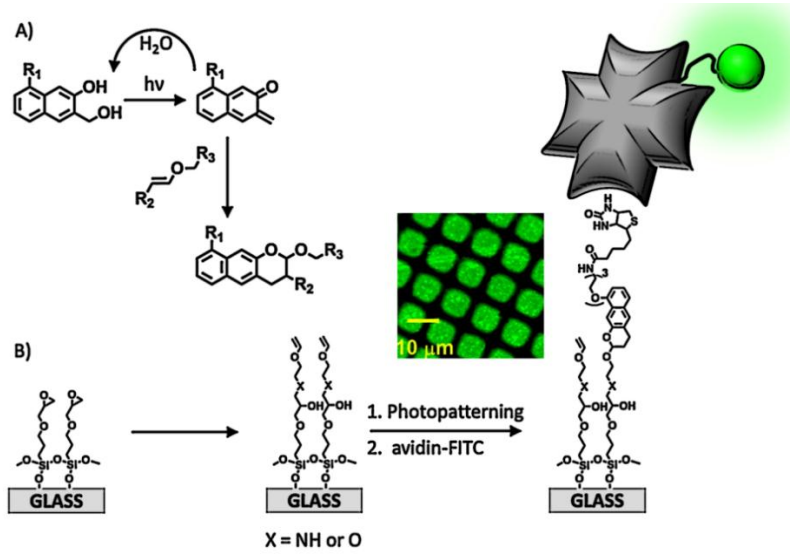

Figure 2.3. A) Mechanism of the dehydration of the substrate and the formation of oNQM and quantitative Diels-Alder cycloaddition to yield photostable benzo[g]chromans. B) Schematic representation of the preparation and light-directed biotinylation of vinyl ether-coated slides followed by immobilization of FITC-avidin. The insert shows a fluorescence microscopy image of a vinyl ether-coated surface irradiated through a 12.5 µm pitch copper grid. Adapted from Ref. 85. © 2011, American Chemical Society.

2.2.4 Imine and oxime formation

The reaction between an amine or an aminooxy moiety and an aldehyde (or a ketone) for the preparation of an imine or oxime, respectively, is widely employed in the fabrication of monolayers in which the interactions between the molecules in solution and the counterpart immobilized on the surface occur through the formation of reversible molecular bonds.

Ravoo *et al.* have described a method for the reversible formation of imines from the reaction of amines/aldehydes with aldehyde/amine monolayers on gold and silicon oxide.[86] An amino-terminated monolayer on gold or silicon was directly reacted with aldehydes in

solution or via μCP to form full or patterned imine monolayers. Alternatively, the amine-reactive functionality was switched to aldehyde via reaction with terephthalaldehyde to allow the reaction with aliphatic amines or the fluorescent Lucifer Yellow for the optical readout of the imine formation. Contact angle goniometry, FT-IRRAS, AFM and fluorescence microscopy attested the reversibility of the obtained imine monolayers under acid-catalyzed hydrolysis. In a following study, aldehyde-terminated monolayers were employed for the microcontact printing-mediated covalent immobilization of collagen-type protein col3a1 for studies on adhesion, proliferation and migration of HeLa cells.[87]

Barner-Kowollik and coworkers combined the phototriggered deprotection of an *o*-nitrobenzyl derivative to obtain spatial and temporal control of the oxime reaction.[88] Silicon wafers were coated with a 2-[(4,5-dimethoxy-2-nitrobenzyl)oxy]tetrahydro-2H-pyranyl (NOTP) silane derivative that experienced fast photocleavage upon irradiation at 370 nm, yielding a nitrosobenzaldehyde-terminated monolayer. When the silicon wafer was covered with a photomask, the photo-deprotection led to the formation of a pattern of aldehyde groups. Next, the oxime formation was demonstrated by means of the reaction with O-[(perfluorophenyl)methyl] hydroxylamine hydrochloride (fluoro marker) and GRGSGR peptide, and subsequent surface imaging via time-of-flight secondary ion mass spectrometry (ToF-SIMS).

Yousaf *et al.* proposed, in a set of studies, a system for the reversible and tunable attachment of aminooxy-functionalized ligands: a redox-active hydroquinone monolayer on gold was electrochemically oxidized to benzoquinone, which was subsequently reacted with aminooxy-containing molecules to form the corresponding oxime (Figure 2.4A).[89] Since both quinone and oxime are electrochemically active (characterized by different redox potentials) the yield of the reaction and the density of the immobilized ligand were determined and modulated (Figure 2.4B). The versatility of this method was demonstrated by the immobilization of peptides for protein binding,[89] for cell adhesion[89] (Figure 2.4C) and differentiation[90] studies and by the fabrication of renewable microarrays.[91]

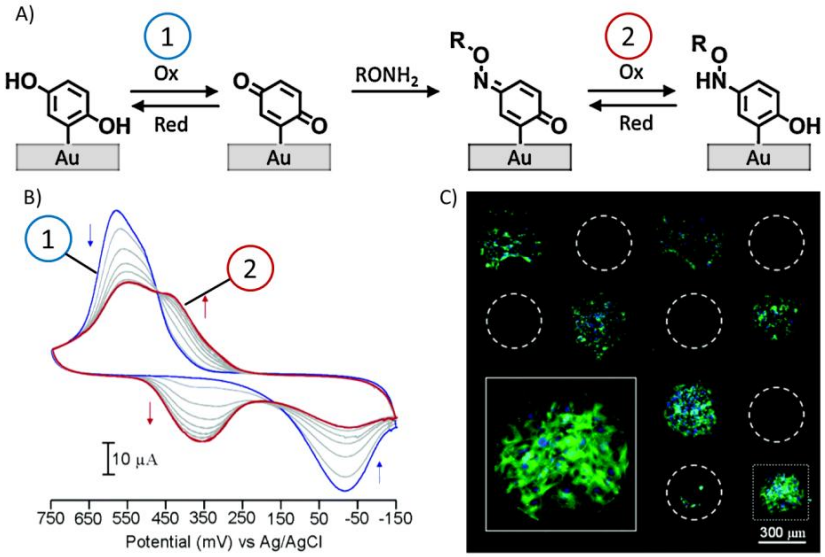

Figure 2.4. A) Redox-active hydroquinone monolayer undergoes electrochemical oxidation to the benzoquinone. The resulting quinone then reacts chemoselectively with aminooxy acetic acid to give the corresponding oxime. B) Cyclic voltammograms showing the extent of the interfacial reaction between soluble aminooxy acetic acid and a quinone monolayer. C) A fluorescence microscopy image of attached cells on a surface arrayed with immobilized aminooxy-modified RGD and GRD peptides. Cells attached only to the spots presenting the RGD peptide. Adapted from Ref. 89. © 2006, American Chemical Society.

2.2.5 Fluorogenic monolayers

Fluorescence-based technologies are employed in materials science and (bio)sensing since they allow the fast, simple, sensitive and non-destructive detection, diagnosis and investigation of (bio)chemical processes.[92-95] Many fluorescent probes have been designed and employed to be selective and sensitive towards various analytes operating through specific chemical reactions.

Fluorogenic molecules have been employed as reactive monolayers for the fabrication of microarrays[96-98] and for the simultaneous immobilization and detection of bio- and macro-molecules.[99,100] To this end, Salisbury *et al.* synthesized a wide range of fluorogenic peptidyl coumarin substrates, 7-amino-4-carbamoylmethyl coumarin peptides, to study protease activity.[97] The set of peptide-modified fluorogenic coumarins were spotted and immobilized via oxime ligation on an aldehyde-terminated monolayer. The microarrays were incubated with a variety of serine proteases. The fluorescence intensity recorded after proteolysis was used to quantify the extension of the cleavage, giving direct information on the enzyme/peptide specificity. In a similar approach, Zhu *et al.* described the synthesis of different coumarin-based fluorogenic molecules and their use in

microarrays to quantitatively and specifically detect the activity of four classes of enzyme hydrolases.[98]

Also in our group technologies based on the construction of fluorogenic platforms were recently developed. Huskens *et al.* described the immobilization of a pyrylium derivative on a glass substrate for the anchoring of amines (e.g. aliphatic amines, a fluorescent protein and a lissamine rhodamine B ethylenediamine) through μCP and dip-pen nanolithography (Scheme 2.10).[99] Upon reaction with a primary amine the initially intense fluorescence of the pyrylium monolayer faded out proving the actual covalent immobilization.

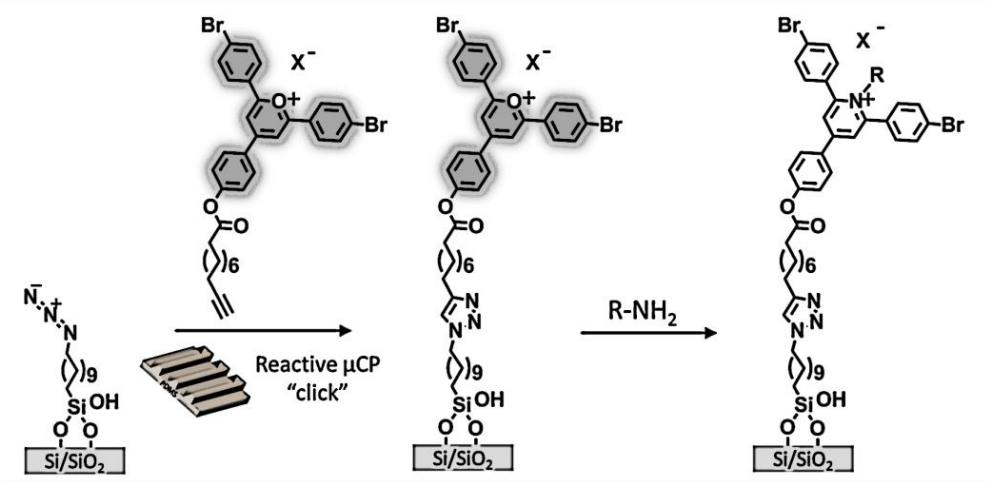

Scheme 2.10. Preparation of a pyrylium-terminated monolayer. The printing of the alkyne-functionalized pyrylium is followed by the covalent immobilization and detection of amines. Adapted from Ref. 99.

Velders and coworkers demonstrated the selectivity and specificity of orthogonal covalent and noncovalent functionalization for small molecules.[100] In their work bifunctional alkyne-cyclodextrin patterned surfaces were prepared via reactive μCP of an azido-modified β-cyclodextrin on a fluorogenic alkyne-modified coumarin monolayer. The fluorescence enhancement upon alkyne-azide cycloaddition was used to monitor the effective bond formation and to localize the β-cyclodextrin monolayer.

2.3 Surface chemical gradients of self-assembled monolayers

Surface chemical gradients are surfaces with gradual, continuous or discrete, variation in space and/or time of physicochemical properties. They have been successfully employed for the study of interfacial phenomena in the areas of, among others, biology to investigate cell migration (haptotaxis) and polarization, materials science, *e.g.* for the study of the driven motion of liquid droplets,[101, 102] and combinatorial/analytical chemistry.[103-105]

The first study describing the fabrication of surface chemical gradients was illustrated by Elwing *et al.* in 1987.[106] The gradient was the result of controlled silane diffusion in liquids. An hydrophilic silicon plate was placed in a cuvette filled with a biphasic solution of dimethyldichlorosilane in trichloroethylene covered with xylene. In this system, organosilane molecules diffuse to the xylene phase and deposit on the silicon substrate yielding surface gradients. The resulting gradient was employed to study the wettability-driven adsorption and interaction of proteins and polymers at liquid/solid interfaces. From that very first work, a wide variety of methods and techniques was developed for the generation of surface chemical gradients mainly based on the controlled adsorption/desorption of monolayers on substrates.

An exhaustive description of gradient fabrication methods has been reported in recent comprehensive reviews.[39-42] Here we focus on two different methods for the preparation of surface chemical gradients of self-assembled monolayers: (i) the controlled physical adsorption, desorption and exchange of monolayer adsorbates on gold and silicon and (ii) the local chemical modification of terminal functional groups of SAMs.

2.3.1 Surface chemical gradients by adsorption/desorption of monolayer adsorbates

The most commonly used technique to prepare silane-based gradients was developed in 1992 by Chaudhury and Whitesides.[38] Wettability surface gradients were prepared by vapor diffusion of decyltrichlorosilane along a silicon substrate, and the surface free energy gradient obtained was employed to study the motion of water droplets based on the surface tension acting on the liquid-solid interface on the two opposite sides of the drop. Genzer *et al.* employed this method to generate gradients of different chemical functionalities on various substrates.[107, 108]

A cross-diffusion method was employed by Liedberg and Tengvall in 1995 to prepare the first alkanethiol gradient on gold.[109] A gold substrate was covered with a polysaccharide matrix and different ω-substituted alkanethiols were added at the two opposite ends of the substrate. The diffusion of the two alkanethiols generated surface chemical gradients with gradual variation of the terminal functional groups that were thoroughly investigated by IR and XP spectroscopies and ellipsometry.

2.3.1.1 Electrochemically derived surface gradients of SAMs on gold

Since 2000, in several works, Bohn and coworkers illustrated an electrochemical method for the gradual desorption of alkanethiol SAMs on gold.[110,114] The working principle is based on the application of an in-plane potential gradient across a surface of a gold electrode fully covered with an alkanethiol SAM. In the areas where the potential is

sufficiently negative (V < -0.8 V vs Ag/AgCl) the reductive desorption of alkanethiols prevails. This leads to the formation of dynamic surface gradients whose shape is dependent on the applied potential window and offset. This technique was employed to study the effects and utility of surface gradients on the attachment of nanoparticles[111] and the immobilization of proteins[112] (e.g. fibronectin) for cell adhesion and motility experiments.

Ulrich *et al.* obtained a potential gradient across a surface by means of a bipolar electrode and employed it for the preparation of surface chemical gradients.[115] A potential difference applied between two electrodes induced an electric field in a solution containing a conductive surface (e.g. SAMs on gold). When the electric field parallel to the surface exceeded a threshold value, the conductive surface of the substrate became a bipolar electrode (an electrode that acts as both anode and cathode). The redox reactions occurred mainly at the edges of the electrode and decreased towards the center of the surface. Thus, the cathodic side of a SAM on gold experienced the reduction and desorption of the alkanethiol monolayer, while the anodic side remained unchanged with the consequent formation of a surface gradient.

Fuierer *et al.* adapted a scanning probe lithography technique to pattern SAMs at the sub-micrometer length scale.[116] They reported an STM-based replacement lithographic technique in which a dodecanethiol SAM on gold is selectively desorbed and *in-situ* replaced by ferrocenyl-undecanethiol resulting in a two-component gradient in the sub-micrometer range (Figure 2.5). The extent of desorption was tuned by gradual variation of the applied bias and/or scan speed.

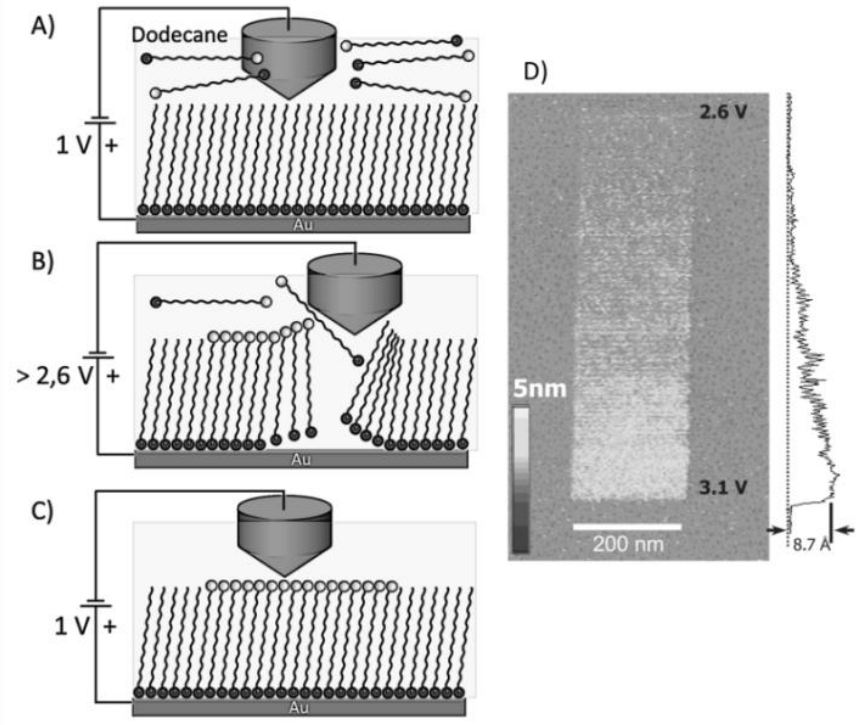

Figure 2.5 Replacement lithography: A) imaging of the substrate; B) thiolate desorption from the Au substrate with gradual increase of the tip-substrate bias until +3.1 V. The localized desorption allows the replacement by other thiol molecules present in solution to adsorb onto the freshly exposed gold regions, creating a new monolayer. C) The STM parameters were returned to the lower bias values to image the monolayer gradient. D) STM image of ferrocenyl-undecanethiol mesoscale chemical gradients fabricated by systematically varying replacement bias. Adapted from Ref. 116. © 2002 Wiley-VCH Verlag GmbH, Weinheim, Germany.

2.3.1.2 Contact printing techniques

Microcontact printing has also been employed as a technique for surface gradient fabrication. Kraus *et al.* exploited a mass transfer-limited μCP process to pattern alkanethiol gradients on gold.[117] By using PDMS stamps with tailored thickness and shape the amount of alkanethiols diffusing into the stamp, from an ink pad, changed along the surface. In particular a higher amount was transferred in the thicker region of the stamp compared to the thinner region (Figure 2.6A). Hexadecanethiol (HDT) gradients on gold were obtained upon diffusion-controlled printing. Two-component gradients were achieved after backfilling with perfluorododecanethiol (PFDDT) in a second step. Using stamps with different geometries they were able to prepare linear and nonlinear (e.g. radial) gradients. Upon extensive investigation of the transfer process responsible for the formation of the surface gradient, it was demonstrated that hexane and heptane deposited on the

fluorinated side of the gradient (oleophobic) move toward the HDT side (oleophilic) (Figure 2.6B).

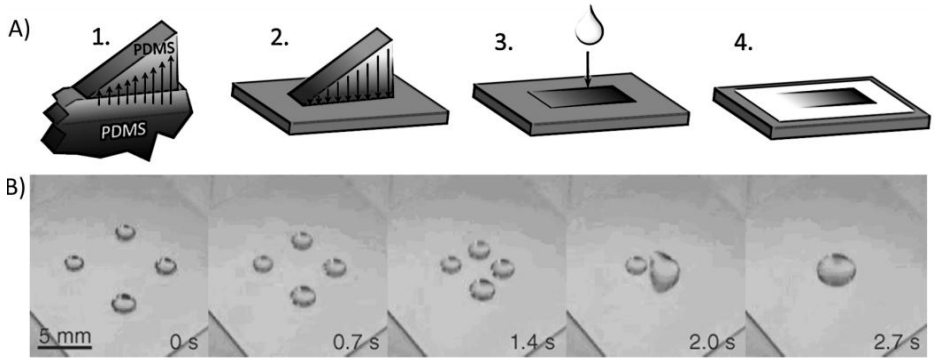

Figure 2.6. A) Scheme of the diffusion-controlled depletion printing: 1. Thiol diffuses into the stamp from an ink pad. 2. The ink leaves the stamp because of adsorption to the gold surface and creates a partially covered surface. 3. The voids can be filled with other thiols to form 4. a two-component surface composition gradient B) Droplets of heptane moving on a radial surface energy gradient. The substrate is vibrated to excite the droplet movement. Adapted from Ref. 117. © 2005, American Chemical Society.

Using a μCP technique, Choi *et al.* fabricated micrometer-scale surface energy gradients on silicon substrates.[118] Curved PDMS stamps inked with octadecyltrichlorosilane were employed to control the contact time over the contacted area, and the obtained surface energy gradients were shown to be able to move nano-liter water droplets on the surface.

Geissler and coworkers used a method called edge-spreading lithography to generate nanometer-scale radial gradients by means of printing of a mixture of alkanethiols on particle arrays on gold.[119] The formation of the surface gradients on the gold substrate is due to the different diffusion constants of the thiols along the microspheres during the transfer between PDMS stamp and substrate.

In a recent report, Yousaf and coworkers fabricated micrometer-scale gradients via solute (e.g. alkanethiol) permeation and diffusion in a PDMS microfluidic cassette.[120] Using this technique the PDMS microfluidic cassette was inked via permeation and diffusion with an oxyamine-terminated alkanethiol, creating a chemical gradient that was transferred via printing onto a gold substrate (Figure 2.7). The gradient was therefore visualized via reaction of the oxyamine-terminated monolayer with a ketone-functionalized dye. The immobilization of a cell adhesive Arg-Gly-Asp (RGD)-ketone peptide provided a stable interfacial oxime linkage for biospecific studies of cell adhesion, polarity, and migration.

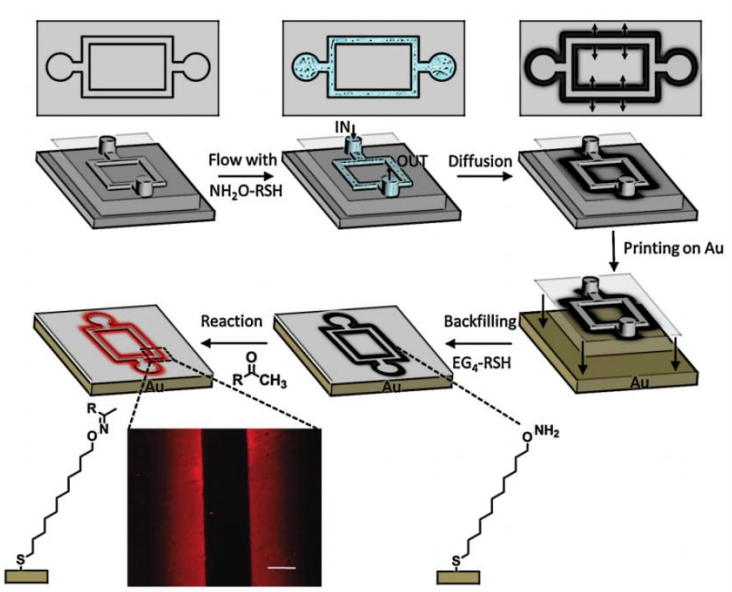

Figure 2.7 Strategy for generating gradients of molecules in PDMS microfluidic cassettes via solute permeation and diffusion. A PDMS microfluidic cassette is placed directly onto the surface of a glass substrate. An oxyamine alkanethiol (NH_2O-RSH) is flowed into the cassette and permeates and diffuses through the walls of the microfluidic channels providing a PDMS stamp with gradients of alkanethiol molecules. The inked microfluidic cassette is stamped onto a bare gold surface. The oxyaminealkanethiol rapidly forms a gradient SAM. The remaining bare gold regions are backfilled with tetra(ethylene glycol) undecanethiol (EG_4-RSH). Addition of a ketone-tethered ligand (ketone-functionalized rhodamine) to the surface allows for the formation of an oxime linkage. The insert shows the fluorescence microscopy image of the resulting surface gradient (scale bar = 200 µm). Adapted from Ref. 120. © 2010, American Chemical Society.

2.3.1.3 Irradiation-driven desorption of SAMs on gold

Irradiation techniques (e.g. (photocatalytic) UV oxidation and low energy electron-beam) have been used to promote the degradation of primary SAMs and to prepare two-component surface chemical gradients by means of a second exchange reaction step. Selective photo-oxidation of carboxylic acid-terminated (or methyl-terminated) SAMs on gold was described by Burgos *et al.* using a UV laser (244 nm) coupled to an etched optical fiber in the presence of oxygen to generate molecular-scale chemical gradients.[121,122] The irradiation led to the formation of oxidation products that were easily displaced by immersion in a solution of a second thiol. The surface gradient was formed because of the UV exposure gradient at the perimeter of the exposed region. This surface was employed to study the anisotropic diffusion of single polymer molecules in the vicinity of the chemical surface gradient.[122]

Nanometer-scale gradients were fabricated by Walder and coworkers by UV photodegradation of trimethylsilane-modified surfaces using transmission electron

microscopy (TEM) grids as contact photomasks.[123] The surface gradient was created at the boundaries between masked and unmasked regions owing to diffraction at the mask edges, and diffusion of free radicals between the contact mask and the surface. The hydrophobic gradient obtained in this way was employed to study the directional motion of nanoparticles using total internal reflection fluorescence microscopy.

Surface energy gradients were fabricated by direct laser patterning promoting a gradual desorption of alkanethiols on gold. A gradual variation of the incident laser intensity along the SAM was obtained via inclination of the substrate with respect to the laser focal plane.[124] A combination of photocatalytic oxidation and grayscale lithography was employed by Blondiaux *et al.* for the gradual degradation of alkanethiol SAMs and was followed by thiol replacement.[125] The gradual photocatalytic oxidation was obtained by UV irradiation of a titanium dioxide-coated glass held in close proximity (≈ 60 µm) of the alkanethiol SAM through a grayscale photomask. When the UV light hit the TiO_2 layer, radicals were expelled that diffused towards the gold-coated SAM with concomitant oxidation of the organic layer and easy replacement by immersion in a second alkanethiol solution (Scheme 2.11).

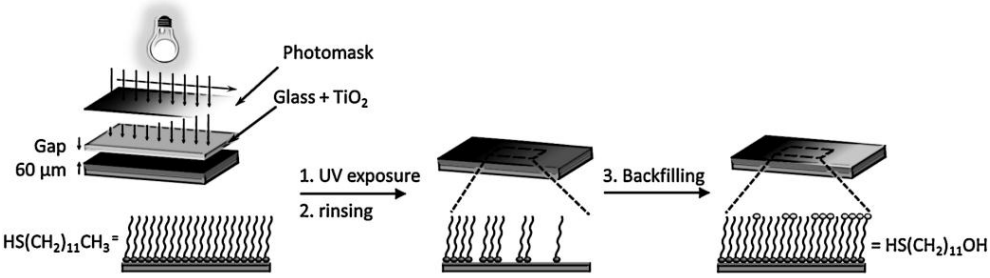

Scheme 2.11. Remote photocatalytic oxidation of a thiol SAM under a gradient of UV illumination and subsequent backfilling with a second component. Adapted from Ref. 125.

A low energy electron-beam was used for the irradiation-promoted exchange reaction of alkanethiols on gold.[126] Winkler *et al.* have recently demonstrated that electron-beam irradiation of alkanethiol SAMs on gold is suitable to introduce surface defects in a micron-scale gradient manner. The surface alteration was employed for the fabrication of bio-resistant micrometer-scale gradients by means of a surface exchange reaction with oligo(ethylene glycol)-terminated thiols.[127]

2.3.1.4 Surface gradients by immersion methods

Spencer and coworkers have fabricated surface chemical gradients via a simple gradual immersion of a vertically positioned substrate (e.g. gold) into a solution of an adsorbate (e.g. thiol) followed by subsequent immersion into a dilute solution of a second

adsorbate.[128,129] A coverage gradient was obtained upon optimization of the concentration of the adsorbate and the maximum immersion time. Gradients by gradual immersion can be achieved by slow withdrawal/immersion of the substrate in the solution or by addition/removal of the solution.

Reinhoudt, Meijer and coworkers reported dendrimer motion driven by interfacial reactions on surface chemical gradients prepared using the immersion method.[130] Aldehyde-terminated surface gradients on glass were prepared by gradual immersion of the substrate into solutions of organosilane-based aldehyde. Amine-functionalized dendrimers, labeled with rhodamine B, were printed on such aldehyde gradients and immobilized via formation of multiple imine bonds. Upon incubation in water, dendrimers experienced directional motion towards the highest surface aldehyde concentration as a consequence of the gradient-driven imine hydrolysis and reformation reactions.

2.3.2 Surface chemical gradients by means of reactive SAMs

The fabrication of the gradients described so far is dictated by the adsorption/desorption of SAMs (e.g. silanes or thiols) on inorganic substrates (e.g. silicon or gold). Below are described flexible and dynamic methods for which the formation of surface gradients is driven by interfacial chemical reactions and interactions with the possibility to tailor and control the functionalization of arbitrary surfaces in space and time.

2.3.2.1 Photochemically controlled surface reactions

A common strategy to develop surface patterns is based on the photochemical deprotection of terminal photosensitive groups of SAMs. Yousaf and coworkers have employed this methodology to pattern ligands and cells in gradients on inert surfaces.[131, 132] A nitroveratryloxycarbonyl (NVOC)-protected hydroquinone ethylene glycol-terminated alkanethiol monolayer on gold underwent photochemical deprotection upon UV illumination to reveal the electrochemically active hydroquinone unit. When the irradiation was performed in the presence of a grayscale photomask, a surface gradient of hydroquinone moieties was obtained. An aminooxy reactive quinone was obtained upon electrochemical oxidation of the hydroquinone while the NVOC-protected units remained completely redox inactive. The quinone gradient was reacted with soluble aminooxy-tagged ligands to form a stable oxime conjugate via chemoselective ligation. A rhodamine-oxyamine was used to visualize the surface gradient while an RGD-oxyamine peptide was immobilized to study cell migration and proliferation along the gradient. Interestingly the dynamic character of the monolayers allowed the electrochemical release of the ligands by

means of the reduction of the oxyamine bond and the restoration of the surface for a further ligand immobilization step.

Ito and coworkers prepared a surface chemical gradient via photodegradation of an octadecylsilane (ODS) monolayer on silicon.[133] The photodegradation was performed using a vacuum UV light (VUV) setup with an excitation wavelength of 172 nm. The VUV light was absorbed by the ODS layer with formation of radicals due to the dissociation of C-C, C-H and C-Si bonds that can react with oxygen and water to give surface oxidized species. A millimeter-scale surface gradient of oxidized groups (e.g. carboxy, aldehyde and hydroxy) was obtained by moving the substrate, positioned on a sample holder, at a controlled velocity of 50-100 μm/s. The formation of the gradient was confirmed by water contact angle goniometry and fluorescence microscopy after labelling the carboxylate groups with fluoresceinamine. Furthermore, the obtained surface gradient was employed to investigate the motion of water micro-droplets from the hydrophobic to the hydrophilic side. A similar approach was described by Gallant and coworkers.[134] An ODS monolayer on silicon was gradually oxidized placing the substrate on a motorized stage next to the slit aperture of a UV lamp. The exposure time-dependent ozone-derived oxidation of the monolayer resulted in the formation of surface gradients of oxidized species (alcohols, aldehydes, and carboxylic acids). A bifunctional propargyl-derivatized amino linker was attached to the acid gradient by using standard amidation methods. The resulting surface possessed varying coverages of alkyne groups: a useful platform for the subsequent "click" modification. In this way an RGD peptide surface gradient was fabricated to investigate cell adhesion and spreading behavior.

2.3.2.2 Electrochemically driven surface chemical reactions

Control over the length-scale, shape and functionality of surface chemical gradients was recently achieved by means of electrochemically mediated reactions, in particular the electrochemically activated copper(I) azide-alkyne cycloaddition ("e-click") and atom transfer radical polymerization ("e-ATRP").

By means of stenciled[135] or bipolar[136] "e-click", surface gradients of covalently bound alkyne-bearing molecules were created on azide-functionalized conductive polymers. Hansen *et al.* fabricated surface gradients of fluorine-rich and bioactive alkyne-modified molecules using a stencilled electro-click process, by tuning the amount of electrochemically generated Cu(I) (by reduction of $CuSO_4$) by spatial confinement of the active electrodes.[135] The shape of the gradient obtained on the conductive polymer (poly-3,4-(1-azidomethylethylene)-dioxythiophene (PEDOT-N_3)) was defined by the geometry of the insulating layer positioned on the copper counter electrode. The distance between the

counter electrode and the reactive surface dictates the speed of generation of the catalyst while the reaction conditions (e.g. concentration of reagents and catalyst, applied potential and reaction time) control the steepness and density of the gradient. The parameters affecting the formation of the surface gradient were first investigated by immobilization of a fluorine-rich alkyne-bearing molecule and characterization by XPS. Thereafter, biological applications were demonstrated by fabrication of cell adhesion peptide and protein gradients.

Li and coworkers demonstrated that a solution concentration gradient of Cu(I) can be exploited to initiate ATRP on non-conducting substrates (silicon) for the preparation of grafted gradient polymer brushes.[137] A stable diffusion gradient of activator Cu(I) and deactivator Cu(II) was formed at the gap between the working electrode and the initiator-terminated substrate. The ratio of Cu(I)/Cu(II) was tuned on different locations of the surface placing the substrate at a tilted angle along the Cu(II)/Cu(I) gradient, thereby creating different polymerization rates at different areas, leading to a gradient in polymer brush length (Scheme 2.12).

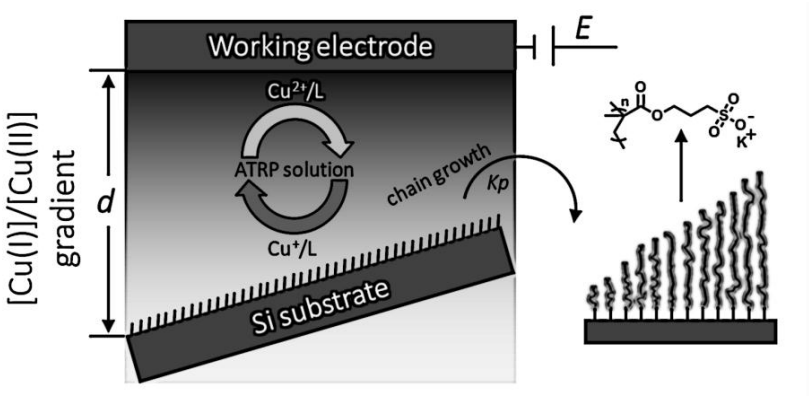

Scheme 2.12. Illustration of the diffusion-controlled eATRP for the fabrication of a surface gradient of polymer brushes. Adapted from Ref. 137.

2.3.2.3 Non-covalent interactions and dynamic chemical reactions

Huskens and coworkers analyzed the directional spreading of multivalent ligands along self-developing gradients on a receptor platform.[138] To this end, fluorescent ligands bearing one, two or three legs functionalized with adamantyl units were microcontact printed on a cyclodextrin monolayer on glass. The surface diffusion of the ligands was driven by the developing concentration gradient of free surface receptors. The multivalent surface diffusion was monitored by fluorescence microscopy and the mechanisms involved were investigated using different concentrations of a soluble receptor (cyclodextrin) as a

competitor: in pure water the divalent ligand was strongly engaged with the surface receptor monolayer and thus it walked slowly down the receptor concentration gradient; at moderate concentrations of soluble cyclodextrin, the system experienced a weakening of the multivalent interaction and one of its feet was capable of making a 'solution' complex, allowing the ligand to hop along the surface using the second foot; when the cyclodextrin concentration was increased, the probability of both feet binding to soluble cyclodextrin increased, and the ligand became free to fly further across the surface leading to more rapid spreading of the fluorescent ligands (Figure 2.8).

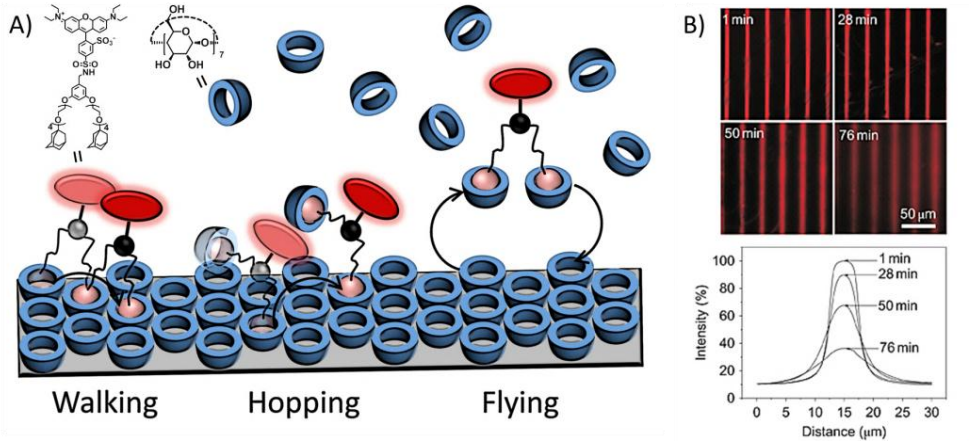

Figure 2.8. A) Schematic representation of the basic mechanisms involved in multivalent surface diffusion. B) Fluorescence microscopy images (top) and integrated line profiles (bottom) of printed lines of a bis-adamantyl fluorescent ligand on a β-cyclodextrin-terminated surface after incubation for given amounts of time in a solution with 2 mM β-cyclodextrin. Adapted from Ref. 138. © 2011, Nature Publishing Group.

Giuseppone and coworkers developed dynamic self-assembled monolayers for the fabrication of mixed surface gradients of small molecules and proteins.[139] In particular they used dynamic covalent chemistry as a tool to control the selective functionalization of surfaces in space and time: an aldehyde-terminated monolayer on silicon was incubated in a solution of various amine-functionalized fluorophores of different pK_a values (e.g. benzylamine (9.5) and alkylamine (10.5)) with simultaneous modulation of the pH (time-dependent parameter) and withdrawal of the sample at constant speed (space-dependent parameter). As a result, highly modular (bio)functional surface imine gradients were obtained with applications for the fabrication of protein and wettability gradients. This example represents a method to design new responsive interfacial systems that can adapt their constituents to external parameters.

2.4 Conclusions

Reactive monolayers constitute a powerful strategy for the introduction of new functionalities on surfaces. This strategy has already led to a number of breakthroughs in a wide range of fields including constructions of biological microarrays, drug discovery and surface science. A vast number of chemical reactions can be successfully applied to monolayers in order to tailor the nature of the terminal functional groups. On the other hand, yields or rate of reactions at the surface are limited by steric hindrance and diffusion at the solid/liquid interface. Moreover, since purification of the monolayer is impossible, high-yielding, efficient, selective and clean reactions are required. To this end, the introduction of the click chemistry approach has given a beneficial propulsion to materials science with the implementation of simple, orthogonal and highly efficient reactions. Development of strategies to control and switch the surface chemistry and properties by means of the integration of dynamic monolayers (e.g electro- and photo-active SAMs) have seen numerous applications for the investigation of the behavior of biological systems at interfaces, in particular for cell adhesion and migration studies.

Control of the local surface composition of monolayers appeared remarkably important for the systematic investigation of physicochemical phenomena at the interface in space and time, laying the foundation of gradient surfaces. In the last two decades this field exhibited an incredible growth and only some fabrication methods have been highlighted here. More importantly, surface chemical gradients recently evolved in combination with reactive monolayer technologies with the development of novel flexible and powerful strategies allowing the exploration of new surface properties. Existing space and time-dependent surface reactions are good candidates for the development of powerful dynamic surface chemical gradients. We expect that these highly efficient and flexible reactions will be used for the development and implementation of new functional surfaces with tailored surface properties and performances for important applications, among others, in the fields of biology and surface science.

2.5 References

(1) R. P. Feynman, *Eng. Sci*. 1960, *23*, 22
(2) G. M. Whitesides, *Small* 2005, *1*, 172.
(3) A. Dowling, R. Clift, N. Grobert, D. Deirdre Hutton, R. Oliver, O. O'Neill, J. Pethica, N. Pidgeon, J. Porritt, J, Ryan, A. Seaton, S. Tendler, M. Welland, R. Whatmore, Nanoscience and nanotechnologies: opportunities and uncertainties, A Report by The Royal Society & The Royal Academy of Engineering, London, July 2004. http://www.nanotec.org.uk/index.htm.
(4) A. Ulman, *Chem. Rev.* 1996, *96*, 1533.

(5) J. C. Love, L. A. Estroff, J. K. Kriebel, R. G. Nuzzo, G. M. Whitesides, *Chem. Rev.* 2005, *105*, 1103.
(6) S. Onclin, B. J. Ravoo, D. N. Reinhoudt, *Angew. Chem. Int. Ed*. 2005, *44*, 6282.
(7) J. Sagiv, *J. Am. Chem. Soc.* 1980, *102*, 92.
(8) L. Netzer and J. Sagiv, *J. Am. Chem. Soc.* 1983, *105*, 674.
(9) C. Haensch, S. Hoeppener, U. S. Schubert, *Chem. Soc. Rev.* 2010, *39*, 2323.
(10) R. G. Nuzzo and D. L. Allara, *J. Am. Chem. Soc.* 1983, *105*, 4481.
(11) C. Vericat, M. E. Vela, G. Benitez, P. Carro, R. C. Salvarezza, *Chem. Soc. Rev.* 2010, *39*, 1805.
(12) H. Hakkinen, *Nat. Chem.* 2012, *4*, 443.
(13) C. D. Bain, J. Evall, G. M. Whitesides, *J. Am. Chem. Soc.* 1989, *111*, 7155.
(14) T. P. Sullivan, W. T. S. Huck, *Eur. J. Org. Chem.* 2003, 17.
(15) P. Jonkheijm, D. Weinrich, H. Schroder, C. M. Niemeyer, H. Waldmann, *Angew. Chem. Int. Ed.* 2008, *47*, 9618.
(16) V. Chechik, R. M. Crooks, C. J. M. Stirling, *Adv. Mater.* 2000, *12*, 1161.
(17) N. Balachander, C. N. Sukenik, *Langmuir* 1990, *6*, 1621.
(18) N. Balachander, C. N. Sukenik, *Tetrahedron Lett.* 1988, *29*, 5593.
(19) G. E. Fryxell, P. C. Rieke, L. L. Wood, M. H. Engelhard, R. E. Williford, G. L. Graff, A. A. Campbell, R. J. Wiacek, L. Lee, A. Halverson, *Langmuir* 1996, *12*, 5064.
(20) D. A. Hutt, G. J. Leggett, *Langmuir* 1997, *13*, 2740.
(21) J. M. Brockman, A. G. Frutos, R. M. Corn, *J. Am. Chem. Soc.* 1999, *121*, 8044.
(22) L. Yan, C. Marzolin, A. Terfort, G. M. Whitesides, *Langmuir* 1997, *13*, 6704.
(23) S. H. Hsu, D. N. Reinhoudt, J. Huskens, A. H. Velders, *J. Mater. Chem.* 2008, *18*, 4959.
(24) V. V. Rostovtsev, L. G. Green, V. V. Fokin, K. B. Sharpless, *Angew. Chem. Int. Ed.* 2002, *41*, 2596.
(25) H. C. Kolb, M. G. Finn, K. B. Sharpless, *Angew. Chem. Int. Ed.* 2001, *40*, 2004.
(26) H. Nandivada, X. Jiang, J. Lahann, *Adv. Mater.* 2007, 19, 2197.
(27) B. J. Adzima, C. N. Bowman, *Aiche J.* 2012, *58*, 2952.
(28) L. Nebhani, C. Barner-Kowollik, *Adv. Mater.* 2009, *21*, 3442.
(29) J.-F. Lutz, *Angew. Chem. Int. Ed.* 2007, *46*, 1018.
(30) W. H. Binder, R. Sachsenhofer, *Macromol. Rapid Commun.* 2007, *28*, 15.
(31) R. K. Iha, K. L. Wooley, A. M. Nyström, D. J. Burke, M. J. Kade, C. J. Hawker, *Chem. Rev.* 2009, *109*, 5620.
(32) Y. Xia, G. M. Whitesides, *Angew. Chem. Int. Ed.* 1998, *37*, 550.
(33) A. Kumar, H. A. Biebuyck, G. M. Whitesides, *Langmuir* 1994, *10*, 1498.
(34) A. Perl, D. N. Reinhoudt, J. Huskens, *Adv. Mater.* 2009, *21*, 2257.
(35) L. Yan, W. T. S. Huck, X.-M. Zhao, G. M. Whitesides, *Langmuir* 1999, *15*, 1208.
(36) B. J. Ravoo, *J. Mater. Chem.* 2009, *19*, 8902.
(37) C. Wendeln, B. J. Ravoo, *Langmuir* 2012, *28*, 5527.
(38) M. K. Chaudhury, G. M. Whitesides, *Science* 1992, *256*, 1539.
(39) A. Pulsipher, M. N. Yousaf, *ChemBioChem* 2010, *11*, 745.
(40) J. Genzer, R. R. Bhat, *Langmuir*, 2008, *24*, 2294.
(41) S. Morgenthaler, C. Zink, N. D. Spencer, *Soft Matter* 2008, *4*, 419.
(42) C. G. Simon, S. Lin-Gibson, *Adv. Mater.* 2011, *23*, 369.
(43) C. W. Tornøe, C. Christensen, M. Meldal, *J. Org. Chem.* 2002, *67*, 3057.
(44) B. T. Worrell, J. A. Malik, V. V. Fokin, *Science* 2013, *340*, 457.

(45) M. Meldal and C. W. Tornøe, *Chem. Rev.* 2008, *108*, 2952.
(46) V. D. Bock, H. Hiemstra, J. H. van Maarseveen, *Eur. J. Org. Chem.* 2006, 51.
(47) F. Fazio, M. C. Bryan, O. Blixt, J. C. Paulson, C.-H. Wong, *J. Am. Chem. Soc.* 2002, *124*, 14397.
(48) V. Hong, A. K. Udit, R. A. Evans, M. G. Finn, *ChemBioChem* 2008, *9*, 1481.
(49) T. R. Chan, R. Hilgraf, K. B. Sharpless, V. V. Fokin, *Org. Lett*, 2004, *6*, 2853.
(50) J. P. Collman, N. K. Devaraj, T. P. A. Eberspacher, C. E. D. Chidsey, *Langmuir* 2006, *22*, 2457.
(51) J. P. Collman, N. K. Devaraj, C. E. D. Chidsey, *Langmuir* 2004, *20*, 1051.
(52) N. K. Devaraj, P. H. Dinolfo, C. E. D. Chidsey, J. P. Collman *J. Am. Chem. Soc.* 2006, *128*, 1794.
(53) S. Y. Ku, K. T. Wong, A. J. Bard, *J. Am. Chem. Soc.* 2008, *130*, 2392.
(54) J. K. Lee, Y. S. Chi, I. S. Choi, *Langmuir* 2004, *20*, 3844.
(55) X.-L. Sun, C. L. Stabler, C. S. Cazalis, E. L. Chaikof, *Bioconjugate Chem.* 2005, *17*, 52.
(56) D. I. Rozkiewicz, D. Janczewski, W. Verboom, B. J. Ravoo, D. N. Reinhoudt, *Angew. Chem. Int. Ed.* 2006, *45*, 5292.
(57) J. M. Spruell, B. A. Sheriff, D. I. Rozkiewicz, W. R. Dichtel, R. D. Rohde, D. N. Reinhoudt, J. F. Stoddart, J. R. Heath, *Angew. Chem. Int. Ed.* 2008, *47*, 9927.
(58) K. Godula, D. Rabuka, K. T. Nam, C. R. Bertozzi, *Angew. Chem. Int. Ed.* 2009, *48*, 4973.
(59) O. Michel, B. J. Ravoo, *Langmuir* 2008, *24*, 12116.
(60) W. F. Paxton, J. M. Spruell, J. F. Stoddart, *J. Am. Chem. Soc.* 2009, *131*, 6692.
(61) N. J. Agard, J. A. Prescher, C. R. Bertozzi *J. Am. Chem. Soc.*, 2004, *126*, 15046.
(62) X. H. Ning, J. Guo, M. A. Wolfert, G. J. Boons, *Angew. Chem. Int. Ed.* 2008, *47*, 2253.
(63) J. C. Jewett, C. R. Bertozzi, *Chem. Soc. Rev.* 2010, *39*, 1272.
(64) J. M. Baskin, J. A. Prescher, S. T. Laughlin, N. J. Agard, P. V. Chang, I. A. Miller, A. Lo, J. A. Codelli, C. R. Bertozzi, *Proc. Natl. Acad. Sci.* 2007, *104*, 16793.
(65) A. Kuzmin, A. Poloukhtine, M. A. Wolfert, V. V. Popik, *Bioconjugate Chem.* 2010, *21*, 2076.
(66) S. V. Orski, A. A. Poloukhtine, S. Arumugam, L. Mao, V. V. Popik, J. Locklin, *J. Am. Chem. Soc.* 2010, *132*, 11024.
(67) C. Wendeln, I. Singh, S. Rinnen, C. Schulz, H. F. Arlinghaus, G. A. Burley, B. J. Ravoo, *Chem. Sci.* 2012, *3*, 2479.
(68) K. Blank, J. Morfill, H. E. Gaub, *ChemBioChem* 2006, *7*, 1349.
(69) B. T. Houseman, E. S. Gawalt, M. Mrksich, *Langmuir* 2002, *19*, 1522.
(70) J. Wetterö, T. Hellerstedt, P. Nygren, K. Broo, D. Aili, B. Liedberg, K.-E. Magnusson, *Langmuir* 2008, *24*, 6803.
(71) P. Jonkheijm, D. Weinrich, M. Koehn, H. Engelkamp, P. C. M. Christianen, J. Kuhlmann, J. C. Maan, D. Nuesse, H. Schroeder, R. Wacker, R. Breinbauer, C. M. Niemeyer, H. Waldmann, *Angew. Chem. Int. Ed.* 2008, *47*, 4421.
(72) J. Escorihuela, M. Jose Banuls, R. Puchades, A. Maquieira, *Chem. Commun.* 2012, *48*, 2116.
(73) C. Wendeln, S. Rinnen, C. Schulz, H. F. Arlinghaus, B. J. Ravoo, *Langmuir* 2010, *26*, 15966.
(74) C. Wendeln, S. Rinnen, C. Schulz, T. Kaufmann, H. F. Arlinghaus, B. J. Ravoo, *Chem. Eur. J.* 2012, *18*, 5880.

(75) M. N. Yousaf, M. Mrksich, *J. Am. Chem. Soc.* **1999**, *121*, 4286.
(76) M. N. Yousaf, E. W. L. Chan, M. Mrksich, *Angew. Chem. Int. Ed.* **2000**, *39*, 1943.
(77) E. W. L. Chan, M. N. Yousaf, M. Mrksich, *J. Phys. Chem. A* **2000**, *104*, 9315.
(78) Y. Kwon, M. Mrksich, *J. Am. Chem. Soc.* **2002**, *124*, 806.
(79) M. N. Yousaf, B. T. Houseman, M. Mrksich, *Proc. Natl. Acad. Sci.* **2001**, *98*, 5992.
(80) M. N. Yousaf, B. T. Houseman, M. Mrksich, *Angew. Chem. Int. Ed.* **2001**, *40*, 1093.
(81) B. T. Houseman, J. H. Huh, S. J. Kron, M. Mrksich, *Nat. Biotechnol.* **2002**, *20,* 270.
(82) W. S. Dillmore, M. N. Yousaf, M. Mrksich, *Langmuir* **2004**, *20*, 7223.
(83) C. Wendeln, A. Heile, H. F. Arlinghaus, B. J. Ravoo, *Langmuir* **2010**, *26*, 4933.
(84) T. Pauloehrl, G. Delaittre, V. Winkler, A. Welle, M. Bruns, H. G. Boerner, A. M. Greiner, M. Bastmeyer, C. Barner-Kowollik, *Angew. Chem. Int. Ed.* **2012**, *51*, 1071.
(85) S. Arumugam, V. V. Popik, *J. Am. Chem. Soc.* **2011**, *133*, 15730.
(86) D. I. Rozkiewicz, B. J. Ravoo, D. N. Reinhoudt, *Langmuir* **2005**, *21*, 6337.
(87) D. I. Rozkiewicz, Y. Kraan, M. W. T. Werten, F. A. de Wolf, V. Subramaniam, B. J. Ravoo, D. N. Reinhoudt, *Chem. Eur. J.* **2006**, *12*, 6290.
(88) T. Pauloehrl, G. Delaittre, M. Bruns, M. Meissler, H. G. Boerner, M. Bastmeyer, C. Barner-Kowollik, *Angew. Chem. Int. Ed.* **2012**, *51*, 9181.
(89) E. W. L. Chan, M. N. Yousaf, *J. Am. Chem. Soc.* **2006**, *128*, 15542.
(90) W. Luo, E. W. L. Chan, M. N. Yousaf, *J. Am. Chem. Soc.* **2010**, *132*, 2614.
(91) A. Pulsipher, M. N. Yousaf, *Chem. Commun.* **2011**, *47*, 523.
(92) M. Eun Jun, B. Roy, K. Han Ahn, *Chem. Commun.* **2011**, *47*, 7583.
(93) O. S. Wolfbeis, *J. Mater. Chem.* **2005**, *15*, 2657.
(94) H. Kobayashi, M. Ogawa, R. Alford, P. L. Choyke, Y. Urano, *Chem. Rev.* **2009**, *110*, 2620.
(95) X. Qian, Y. Xiao, Y. Xu, X. Guo, J. Qian, W. Zhu, *Chem. Commun.* **2010**, *46*, 6418.
(96) S. Y. Lim, W.-y. Chung, H. K. Lee, M. S. Park, H. G. Park, *Biochem. Biophys. Res. Commun.* **2008**, *376*, 633.
(97) C. M. Salisbury, D. J. Maly, J. A. Ellman, *J. Am. Chem. Soc.* **2002**, *124*, 14868.
(98) Q. Zhu, M. Uttamchandani, D. Li, M. L. Lesaicherre, S. Q. Yao, *Org. Lett.* **2003**, *5*, 1257.
(99) F. A. Scaramuzzo, A. Gonzalez-Campo, C.-C. Wu, A. H. Velders, V. Subramaniam, G. Doddi, P. Mencarelli, M. Barteri, P. Jonkheijm, J. Huskens, *Chem. Commun.* **2010**, *46*, 4193.
(100) A. Gonzalez-Campo, S. H. Hsu, L. Puig, J. Huskens, D. N. Reinhoudt, A. H. Velders, *J. Am. Chem. Soc.* **2010**, *132*, 11434.
(101) R. B. van Dover, L. F. Schneemeyer, R. M. Fleming, *Nature* **1998**, *392*, 162.
(102) S. Suresh, *Science* **2001**, *292*, 2447.
(103) J. Genzer, D. A. Fischer and K. Efimenko, *Appl. Phys. Lett.* **2003**, *82*, 266.
(104) C. M. Stafford, C. Harrison, K. L. Beers, A. Karim, E. J. Amis, M. R. VanLandingham, H.-C. Kim, W. Volksen, R. D. Miller, E. E. Simonyi, *Nat. Mater.* **2004**, *3*, 545.
(105) D. Julthongpiput, M. J. Fasolka, W. Zhang, T. Nguyen, E. J. Amis, *Nano Lett.* **2005**, *5*, 1535.
(106) H. Elwing, S. Welin, A. Askendal, U. Nilsson, I. Lundstrom, *J. Colloid Interface Sci.* **1987**, *119*, 203.
(107) K. Efimenko, J. Genzer, *Adv. Mater.* **2001**, *13*, 1560.
(108) R. R. Bhat, D. A. Fischer, J. Genzer, *Langmuir* **2002**, *18*, 5640.

(109) B. Liedberg, P. Tengvall, *Langmuir*, 1995, *11*, 3821.
(110) R. H. Terrill, K. M. Balss, Y. M. Zhang, P. W. Bohn, *J. Am. Chem. Soc.* 2000, *122*, 988.
(111) S. T. Plummer, P. W. Bohn, *Langmuir* 2002, *18*, 4142.
(112) S. T. Plummer, Q. Wang, P. W. Bohn, R. Stockton, M. A. Schwartz, *Langmuir* 2003, *19*, 7528.
(113) X. J. Wang, P. W. Bohn, *J. Am. Chem. Soc.* 2004, *126*, 6825.
(114) X. J. Wang, P. W. Bohn, *Adv. Mater.* 2007, *19*, 515.
(115) C. Ulrich, O. Andersson, L. Nyholm, F. Bjorefors, *Angew. Chem. Int. Ed.* 2008, *47*, 3034.
(116) R. R. Fuierer, R. L. Carroll, D. L. Feldheim, C. B. Gorman, *Adv. Mater.* 2002, *14*, 154.
(117) T. Kraus, R. Stutz, T. E. Balmer, H. Schmid, L. Malaquin, N. D. Spencer, H. Wolf, *Langmuir* 2005, *21*, 7796.
(118) S. H. Choi, B. M. Z. Newby, *Langmuir* 2003, *19*, 7427.
(119) M. Geissler, P. Chalsani, N. S. Cameron, T. Veres, *Small* 2006, *2*, 760.
(120) B. M. Lamb, S. Park, M. N. Yousaf, *Langmuir* 2010, *26*, 12817.
(121) P. Burgos, M. Geoghegan, G. J. Leggett, *Nano Lett.* 2007, *7*, 3747.
(122) P. Burgos, Z. Zhang, R. Golestanian, G. J. Leggett, M. Geoghegan, *ACS Nano* 2009, *3*, 3235.
(123) R. Walder, A. Honciuc, D. K. Schwartz, *Langmuir* 2010, *26*, 1501.
(124) S. Meyyappan, M. R. Shadnam, A. Amirfazli, *Langmuir* 2008, *24*, 2892.
(125) N. Blondiaux, S. Zurcher, M. Liley, N. D. Spencer, *Langmuir* 2007, *23*, 3489.
(126) N. Ballav, A. Shaporenko, A. Terfort, M. Zharnikov, *Adv. Mater.* 2007, *19*, 998.
(127) T. Winkler, N. Ballav, H. Thomas, M. Zharnikov, A. Terfort, *Angew. Chem. Int. Ed.* 2008, *47*, 7238.
(128) S. M. Morgenthaler, S. Lee, N. D. Spencer, *Langmuir* 2006, *22*, 2706.
(129) E. Beurer, N. V. Venkataraman, A. Rossi, F. Bachmann, R. Engeli, N. D. Spencer, *Langmuir* 2010, *26*, 8392.
(130) T. Chang, D. I. Rozkiewicz, B. J. Ravoo, E. W. Meijer, D. N. Reinhoudt, *Nano Lett.* 2007, *7*, 978.
(131) E.-J. Lee, E. W. L. Chan, M. N. Yousaf, *ChemBioChem* 2009, *10*, 1648.
(132) E. W. L. Chan, M. N. Yousaf, *Mol. Biosys.* 2008, *4*, 746.
(133) Y. Ito, M. Heydari, A. Hashimoto, T. Konno, A. Hirasawa, S. Hori, K. Kurita, A. Nakajima, *Langmuir* 2007, *23*, 1845.
(134) N. D. Gallant, K. A. Lavery, E. J. Amis, M. L. Becker, *Adv. Mater.* 2007, *19*, 965.
(135) T. S. Hansen, J. U. Lind, A. E. Daugaard, S. Hvilsted, T. L. Andresen, N. B. Larsen, *Langmuir* 2010, *26*, 16171.
(136) N. Shida, Y. Ishiguro, M. Atobe, T. Fuchigami, S. Inagi, *ACS Macro Lett.* 2012, *1*, 656.
(137) B. Li, B. Yu, W. T. S. Huck, W. Liu, F. Zhou, *J. Am. Chem. Soc.* 2013, *135*, 1708.
(138) A. Perl, A. Gomez-Casado, D. Thompson, H. H. Dam, P. Jonkheijm, D. N. Reinhoudt, J. Huskens, *Nat. Chem.* 2011, *3*, 317
(139) L. Tauk, A. P. Schroeder, G. Decher, N. Giuseppone, *Nat. Chem.* 2009, *1*, 649..

Chapter 3

"If you're not prepared to be wrong, you'll never come up with anything original."
— Ken Robinson, How schools kill creativity, TED Talks.

A fluorogenic reactive monolayer platform for the signaled immobilization of thiols*

A thiol-sensitive fluorogenic reactive platform has been developed by "clicking" an orthogonally modified coumarin onto an azide monolayer on glass. Fluorescent signaling reports the immobilization of thiols in a second "click" step. The platform's effectiveness, in terms of selectivity and ease of identifying the place of functionalization, was demonstrated for supramolecular and biomolecular applications.

*Parts of this chapter have been published in: C. Nicosia, J. Cabanas-Danés, P. Jonkheijm, J. Huskens, *ChemBioChem* **2012**, 13, 778–782; J. Cabanas-Danés, C. Nicosia, E. Landman, M. Karperien, J. Huskens, P. Jonkheijm, *J. Mater. Chem. B* **2013**, *1*, 1903-1908.

3.1 Introduction

The overwhelming majority of reactions and interactions in biology does not occur in solution, but at interfaces. Therefore, the study of how surfaces play a role in the control of biological interactions poses a great challenge. The interface between a cell and a synthetic biomaterial, among others, is of particular interest owing to its high impact in the design of novel biomaterials for tissue engineering and biomedical applications.[1]

A key aspect of the interfacing of biological material with an artificial substrate is the surface chemistry. This has led to the development of various types of surface chemistries, often in the form of reactive monolayers, allowing the controlled immobilization of biomolecules while paying attention to the control over orientation, the retention of biological activity, the selectivity and specificity of the biological interaction, etc.[2] The fabrication of fluorogenic monolayers on surfaces aims for the fast, simple, sensitive and non-destructive detection of the immobilization products by fluorescence microscopy. For example, reporter monolayers for immobilization of amine-terminated (bio)molecules,[3] for microarrays fabrication[4] and for orthogonal surface modification[5] have been published. This methodology allows a faster and cheaper surface imaging and avoids the use of other techniques such as X-ray photoelectron spectroscopy (XPS), time-of-flight secondary ion mass spectrometry (ToF SIMS) and scanning probe microscopy (SPM), while preserving a high spatial resolution.

The important role that thiols play in nature has encouraged scientists to develop molecular probes for their sensing and quantification in biological systems.[6] For this reason, there are several recent examples of fluorescent or colorimetric sensors for the detection of thiols in solution. However, to our knowledge, no examples exist in the area of surface platforms for biological applications. Developing a platform chemistry for thiols has a high potential for reasons of selectivity and orthogonality of immobilization, the controlled orientation of appropriately bioengineered (e.g. cysteine-modified) peptides and proteins, etc.

Maleimide chemistry, owing to its highly selectivity with thiols under physiological conditions, is frequently employed for the surface immobilization of biomolecules.[2, 7] Therefore, this reaction is a good candidate for the design of rapid methods to visualize the in situ covalent binding of thiols on surfaces with applications in bioconjugation, bioassays, and materials science.

Here we report a strategy for the simultaneous anchoring and detection of molecular and biomolecular thiols in a fast manner by using a fluorogenic reactive monolayer on glass (Scheme 3.1A). This monolayer acts as a molecular construction platform in which the

fluorogenic response upon immobilization provides a useful function for spatial identification and coverage assessment of the thiol immobilization step.

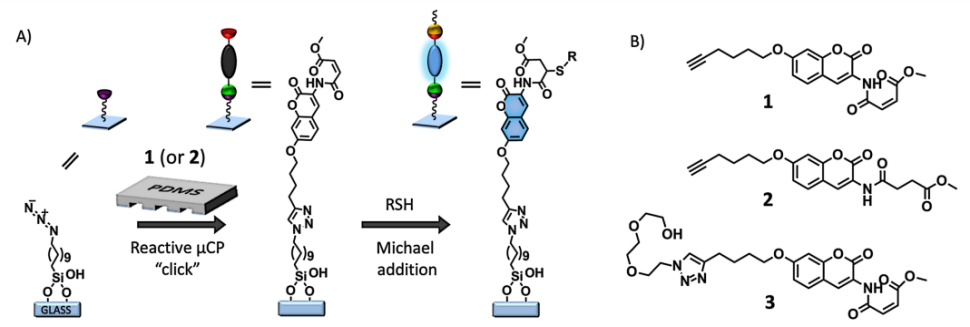

Scheme 3.1. A) Schematic procedure of the surface functionalization by printing **1** (or **2**) via "click" chemistry onto an azide monolayer. The printing of **1** is followed by the covalent immobilization and detection of thiols by means of the fluorogenic Michael addition to the methyl-4-oxo-2-butenoate moiety. B) Chemical structures of the compounds employed for the surface immobilization (**1** and **2**) and for the characterization in solution (**3**).

We show its potential in three applications: (i) the co-localization of a dye via supramolecular host-guest chemistry on signaled and pre-immobilized thiol-functionalized cyclodextrin; (ii) the co-localization of mouse myoblast cells on fluorescently visualized regions with a pre-immobilized RGD peptide, and (iii) cell differentiation by means of specific binding and delivery of growth factors. The fluorogenic probe consists of a coumarin unit equipped with an alkyne moiety that allows its directed immobilization on an azide monolayer on glass by reactive microcontact printing (µCP) via the Huisgen 1,3-dipolar cycloaddition.[8] We incorporate a methyl-4-oxo-2-butenoate group next to the coumarin unit (compound **1** in Scheme 3.1B) for the binding of thiols via a Michael addition. Yi et al.[6a] have recently reported a similar dye for the detection of thiols in solution. The carbon-carbon double bond of the methyl-4-oxo-2-butenoate group quenches the intrinsic fluorescence of the coumarin unit by photoinduced electron transfer (PeT). Upon nucleophilic addition of thiols to the unsaturated system the quenching disappears and the strong fluorescence of the coumarin unit is restored.

3.2 Results and discussion

3.2.1 Synthesis

A fluorogenic coumarin **1** with alkyne and methyl-4-oxo-2-butenoate groups at the 7- and 3-positions was synthesized (Scheme 3.2). The double functionalization allows the immobilization of the coumarin on an azide monolayer through "click chemistry" and the consecutive immobilization of thiols via Michael addition.

3-Amino-7-hydroxycoumarin[9] in dry DMF was stirred with NaH at 0 °C for 1 h, and reacted overnight at room temperature with 6-chloro-1-hexyne to give **5**. The reaction of the amino group with maleic or succinic anhydride in acetone under reflux and the further acid-catalyzed esterification gave compounds **1** or **2**, respectively. The water soluble compound **3** was synthesized by means of the Cu(I) alkyne-azide cycloaddition between compound **2** and azido-tri(ethylene glycol). The further reaction of **3** with β-mercaptoethanol in the presence of a base yielded quantitatively the highly fluorescent compound **4**.
While compounds **1** and **2** were used for surface immobilization, compounds **3** and **4** were employed for the photophysical characterization in solution.

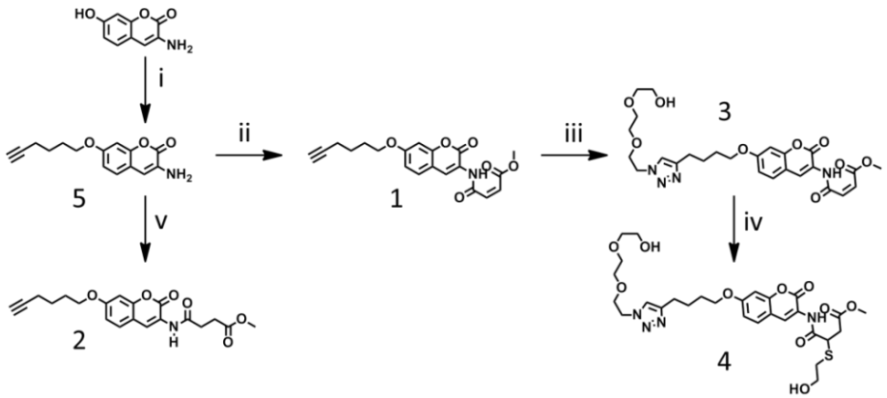

Scheme 3.2. i) NaH, 6-chloro-1-hexyne, DMF, r.t, o.n. ii) a) maleic anhydride, acetone, reflux, o.n. b) TsOH, MeOH, reflux, o.n., iii) azido-tri(ethylene glycol), $Cu(CN)_4PF_6$, TBTA, MeOH/DCM, r.t., o.n. iv) β-mercaptoethanol, MeOH, r.t., o.n. v) a) succinic anhydride, acetone, reflux, o.n. b) TsOH, MeOH, reflux, o.n.

3.2.2 Photophysical properties and reactivity in solution

To study the effect of the alkylation of the oxydryl group in position 7 of the coumarin, which is required for the surface immobilization, on the fluorescent properties of the probe, compound **1** was first reacted with azido-tri(ethylene glycol) to prepare the water soluble compound **3**. The spectroscopic characterization of compound **3** before and after the reaction with thiols shows that the fluorescence properties were not affected by the alkylation and they are independent from the pH of the solution (Figure 3.1A). The quantum yield (ϕ) before (0.01) and after (0.42) the reaction of **3** with β-mercaptoethanol shows more than a 40-fold increase, illustrating the excellent reporting properties of the probe for thiols (Table 3.1).

Disulfide bonds play an important role in the folding and stability of some proteins and since they can be reversibly reduced and re-oxidized, the redox state of these bonds has evolved into a signalling element.[10] The reaction of the probe in the presence of an excess of L-cysteine or L-cystine (Figure 3.1B) shows the bioselectivity towards thiols in the

presence of disulfide. The result is the 20-fold fluorescence enhancement in the presence of L-cysteine in comparison with L-cystine.

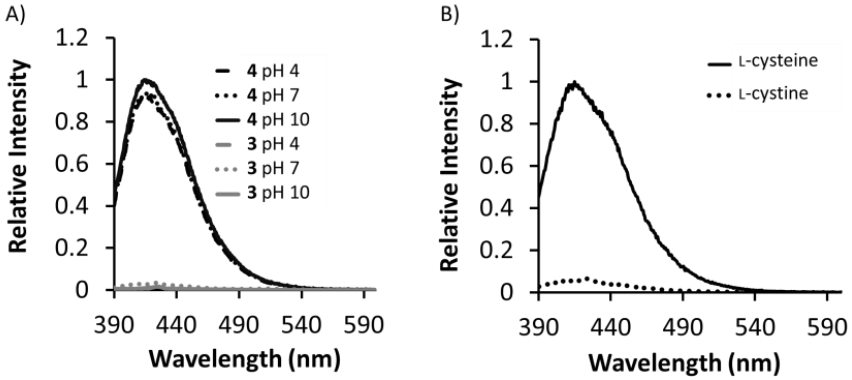

Figure 3.1. A) Fluorescence spectra of 2 µM of compounds **3** (grey lines) and **4** (black lines) at different pHs. B) Fluorescence spectra of 2 µM of compound **3** in the presence of 500 equiv of L-cysteine (solid lines) or 500 equiv of L-cystine (dashed lines).

Compound	ε (λ = 345 nm)	$\lambda_{em,max}$ (nm)	Φ (in air)
3	18000	412	0.01
4	19500	420	0.42

Table 3.1. Absorption coefficient (ε), maximum emission wavelength ($\lambda_{em\ max}$) and quantum yield (Φ) of compounds **3** and **4** in water (50 mM buffer pH 7) (anthracene was used as reference compound for the calculation of the quantum yield; Φ (ethanol) = 0.21 in air).

The reaction kinetics of the addition of cysteine to **3** in solution was monitored by fluorescence spectroscopy. Kinetic studies were performed at different pHs under pseudo-first order conditions (0.2 µM of **3** and 0.2 mM of L-cysteine). The observed rate constant (k_{obs}) at pH 4 (2.2×10^{-2} s^{-1}) is about 60 times higher than the one found at pH 10 (3.7×10^{-4} s^{-1}) while at pH 7.5 the reaction rate reached its maximum (Figure 3.2), as has been observed before for a similar derivative,[6a] making the system compatible for bio-applications. While the fluorescence spectra show a drastic change, moderate alterations are observed in the absorption spectra (Figure 3.3), in accordance with the mediated photo-induced electron transfer phenomena.

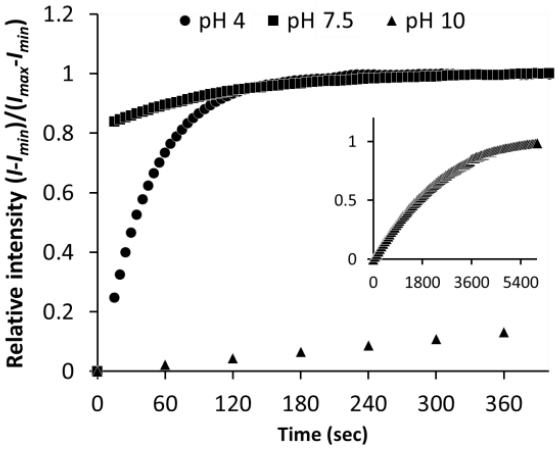

Figure 3.2. Time dependent curves for the reaction of 0.2 μM of **3** and 0.2 mM of L-cysteine at different pHs (λ_{exc}= 370 nm, λ_{em}= 410 nm) The inset shows the time dependent curve at pH 10.

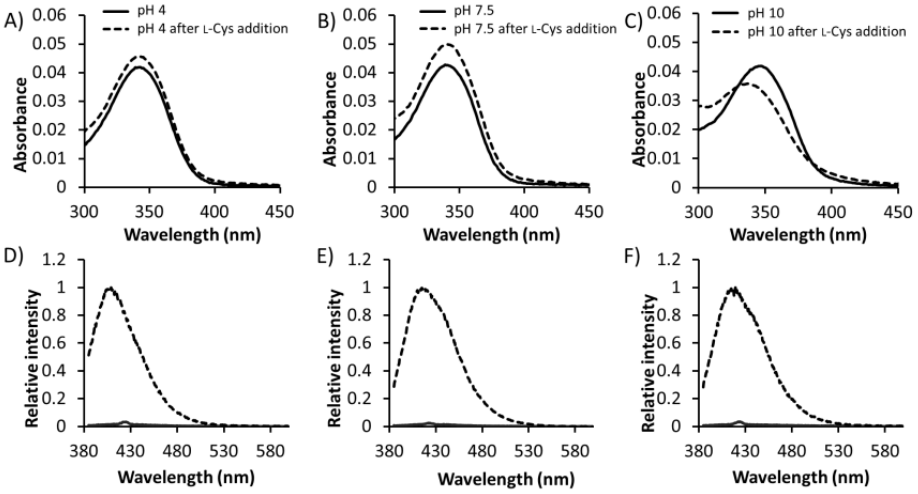

Figure 3.3. Absorption (A-C) and fluorescence spectra (λ_{exc}= 370 nm) (D-F) of a 0.2 μM of **3** at different pHs (50 mM buffer) before (solid line) and after (dashed line) addition of 1000 equiv of Cys.

Reactions between **3** and thiols were always performed with freshly prepared solutions of thiols to reduce the exposure time to air and the consequent undesired oxidation to the inert disulfide. Reducing agents, such as dithiothreitol (DTT) and tris-(2-carboxyethyl)phosphine hydrochloride (TCEP) could not be used because they compete with the Michael addition reaction. For instance, upon addition of TCEP to a solution of **3**, a strong and fast enhancement of fluorescence was observed (Figure 3.4).

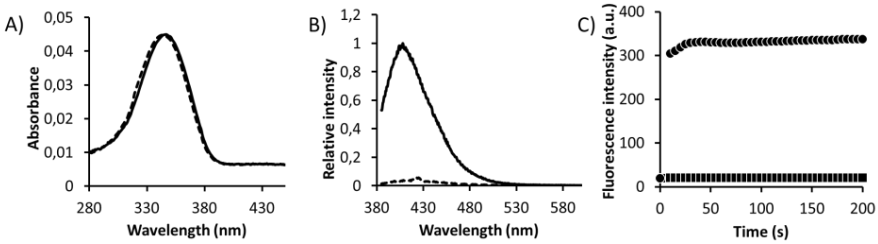

Figure 3.4 Absorption (A) and fluorescence (λ_{exc}= 370 nm) (B) spectra before (broken line) and after (line) addition of 100 equiv of TCEP to a 0.2 μM of **3** in a phosphate buffer solution at pH 7.5. C) Time dependent fluorescence curves upon reaction of 20 μM of TCEP with 0.2 μM of **3** in a phosphate buffer solution at pH 7.5.

3.2.3 Characterization and reactivity of the platform

Since **1** is weakly fluorescent, we initially performed reactive μCP via "click" chemistry using the methyl-4-oxobutanoate modified coumarin **2**. This modification does not affect PeT-mediated fluorescence of coumarin. The presence of an electron-withdrawing group at the 3-position and an electron-donating group at the 7-position ensures good optical properties.[11] An oxidized polydimethylsiloxane (PDMS) stamp was inked with a solution of **2**, Cu(I)$(CH_3CN)_4PF_6$ and tris[(1-benzyl-1*H*-1,2,3-triazol-4-yl)methyl]amine (TBTA), dried under nitrogen flow and brought into conformal contact for 1 h with a glass slide which was functionalized with an azide monolayer.[12] After stamp removal, the substrates were rinsed with acetonitrile, blown dry with nitrogen and imaged by fluorescence microscopy (Figure 3.5A). The same conditions described above for compound **2** were used for compound **1** allowing the preparation of the thiol-sensitive monolayer on glass. Owing to the PeT-mediated quenching, upon printing of compound **1** on an azide-modified glass slide, the fluorescence of the pattern is almost indistinguishable from the background (Figure 3.5B).

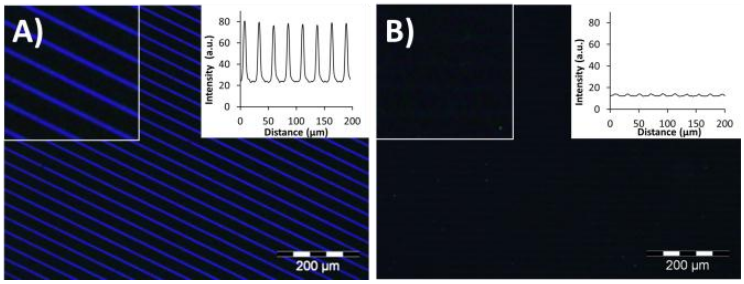

Figure 3.5. Fluorescence microscopy images (inserts show intensity profiles): A) after printing of **2** (5×20 μm lines) or B) **1** (5×15 μm lines) (1.5 mM coumarin **1** or **2** in CH_3CN, 0.5 mM Cu(I)$(CH_3CN)_4PF_6$ and 0.5 mM TBTA (CH_3CN/EtOH 2/1), 4 min inking, 1 h μCP (Images were recorded at an excitation wavelength of 350 nm and an emission wavelength of 420 nm (exposure time: 1000 ms).

For XPS characterization (Figure 3.6 and Table 3.2) compound **1** was printed using the above protocol on an azide-terminated silicon oxide slide using a flat PDMS stamp, thus

obtaining a full monolayer. The XP spectrum of the azide monolayer showed the characteristic peaks for N_{1s} at 405 eV (1N) and 401 eV (2N) indicating the presence of azide groups (Figure 3.6A), and the observed C/N ratio (4.5) is in reasonable agreement with the predicted value (3.7). The N_{1s} signal confirmed the triazole formation resulting from the reaction between the azide monolayer and the alkyne-modified coumarin **1**. Further evidence for the formation of the coumarin monolayer is the increased C/N ratio (observed 8.4, predicted 7.8) and the appearance of a peak at 289 eV in the C_{1s} spectrum owing to the introduction of carbonyl groups (Figure 3.6B).

Monolayer	C/N (exp)	C/N (calc)
Azide	4.5	3.7
Coumarin	8.4	7.8
CD-SH	13.3	-

Table 3.2. Atomic ratios of elements C and N from X-ray photoelectron spectroscopy of the monolayers.

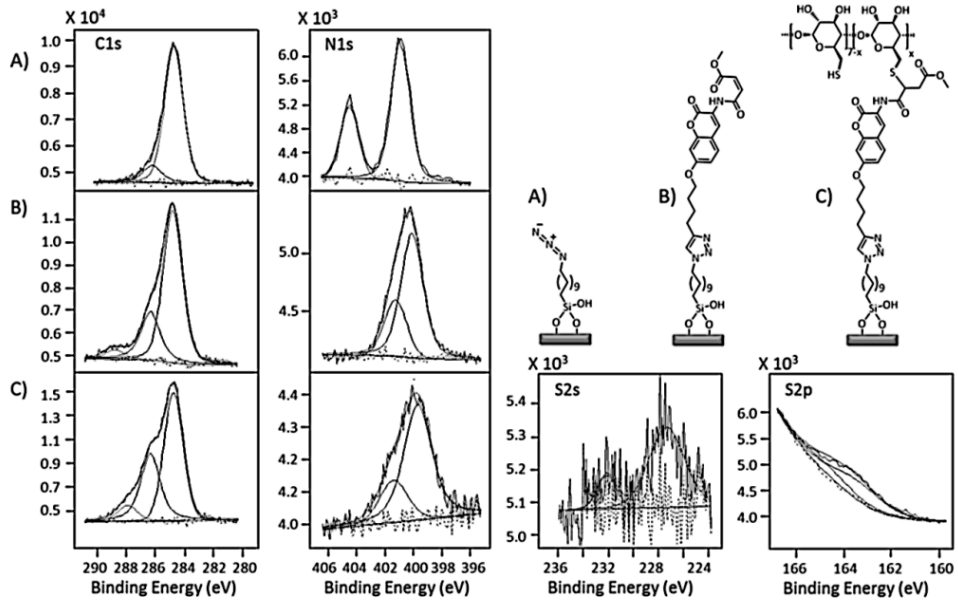

Figure 3.6. X-ray photoelectron spectra of the C_{1s}, N_{1s}, S_{2s} and S_{2p} regions for A) azide, B) coumarin and C) heptakis-thio-β-cyclodextrin (β-CD-$(SH)_7$) terminated monolayers.

Subsequently, the thiol-sensitive probe **1** was used as a reactive platform for the signaled immobilization of thiols. The selectivity for thiols was investigated by comparing the fluorescence change upon incubation of substrates patterned with compound **1** (Figure 3.5B) in a 10 mM cysteine or methionine or 1 mM cystine solution at pH 7.5.[13] After one

hour of incubation in the cysteine solution, the fluorescence intensity increased 20-fold (Figure 3.7A) reaching the saturation limit while after incubation in the methionine (Figure 3.7B) or the cystine solution (Figure 3.7C), the intensity remained unchanged. This confirms the selectivity of the platform for free thiols, showing in particular the ability of the platform of distinguish them from disulfide which is critical for the biological activity of the redox-active moiety. Moreover, for a fair comparison with L-cystine in which case, owing to its low solubility in water, it is not possible to work above 1 mM, we performed the reaction using only 1 mM of L-cysteine. In this case we observed a distinct enhancement of fluorescence, a clear indication of the high sensitivity of the platform (Figure 3.7D).

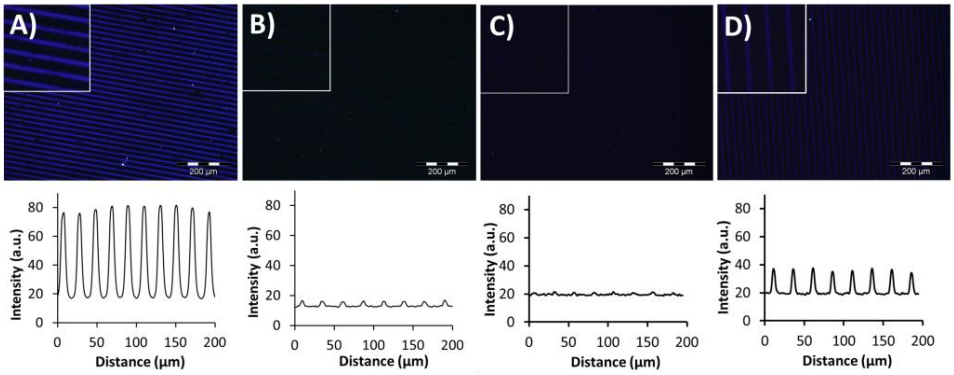

Figure 3.7. Fluorescence microscopy images (inserts show zoom-ins, intensity profiles are shown below): substrates patterned with **1** after incubation in a solution of: A) 10 mM cysteine (5×20 µm lines) or B) 10 mM methionine (5×20 µm lines) (pH 7.5) or C) 1 mM cystine (5×15 µm lines) or D) 1 mM cysteine (5×20 µm lines) for 1 h. Images were recorded at an excitation wavelength of 350 nm and an emission wavelength of 420 nm (exposure time: 1000 ms).

The pseudo-first order interfacial reaction between immobilized compound **1** and cysteine from a 10 mM solution (in 50 mM phosphate buffer at pH 7.5) was complete after 20 min incubation (Figure 3.8). This is however significantly slower than in solution: the pseudo-first order rate constant (k_{obs}) for the reaction on the surface ($4.2 \cdot 10^{-3}$ s^{-1}, Figure 3.8C) is about 5 orders of magnitude lower than the one obtained for a similar reaction in solution.[6a] Nevertheless, this difference does not hinder the practical use of the platform for sensing applications.

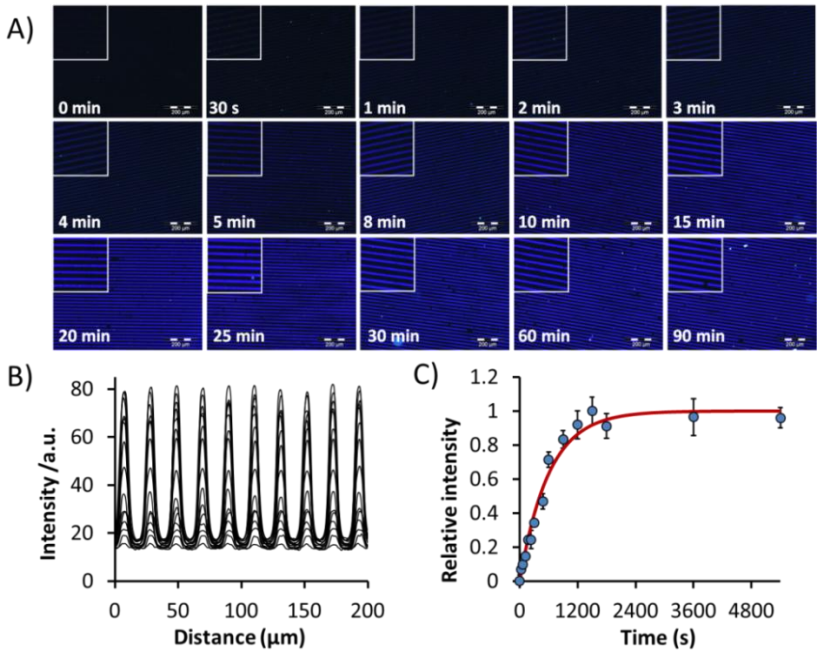

Figure 3.8. A) Fluorescence microscopy images after printing **1** (0 min) and after subsequent incubation in 10 mM cysteine solution at pH 7.5 (phosphate buffer) at different incubation times. (λ_{exc} = 350 nm, λ_{em} = 420 nm; exposure time: 1000 ms) B) Intensity profiles of the surface reaction between immobilized **1** and 10 mM cysteine solution at pH 7.5 at different incubation times. C) Time trace of the surface reaction between immobilized **1** and 10 mM cysteine solution at pH 7.5 (error bars represent a single standard deviation obtained from three different samples for each data point).

3.3 Supramolecular and biological applications

3.3.1 Co-localization via host-guest interactions

In order to show the versatility of the platform, we investigated both its supramolecular and biomolecular potential. In the first place, a supramolecular immobilization platform was created by reacting the substrate patterned with **1** with thiol-modified β-cyclodextrin (heptakis-thio-β-cyclodextrin, β-CD-$(SH)_7$) (Scheme 3.3), which yielded a 15-fold increase of the blue emission (Figure 3.9A). Upon β-CD immobilization on a full monolayer of **1**, XPS showed the expected increase of the C/N ratio (to 13.3) and the appearance of S_{2s} and S_{2p} signals (Figure 3.6C). Subsequently, the patterned β-CD monolayer was incubated for 5 min with a red fluorescent bisadamantyl guest (Scheme 3.3) showing the perfect co-localization of the fluorescent dye on the β-CD areas, which is attributed to the specific host-guest interactions between them (Figures 3.9C and 3.9D). This co-localization exemplifies the power of the use of the platform in signalling the success of multistep covalent/noncovalent micro/nano fabrication schemes.

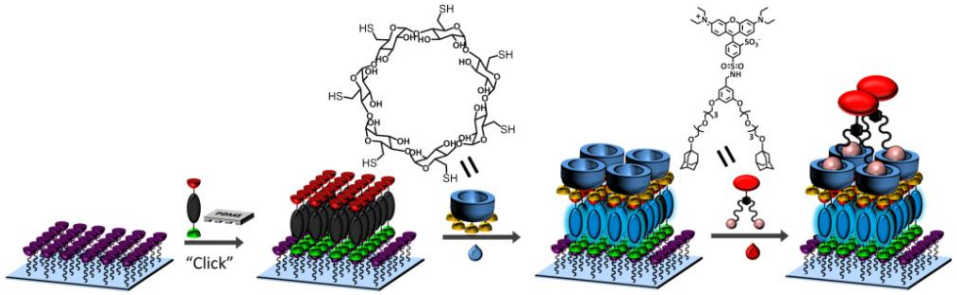

Scheme 3.3 Chemical structures of heptakis-thio-β-cyclodextrin (β-CD-$(SH)_7$) and the bis-adamantyl-functionalized rhodamine dye, and the schematic procedure of the surface functionalization by printing **1** via "click" chemistry on an azide monolayer, followed by covalent immobilization of β-CD-$(SH)_7$ which is reported by the fluorogenic reaction, and subsequent noncovalent guest dye immobilization with co-localization of the dye and the β-CD receptor areas.

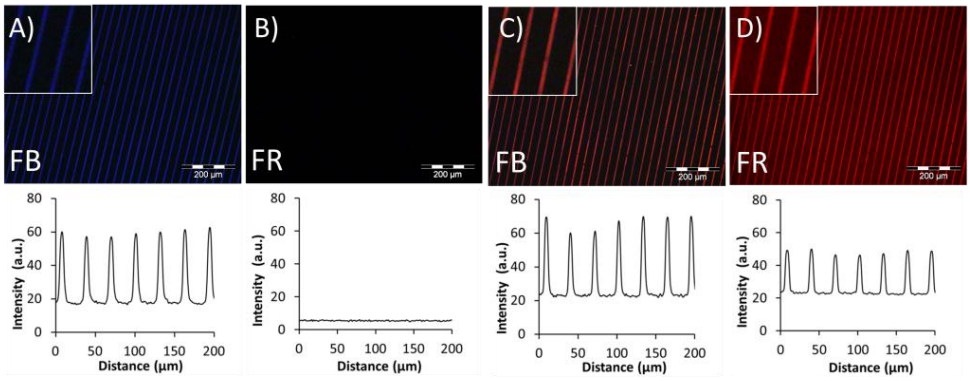

Figure 3.9. Fluorescence microscopy images (inserts show intensity profiles): A, B) after incubation of the substrate printed with **1** in 1 mM β-CD-$(SH)_7$ DMSO/phosphate buffer pH 7.5 = 3/1 (5×25 µm lines) and C, D) after subsequent incubation in an aqueous 10 µM bis-adamantyl-functionalized rhodamine dye solution (owing to the use of an open UV filter (FB) the image D is affected by the red fluorescence of the rhodamine dye). FB and FR refer to the filter sets used for imaging: FB: λ_{exc} = 350 nm, λ_{em} = 420 nm FR: λ_{exc} = 510-550 nm, λ_{em} = 590 nm (exposure time: 1000 ms).

3.3.2 Immobilization of peptides for localized cell adhesion

The visualization of the position of the surface modification is important for cell adhesion and migration experiments allowing the direct study of specific interactions in space. The patterning of mouse myoblast (C2C12) cells on a platform functionalized with a cell adhesion-promoting peptide has been investigated as a model for biological applications. We demonstrate here that surfaces patterned with **1** are useful for the fast and unequivocal covalent immobilization of cysteine-functionalized peptides while preserving their function and show the co-localization of the bound peptide and cells immobilized onto the peptide layer. Fibronectin has been used for several decades as the main cell adhesive protein. Its primary sequence motif for integrin binding is the tripeptide,

Arg-Gly-Asp (RGD).[14] Therefore the sequence Cys-Gly-Arg-Gly-Asp-Ser (Cys-GRGDS)[15] as well as the control sequence Met-Gly-Arg-Gly-Asp-Ser (Met-GRGDS) lacking a reactive SH group, were synthesized and tested on the signalling platform.

As shown in the schematic procedure (Scheme 3.4), **1** was immobilized by µCP in patterns of 100 µm wide lines separated by 100 µm gaps and the patterned surface was incubated in a 10 mM Cys-GRGDS or Met-GRGDS solution for 1 h. Only the sample treated with the cysteine-modified RGD showed a strong enhancement of fluorescence (Figure 3.10A) while the intensity remained unchanged in the case of the methionine-modified RGD (Figure 3.10B).

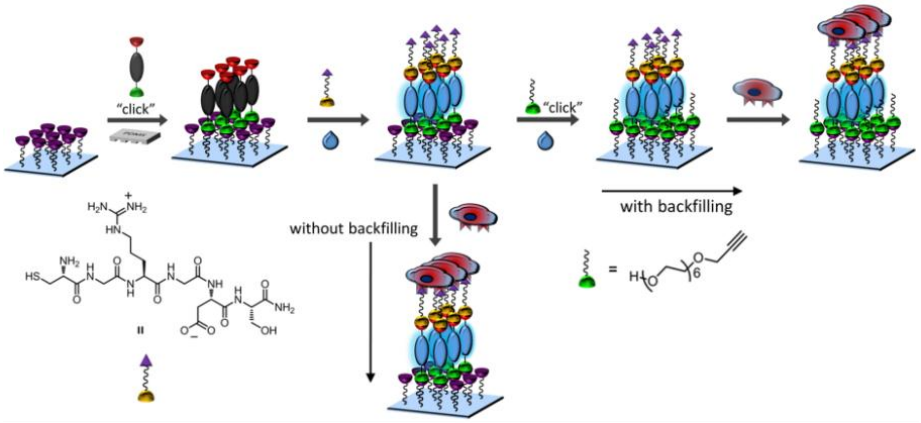

Scheme 3.4. Schematic procedure of the surface functionalization by reactive µCP of **1** on an azide monolayer, followed by immobilization of Cys-GRGDS reported by the fluorogenic reaction, and subsequent cell patterning experiments with or without backfilling with propargyl hexa(ethylene glycol).

Cell adhesion experiments, using mouse myoblast cells (C2C12), were carried out on Cys-GRGDS-patterned surfaces, with or without backfilling. Backfilling of the remaining unfunctionalized azide areas was achieved by "click" reaction with propargylhexa(ethylene glycol). We observed in both cases the co-localization of cells on top of the blue fluorescent pattern at which a high density of the RGD peptide is present. We found that when the samples were not backfilled, cells partially spread onto areas which were not functionalized with RGD (Figures 3.10C, D and G). Backfilling with hexa(ethylene glycol), however, led to significant increase of the selectivity and clear localization of the cells on the RGD patterns (Figures 3.10E, F and H).

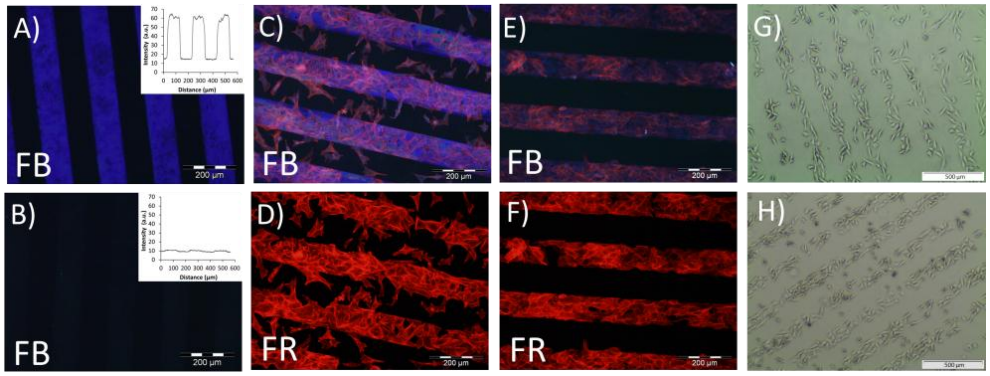

Figure 3.10. Fluorescence microscopy images: A) after incubation of the substrate printed with **1** in 10 mM Cys-GRGDS solution or B) 10 mM Met-GRGDS; C, D) after subsequent incubation of the Cys-GRGDS-modified substrate with C2C12 (mouse myoblast) cells at a density of 50000 cells/cm^2 and cultured at 37°C in a humidified 5% CO_2 atmosphere for 6 h; E, F) after incubation of a backfilled substrate with C2C12 cells under the same conditions. Bright field microscopy images after 4 h incubation of a substrate without G) and with H) backfilling. The red fluorescence in images D) and F) comes from the actin filaments staining with phalloidin. FB and FR refer to the filter sets used for imaging: FB: λ_{exc} = 350 nm, λ_{em} = 420 nm FR: λ_{exc}= 510-550 nm, λ_{em}= 590 nm.

3.3.3 Detected immobilization of peptides for binding of growth factors

Employing peptides with specific targeting and regenerative properties is an effective strategy to induce the desired biological function. The self-reporting fluorogenic reactive monolayer was employed to immobilize a peptide (Cys-Leu-Pro-Leu-Gly-Asn-Ser-His, Cys-LPLGNSH, **6**) for the delivery of growth factors TGF-β1, which maintains articular cartilage cells in its differentiated phenotype[16] while inducing chondrogenic differentiation in bone marrow mesenchymal progenitor cells (Scheme 3.5).[17] As control for assessing the specificity of binding of the protein to the immobilized peptide, a scrambled peptide was synthesized (Cys-HNLGLPS, **7**).

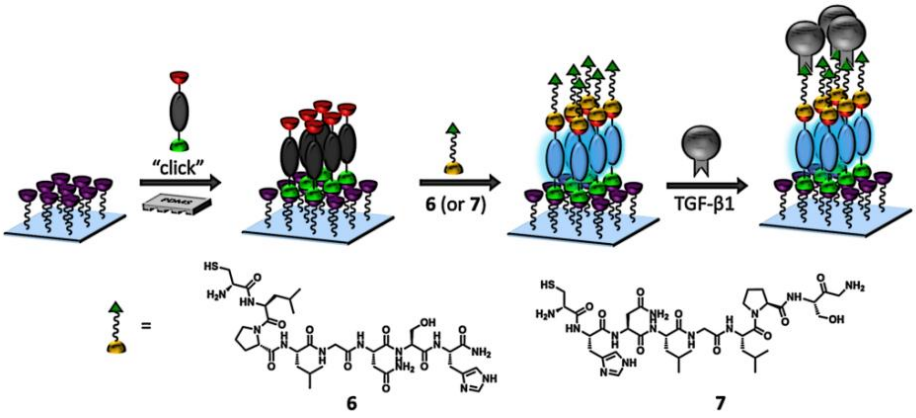

Scheme 3.5. Schematic procedure of the surface functionalization by reactive μCP of **1** on an azide monolayer, followed by reported immobilization of **6** (or **7**) and subsequent binding of TGF-β1.

Incubating fluorogenic platforms with a solution of **6** or **7** led to a strong enhancement of fluorescence (Figure 3.11A and 3.11D respectively) indicating the successful immobilization of the peptides.

After incubation of platforms functionalized with **6** in a solution containing TGF-β1 (1 µg/mL) in PBS for 1 h, an immunofluorescence assay was performed to visualize the binding of TGF-β1 to the immobilized peptide. First a primary antibody was incubated for 1 h followed by an incubation of a secondary antibody labeled with Alexa Fluor® 546 for 1 h. After rinsing, the substrates were analyzed using fluorescence microscopy showing clearly red fluorescent patterns that coincide with the coumarin patterns (Figure 3.11B and C). When this assay was performed on substrates functionalized with a scrambled peptide sequence (**7**) (Figure 3.11D), no red fluorescent patterns could be discerned (Figure 3.11E) while the blue fluorescence was retained (Figure 3.11F).

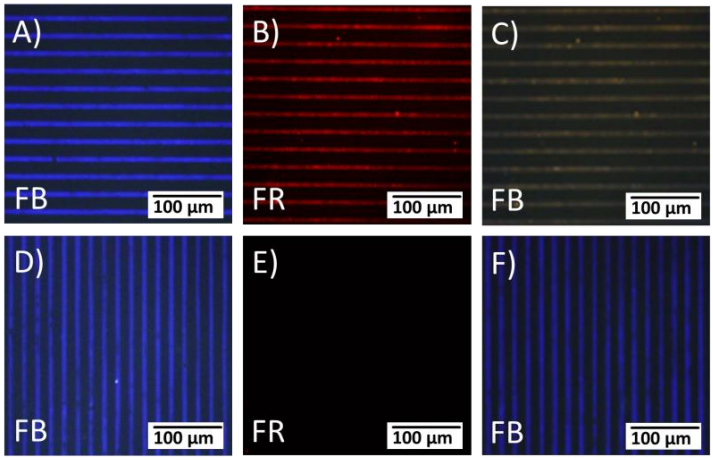

Figure 3.11. Fluorescence microscopy images: after 1 h incubation of the substrate printed with **1** in 10 mM Cys-LPLGNSH, **6** solution A) or Cys-HNLGLPS, **7** D); B), C), E), F) after 1 h incubation of the previous substrates with 1 µg/mL TGF-β1 and immunofluorescence staining (red). FB and FR refer to the filter sets used for imaging: FB: λ_{exc} = 350 nm, λ_{em} = 420 nm FR: λ_{exc} = 510-550 nm, λ_{em} = 590 nm.

To demonstrate the biological activity of bound TGF-β1, a platform was fabricated that consisted of a full layer of **6**. After printing **1** on an azide-terminated SAM using a flat featureless PDMS stamp (Figure 3.12A), the fluorogenic surface was incubated with either a solution containing **6** or **7**. The increase in the fluorescence intensity (Figure 3.12B and C) indicates that the peptides were successfully immobilized. These platforms were then incubated with TGF-β1 (100 ng) and used for culturing human articular chondrocytes (HACs) for one week and the cellular morphology was analyzed (Figure 3.12D-J). After 7 days, cells cultured in absence of TGF-β1 exhibited an elongated morphology, which

resembles a fibroblast-like phenotype (Figure 3.12D-G).[18] Although a similar spreading behavior was observed irrespective of the surface in the absence of TGF-β1, higher numbers of adhered cells were observed on surfaces functionalized with **1** (Figure 3.12E) or peptide (Figure 3.12F and G) when compared to the bare azide-SAM (Figure 3.12D). In contrast, those cultured in the presence of TGF-β1, either bound (Figure 3.12I and J) or supplemented in the culture medium (Figure 3.12H), showed a more round to polygonal morphology, which resembles chondrocyte-like phenotypes. In addition, the presence of pre-chondrogenic cell condensations was observed as an early skeletogenesis event, common in cultures supplemented with TGF-β1.[19] These cellular condensations ranged in size and number being maximized for cells cultured on platforms of **6** with bound TGF-β1 (Figure 3.12I), followed by cells seeded on a glass slide with TGF-β1 (100 ng) supplemented in the medium (Figure 3.12H) while cells seeded on a platform of **7** pre-loaded with 100 ng of growth factor showed the fewest and smallest cell condensations of them all (Figure 3.12J).

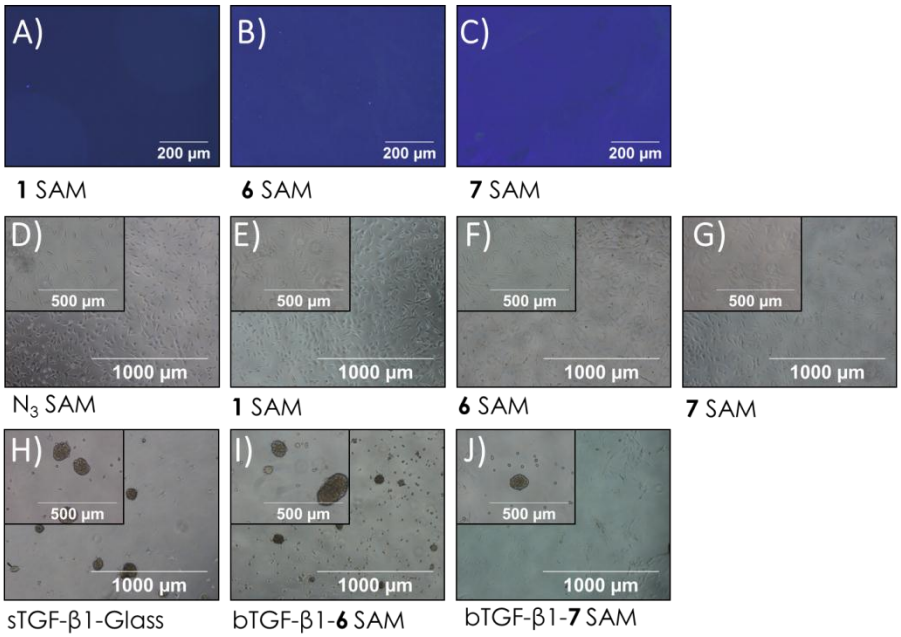

Figure 3.12 A-C) Fluorescence images corresponding to the functionalization of an azide-terminated SAM with **1** using a flat PDMS stamp and after incubation with **6** and **7**. D-J) HACs morphology after 7 days on the different functionalized substrates by bright field microscopy. sTGF-β1 refers to soluble (s) growth facor while bTGF-β1 indicates bound (b) protein.

These results not only show again that platforms of surface-bound **6** are useful for the binding with TGF-β1 but also that the growth factor remains active and is readily accessible for interacting with specific cellular receptors. When comparing to the case in which the

same amount of TGF-β1 was delivered in solution (Figure 3.12H), the observed stimulation in the case of TGF-β1 bound to **6** was enhanced (Figure 3.12I). This could be related to a higher local concentration of growth factor at the surface. The enhanced stimulation led to larger sizes and higher quantities of cell condensations. These observations were in agreement with the observations made on platforms with immobilized **7**. In this case reduced sizes and quantities of pre-chondrogenic cell condensations were observed when compared to those with bound **6**. This indicates that the presence of TFG-β1 was important and confirms the specific binding between peptide **6** and TGF-β1.

3.4 Conclusions

In conclusion, we have developed a highly sensitive and selective fluorogenic platform for the immobilization of thiols under physiological conditions. The strong fluorescence intensity enhancement upon the interfacial Michael addition of thiols is a unique feature of the system which allows the easy identification of the place of functionalization as well as the selectivity. We have attested the versatility of the platform in different examples: the fabrication of a supramolecular platform and the immobilization of peptides for cell adhesion studies and cell differentiation by means of growth factor delivery. In all cases clear co-localization was observed. Owing to the simplicity, sensitivity and biocompatible working conditions of the platform, we believe that this system will find many applications for a fast and selective covalent binding of relevant thiols and for the direct attachment of proteins.

3.5 Acknowledgments

Dr. Jordi Cabanas-Danés is gratefully acknowledged for the synthesis of all peptides, for the cell adhesion experiments, and for the immobilization and assessment of biological activity of bound growth factors.

3.6 Experimental section

3.6.1 Materials

The following materials and chemicals were used as received without further purification: 11-bromoundecyltrichlorosilane (ABCR), sodium azide (Acros), sodium hydride (Aldrich), 6-chloro-1-hexyne (Aldrich), maleic anhydride (Aldrich), succinic anhydride (Aldrich), p-toluenesulfonic acid monohydrate (Fluka), β-mercaptoethanol (Acros), L-cysteine (Sigma), L-methionine (Aldrich). 3-Amino-7-hydroxycoumarin,[11,6a] tris-(benzyltriazolylmethyl)amine (TBTA),[20] red fluorescent bisadamantyl guest,[21] heptakis-thio-β-cyclodextrins (β-CD-SH_7),[22] propargylhexaethyleneglycol[23] were prepared as described in literature .

3.6.2 Synthetic procedures

Synthesis of 5

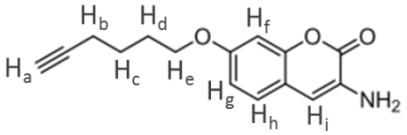

Under N_2, 3-amino-7-hydroxycoumarin (0.19g, 1.1 mmol) was dissolved in dry DMF (10 mL). At 0 °C, NaH (60 % in mineral oil, 43 mg) was added and the solution was allowed to stir for 1 h, while warming to room temperature. Subsequently, a solution of 6-chloro1-hexyne (143 µL, 1.18 mmol) in dry DMF (5 mL) was added dropwise. After stirring over night at room temperature, brine (30 mL) was added and the mixture was extracted with Et_2O (5 x 30 mL). The combined organic phases were washed with brine, dried (Na_2SO_4) and concentrated under reduced pressure. Flash column chromatography (SiO_2, CH_2Cl_2/MeOH 99:1, Rf=0.65) gave hexynyl amino coumarin **5** as a yellowish powder. (Yield: 90 mg, 37 %)

^{1}H NMR (300 MHz, $CDCl_3$): δ = 7.18 (H_h, 1H, d, J_o=8.64 Hz), 6.81 (H_f, H_g, 2H, m), 6.70 (H_i, s, 1H), 4.04 (NH_2, s, 2H), 4.00 (H_e, t, 2H, J=6.21 Hz), 2.28 (H_b, m, 2H, J_1=7.05 Hz , J_2=2.67 Hz), 1.98 (H_a, t, 1H, J=2.67), 1.92 (H_d, m, 2H), 1.74 (H_c, m, 2H).

^{13}C NMR (75 MHz, $CDCl_3$): δ = 159.74, 158.39, 150.28, 129.61, 125.78, 114.25, 112.93, 112.31, 101.20, 83.94, 68.74, 67.71, 28.08, 24.93, 18.12.

MS (ESI): m/z = 258.1 $[M+H]^+$, (calcd. 258.1 for $C_{15}H_{15}NO_3$).

Synthesis of 1

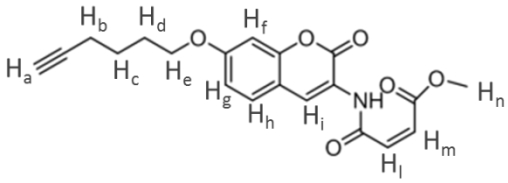

A mixture of hexynyl amino coumarin **5** (70 mg, 0.27 mmol) and maleic anhydride (23.5 mg, 0.24 mmol) in 15 ml acetone was stirred at reflux overnight. After cooling the mixture to 0°C and filtration, the yellow solid was washed with cold acetone to give the carboxylic acid product (85.2 mg, 0.23 mmol, 86%). A mixture of the carboxylic acid (85.2 mg, 0.23 mmol) and p-toluenesulfonic acid monohydrate (8.7 mg, 0.05 mmol) in 30 ml methanol was

refluxed overnight. After cooling of the mixture to 0°C and filtration, the yellowish solid was washed with cold methanol to give product **1** (Yield: 76 mg, 0.21 mmol, 90%).

^{1}H NMR (300 MHz, $CDCl_3$): δ = 9.98 (NH, s, 1H), 8.76 (H_i, s, 1H), 7.39 (H_h, 1H, d, J_o=8.64 Hz), 6.86 (H_g, dd, 1H, J_o=8.64 Hz, J_m=2.40 Hz), 6.81 (H_f, d, 1H, J_m=2.40 Hz), 6.42 (H_l, d, 1H, J=12.72 Hz), 6.26 (H_m, d, 1H, J=12.72 Hz), 4.03 (H_e, t, 2H, J=6.21 Hz), 3.86 (H_n, s, 3H), 2.28 (H_b, m, 2H, J_1=7.05 Hz , J_2=2.67 Hz), 1.98 (H_a, t, 1H, J=2.67), 1.93 (H_d, m, 2H), 1.74 (H_c, m, 2H).

^{13}C NMR (75 MHz, $CDCl_3$): δ = 166.43, 163.17, 161.12, 158.94, 152.02, 136.46, 129.01, 127.24, 125.80, 121.71, 113.78, 113.10, 101.38, 84.10, 69.08, 68.13, 53.00, 28.24, 25.13, 18.36.

HRMS (ESI): *m/z* = 392.1107 $[M+Na]^+$ (calcd. 392.1110 for $C_{20}H_{20}NO_6Na$).

Synthesis of 2

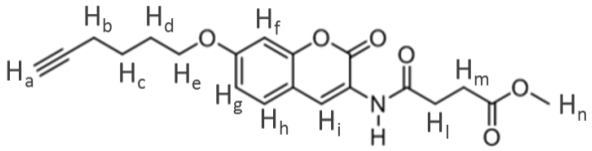

A mixture of **5** (70 mg, 0.27 mmol) and succinic anhydride (41 mg, 0.41 mmol) in 15 ml acetone was stirred at reflux overnight. After cooling of the mixture to 0°C and filtration, the yellow solid was washed with cold acetone to give the carboxylic acid product. Yield: 92 mg, 95%. A mixture of the carboxylic acid (60 mg, 0.17 mmol) and p-toluenesulfonic acid monohydrate (6 mg, 0.034 mmol, 0.2 eq) in 20 ml methanol was refluxed overnight. After cooling the mixture to 0°C and filtration, the yellow solid was washed with cold methanol to give product **2**. Yield: 55 mg, 88%.

^{1}H NMR (300 MHz, $CDCl_3$): δ = 8.62 (NH, s, 1H), 8.10 (H_i, s, 1H), 7.36 (H_h, 1H, d, J_o=8.64 Hz), 6.88 (H_g, dd, 1H, J_o=8.64 Hz, J_m=2.40 Hz), 6.82 (H_f, d, 1H, J_m=2.40 Hz), , 4.03 (H_e, t, 2H, J=6.21 Hz), 3.72 (H_n, s, 3H), 2.74 (H_m, H_l, s, 4H), 2.28 (H_b, m, 2H, J_1=7.05 Hz , J_2=2.67 Hz), 1.99 (H_a, t, 1H, J=2.67), 1.95 (H_d, m, 2H), 1.72 (H_c, m, 2H).

^{13}C NMR (75 MHz, $CDCl_3$): δ = 173.14, 170.79, 160.90, 159.21, 151.65, 128.79, 124.55, 121.60, 113.79, 113.15, 101.41, 69.06, 68.12, 52.30, 32.18, 31.20, 29.06, 28.25, 25.14, 18.36.

HRMS (ESI): *m/z* = 394.133 $[M+Na]^+$ (calcd. 394.127 for $C_{20}H_{21}NO_6Na$).

Synthesis of 3

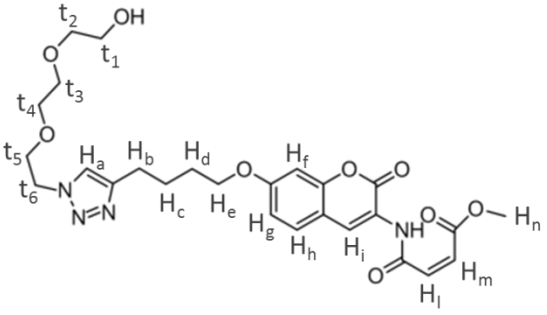

Under nitrogen, **1** (60 mg, 0.16 mmol) was dissolved in dichloromethane (10 mL) and a solution of azide triethylenglycol (29 mg, 0.16 mmol) in methanol (5 mL) was added. A solution of TBTA (8 mg, 16 µmol) and $Cu(CH_3CN)_4PF_6$ (6 mg, 16 µmol) in methanol (10 mL) was added to the reaction mixture, which was allowed to stir overnight at room temperature. Evaporation of the solvent under reduced pressure and flash column chromatography (SiO_2, CH_2Cl_2/MeOH 97/3) gave **3** as a colorless solid (Yield: 69 mg, 0.14 mmol, 78%).

^{1}H NMR (300 MHz, $CDCl_3$): δ = 9.98 (NH, s, 1H), 8.76 (H_i, s, 1H), 7.61 (H_a, s, 1H), 7.41 (H_h, 1H, d, J_o=8.64 Hz), 6.86 (H_g, dd, 1H, J_o=8.64 Hz, J_m=2.40 Hz), 6.83 (H_f, d, 1H, J_m=2.40 Hz), 6.44 (H_l, d, 1H, J=12.72 Hz), 6.29 (H_m, d, 1H, J=12.72 Hz), 4.55 (t_1, bt, 2H), 4.06 (H_e, t, 2H, J=6.21 Hz), 3.91 (t_2, bt, 2H) 3.88 (H_n, s, 3H), 3.75-3.58 (t_3-t_6, m, 8H), 2.82 (H_b, t, 2H), 2.35 (OH, s, 1H), 1.92 (H_c, H_d, m, 4H).

^{13}C NMR (75 MHz, $CDCl_3$): δ = 166.42, 163.16, 161.15, 158.94, 152.02, 136. 46, 129.01, 127.23, 125.81, 121.69, 113.73, 113.07, 101.44, 70.50, 69.75, 68.42, 61.94, 52.99, 29.93, 28.77, 26.05, 25.58.

HRMS (ESI): *m/z* = 545.225$[M+H]^+$ (calcd. 545.225 for $C_{26}H_{33}N_4O_9$).

Synthesis of 4

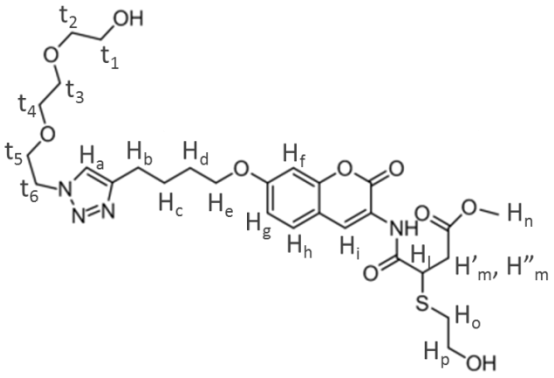

A mixture of **3** (16 mg, 0.032 mmol), NEt_3 (1 µl, 0.007 mmol), and β-mercaptoethanol (2.7 µl, 0.038 mmol) in 10 ml of methanol was stirred overnight. After evaporation of the solvent, a white solid was obtained via LC (silica, CH_2Cl_2/MeOH, 95/5, V/V). (Yield: 18 mg, 100%)

^{1}H NMR (300 MHz, $CDCl_3$): δ = 9.58 (NH, s, 1H), 8.64 (H_i, s, 1H), 7.52 (H_a, s, 1H), 7.38 (H_h, 1H, d, J_o=8.64 Hz), 6.88 (H_g, dd, 1H, J_o=8.64 Hz, J_m=2.40 Hz), 6.82 (H_f, d, 1H, J_m=2.40 Hz), 4.55 (t_1, t, 2H, J=4.92 Hz), 4.10 (H_l, t, 1H, J=7.3 Hz), 4.05 (H_e, t, 2H, J=6.21 Hz), 4.01 (H_q, m, 2H), 3.89 (t_2, t, J=5.04 Hz, 2H), 3.75-3.59 (H_n, t_3-t_6, 11H), 3.19 (H'_m, dd, 1H, J_1=7.62 Hz, J_2= 17.04 Hz) 2.99 (H_q, OH, m, 3H), 2.82 (H_b, H''_m, m, 3H) 2.35 (OH, s, 1H), 1.91 (H_c, H_d, m, 4H) Assignment of the signals was accomplished by means of 2D NMR ^{1}H-^{1}H COSY.

^{13}C NMR (75 MHz, $CDCl_3$): δ = 171.58, 170.49, 160.81, 159.06, 147.66, 128.63, 124.88, 122.04, 121.64, 113.57, 112.90, 101.20, 72.41, 70.58, 70.28, 69.59, 68.20, 63.27, 61.73, 52.17, 50.15, 45.23, 37.11, 35.20, 29.71, 28.54, 25.92, 25.28.

HRMS (ESI): *m/z* = 623.239 $[M+H]^+$ (calcd. 623.239 for $C_{28}H_{39}N_4O_{10}S$).

3.6.3 Methods

Automated solid-phase peptide synthesis. Fmoc-Rink amide MBHA resin (50 mg, substitution 0.64 mmol/g) was placed in the reaction vessel of the fully-automated peptide synthetizer (Syro), and swollen for 30 min in 3 mL N-methyl-2-pyrrolidinone (NMP), the vessels were subsequently emptied. The resin was washed with 1 mL piperidine (20%v)/NMP for 3 minutes and with 1 mL piperidine (20%v)/NMP for 12 min. The resin was washed with NMP (6x 1mL) before the following solutions: Fmoc-amino acid (4.5 equiv

respect to the resin) dissolved in a solution of HOBT (0.3 M) in NMP, HBTU (0.29 M) in NMP and DIPEA (0.58 M) in NMP were added to the vessel. The solid phase reaction was carried out for 80 min at room temperature and the vessel was emptied under reduced pressure before rinsing with NMP. The deprotection and coupling cycles were repeated until the assembly of the Fmoc protected peptide sequence was complete. The cleavage of the side chain protecting groups and the release of the sequence from the resin was achieved by manually incubating the resin with a mixture of 95% trifluoroacetic acid (TFA), 2.5% H_2O, 2.5% 1,2-ethanedithiol (EDT) and 1% triisopropylsilane (TIS) overnight.

The peptide was purified by several reprecipitation cycles in cold diethyl ether, redissolved in water and lyophilized overnight.

MS (ESI): *m/z* = 593.2 $[M+H]^+$, (calcd. 592.6 for $C_{20}H_{36}N_{10}O_9S$) for Cys-GRGDS

MS (ESI): *m/z* = 621.3 $[M+H]^+$, (calcd. 620.7 for $C_{22}H_{40}N_{10}O_9S$) for Met-GRGDS

MS (ESI): m/z = 839.8 $[M+H]^+$, (calcd. 839.0 for $C_{35}H_{58}N_{12}O_{10}S$) for Cys-LPLGNSH.

MS (ESI): m/z = 840.2 $[M+H]^+$, (calcd. 839.0 for $C_{35}H_{58}N_{12}O_{10}S$) for Cys-HNLGLPS.

Substrate and monolayer preparation. Microscope glass slides were used for monolayer preparation.[12] The substrates were oxidized with piranha solution for 45 min (concentrated H_2SO_4 and 33 % aqueous H_2O_2 in a 3:1 ratio; Warning: piranha should be handled carefully: it has been reported to detonate unexpectedly) and rinsed with water (MilliQ). After drying in a nitrogen stream, the substrates were used immediately to form a silanized monolayer. The substrates were immersed in 0.1 vol% 11-bromoundecyltrichlorosilane in dry toluene for 45 min at room temperature. Following monolayer formation, the substrates were rinsed with toluene to remove any excess of silanes, with ethanol and subsequently dried in a nitrogen flow. The bromide/azide nucleophilic substitution was carried out by the reaction with a saturated solution of NaN_3 in DMF for 48 h at 70^{o}C. The substrates were thoroughly rinsed with MilliQ water and ethanol and dried in a nitrogen flow.

Microcontact printing. Stamps were prepared by casting a 10:1 (v/v) mixture of poly(dimethylsiloxane) and curing agent (Sylgard 184, Dow Corning) against a silicon master. After overnight curing at 60^{o}C, the stamps were oxidized by oxygen plasma for 10 sec (power tuned at 50 mA) and subsequently inked by dropping the inking solution onto the stamp (1.5 mM **1** or **2** (in CH_3CN), 0.5 mM $Cu(I)(CH_3CN)_4PF_6$ and 0.5 mM TBTA (CH_3CN/EtOH=2/1) (catalyst mixture), prepared by mixing 75 µL of 2 mM solution of **1** or **2** in CH_3CN and 25 µL of 2 mM of catalyst mixture). After 4 min incubation the stamps were blown dry in a stream of nitrogen and brought into conformal contact with the substrate for 60 min. The stamps were changed for each new printing, and the same inking

procedure was used. After stamp removal, the printed substrates were rinsed with ethanol, sonicated in acetonitrile for 2 min, rinsed again with ethanol, blown dry with nitrogen and imaged by fluorescence microscopy.

Interfacial reaction with thiols. After immobilization of **1**, the platform was further reacted via incubation with thiols. In the case of the preparation of the β-CD monolayer, the patterned substrate was incubated in 1 mM heptakis-thio-β-cyclodextrin (β-CD-$(SH)_7$) in DMSO/PBS 3/1 at pH 7.5 for about 20 min. The substrate was then cleaned via sonication in DMF and in PBS buffer, rinsed with MQ water and ethanol and blown dry with nitrogen.
In the case of the immobilization of L-cysteine or Cys-GRGDS the substrate patterned with **1** was incubated with 10 mM solution of the thiol in PBS at pH 7.5 for 1 h, then was rinsed via sonication in PBS and in MilliQ water. For cell adhesion experiments a backfilling with a hydrophilic compound was necessary to improve the selectivity of the cell patterning. Therefore after reaction with Cys-GRGDS some samples were incubated in a water solution containing 30 mM propargylhexaethyleneglycol (offering cell adhesion resistance), 50 mM NaCl, 1mM $CuSO_4$, 40 mM ascorbic acid over night at room temperature.
In the case of the control experiment with L-cystine the substrate patterned with **1** was incubated with 1 mM solution of the thiol in PBS at pH 7.5 for 2 h, then was rinsed via sonication in PBS and in MilliQ water. The concentration was limited to 1 mM due to the low solubility of L-cystine. For a fair comparison we performed also experiments using 1mM L-cysteine for 2 h incubation.

Cell culture and adhesion studies. Every substrate was sterilized prior to cell seeding with 70% ethanol and subsequently washed twice with PBS to remove any excess of ethanol.
C2C12 (Mouse myoblast) cells were plated at a density of 50,000 cells/cm^2 in Dulbecco's modified eagle medium (DMEM) media (Sigma-Aldrich), supplemented with 4.5 g/L glucose, L-glutamine and $NaHCO_3$; 1% (v/v) Penicillin-Streptomycin solution (with 10,000 units penicillin and 10 mg streptomycin/mL, Sigma-Aldrich) and cultured at 37°C in a humidified 5% CO_2 atmosphere for 6 hours. Subsequent to incubation, adhered cells were carefully washed twice with sterile PBS to remove loosely attached cells.
Cells were fixed with a 4% formaldehyde solution in PBS for 10 minutes at room temperature and stained for F-actin with Alexa Fluor® 568 phalloidin (Invitrogen) following the protocol from the provider. Afterwards, the substrates were washed two times with PBS, water and they were carefully blown-dry with N_2.

TGF-β1 binding and immunofluorescent staining. Upon functionalization of the surfaces with peptides, the substrates were incubated with solutions containing either 1 µg/mL TGF-β1 in PBS. The substrates were then rinsed three times 10 min with PBS buffer including 1 mM Tween-20 on the orbital shaker and finally rinsed with PBS buffer. Afterwards, substrates were incubated with PBS containing 1% BSA for 1 h and washed again three times as described above to block the background against non-specific protein interactions. Protein patterns were then incubated with 200 µL of a solution of 5 µg/mL of monoclonal anti-TGF-β1 antibody (R&D systems) produced in mouse (mouse IgG_{2b} isotype, clone 141322) in PBS buffer including 1% BSA. After 1 h, the substrates were washed three times 10 min with PBS buffer including 1 mM Tween-20, rinsed with water and dried with a flow of dry N_2. Consecutively, 200 µL of a solution (4 µg/mL) of anti-mouse IgG_{2b} labeled with Alexa Fluor® 546 produced in goat (Invitrogen) in PBS buffer (including 1% BSA) was used to incubate the samples for 1 h. The substrates were then washed again three times 10 min with PBS buffer including 1 mM Tween-20, rinsed with water and dried with a flow of dry N_2 and used for fluorescence microscopy imaging.

Cell differentiation studies. Macroscopically intact articular cartilage from femoral condyles was obtained from patients undergoing total knee replacement. Chondrocytes were isolated after overnight digestion with Collagenase type II and used at passage two.
Chondrocytes were plated at a density of 5,000 cells/cm^2 in Dulbecco's modified eagle medium (DMEM) (Sigma-Aldrich), supplemented with 4.5 g/L glucose, 1% (v/v) penicillin-streptomycin solution (with 10,000 units penicillin and 10 mg streptomycin/mL, Sigma-Aldrich), 50 µg/mL L-ascorbic acid-2-phosphate (AsAP), 100 µg/mL sodium pyruvate 40 µg/ml proline, 1% of a mixture of 1.0 mg/ml recombinant human insulin, 0.55 mg/ml human transferrin (substantially iron-free), and 0.5 µg/ml sodium selenite (ITS supplement) and 10^{-7} M dexamethasone. 100 ng of TGF-β1 was either supplemented to the medium or bound to the surfaces as indicated in the results and discussion section. Cells were cultured at 37°C in a humidified 5% CO_2 atmosphere for 7 days.
Live/Dead assay (LIVE/DEAD® Viability/Cytotoxicity Kit, for mammalian cells, Molecular Probes®) was performed according to the protocol from the provider.

3.6.4 Equipment

Fluorescence microscopy. Fluorescence microscopy images were taken using an Olympus inverted research microscope IX71 equipped with a mercury burner U-RFL-T as light source and a digital Olympus DR70 camera for image acquisition. UV excitation (300 nm ≤ λ_{ex} ≤ 400

nm) and blue emission (410 nm ≤ λ_{em} ≤ 510 nm) was filtered using a Dapi Olympus filter cube. Green excitation (510 nm ≤ λ_{ex} ≤ 550 nm) and red emission (λ_{em} ≥ 580) was filtered using a Olympus filter cube. All fluorescence microscopy images were acquired in air.

XPS. XPS spectra were obtained on a Physical Electronics Quantera Scanning X-ray Multiprobe instrument, equipped with a monochromatic AlKα X-ray source operated at 1486.6 eV and 26.18 W. Spectra were referenced to the main C_{1s} peak set at 284.0 eV. The X-ray beam size was 100 µm and the data were collected from surface areas of 100 µm × 300 µm with a pass energy of 224 eV and a step energy of 0.8 eV for survey scans and 0.4 eV for high resolution scans. For quantitative analysis, the sensitivity factors used to correct the number of counts under each peak were: C_{1s}, 1.00; N_{1s}, 1.59. The measurement was collected after 25 scanning cycles.

Mass spectra. ESI-TOF-MS mass spectra were recorded using a LCT Mass spectrometer (Waters/Micromass).

NMR. ^{1}H and ^{13}C NMR spectra were recorded on Varian Unity (300MHz) spectrometer. ^{1}H and ^{13}C chemical shifts values, 300 MHz and 75 MHz, are reported as δ using the residual solvent signal as internal standard.

3.7 References

(1) a) D. G. Castner, B. D. Ratner, *Surf. Sci.* **2002**, *500*, 28-60; b) M. D. Mager, V. LaPointe, M. M. Stevens, *Nat. Chem.* **2011**, *3*, 582.

(2) P. Jonkheijm, D. Weinrich, H. Schroeder, C. M. Niemeyer, H. Waldmann, *Angew. Chem. Int. Ed.* **2008**, *47*, 9618.

(3) F. A. Scaramuzzo, A. Gonzalez-Campo, C. C. Wu, A. H. Velders, V. Subramaniam, G. Doddi, P. Mencarelli, M. Barteri, P. Jonkheijm, J. Huskens, *Chem. Commun.* **2010**, *46*, 4193.

(4) a) C. M. Salisbury, D. J. Maly, J. A. Ellman, *J. Am. Chem. Soc.* **2002**, *124*, 14868-14870; b) N. Winssinger, R. Damoiseaux, D. C. Tully, B. H. Geierstanger, K. Burdick, J. L. Harris, *Chem. Biol.* **2004**, *11*, 1351; c) S. Y. Lim, W. Y. Chung, H. K. Lee, M. S. Park, H. G. Park, *Biochem. Biophys. Res. Commun.* **2008**, *376*, 633.

(5) A. Gonzalez-Campo, S. H. Hsu, L. Puig, J. Huskens, D. N. Reinhoudt, A. H. Velders, *J. Am. Chem. Soc.* **2010**, *132*, 11434.

(6) a) L. Yi, H. Li, L. Sun, L. Liu, C. Zhang, Z. Xi, *Angew. Chem. Int. Ed.* **2009**, *48*, 4034; b) X. Chen, Y. Zhou, X. J. Peng, J. Yoon, *Chem. Soc. Rev.* **2010**, *39*, 2120.

(7) a) Y. Y. Wang, J. Cai, H. Rauscher, R. H. Belun, W. A. Goedel, *Chem. Eur. J.* **2005**, *11*, 3968; b) B. T. Houseman, E. S. Gawalt, M. Mrksich, *Langmuir* **2003**, *19*, 1522.

(8) D. I. Rozkiewicz, D. Jańczewski, W. Verboom, B. J. Ravoo, D. N. Reinhoudt, *Angew. Chem. Int. Ed.* **2006**, *45*, 5292.

(9) K. Sivakumar, F. Xie, B. M. Cash, S. Long, H. N. Barnhill, Q. Wang, *Org. Lett.* 2004, *6*, 4603.
(10) C. S. Sevier, C. A. Kaiser, *Nat. Rev. Mol. Cell Biol.* 2002, *3*, 836.
(11) M. S. Schiedel, C. A. Briehn, P. Bauerle, *Angew. Chem. Int. Ed.* 2001, *40*, 4680.
(12) N. Balachander, C. N. Sukenik, *Langmuir* 1990, *6*, 1621.
(13) R. Carta, G. Tola, *J. Chem. Eng. Data* 1996, *41*, 414.
(14) a) R. Pankov, K. M. Yamada, *J. Cell Sci.* 2002, *115*, 3861; b) S. J. Xiao, M. Textor, N. D. Spencer, H. Sigrist, *Langmuir* 1998, *14*, 5507.
(15) a) D. B. Liu, Y. Y. Xie, H. W. Shao, X. Y. Jiang, *Angew. Chem. Int. Ed.* 2009, *48*, 4406; b) W. S. Yeo, M. Mrksich, *Langmuir* 2006, *22*, 10816.
(16) J. S. Dounchis, R. S. Goomer, F. L. Harwood, M. Khatod, R. D. Coutts, D. Amiel, *J. Orthop. Res.* 1997, *15*, 803.
(17) B. Johnstone, T. M. Hering, A. I. Caplan, V. M. Goldberg, J. U. Yoo, *Exp. Cell Res.* 1998, *238*, 265.
(18) M. Schnabel, S. Marlovits, G. Eckhoff, I. Fichtel, L. Gotzen, V. Vécsei, J. Schlegel, *Osteoarth. Cart.* 2002, *10*, 62.
(19) a) A. M. DeLise, L. Fischer, R. S. Tuan, *Osteoarth. Cart.* 2000, *8*, 309. b) H. J. Kwon, *Biochem. Biophys. Res. Commun.* 2012, *424*, 793.
(20) T. R. Chan, R. Hilgraf, K. B. Sharpless, V. V. Fokin, *Org. Lett.* 2004, *6*, 2853.
(21) A. Mulder, S. Onclin, M. Peter, J. P. Hoogenboom, H. Beijleveld, J. ter Maat, M. F. Garcia-Parajo, B. J. Ravoo, J. Huskens, N. F. van Hulst, D. N. Reinhoudt, *Small* 2005, *1*, 242.
(22) M. T. Rojas, R. Koniger, J. F. Stoddart, A. E. Kaifer, *J. Am. Chem. Soc.* 1995, *117*, 336.
(23) H. S. Gill, J. N. Tinianow, A. Ogasawara, J. E. Flores, A. N. Vanderbilt, H. Raab, J. M. Scheer, R. Vandlen, S. P. Williains, J. Marik, *J. Med. Chem.* 2009, *52*, 5816.

Chapter 4

"I don't know, and I would rather not guess." — John R. R. Tolkien

Oriented protein immobilization using covalent and non-covalent chemistry on a thiol-reactive self-reporting surface*

We report the fabrication of a patterned protein array using three orthogonal methods of immobilization that are detected exploiting a fluorogenic surface. Upon reaction of thiols, the fluorogenic tether reports the bond formation by an instantaneous rise in (blue) fluorescence intensity providing a means to visualize the immobilization even of non-fluorescent biomolecules. First, the covalent, oriented immobilization of a visible fluorescent protein (TFP) modified to display a single cysteine residue was detected. Co-localization of the fluorescence of the immobilized TFP and the fluorogenic group provided a direct tool to distinguish covalent bond formation from physisorption of proteins. Subsequent orthogonal immobilization of thiol-functionalized biomolecules could be conveniently detected by fluorescence microscopy using the fluorogenic surface. A thiol-modified nitrilotriacetate ligand was immobilized for binding of hexahistidine-tagged red-fluorescing TagRFP, while a suitably modified biotin was immobilized for binding of Cy5-labelled streptavidin.

*Part of this chapter has been published in: D. Wasserberg,[#] C. Nicosia,[#] E.E. Tromp, V. Subramaniam, J. Huskens, P. Jonkheijm, *J. Am. Chem. Soc.*, **2013**, *135*, 3104-3111 ([#] equal authorship).

4.1 Introduction

Convenient ways to link proteins to predefined locations on molecular and supramolecular reactive surfaces are of great importance for bottom-up engineering in nanotechnology and life sciences.[1] Site-specific chemical strategies, as opposed to random attachment, provide precise control over immobilizing proteins in homogeneously oriented layers and yield improved performance of protein biochips.[2-4] For the immobilization of structurally sensitive proteins, chemical reactions with high specificity towards the protein of interest, mild reaction conditions compatible with physiological conditions, and rapid and quantitative conversion are essential.[2] Among the bio-analytical platforms under development, interfaces with multiple proteins on a single surface with predetermined density, spacing and orientation have attracted much attention.[5] Promising progress has been reported on developing multifunctional protein surfaces using diverse surface-bound orthogonal chemical functionalities for subsequent protein attachment via covalent and non-covalent chemistry. To achieve spatial surface patterning of orthogonal chemical groups, elegant techniques have been developed,[6] including photolithography,[7] spot arraying,[8] electron-beam lithography,[9] dip-pen and other probe lithographies,[10] and imprint lithography[11] as well as microcontact printing (μCP).[12] Whilst a few of the above-mentioned spatially multi-functionalized surfaces are documented in the literature, where site-specific protein attachment has been realized, only a small number are shown to combine orthogonal covalent with non-covalent protein immobilization strategies. Employing such multifunctional protein-binding surfaces is attractive to achieve differentiated responsive biomimetic functions.[13] Recently, Velders and coworkers demonstrated the selectivity and specificity of orthogonal covalent and non-covalent functionalization for small molecules.[14] In their work bi-functional alkyne-cyclodextrin patterned surfaces were prepared via reactive μCP. Microcontact printing is a versatile surface patterning method that has been exploited for the immobilization of many different molecules by inducing a variety of reactions.[15] In a very recent example, Ravoo and coworkers fabricated tetra-functional chemical patterns on silicon oxide by consecutive reactive prints of hetero-functional linkers, each with a ligand attached, displaying excellent biomolecular specificity.[12d]

Here, we employ our recently developed self-reporting thiol-reactive fluorogenic platform[16] (described in Chapter 3) to fabricate an interface with covalently and non-covalently bound proteins. Oriented protein immobilization can be conveniently achieved if the protein possesses a single accessible, reactive cysteine (Cys), which is the only naturally occurring amino acid containing a thiol group in its side-chain, and whose relative abundance in proteins is rather small (< 1%). Thiols have a pK_a of around 8.5 and are

sufficiently nucleophilic at pH 7. When Cys residues are introduced into a protein through site-specific mutation of, for example, Ser or Ala residues, preferably in a remote solvent-accessible epitope of the protein, the specific reaction of an engineered cysteine moiety with our fluorogenic maleimide-terminated monolayers can be conveniently detected. Co-localization of the fluorescence of the immobilized protein and of the fluorogenic group provides a direct tool to discern covalent bond formation from physisorption. Similarly, the orthogonal attachment of subsequent immobilization steps of thiol-functionalized biomolecules can be identified via this co-localization of fluorescence signatures.

4.2 Results and discussion

4.2.1. Direct oriented immobilization of cysteine-modified proteins from solution

Visible fluorescent proteins were used as model proteins in this study as they provide an intrinsic probe for their structural integrity upon immobilization, as their fluorescence characteristics are highly sensitive to even minute changes in their native structure.[17] For the preparation of micro-patterned protein surfaces, glass slides were first modified with an azide-terminated monolayer (Scheme 4.1, step 1).[18] Then, a one-hour single reactive μCP step (Scheme 4.1, step 2), by the Huisgen 1,3-dipolar cycloaddition,[19] was performed employing an oxidized poly(dimethylsiloxane) (PDMS) stamp inked with a solution of alkyne-functionalized fluorogenic coumarin **1** (Scheme 4.1), Cu(I)$(CH_3CN)_4PF_6$ and tris[(1-benzyl-1H-1,2,3-triazol-4-yl)methyl]amine (TBTA). As described in Chapter 3, the presence of a methyl-4-oxo-2-butenoate group adjacent to the coumarin allows reaction with thiols and quenches the coumarin emission prior to reaction with such thiols.[16,20] Owing to this phenomenon, upon printing of **1**, the fluorescence of the pattern was almost indistinguishable from the background (Figure 4.1A).[16] Subsequently, onto this self-reporting platform the covalent immobilization of thiol-containing compounds was performed by means of the fluorogenic Michael addition to the methyl-4-oxo-2-butenoate moiety of **1** (Scheme 4.1, step 3, center).

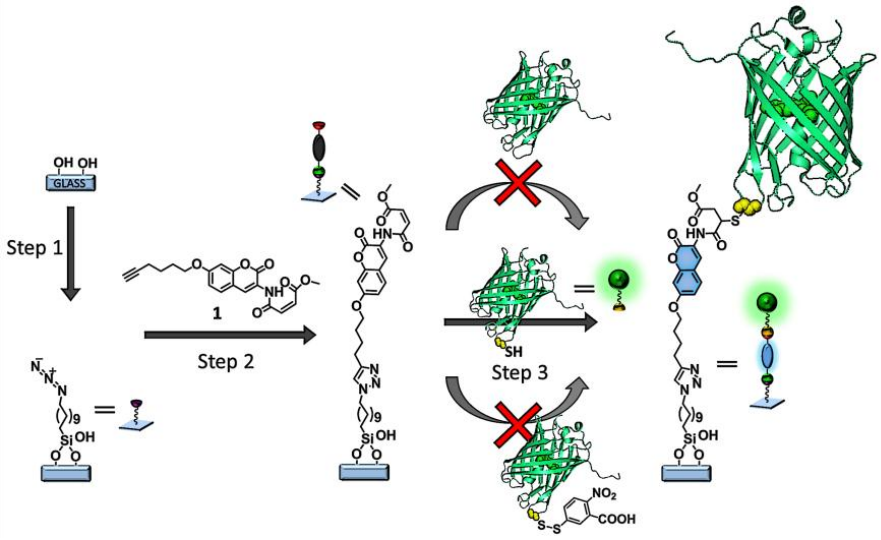

Scheme 4.1. Schematic representation of the surface functionalization by reactive µCP of **1** (step 2) on an azide monolayer (from step 1), followed by immobilization of a single-cysteine-containing mutant of TFP (**^{G174C}TFP**, step 3) reported by the fluorogenic reaction of **1**, (step 3, center). Schematic representation of the protein structures: control cysteine-free **TFP** (step 3, top), **^{G174C}TFP** (step 3, center) and blocked **^{G174C}TFP** after derivatization with Ellman's reagent (step 3, bottom).

To establish the method for the direct covalent immobilization on the self-reporting surface of a cysteine-modified protein (Scheme 4.1), a single-cysteine-containing mutant of a monomeric variant of *Clavularia* cyan fluorescent protein, **mTFP1**,[21] was recombinantly expressed and purified. **mTFP1** was modified to contain no hexa-histidine (His_6)-tags and, additionally, was site-selectively mutated to introduce a single cysteine group at position 174, which is located in a flexible loop on top of the β-barrel of the fluorescent protein, yielding **^{G174C}TFP**. To investigate the applicability of the direct protein immobilization, a 20 µM phosphate-buffered solution (pH 7.5) of **^{G174C}TFP** was used for overnight incubation of substrates patterned with **1**. As control for the specificity of the immobilization reaction, an otherwise unchanged cysteine-free **TFP** was used at even higher concentrations (40 µM) but otherwise identical conditions. After overnight incubation fluorescence micrographs showed protein patterns co-localized on the fluorescent coumarin patterns only in the case of **^{G174C}TFP** (Figures 4.1C and D), whereas no enhancement of fluorescence of the fluorogenic coumarin or any other part of the pattern in the case of the native protein (Figures 4.1A and B) could be observed, proving that the reaction indeed proceeds exclusively with thiol-containing proteins.

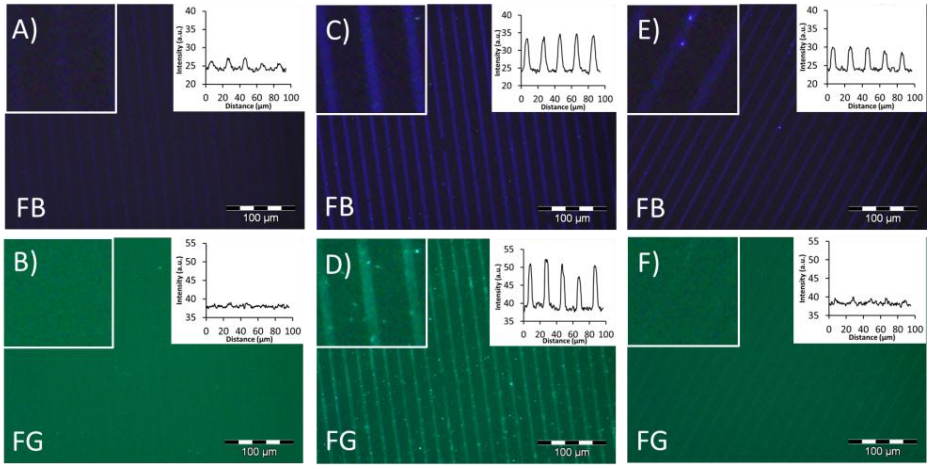

Figure 4.1. A-F) Fluorescence microscopy images (inserts: corresponding intensity profiles) of substrates patterned with **1**, after overnight incubation with A,B) 40 µM **TFP**; C,D) 20 µM **^{G174C}TFP**; E,F) 30 µM **^{G174C}TFP** after reaction with Ellman's reagent. FB/FG refer to blue and green channels, respectively. FB: λ_{exc} = 350 nm, λ_{em} > 420 nm; FG: λ_{exc} = 460 nm, λ_{em} = 520 nm.

The thus generated signaling platform is indeed so specific to thiol moieties that it may become a valuable tool for the identification of the redox state of cysteines, which are important to the folding and stability of some proteins that are part of various signaling pathways.[22] To prove the ability of our platform to selectively distinguish between thiols and disulfides a series of substrates were patterned with fluorogenic coumarin **1** and subsequently incubated with a disulfide conjugate of **^{G174C}TFP**. To yield a disulfide conjugate of **^{G174C}TFP**, a 20 µM solution of **^{G174C}TFP** was reacted with an excess of Ellman's reagent.[23] Slides patterned with **1** were incubated overnight in solution of the reaction mixture of **^{G174C}TFP** with Ellman's reagent. No green fluorescent pattern could be observed (Figure 4.1F). A modest increase of blue fluorescence from the coumarin lines was detected (Figure 4.1E), probably due to the reaction with residual free thiol-containing by-products from the disulfide formation with Ellman's reagent. These results show that only **^{G174C}TFP** is immobilized (Figure 4.1C and D) but not its disulfide conjugate (Figure 4.1E and F).

The above series of experiments proves that: a) thiol-containing proteins can be directly immobilized on fluorogenic coumarin patterns; b) direct protein immobilization gives rise to the self-reporting blue fluorescence signal of the thiol addition product of the tethered coumarin; c) immobilization from a solution of **^{G174C}TFP** results in co-localized patterns of protein and fluorogenic coumarin, and d) immobilization of **^{G174C}TFP** on fluorogenic coumarin is chemo-selective, i.e. only thiol-containing **^{G174C}TFP** but neither thiol-free **TFP** nor **^{G174C}TFP**-disulfide conjugates are being immobilized.

4.2.2. Supramolecular oriented immobilization of His_6-tagged proteins

In contrast to our previous work[16] where thiolated molecules, a pentapeptide and a protein (vide supra) were immobilized from solution, the viability of reactive µCP of thiol-containing compounds on pre-patterned fluorogenic coumarin was tested. To this end, cysteine was selected for immobilization via reactive µCP on the self-reporting platform. A flat PDMS stamp was inked with a 10 mM cysteine solution in PBS for 30 min and dried in a flow of nitrogen, and subsequently brought into conformal contact with the self-reporting coumarin-patterned substrate for 10 min. The fluorescence microscopy characterization of the monolayers showed a very weak signal for the unreacted fluorogenic moiety before (Figure 4.2A) and a strong blue fluorescence emission after reactive µCP of cysteine (Figure 4.2B).

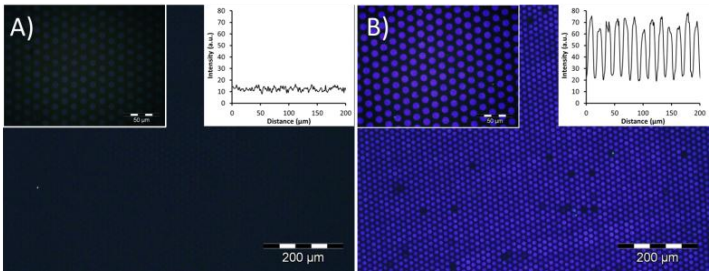

Figure 4.2. Fluorescence microscopy images (inserts show intensity profiles) A) before and B) after printing a 10 mM cysteine solution on the fluorogenic platform. λ_{exc} = 350 nm, λ_{em} > 420 nm (FB).

Due to immobilization via reactive µCP, the required sample volume and concentration were much reduced compared to that required for the previously reported immobilization from solution.[16] From the fluorescence images it is evident that after performing two reactive µCP steps, a Huisgen 1,3-dipolar cycloaddition of **1** on the azide-functionalized monolayer followed by a fluorogenic Michael addition on patterns of **1**, the cysteine-printed areas of the fluorogenic coumarin pattern had indeed increased in fluorescence intensity. This demonstrates the viability of using reactive µCP to immobilize thiols on our fluorogenic platform.

With the goal of fabricating a multifunctional patterned surface that allows for oriented covalent and non-covalent protein immobilization, we decided to make use of the Ni(II)-nitrilotriacetic acid (NiNTA)/His_6-tag technology. Following the same procedure as described above for cysteine, thiol-NTA was immobilized via reactive µCP (using a flat stamp) on fluorogenic coumarin reporter patterns (Scheme 4.2).

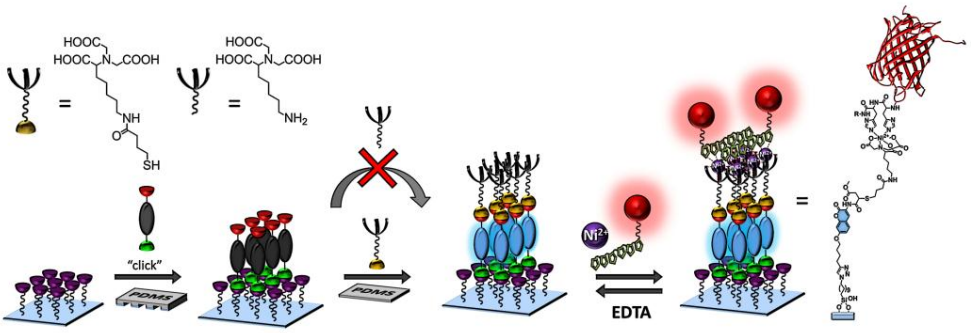

Scheme 4.2. Schematic representation of the procedure of the supramolecular protein immobilization by reactive μCP of **1** on an azide monolayer, followed by immobilization of a thiol-NTA reported by the fluorogenic reaction and subsequent co-localization of **His_6-^{14}TagRFP-His_6** immobilized via NiNTA/His_6 interactions. The molecular structure of the NiNTA/His_6 complex represents one of the possible species formed upon interactions of a His_6-tag with a single NiNTA unit.

After printing, the blue fluorescent coumarin pattern was clearly visible (Figure 4.3A) confirming the successful immobilization of thiol-NTA. Subsequently, a variant **His_6-^{14}TagRFP-His_6** of monomeric red fluorescent protein, derived from Entacmaea quadricolor, TagRFP,[24] carrying His_6-tags at both N- and C-termini was used for supramolecular immobilization on the NTA-patterns. The NTA-patterned sample was incubated with a solution of 1 μM **His_6-^{14}TagRFP-His_6** and $NiCl_2$ in a 1:2 ratio for 30 min, washed for 1 h, dried, and imaged using fluorescence microscopy. The fluorescence characterization (Figure 4.3C and D) shows a perfect co-localization of the covalently attached NTA (determined via coumarin) and the assembled fluorescent protein. Then, the sample was shortly immersed in a 10 mM ethylene diamine tetraacetic acid (EDTA) solution in order to remove the protein from the NTA monolayer via competitive complexation of Ni^{2+} ions by EDTA. This resulted in the retention of the immobilized NTA as seen by the remaining signal from the coumarin (Figure 4.3E) and, at the same time, a substantial loss of the red fluorescence intensity (Figure 4.3F) indicating desorption of the protein. This demonstrates the reversibility and specificity of the **His_6-^{14}TagRFP-His_6** interaction with the NTA-patterns.

The selectivity of the immobilization for thiols was further confirmed using an amino-NTA, lacking a thiol group (Scheme 4.2). After printing the amino-NTA on fluorogenic coumarin patterns using a flat stamp, negligible enhancement of fluorescence was observed (Figure 4.3G). Upon subsequent incubation with **His_6-^{14}TagRFP-His_6** and $NiCl_2$ the slight increase in red fluorescent patterns (Figure 4.3H) indicates that hardly any non-specific interactions occur between the protein and the Ni^{2+}-free surface.

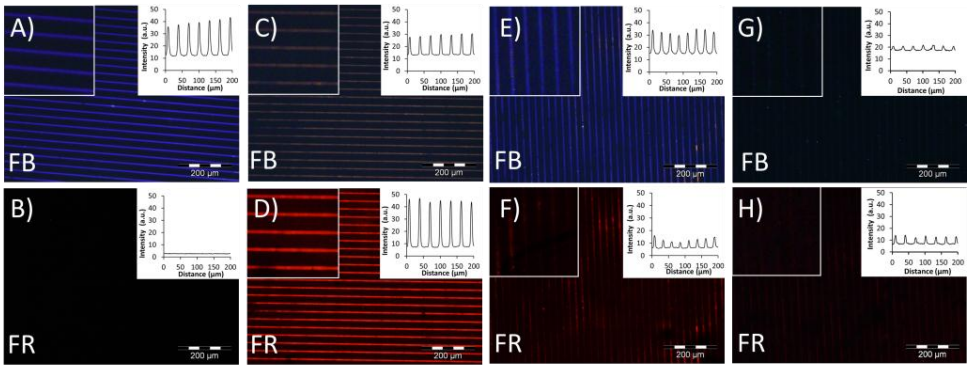

Figure 4.3. Fluorescence microscopy images (insets: corresponding intensity profiles): A, B) after printing of thiol-NTA with a flat PDMS stamp on a substrate patterned with compound **1**; C, D) after incubation of the previous substrate in **His_6-^{14}TagRFP-His_6**:$NiCl_2$ (1:2) in PBS; E, F) after immersion in 10 mM EDTA in PBS (different substrate); G) after printing amino-NTA with a flat PDMS stamp and H) after incubation of this substrate in **His_6-^{14}TagRFP-His_6**:Ni^{2+} in PBS. FB/FR refer to blue (monitoring coumarin) and red (monitoring RFP) channels, respectively (FB: λ_{exc} = 350 nm, λ_{em} > 420 nm FR: λ_{exc}= 510-550 nm, λ_{em}= 590 nm).

From this series of experiments we conclude that a) thiol-NTA is site-selectively immobilized on our fluorogenic platform following a reactive μCP approach; b) immobilization gives rise to the self-reporting blue fluorescence signal of the thiol addition product of coumarin upon reactive μCP; c) immobilization from a solution of **His_6-^{14}TagRFP-His_6** with $NiCl_2$ results in co-localized patterns of protein and NTA; d) immobilization of **His_6-^{14}TagRFP-His_6** in the presence of Ni^{2+} ions on NTA patterns on fluorogenic coumarin is selective and reversible.

4.2.3 Protein arrays through oriented covalent and non-covalent immobilization

To fabricate arrays using covalent and non-covalent immobilization of two different proteins, we next set out to show immobilization of NTA ligands only on defined areas of the fluorogenic coumarin patterns (Scheme 4.3).

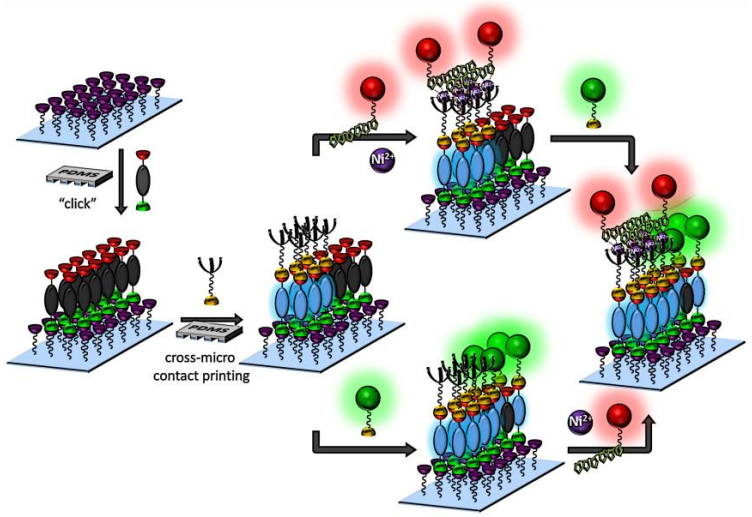

Scheme 4.3. Schematic representation of the fabrication of a dual protein array: surface functionalization by reactive µCP of **1** on an azide monolayer, followed by immobilization of thiol-NTA by cross-µCP. The next step consists of the subsequent immobilization of **His$_6$-^{14}TagRFP-His$_6$**:Ni^{2+} on the NTA pattern (upper route) and consecutive immobilization of cysteine-containing **^{G174C}TFP** from solution on the rest of the pattern of as yet unreacted coumarin tether or, alternatively, vice versa (lower route) the immobilization of **^{G174C}TFP** with the consecutive immobilization of **His$_6$-^{14}TagRFP-His$_6$**:Ni^{2+}.

To this end, a line-patterned PDMS stamp inked with a thiol-NTA solution was cross-microcontact printed on a substrate pre-patterned with lines of **1** so that the two line patterns were oriented perpendicular to each other. This resulted in NTA-functionalized squares at the locations where the two patterns overlap (Figure 4.4A), while the rest of the lines functionalized with the fluorogenic unit **1** remained unreacted and thus still thiol-reactive. Upon incubation of such a substrate with 1 µM **His$_6$-^{14}TagRFP-His$_6$**:Ni^{2+} (1:2 ratio) in PBS, the selective co-localization of protein on the NTA-functionalized squares was observed (Figure 4.4B and C).

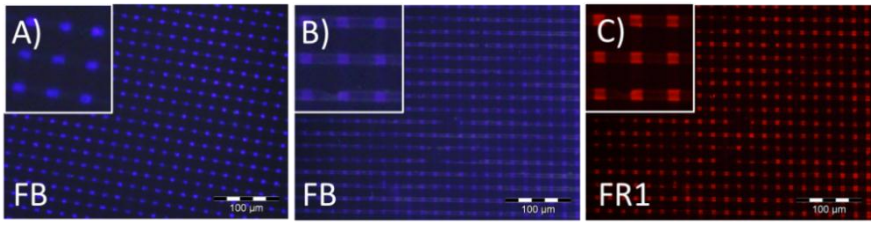

Figure 4.4. A) Fluorescence microscopy image of a substrate patterned with **1** and cross-microcontact printed with thiol-NTA. **B, C)** Fluorescence microscopy images after 1 h incubation of the previous substrate in 1 µM **His$_6$-^{14}TagRFP-His$_6$**:$NiCl_2$ (1:2) in PBS. FB: λ_{exc} = 350 nm, λ_{em} > 420 nm; FR=FR1: λ_{exc} = 510-550 nm, λ_{em} = 590 nm; FR2: λ_{exc} = 650 nm, λ_{em} = 670 nm.

To test the ability to immobilize ^{G174C}**TFP** onto the remaining 'dark' areas of the as yet unreacted lines of fluorogenic coumarin and, at the same time, the His_6-tagged protein on the NTA-functionalized areas of the same substrate, two procedures comprising two consecutive immobilization steps were carried out (Scheme 4.3). In one procedure the His_6-tagged proteins were supramolecularly immobilized on the NTA patterns prior to the direct covalent immobilization of the cysteine-containing variant ^{G174C}**TFP** on the as yet unreacted fluorogenic patterns (Scheme 4.3, upper route), while in the other procedure the order of the two immobilization steps was reversed (Scheme 4.3, lower route). Both routes lead to the same result: dual protein patterns of oriented, non-covalently immobilized **His_6-^{14}TagRFP-His_6** on NTA and covalently immobilized ^{G174C}**TFP** on the non-NTA functionalized coumarin, respectively.

In detail, following the lower route in Scheme 4.3, a square cross-micro contact printed substrate of thiol-NTA on patterns of **1** (Figure 4.4) was incubated overnight with a 20 µM solution of ^{G174C}**TFP**, with immobilization of the protein on the unreacted coumarin areas (Figure 4.5). The coumarin lines are fully functionalized, as they show highly intense blue fluorescence along their entire lengths (Figure 4.5A). Remarkably, there seems to be a systematically higher intensity in the blue coumarin fluorescence co-localized exactly at the squares of cross-microcontact printed thiol-NTA, while the rectangular parts of the coumarin lines in-between, functionalized with ^{G174C}**TFP** (Figure 4.5B), consistently show a lower blue (coumarin) fluorescence intensity. Since our self-reporting platform reflects bond formation, we correlate this observation to a higher surface coverage in the case of the small molecule, thiol-NTA, in comparison to the much larger protein.

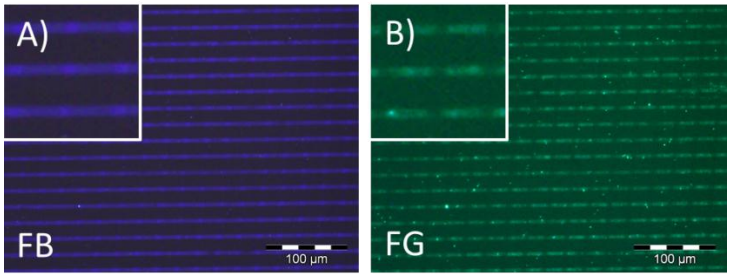

Figure 4.5. Fluorescence microscopy images after overnight incubation of a substrate patterned with **1** and cross-microcontact printed with thiol-NTA in 20 µM ^{G174C}**TFP** in PBS. FB: λ_{exc} = 350 nm, λ_{em} > 420 nm; FG: λ_{exc} = 460 nm, λ_{em} = 520 nm.

The previous sample was incubated 1 h with a solution of 1 µM **His_6-^{14}TagRFP-His_6**:Ni^{2+} (1:2 ratio), and finally washed and dried in a flow of nitrogen. Then a series of fluorescence micrographs were recorded using different filters (Figure 4.6). As can be concluded from

the merged fluorescence images (Figure 4.6D), squares of **His_6-^{14}TagRFP-His_6**:Ni^{2+} are localized on parts of the blue fluorescent coumarin lines complementary to the ones where **^{G174C}TFP** is localized.

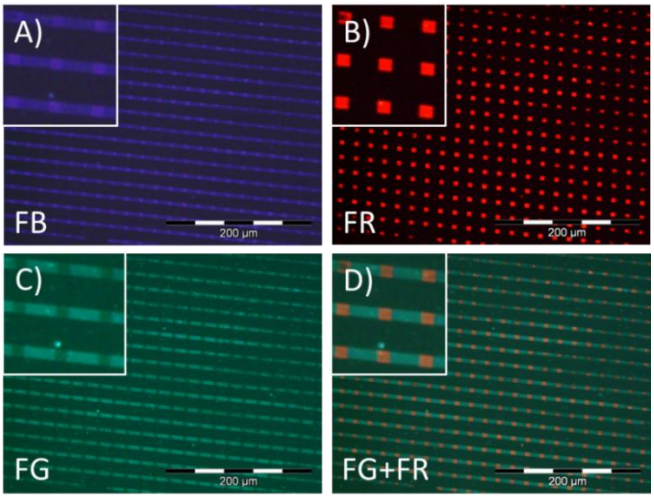

Figure 4.6. A-C) Fluorescence microscopy images after overnight incubation of a substrate patterned with **1** and cross-micro contact printed with thiol-NTA in 20 µM **^{G174C}TFP** and subsequent incubation with 1 µM **His_6-^{14}TagRFP-His_6**:$NiCl_2$ (1:2) in PBS for 1 h; D) merged image of FR+FG. FB/FG/FR refer to blue (monitoring coumarin), green (monitoring TFP) and red (monitoring RFP) channels, respectively.

When the order of incubation was reversed, following the upper route in Scheme 4.3, i.e. first **His_6-^{14}TagRFP-His_6** and then **^{G174C}TFP**, equally specific complementary patterns were observed, with similar fluorescence intensity ratios in both cases.

With this series of experiments, we show that a) NiNTA and thiol-sensitive coumarin tethers can be used to orthogonally immobilize two different proteins, one containing His_6-tags and one containing free cysteines regardless of the order in which the proteins are immobilized; b) the immobilization strategies are orthogonal and (chemo-)selective; c) the fluorogenic tether acts as fluorescent reporter for the immobilization of thiols, while d) a correlation between fluorescence intensity and coverage of bound thiols can be detected.

After optimizing the conditions for fabricating a bifunctional surface for dual protein patterns, the use of the residual azide groups using reactive µCP for further functionalization via an additional orthogonal 'click'-reaction with alkyne-modified biotin was investigated (Scheme 4.4).

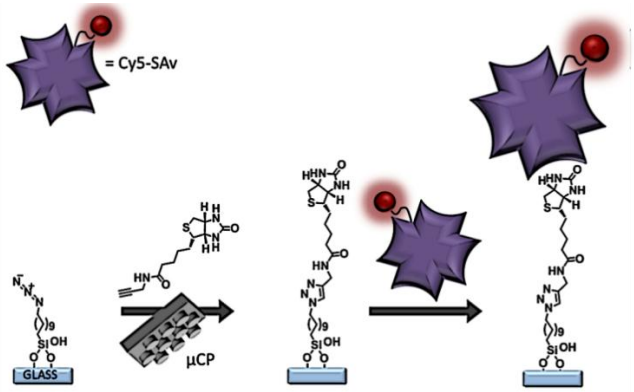

Scheme 4.4. Immobilization of alkyne-modified biotin/**Cy5-SAv** on an azide monolayer on glass by means of reactive microcontact printing.

For the preparation of micro-patterned biotinylated surfaces, we proceeded as described previously for patterning of **1**. An oxidized PDMS stamp was inked with a solution of alkyne-modified biotin, Cu(I)$(CH_3CN)_4PF_6$ and TBTA, dried in a stream of nitrogen and brought into conformal contact with the azide-terminated glass slide for 1 h. In order to visualize the biotinylation of the surface, the substrate was incubated with a solution of 0.6 µM Cy5-labeled streptavidin (**Cy5-SAv**) showing the successful specific binding of streptavidin on the biotin pattern (Figure 4.8D). Moreover, the pattern was imaged using the fluorescent filters employed for the visualization of **1** (Figure 4.8A), **His_6-^{14}TagRFP-His_6** (Figure 4.8B) and **^{G174C}TFP** (Figure 4.8C) resulting in none or negligible fluorescence interference, confirming the possibility of monitoring the simultaneous attachment of the three different proteins on one substrate.

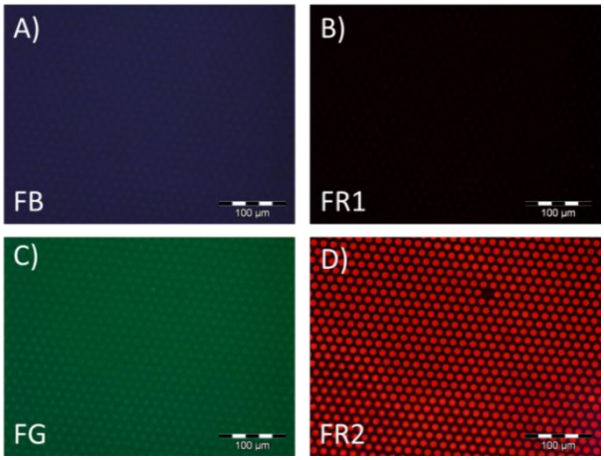

Figure 4.8. A-D) Fluorescence microscopy images after µCP of alkyne-modified biotin and 1 h incubation with 0.6 µM **Cy5-SAv** in PBS. FB: λ_{exc} = 350 nm, λ_{em} > 420 nm; FG: λ_{exc} = 460 nm, λ_{em} = 520 nm; FR=FR1: λ_{exc} = 510-550 nm, λ_{em} = 590 nm; FR2: λ_{exc} = 650 nm, λ_{em} = 670 nm.

In order to fabricate a triple protein pattern, the biotin-SAv interaction was combined with the dual protein pattern introduced above. To achieve a triple protein array such as that shown in the surface layout in Scheme 4.5, first the fluorogenic platform was prepared via reactive μCP of lines of the fluorogenic coumarin **1** on the azide monolayer, followed by immobilization of thiol-NTA in squares using a cross-μCP step. Subsequently, a dot-pattern of alkyne-biotin was cross-microcontact printed onto the remaining areas of azide groups on the substrate. After the triple printing steps, three different proteins were immobilized consecutively (i) **^{G174C}TFP** via the direct Michael addition on the residual thiol-reactive coumarin tether (Figure 4.9C); (ii) **His$_6$-^{14}TagRFP-His$_6$** via formation of a supramolecular complex with NTA ligands in the presence of Ni^{2+} ions (Figure 4.9B); and (iii) **Cy5-SAv** via complexation with immobilized biotin (Figure 4.9D). As it can be seen from the merged fluorescent images (Figure 4.9E), the formation of blue fluorescent lines (Figure 4.9A) reports the successful direct immobilization of thiol-NTA and of **^{G174C}TFP** (Figure 4.9B and C) onto the fluorogenic tether. The incubation of the substrate with a solution of **His$_6$-^{14}TagRFP-His$_6$** in PBS resulted in selective, non-covalent immobilization of **His$_6$-^{14}TagRFP-His$_6$** solely on the NTA-functionalized cross-micro contact printed squares (Figure 4.9A and B). The successful immobilization of **Cy5-SAv** exclusively on the printed biotin dots is shown in Figure 4.10D.

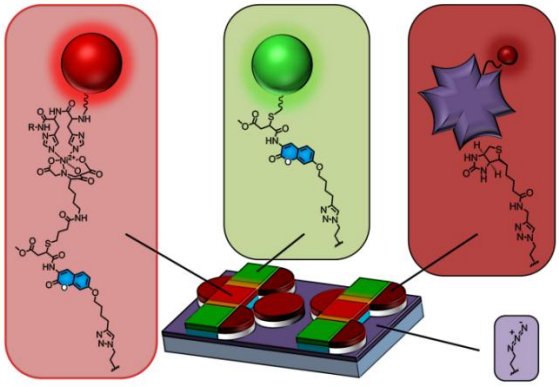

Scheme 4.5. Schematic representation of the triple protein array. The molecular structure of the NiNTA/His_6 complex represents one of the possible species formed upon interactions of a His_6-tag with a single NiNTA unit.

The overlay of the fluorescent images (Figure 4.9E) of the three individual immobilizations of the three different proteins on the same surface proves the expected localization of the proteins on the doubly cross-micro contact printed array. With the above series we could show that a) we were able to specifically immobilize three different proteins on different parts of a pattern on one substrate; b) the three methods of immobilization employed here

are orthogonal and specific with regard to their respective surface functionalities; c) triple μCP is a viable patterning technique for the fabrication of a triple protein array.

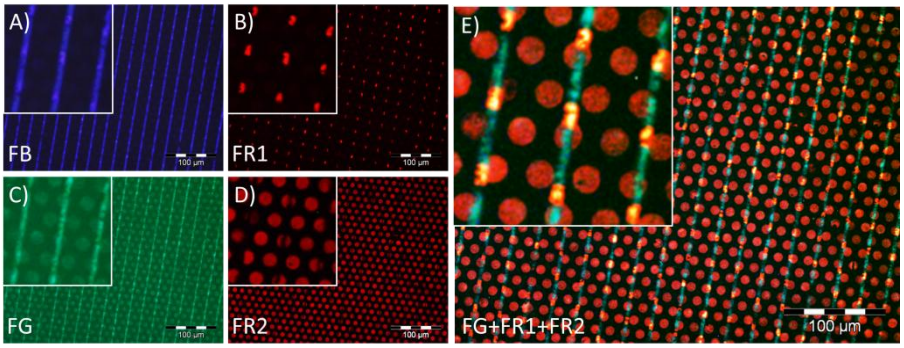

Figure 4.9. Fluorescence microscopy images A-D) after cross-micro contact printed thiol-NTA on the fluorogenic coumarin, μCP of alkyne-modified biotin and overnight incubation with ^{G174C}**TFP** solution, 1 h incubation with **His$_6$-^{14}TagRFP-His$_6$**:Ni^{2+} (1:2) and 1 h incubation with **Cy5-SAv**; E) merged image of FG, FR1 and FR2. FB/FG/FR (=FR1)/FR2 refer to blue (monitoring coumarin), green (monitoring TFP), red (monitoring RFP) and far-red (monitoring Cy5) channels, respectively.

4.3 Conclusions

A fluorogenic platform was employed to selectively immobilize, and fluorescently report on the immobilization of, thiol-containing, proteins and thiol-modified biomolecules. The fluorogenic platform proved to be an excellent tool to visualize the bond formation between biomolecule and surface, as well as the orthogonal immobilization at different parts of the patterned substrate. The flexibility of this approach will allow for the fabrication of specific protein patterns and represents an important achievement on the way towards establishing surfaces with differentiated responsive functions. Such interfaces can serve as additional tools for the study of cell-surface interactions in an orientationally controlled, multi-protein environment.

4.4 Acknowledgments

Dr. Dorothee Wasserberg is gratefully acknowledged for providing mutant fluorescent proteins, for her help with experiments and for fruitful discussions.

4.5 Experimental section

4.5.1 Materials

11-Bromoundecyltrichlorosilane (ABCR), sodium azide (Acros), L-cysteine (Sigma), *N,N*-bis(carboxymethyl)- L-lysine (Aldrich), tetrakis(acetonitrile)copper(I) hexafluorophosphate

(Aldrich), ethylenediaminetetraacetic acid (Sigma-Aldrich), γ-thiobutyrolactone (Aldrich) and 5,5′-dithiobis(2-nitrobenzoic acid) (Aldrich) were used as received.
(1S)-*N*-[5-[(4-Mercaptobutanoyl)-amino]-1-carboxypentyl]iminodiacetic acid (thiol-NTA),[25] tris-(benzyltriazolylmethyl)amine (TBTA),[26] propargyl-biotin[27] and compound **1**[16] were prepared as described in literature. Water was of MilliQ quality. Solvents were of p.a. grade unless stated otherwise.

4.5.2 Methods

Substrate and monolayer preparation. Microscope glass slides were used for monolayer preparation. The substrates were cleaned and activated with piranha solution for 45 min (concentrated H_2SO_4 and 33 % aqueous H_2O_2 in a 3:1 ratio; handle with care!) and rinsed with water. After drying in a stream of nitrogen, the substrates were used immediately to form a silanized monolayer. The substrates were immersed in 0.1 vol.% 11-bromoundecyltrichlorosilane in dry toluene for 45 min at room temperature. Following monolayer formation, the substrates were rinsed with toluene to remove any excess of silanes with ethanol and subsequently dried in a flow of nitrogen. The bromide/azide nucleophilic substitution was carried out by reacting with a saturated solution of NaN_3 in DMF for 48 h at 70 ^oC. The substrate were thoroughly rinsed with water and ethanol and gently dried in a flow of nitrogen.

Microcontact printing. Silicon masters were fabricated by photolithography. They consisted of micrometer-sized features (hexagonally arranged 10 µm diameter circular features separated by 5 µm or 5 µm wide lines separated by 15 or 20 µm) and were treated with 1H,1H,2H,2H-perfluoredecyltrichlrorosilane to facilitate separation of the PDMS from the master. Stamps were prepared by casting a 10:1 (v/v) mixture of poly(dimethylsiloxane) and curing agent (Sylgard 184, Dow Corning) onto a silicon master. After overnight curing at 60 ^oC, the stamps were oxidized by oxygen plasma for 10 s (power tuned to 50 mA) and subsequently inked by covering the stamp with an inking solution (1.5 mM **1** or propargyl-biotin (in CH_3CN), 0.5 mM $Cu(I)(CH_3CN)_4PF_6$ and 0.5 mM TBTA (CH_3CN/EtOH=2/1) (catalyst mixture), prepared by mixing 75 µL of 2 mM solution of **1** or propargyl-biotin in CH_3CN and 25 µL of 2 mM of catalyst mixture). After 4 min incubation, the stamps were dried in a stream of nitrogen and brought into conformal contact with the substrate for 60 min. The stamps were changed for each new printing, and the same inking procedure was used. After stamp removal, the printed substrates were rinsed with ethanol, sonicated in acetonitrile for 2 min, rinsed again with ethanol, gently dried with nitrogen and imaged with a fluorescence microscope.

Reactive contact printing of thiols. After immobilization of **1**, the platform was further reacted with thiols via a printing procedure. In the case of the immobilization of cysteine or thiol-NTA, an oxidized PDMS stamp was inked with a 10 mM thiol-NTA solution in PBS (pH 7.5) for 30 min. Stamps were gently dried in a stream of nitrogen and brought into conformal contact with substrates patterned with **1** for 10 min. The PDMS was carefully removed and substrates were washed via sonication in PBS and water.

Cloning of TagRFP and TFP variants for high-level expression. The following primers were used for PCR amplification of *TagRFP* using pTagRFP-C (purchased from Evrogen JSC) as DNA template: 5'-cgcggatccaatgagcgagctgattaaggagaacatgca-3' containing a unique BamHI restriction site (underlined) and 5'-cgcgaattccttgtgccccagtttgctag-3' containing a unique EcoRI restriction site (underlined). The PCR product was purified and digested with BamHI and EcoRI restriction enzymes (NEB) and ligated into pRSETB plasmid (Invitrogen) digested with the same restriction enzymes. pRSETB contains an N-terminal hexahistidine-tag (His_6-tag) for nickel-affinity purification. The resulting plasmid, pRSETB-TagRFP, was first transformed into *E. coli* (XL10 gold, Stratagene) using standard procedures in the presence of ampicillin (100 mg/L). pRSETB-TagRFP plasmid was transformed into *E. coli* BL21 pLysS using standard procedures in the presence of ampicillin (100 mg/L) and chloramphenicol (34 mg/L). Single colony transformants were selected and the pre-culture was grown overnight at 37 ^{o}C. This pre-culture was used to inoculate 2 L of LB medium containing ampicillin (100 mg/L) and chloramphenicol (34 mg/L) at 37 ^{o}C with shaking until an OD_{600} = 0.6 was reached. The culture was cooled to 16 ^{o}C before protein expression was induced with IPTG (isopropyl-D-thiogalactopyranoside) to a final concentration of 1 mM and incubated overnight at 16 ^{o}C. Cells were harvested by centrifugation at 4000x*g* at 4 ^{o}C for 20 min. The resulting cell pellet was resuspended for 20 min in BugBuster reagent with benzonase nuclease (Novagen) according to the supplier's instructions. The lysate was cleared by centrifugation at 16000x*g* for 30 min at 4 ^{o}C. Ni-NTA agarose beads (QIAGEN) were added to the protein supernatant at a 10:1 v/v ratio, respectively and incubated at 4 ^{o}C for at least 1 h with slow but continuous mixing. The agarose beads were filtered and washed with wash buffer (20 mM Tris buffer, 300 mM NaCl, 20 mM imidazole, pH 8.0) and eluted with elution buffer (20 mM Tris buffer, 300 mM NaCl, 1 M imidazole, pH 8.0). The purified protein fractions (~ 30 µM) were subsequently desalted using PD10 columns (GE Healthcare) into 0.1 x PBS (0.8 mM phosphate buffer (PB), 14.4 mM NaCl, 0.27 mM KCl, pH 7.4), aliquoted, snap-frozen in liquid nitrogen and stored at -80 ^{o}C. Proteins were characterized using SDS- and native PAGE, UV-Vis, steady state- and time-resolved fluorescence spectroscopy and MALDI-TOF mass spectrometry.[28]

For the insertion of a second, C-terminal His_6-tag, the *TagRFP* gene was amplified using 5'-cgcggatccaatgagcgagctgattaaggagaacatgca-3' (BamHI restriction site is underlined) and 5'-gcggaattcttagtggtggtggtggtggtgcttgtgccccagtttgcta-3' (EcoRI restriction site is underlined) as forward and reverse primers, respectively, and pRSETB-TagRFP as DNA template. After PCR purification, the gene product and pRSETB-TagRFP were digested sequentially, first with EcoRI, then BamHI according to the manufacturer's instructions. DNA ligations were performed using T4-ligase (NEB) at 16 ^{o}C overnight and the resulting pRSETB-TagRFP-His_6 plasmid was transformed into *E. coli* XL10 gold competent cells according to standard procedures.

pRSETB-TagRFP-His_6 plasmid was transformed into *E. coli* BL21 pLysS in the presence of ampicillin (100 mg/L) and chloramphenicol (34 mg/L). Single colony transformants were selected and the pre-culture was grown overnight at 37 ^{o}C. The pre-culture was used to inoculate 2 L cultures of *E. coli* BL21 pLysS cells, which were grown at 37 ^{o}C to OD_{600} = 0.6 before protein expression was induced upon addition of IPTG to a final concentration of 1 mM (left overnight, 16 ^{o}C). The cells were harvested by centrifugation (4000x*g*, 20 min) and lysed using BugBuster (as described above). Protein purification and characterisation of the N- and C-terminal (doubly) His_6-tagged TagRFP (His_6-TagRFP-His_6) was carried out as described for His_6-TagRFP.[28]

By site-directed mutagenesis (QuikChange Multi kit, Stratagene Technologies), selected mutations were introduced into pRSETB-TagRFP (both, singly and doubly His_6-tagged TagRFP) using the following primers: C222S forward: 5'-ggctgtggccagatactccgacctccc-3'; reverse: 5'-gggaggtcggagtatctggccacagcc-3' and C114S forward: 5'-gcctccaggacggctccctcatctacaac-3' and reverse: 5'-gttgtagatgagggagccgtcctggaggc-3'.

The mutant variants were expressed and purified under the same conditions as for the wild-type protein, to yield His_6-TagRFP and His_6-TagRFP-His_6. Mutations C222S and C114S yielded mutants '^{14}TagRFP' containing no accessible cysteine residues. Characterisation by SDS- and native PAGE, UV-Vis, steady state and time-resolved fluorescence spectroscopy and MALDI-TOF mass spectrometry were carried out and the mutants showed no discernible differences in their photophysical properties to the wild type, thus indicating that their overall structure upon site-directed mutagenesis is retained.[28]

For monomeric teal fluorescent protein TFP, the following primers were used for PCR amplification using pET15b-TFP (kindly provided by Rik Rurup, University of Twente, The Netherlands) as DNA template: 5'-ctccacggatccatggtgagcaagggcgag-3' containing a unique BamHI site (underlined) and 5'-ctccacgaattccttgtacagctcgtccatgc-3' containing a unique EcoRI restriction site (underlined). The PCR product was cloned into pRSETB as described

above resulting in pRSETB-TFP, lacking a His_6-tag due to a frameshift just before the inserted gene. Site-directed mutagenesis was carried out to yield pRSETB-^{G174C}TFP using the above protocol and the following primers: forward 5'-tgctggagggctgcggccaccac-3' and reverse 5'-gtggtggccgcagccctccagca-3'.

Purification of TFP and ^{G174C}TFP were carried out using an Äkta FPLC system with a 5 mL ResourceQ anion exchange chromatography column (GE Healthcare) according to the manufacturer's instructions using sterile filtered wash buffer (40 mM PB, pH 8.0) and elution buffer (40 mM PB, 1 M NaCl pH 8.0). Both proteins were characterized using the same techniques as mentioned above.[28]

Protein immobilization. Substrates patterned with **1**, further reacted with thiol-NTA and then incubated in a solution of 1 µM ^{14}TagRFP and 2 µM $NiCl_2$ in PBS buffer for 30 min. Substrates were rinsed with PBS containing 0.01% of surfactant Tween-20 for 1 h, with water and dried in a stream of nitrogen. The selectivity and reversibility was tested via incubation in a 10 mM EDTA solution in PBS overnight. Substrates patterned with **1** were incubated in a 20 µM cysteine-containing ^{G174C}TFP (or the native TFP or the ^{G174C}TFP conjugate with Ellman's reagent) overnight. Samples were then rinsed in PBS containing 0.01% of surfactant Tween-20 for 2 h, with water and dried in a stream of nitrogen prior to fluorescence microscopy imaging.

The free thiol group (after overnight reduction using 1 mM DTT and its subsequent removal with Zebaspin desalting columns, MWCO 7000, Thermo Fisher) of the cysteine-containing ^{G174C}TFP was converted to disulfide groups by the use of the Ellman's reagent (5,5'-dithiobis-(2- nitrobenzoic acid) or DTNB). 20 µM Solutions of ^{G174C}TFP and, as negative control, TFP were reacted overnight with 2 mM DTNB in 40 mM PB, pH 7.8, and subsequently desalted using Zebaspin desalting columns to remove by-products (in particular to separate the protein from 5-thio-2-nitrobenzoic acid that, as it contains a free thiol group, would react with the thiol-sensitive coumarin on the surface). Substrates patterned with propargyl-biotin were incubated in a 0.6 µM Cy5-labelled streptavidin in PBS (pH 7.4) for 30 min and washed with PBS containing 0.01% of Tween-20 for 1 h.

4.5.3 Equipment

Fluorescence microscopy. Fluorescence microscopy images were taken using an Olympus inverted research microscope IX71 equipped with a mercury burner U-RFL-T as light source and a digital Olympus DR70 camera for image acquisition. For UV excitation and blue emission imaging a standard DAPI Olympus filter cube was used to image the fluorogenic platform. A standard Cy5 Olympus filter cube was used to image emission of Cy5-labelled

streptavidin and Olympus filter cubes with appropriate band pass and long pass filters for TFP (excitation 460 nm, emission 490 nm) and TagRFP (excitation 555 nm, emission 580 nm) imaging were used. All fluorescence microscopy images were acquired on dry samples using a 20x Fluorplan objective from Olympus. Filter settings used: λ_{exc} = 350 nm, λ_{em} > 420 nm (FB); λ_{exc} = 460 nm, λ_{em} = 520 nm (FG); λ_{exc} = 510-550 nm, λ_{em} = 590 nm, (FR=FR1); λ_{exc} = 650 nm, λ_{em} = 670 nm (FR2).

Mass spectra. ESI-ToF-MS spectra were recorded using a LCT Mass spectrometer (Waters/Micromass). Protein masses were determined using a BioSystems, VoyagerII MALDI-ToF mass spectrometer using sinapinic acid as matrix.

NMR. ^{1}H and ^{13}C NMR spectra were recorded on a Varian Unity (300MHz) spectrometer. ^{1}H and ^{13}C chemical shifts values, δ (in ppm) at 300 MHz and 75 MHz, respectively, are reported using the residual solvent as internal standard.

4.6 References

(1) For reviews see for example: a) Weinrich, D.; Jonkheijm, P.; Niemeyer, C.M.; Waldmann, H. *Angew. Chem., Int. Ed.* **2009**, *48*, 7744; b) Kingsmore, S.F. *Nat. Rev. Drug Discovery*, **2006**, *5*, 310; c) Dufva, M.; Christensen, C. B. *Experts Rev. Proteomics*, **2005**, *2*, 41; d) Zhu, H.; Snyder, M. *Curr. Opin. Chem. Biol.* **2003**, *7*, 55.

(2) For reviews see for example: a) Y.-X. Chen, G. Triola, H. Waldmann, *Acc. Chem. Res.* **2011**, *44*, 762; b) Wong, L. S.; Khan, F.; Micklefield, J. *Chem. Rev.* **2009**, *109*, 4025; c) Jonkheijm, P.; Weinrich, D.; Schroeder, H.; Niemeyer, C.M.; Waldmann, H. *Angew. Chem. Int. Ed.* **2008**, *47*, 9618.

(3) For a feature article see for example: Ganesan, R.; Kratz, K.; Lendlein, A. *J. Mater. Chem.* **2010**, *20*, 7322.

(4) For examples see: a) Soellner, M.B.; Dickson, K.A.; Nilsson, B.L.; Raines, R.T. *J. Am. Chem. Soc.* **2003**, *125*, 11790; b) Watzke, A.; Koehn, M.; Gutierrez-Rodriguez, M.; Wacker, R.; Schroeder, H.; Breinbauer, R.; Kuhlmann, J.; Alexandrov, K.; Niemeyer, C.N.; Goody, R.S.; Waldmann, H. *Angew. Chem. Int. Ed.* **2006**, *45*, 1408; c) de Araujo, A.D.; Palomo, J.M.; Cramer, J.; Kohn, M.; Schroder, H.; Wacker, R.; Niemeyer, C.; Alexandrov, K.; Waldmann, H. *Angew. Chem. Int. Ed.* **2006**, *45*, 296; d) Duckworth, B.P.; Xu, J.H.; Taton, T.A.; Guo, A.; Distefano, M. *Bioconjugate Chem.* **2006**, *17*, 967; e) Lin, P.C.; Ueng, S.H.; Tseng, M.C.; Ko, J.L.; Huang, K.T.; Yu, S.C.; Adak, A.K.; Cheng, Y.J.; Lin, C.C. *Angew. Chem. Int. Ed.* **2006**, *45*, 4286; f) Govindaraju, T.; Jonkheijm, P.; Gogolin, L.; Schroeder, H.; Becker, C.F.W.; Niemeyer, C.M.; Waldmann, H. *Chem. Commun.* **2008**, 3723; g) Christman, K.L.; Broyer, R.M.; Tolstyka, Z.P.; Maynard, H.D. *J. Mater. Chem.* **2007**, *17*, 2021. h) Lempens, E.H.E.; Helms, B.A.; Merkx, M.; Meijer, E.W. *ChemBioChem*, **2009**, *10*, 658; i) Zhang, K.; Diehl, M.R.; Tirrell, D.A. *J. Am. Chem. Soc.*, **2005**, *127*, 10136; j) Weinrich, D.; Lin, P.C.; Jonkheijm, P.; Nguyen, U.T.T.; Schroder, H.; Niemeyer, C.M.; Alexandrov, K.; Goody, R.S.; Waldmann, H. *Angew. Chem. Int. Ed.*, **2010**, *49*, 1252; k) Hodneland, C.D.; Lee, Y.-S.; Min, D.-H.; Mrksich, M.

Proc. Natl. Acad. Sci. USA, **2002**, *99*, 5048. l) Kindermann, M.; George, N.; Johnsson, N.; Johnsson, K. *J. Am. Chem. Soc.* **2003**, *125*, 7810.

(5) For examples see: a) Becker, C.F.W.; Wacker, R.; Bouschen, W.; Seidel, R.; Kolaric, B.; Lang, P.; Schroeder, H.; Mueller, O.; Niemeyer, C.M.; Spengler, B.; Goody, R.S.; Engelhard, M. *Angew. Chem. Int. Ed.* **2005**, *44*, 7635; b) Hutschenreiter, S.; Tinazli, A.; Model, K.; Tampé, R. *EMBO J.* **2004**, *44*, 2488; c) Kwon, Y.; Coleman, M.A.; Camarero, J.A. *Angew. Chem. Int. Ed.* **2006**, *45*, 1726; d) Escalante, M.; Zhao, Y.; Ludden, M.J.W.; Vermeij, R.; Olsen, J.D.; Berenschot, E.; Hunter, C.N.; Huskens, J.; Subramaniam, V.; Otto, C. *J. Am. Chem. Soc.* **2008**, *130*, 8892; e) Hwang, I.; Baek, K.; Jung, M.; Kim, Y.; Park, K.M.; Lee, D.-W.; Selvapalam, N.; Kim, K. *J. Am. Chem. Soc.* **2007**, *129*, 4170; f) Young, J.F.; Nguyen, H.D.; Yang, L.; Huskens, J.; Jonkheijm, P.; Brunsveld, L. *ChemBioChem.* **2010**, *11*, 180.

(6) Li, Y.; Niehaus, J. C.; Chen, Y.; Fuchs, H.; Studer, A.; Galla, H.-J.; Chi, L. *Soft Matter* **2011**, *7*, 861.

(7) a) Vong, T.; ter Maat, J.; van Beek, T. A.; van Lagen, B.; Giesbers, M.; van Hest, J. C. M.; Zuilhof, H. *Langmuir* **2009**, *25*, 13952; b) del Campo, A.; Boos, D.; Spiess, H. W.; Jonas, U. *Angew. Chem. Int. Ed.* **2005**, *44*, 4707; c) Xu, H.; Hong, R.; Lu, T.; Uzun, O.; Rotello, V. M. *J. Am. Chem. Soc.* **2006**, *128*, 3162; d) Sato, H.; Miura, Y.; Saito, N.; Kobayashi, K.; Takai, O. *Biomacromolecules* **2007**, *8*, 753; e) Pritchard, D. J.; Morgan, H.; Cooper, J. M. *Angew. Chem. Int. Ed.* **1995**, *34*, 91; f) Doh, J.; Irvine, D. J. *J. Am. Chem. Soc.* **2004**, *126*, 9170; g) Holden, M. A.; Cremer, P. S. *J. Am. Chem. Soc.* **2003**, *125*, 8074; h) Dubey, M.; Emoto, K.; Takahashi, H.; Castner, D. G.; Grainger, D. W. *Adv. Funct. Mater.* **2009**, *19*, 3046.

(8) a) Rozkiewicz, D. I.; Brugman, W.; Kerkhoven, R. M.; Ravoo, B. J.; Reinhoudt, D. N. *J. Am. Chem. Soc.* **2007**, *129*, 11593; b) Gupta, N.; Lin, B. F.; Campos, L. M.; Dimitriou, M. D.; Hikita, S. T.; Treat, N. D.; Tirrell, M. V.; Clegg, D. O.; Kramer, E. J.; Hawker, C. J. *Nat. Chem.* **2010**, *2*, 138.

(9) Christman, K. L.; Schnopf, E.; Broyer, R. M.; Li, R. C.; Chen, Y.; Maynard, H. D. *J. Am. Chem. Soc.* **2009**, *131*, 521.

(10) a) Salaita, K.; Wang, Y. H.; Mirkin, C. A. *Nat. Nanotechnol.* **2007**, *2*, 145; b) Paxton, W. F.; Spruell, J. M.; Stoddart, J. F. *J. Am. Chem. Soc.* **2009**, *131*, 6692; c) Wu, C. C.; Reinhoudt, D.N.; Otto, C.; Subramaniam, V.; Velders, A.H. *Small* **2011**, *7*, 989.

(11) a) Subramani, C.; Cengiz, N.; Saha, K.; Gevrek, T. N.; Yu, X.; Jeong, Y.; Bajaj, A.; Sanyal, A.; Rotello, V. M. *Adv. Mater.* **2011**, *23*, 3165; b) Im, S. G.; Bong, K. W. ; Kim, B.-S.; Baxamusa, S. H.; Hammond, P. T.; Doyle, P. S.; Gleason, K. K. *J. Am. Chem. Soc.* **2008**, *130*, 14424; c) Slocik, J. M.; Beckel, E. R.; Jiang, H.; Enlow, J.; Zabinski, J. S.; Bunning, T. J.; Naik, R. R. *Adv. Mater.* **2006**, *18*, 2095.

(12) a) Leibfarth, F. A.; Kang, M.; Ham, M.; Kim, J.; Campos, L. M.; Gupta, N.; Moon, B.; Hawker, C. J. *Nat. Chem.* **2010**, *2*, 207; b) Spruell, J. M.; Sheriff, B. A.; Rozkiewicz, D. L.; Dichtel, W. R.; Rohde, R. D.; Reinhoudt, D. N.; Stoddart, J. F.; Heath, J. R. *Angew. Chem. Int. Ed.* **2008**, *47*, 9927; c) Spruell, J. M.; Wolffs, M.; Leibfarth, F. A.; Stahl, B. C.; Heo, J.; Connal, L. A.; Hu, J.; Hawker, C. J. *J. Am. Chem. Soc.* **2011**, *133*, 16698; d) Wendeln, C.; Rinnen, S.; Schulz, C.; Kaufmann, T.; Arlinghaus, H. F.; Ravoo, B. J. *Chem. Eur. J.* **2012**, *18*, 5880; e) Deng, X.; Friedmann, C.; Lahann, J. *Angew. Chem. Int. Ed.* **2011**, *50*, 6522.

(13) For reviews see for example: a) Mager, M.D.; LaPointe, V.; Stevens, M.M. *Nat. Chem.* 2011, *3*, 582; b) Aida, T.; Meijer, E.W.; Stupp, S.I. *Science* 2012, *335*, 813; c) Fenske, T.; Korth, H.-G.; Mohr, A.; Schmuck, C. *Chem. Eur. J.* 2012, *18*, 738; d) Uhlenheuer, D.A.; Petkau, K.; Brunsveld, L. *Chem. Soc. Rev.* 2010, *39*, 2817.
(14) González-Campo, A.; Hsu, S.-H.; Puig, L.; Huskens, J.; Reinhoudt, D.N.; Velders, A.H. *J. Am. Chem. Soc.* 2010, *132*, 11434.
(15) For a recent review see: Wendeln, C.; Ravoo, B.J. *Langmuir* 2012, *28*, 5527.
(16) Nicosia, C.; Cabanas-Danés, J.; Jonkheijm, P.; Huskens, J. *ChemBioChem* 2012, *13*, 778.
(17) Newman, R.H.; Fosbrink, M.D.; Zhang, J. *Chem. Rev.* 2011, *111*, 3614.
(18) Balachander, N.; Sukenik, C.N. *Langmuir* 1990, *6*, 1621.
(19) Rozkiewicz, D.I.; Janczewski, D.; Verboom, W.; Ravoo, B.J.; Reinhoudt, D.N. *Angew. Chem. Int. Ed.* 2006, *45*, 5292.
(20) Yi, L.; Li, H.; Sun, L.; Liu, L.; Zhang, C.; Xi, Z. *Angew. Chem. Int. Ed.* 2009, *48*, 4034.
(21) Ai, H.; Henderson, J.N.; Remington, S.J.; Campbell, R.E. *Biochem. J.* 2006, *400*, 531.
(22) Sevier, C.S.; Kaiser, C.A. *Nat. Rev. Mol. Cell Biol* 2002, *3*, 836.
(23) Ellman, G.L. *Biochem. Biophys.* 1959, *82*, 70.
(24) Subach, O.M.; Malashkevich, V.N.; Zencheck, W.D.; Morozova, K.S.; Piatkevich, K.D.; Almo, S.C.; Verkhusha, V.V. *Chem. Biol.* 2010, *17*, 333.
(25) Du Roure, O.; Debiemme-Chouvy, C.; Malthête, J.; Silberzan, P. *Langmuir* 2003, *19*, 4138.
(26) Chan, T.R.; Hilgraf, R.; Sharpless, K.B.; Fokin, V.V. *Org. Lett.* 2004, *6*, 2853.
(27) He, B.; Velaparthi, S.; Pieffet, G.; Pennington, C.; Mahesh, A.; Holzle, D.L.; Brunsteiner, M.; van Breemen, R.; Blond, S.Y.; Petukhov, P.A. *J. Med. Chem.* 2009, *52*, 7003.
(28) Wasserberg, D.; Cabanas-Danés, J.; Huskens, J.; Subramaniam, V.; Jonkheijm, P. manuscript in preparation.

Chapter 5

"If you have things that are cheap enough, people will find uses for them, even if they seem very primitive. For example: stones. You can build cathedrals out of stones" — George M. Whitesides, Toward a science of simplicity.

Electrochemical gradients for monitoring reactivity at surfaces in space and time*

Studying and controlling reactions at surfaces is of great fundamental and applied interest in, amongst others, biology, electronics and catalysis. Because reaction kinetics is different at surfaces compared to solution, frequently, solution characterization techniques cannot be used. This chapter presents solution gradients, prepared by electrochemical means, for controlling and monitoring reactivity at surfaces in space and time. As a proof of principle, electrochemically derived gradients of a reaction catalyst (Cu(I)) have been employed to make surface gradients on the micron-scale and to study the kinetics of the ligand-free, surface-confined copper(I)-catalyzed azide-alkyne 1,3-dipolar cycloaddition.

*Part of this chapter has been published in: S. O. Krabbenborg, C. Nicosia, P. Chen, J. Huskens, *Nat. Commun.* **2013**, 4, 1667.

5.1 Introduction

Chemical reactions at surfaces are of great fundamental and applied interest, for example in biology,[1,2] electronics[3] and catalysis.[4-6] Investigating and monitoring reactivity is therefore of paramount importance[7-9] to evaluate a surface reaction's scope and applicability. Monolayers are an excellent platform to investigate interfacial reactions and reactivity because of the ability to precisely control surface composition.[7,10-13] Because reaction kinetics is different at surfaces compared to solution, frequently, solution characterization techniques cannot be used.

Gradients of physicochemical properties, i.e. their continuous variation in space and/or time, are of great value both in solution and on surfaces for many applications and systems, such as for the screening of catalysts[14,15] and biomaterials,[16] and for studying dynamic phenomena such as the chemotaxis of cells[17] and the motion of water droplets[12] or molecules.[18] Many methods have been developed to create static surface gradient patterns on the (sub)mm lengthscale.[19] For the (sub)µm lengthscale, not many methods are available to produce such gradients, which would be worthwhile from the perspective of, for example, studying the motion of individual (bio)molecules and the investigation and screening of nanomaterials. None of the existing (sub)µm gradient methods is compatible with switching on/off or dynamically changing gradient properties in time, which has been done at the sub-mm lengthscale for biological surfaces[20] to study cell chemotaxis.[21]

This chapter presents solution gradients, prepared by electrochemical means, for controlling and monitoring reactivity at surfaces in space and time in a high-throughput manner. Because the solution gradient provides a tunable and intrinsically predictable, spatial concentration variation of a chemically reactive species, and therefore of the reaction parameter, the reaction yields micron-scale surface gradients and the kinetic data is directly correlated to a kinetic model of the surface reaction at hand. In this way, not only kinetic rate constants are obtained, but their spatial variation is directly visualized, and translated into the reaction rate order.

5.2 Results and discussion

Scheme 5.1 shows a schematic overview of the setup, showing the dimensions and overall design. Platinum microelectrode arrays on glass were fabricated using a bilayer lift-off procedure based on a standard photolithographic technique. The glass surface of the platinum microelectrode array on glass was modified by using silane chemistry to prepare an azide monolayer.[22] As a proof of principle, electrochemically derived gradients of the concentration of a homogeneous catalyst (Cu(I)) were employed to make surface gradients on the micron-scale and to study the kinetics of the (surface-confined) copper(I)-catalyzed

azide-alkyne 1,3-dipolar cycloaddition (CuAAC; "click" reaction). Since the introduction of Cu(I) catalysis,[23,24] the Huisgen 1,3-dipolar cycloaddition reaction of organic azides and alkynes, has obtained substantial attention.[25,26] Owing to its high yield, orthogonality and chemoselectivity,[27] it is a useful reaction for surface functionalization.[28]

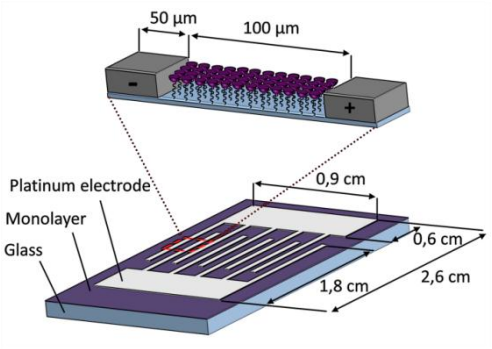

Scheme 5.1. Schematic overview of the setup showing the dimensions and overall design of the interdigitated electrode array, with which the electrochemically derived gradients are formed.

The schematic representation of the system used for the CuAAC reaction is illustrated in Scheme 5.2. A [Cu(I)] gradient is applied on top of the azide-terminated silane layer that is attached to the glass substrate areas between the electrodes of the interdigitated electrode array. The Cu(I) catalyst is formed in-situ by a one-electron reduction of already present Cu(II),[29] at the cathode (source), while oxidation of the generated Cu(I) back to Cu(II) at the anode (sink) makes sure a stable gradient is formed. The solution gradient of [Cu(I)] is then exploited in the electrochemically activated CuAAC ("e-click") of an alkyne from solution to the azide monolayer resulting in a surface gradient. The reaction is monitored ex-situ via immobilization of an alkyne-modified fluorescein (**1**) onto the azide-terminated monolayer. The rate of this reaction is expected to be highest close to the cathode, at which electrode the reduction of Cu(II) to Cu(I) is expected to occur.

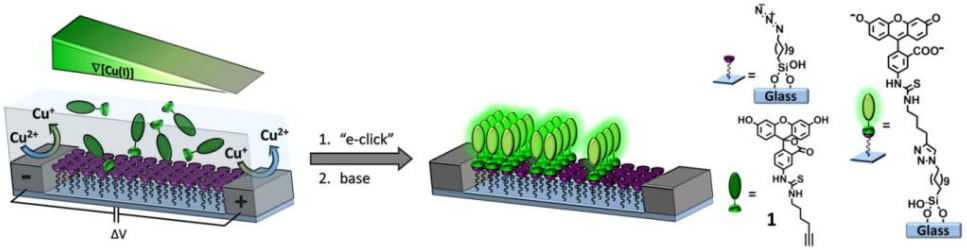

Scheme 5.2. Schematic representation of the electrochemical generation of a [Cu(I)] gradient in solution between the electrodes of an interdigitated electrode array, obtained via the reduction of Cu(II) to Cu(I) and oxidation of the resulting Cu(I) to Cu(II) at the cathode and anode, respectively. This solution gradient is transferred to a surface gradient by means of the electrochemically activated click reaction of a fluorescein-labeled alkyne to an azide monolayer, resulting in a surface-bound fluorescein dye gradient.

Figure 5.1 shows the fluorescence microscopy images of the resulting micron-scale surface gradients after different reaction times, showing clearly the highest intensity, and thus coverage, near the cathode where the electrochemically produced [Cu(I)] is higher. When the reaction was performed using the same conditions but without Cu(II) present in the solution, no reaction occurred.

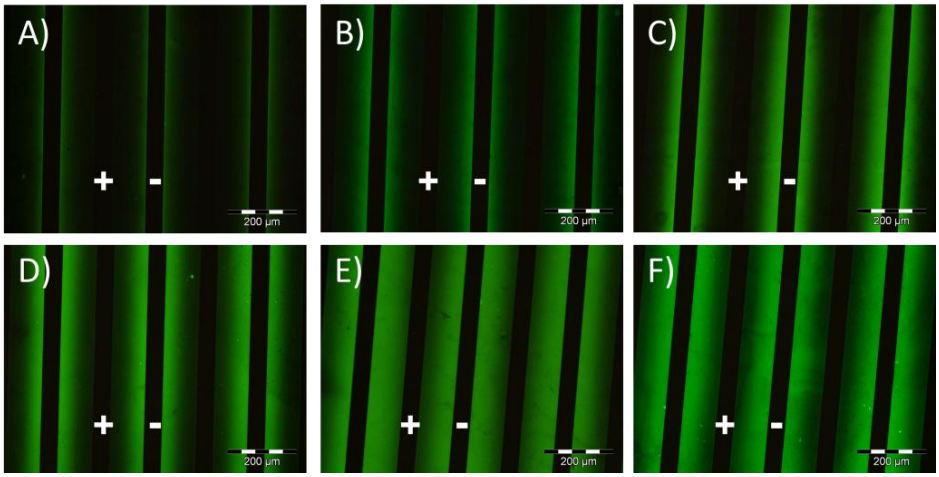

Figure 5.1 Fluorescence microscopy images of the surface gradients fabricated via electrochemically activated CuAAC by using a solution of 1 mM alkyne-modified fluorescein **1** and 1 mM $CuSO_4$ in DMSO upon application of 1.0 V potential difference between the electrodes at different reaction times: A) 1 min; B) 2 min; C) 3 min; D) 4 min; E) 5 min; F) 6 min. λ_{ex} = 460-490 nm, λ_{em} > 520 nm, exposure time 400 ms.

All fluorescence microscopy images (an example batch is shown in Figure 5.1) were analyzed with ImageJ,[30] by extracting cross sections with averaging over 100 µm parallel to the electrode, resulting in fluorescence vs. distance data. Because the dye solution on top of the electrodes prevented us to work in-situ, images were processed ex-situ, and, therefore, a different substrate was used for each reaction time. The cross sections were aligned by the electrode positions. Figure 5.2 shows averaged, normalized fluorescence intensity profiles from four different batches, showing the good reproducibility of this new surface gradient fabrication method. The fluorescence intensity profiles vs. distance from the cathode, illustrated in Figure 5.2, show the increase of coverage upon prolonged reaction times. These profiles confirm that, close to the cathode (high [Cu(I)]), the fluorescence intensity increases more rapidly than near the anode (low [Cu(I)]).

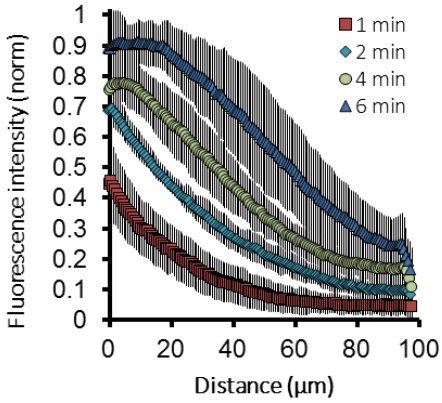

Figure 5.2. Reproducibility of the click gradients. Averaged, normalized fluorescence intensity profiles vs. distance from the cathode showing the reproducibility of the resulting dye gradient for different reaction times, with ± 1 standard deviation from four different batches. All different batches had the same reaction conditions, 1.0 mM fluorescein alkyne, 1.0 mM $CuSO_4$ salt in DMSO, ΔV = 1 V.

Figure 5.3A shows fluorescence intensity profiles vs. distance from the cathode of a representative batch of ex-situ samples (Figure 5.1) at varying reaction times. The fluorescence vs. distance data was plotted vs. time, each at specific distances from the negative electrode (Figure 5.3B).

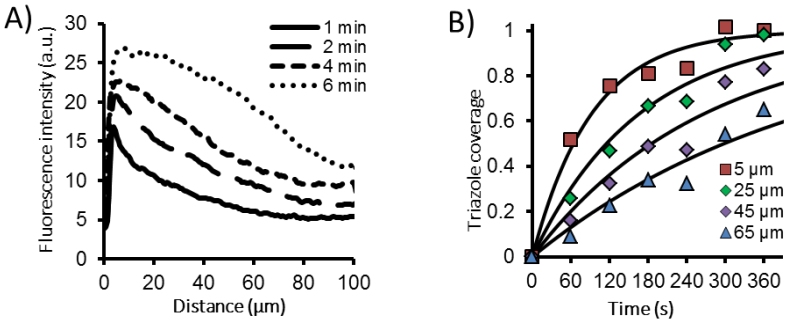

Figure 5.3. A) Fluorescence intensity profiles vs. distance from the cathode visualizing the resulting dye gradient for different reaction times (raw data, obtained ex-situ). B) Data and exponential fits ($I(t) = 1\text{-}e^{-k_{obs}t}$) of the surface-confined e-click reaction at some characteristic distances from the cathode (high [Cu(I)]) for a single batch of samples.

Since the alkyne in solution is present in excess, a first-order dependence on surface-bound azide is expected as well as a second-order dependence on [Cu(I)] (eq. 1).[31]

$$rate = k\,[\text{alkyne}]^2\,[\text{azide}]\,[\text{Cu(I)}]^2 = k_{obs}[\text{azide}] \qquad (1)$$

where k is the reaction rate constant ($m^{12}/(s*mol^4)$), and [alkyne], [azide] and [Cu(I)] are the concentrations of alkyne (mol/m^3), azide (mol/m^2) and Cu(I) (mol/m^3) respectively.

At each specific distance from the cathode we assume [Cu(I)] to be constant, because the [Cu(I)] gradient is relatively stable after 30 s as indicated by modelling (Figure 5.4A) and by the stable current plateau of 1.5 µA from 1 min onward found via amperometric *I-t* measurements (Figure 5.4C). Thus the asymptotic enhancement of fluorescence is directly correlated with the decrease in [azide] and concomitant increase in [triazole] at the surface.

Therefore, k_{obs} is assumed to be the pseudo first-order (in [azide]) rate constant of the e-click reaction (eq. 2):

$$I(t) = 1 - e^{-k_{obs}t} \qquad (2)$$

where I is the normalized fluorescence intensity at time t (s) and k_{obs} is the pseudo first-order rate constant (s^{-1}).

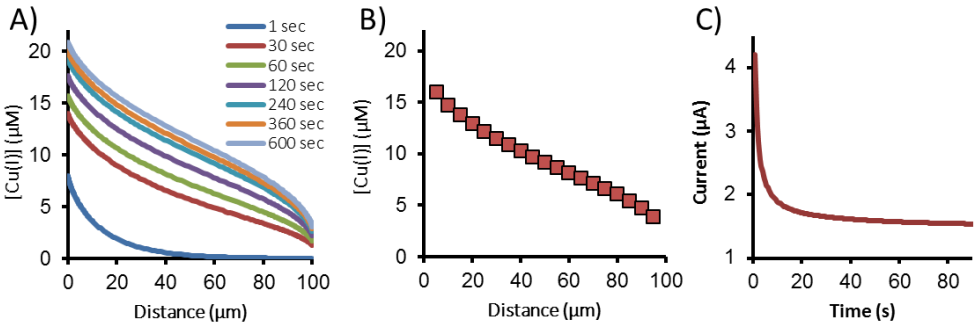

Figure 5.4 A) Development of the Cu(I) solution gradient in between the interdigitated electrodes in time using a finite element model (see Methods, 5.5.4 Finite element modeling, below), showing that the gradient is nearly linear and has a stable shape from 30 s onwards. B) Time-averaged Cu(I) gradient from the time dependence shown in 5.4A. Modeled Cu(I) concentration values were quadratically averaged (to account for the theoretically expected second order rate constant), with a 1 s time step for a total of 360 s. This also shows the negligible influence of the startup of the gradient, at the timescale of the reaction. The average gradient shown here is used for the rate order determination. C) Amperometric *I-t* curve measured while applying 1.0 V potential difference between the electrodes for generating the [Cu(I)] gradient, showing that the current, and thus the [Cu(I)] gradient, does not change significantly after 30 s.

Figure 5.5A shows the resulting k_{obs} values vs. distance from the cathode after averaging the k_{obs} values obtained from four different batches. Because Cu(I) is generated at the cathode, k_{obs} is, as expected, the highest close to the cathode, with a difference of more than an order of magnitude compared to values near the anode. The parabolic profile observed in Figure 5.5A directly visualizes the expected second-order dependence on [Cu(I)]. A finite-element model was set up to estimate the [Cu(I)] gradient and to compare a surface reaction model with the experimental results. The resulting average [Cu(I)] solution

gradient, Figure 5.4B, was used to determine the rate order of Cu(I) in the e-click reaction. Comparison of the experimentally determined k_{obs} (data points, Figure 5.5A) vs. the k_{obs} (k'[Cu(I)]^2 where k' = k[alkyne]^2, see eq. 1) of the finite element simulation (red line, Figure 5.5A), shows good overlap. This confirms that the model includes the most important factors influencing the gradient formation.

Figure 5.5B shows a plot of ln(k_{obs}) vs. ln([Cu(I)]), for data of the first 90 µm (only the last data point was excluded because it was evidently deviating from the linear fit, possibly due to less accurate determination of the conversion in the low conversion regime). The linear fit of this data results in a slope of 2.06 ± 0.07 (R^2 = 0.98), confirming the second-order dependence on [Cu(I)], which is consistent with the literature.[31]

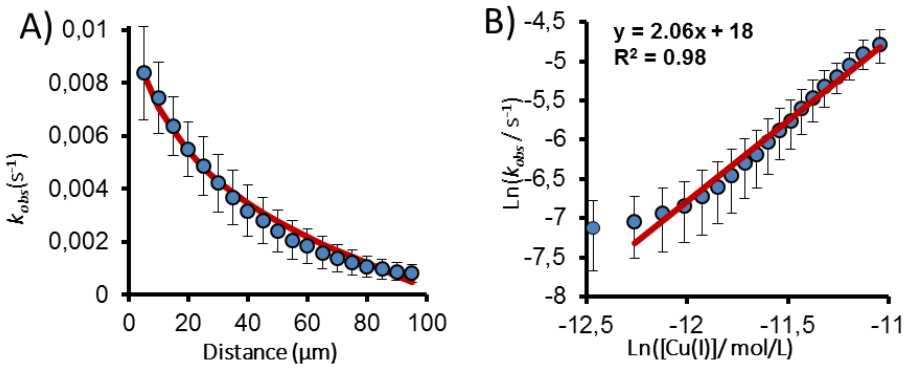

Figure 5.5 A) Resulting (averaged; ± 1 standard deviation) values of the pseudo-first-order rate constant, k_{obs}, of the e-click reaction vs. distance from the cathode. Experimentally determined k_{obs} (data points) were compared with k_{obs} (k'*[Cu(I)]^2) of the finite element simulation (red line), showing good overlap. B) Rate order plot of ln(k_{obs}) vs. modeled ln([Cu(I)]) values showing a second-order rate dependence on Cu(I).

5.3 Conclusions

In conclusion, we have shown an electrochemical method for the fabrication of micron scale surface gradients. A solution gradient of a catalytic species (Cu(I)) was used to study the chemical reactivity of the CuAAC reaction at the surface. As a proof of principle, 1D gradients were used and the detection was done with a fluorescence microscope, but this can potentially be extended to orthogonal gradients, varying two parameters in one experiment, and other surface characterization techniques (e.g. Raman spectroscopy) to remove the constraint of a fluorescent dye present. Furthermore, this method can also be extended to investigate the influence of substrate or reagent concentration by a static surface or solution gradient respectively. It may even be possible to study reactions in a dynamic fashion, by controlling the solution gradient in time. Optimal use of the method of reactivity mapping will allow the study of a wide range of reactions in which one or more

reaction parameters are varied in space and time, while it is envisioned that this method gives the possibility of identification of chemically reactive sites with high spatial resolution.

5.4 Acknowledgments

Sven O. Krabbenborg is gratefully acknowledged for the implementation of the modelling of the system, for the fabrication of the electrode arrays, for his help and fruitful discussions.

5.5 Experimental section

5.5.1 Materials

The following materials and chemicals were used as received without further purification: 11-bromoundecyltrichlorosilane (ABCR), sodium azide, hydrazine hydrate, (Sigma Aldrich), 6-fluorescein 5(6)-isothiocyanate (Sigma) chloro-1-hexyne, copper sulfate pentahydrate (Aldrich), potassium phthalimide (Fluka), HMDS (BASF), LOR 5A (MicroChem), Olin OiR 907-17 photoresist, Olin OPD 4262 developer (FujiFilm), rhodamine B ethylenediamine, 5-(aminoacetamido)fluorescein (Invitrogen). Alkyne-modified coumarin was prepared as described previously.[32]

5.5.2 Synthetic procedures

6-Phthalimido-1-hexyne and 6-amino-1-hexyne were prepared as described in the literature.[33]

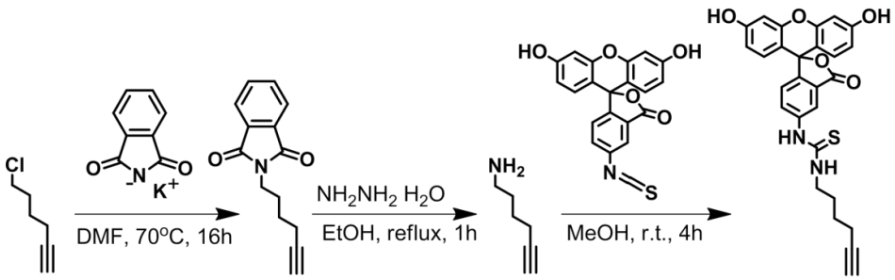

Scheme 5.3. Synthetic procedure for the synthesis of the alkyne-modified fluorescein.

6-Phthalimido-1-hexyne[33]

A suspension of potassium phthalimide (12.43 g, 67 mmol) and 6-chloro-1-hexyne (5 ml, 41 mmol) in 100 ml of dry DMF was stirred at 70 °C for 16 h. The solvent was evaporated and the solid residue was suspended in dichloromethane and filtered through a layer of silica gel 60. Evaporation of the solvent gave the pure product as a white powder (8.90 g, 39 mmol, 95%).

^{1}H-NMR (300 MHz, $CDCl_3$): δ (ppm) 7.83 (m, 2H, phthalimide), 7.70 (m, 2H, phthalimide), 3.71 (t, 2 H, $N_{phthalimide}$-CH_2), 2.25 (dt, 2H, CH_2CCH), 1.94 (t, 1H, CH_2CCH), 1.80 (m, 2H, $N_{phthalimide}$-CH_2CH_2), 1.57 (m, 2H, CH_2CH_2CCH).

^{13}C-NMR (300 MHz, $CDCl_3$): δ (ppm) 168.6, 131.1, 132.3, 123.4, 83.9, 69.0, 37.6, 27.7, 25.8, 18.2.

ESI-MS: measured 228.1 $[M+H]^+$, calculated 228.1 $[M+H]^+$.

6-Amino-1-hexyne[33]

Hydrazine monohydrate (3.2 ml, 66 mmol) was added to a solution of 6-phthalimido-1-hexyne (3,0 g, 13 mmol) in 150 ml of ethanol. The mixture was stirred under reflux for 1 h. After cooled to room temperature the solid was filtered and the solution was acidified to pH =1 by addition of concentrated HCl. The precipitate was filtered off, and aqueous 50% NaOH was carefully added to the solution until pH = 12. The mixture was extracted with CH_2Cl_2 (3 × 30 ml) and the combined organic fractions were dried over Na_2SO_4. Evaporation of the solvent gave the pure product as a light yellow oil (0.43 g, 4.4 mmol, 33%).

^{1}H-NMR (300 MHz, $CDCl_3$): δ (ppm) 2.58 (t, 2 H, NH_2CH_2), 2.08 (dt, 2H, CH_2CCH), 1.84 (t, 1H, CH_2CCH), 1.42 (m, 4H, $NH_2CH_2CH_2CH_2$), 1.20 (s, broad, NH_2).

^{13}C-NMR (300 MHz, $CDCl_3$): δ (ppm) 84.5, 68.6, 41.8, 32.7, 26.0, 18.5.

ESI-MS: measured 98.1 $[M+H]^+$, calculated 98.1 $[M+H]^+$.

N-(3',6'-Dihydroxy-3-oxospiro[isobenzofuran-1(3H),9'-[9H]xanthen]-5-yl)-*N'*-6-hexyn-1-ylthiourea, (alkyne-fluorescein 1)

Fluorescein isothiocyanate (0.38 mmol, 150 mg) and 6-amino-1-hexyne (0.46 mmol, 46 mg) were dissolved in dry methanol, and the mixture was stirred at room temperature for 4 h. Upon addition of dichloromethane, the product was precipitated from the solution as a dark yellow solid. The crude product was collected and recrystallized twice from dichloromethane to yield a dark yellow solid (164 mg, 84%).

^{1}H-NMR (300 MHz, CD_3OD): δ (ppm) 8.13 (s, 1H), 7.75 (d, 1H), 7.15 (d, 1H), 6.71-6.67 (m, 4H), 6.55 (d, 2H), 3.64 (t broad, 2H), 2.25(m, 3H), 1.78 (m, 2H), 1.61 (m, 2H).

^{13}C-NMR (300 MHz, CD_3OD): δ (ppm) 182.84, 171.46, 162.62, 154.62, 142.45, 130.57, 126.11, 120.44, 114.30, 111.91, 103.56, 84.74, 69.87, 45.11, 29.15, 27.06, 18.85

ESI-MS: measured 487.1212 $[M+H]^+$, calculated 487.1249 $[M+H]^+$.

UV/Vis: λ_{max} (carbonate buffer, pH 9) = 493 nm

Fluorescence: λ_{max} (carbonate buffer, pH 9) = 513 nm

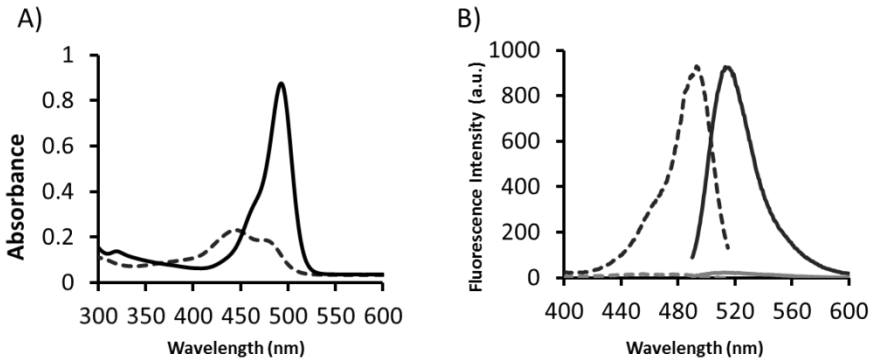

Figure 5.6 A) Absorption spectra of 10 µM alkyne-fluorescein **1** in buffer acetate at pH 4 (broken line) and in buffer carbonate at pH 9 (line). B) Emission (line, excitation at 464 nm) and excitation (broken line, emission at 540 nm) spectra of 0.1 µM alkyne-fluorescein in buffer acetate at pH 4 (grey lines) and in buffer carbonate at pH 9 (black lines).

5.5.3 Methods

Electrode fabrication. A bilayer lift-off recipe was used for fabricating the Pt electrode arrays on borofloat glass wafers. First the electrode pattern was created in a bilayer of sacrificial resist. The process started with a dehydration bake (5 min, 120 °C). Then a HMDS adhesion layer was spincoated (20 s, 5000 rpm), after which LOR 5A was spincoated (20 s, 5000 rpm) followed by a baking step (10 min, 160 °C). For the second resist layer, a standard photolithography recipe was used. First a HMDS adhesion layer was spincoated (5s, 500 rpm followed by 30 s, 4000 rpm). Then Olin OiR 907-17 photoresist was spincoated (5 s, 500 rpm followed by 30 s, 4000 rpm), followed by a pre-bake step (1 min, 95 °C). The photoresist was exposed (4 s, EVG EV620 Mask Aligner, Hg-lamp 12 $mW*cm^{-2}$) through a patterned photomask, followed by a post-exposure bake (1 min, 120 °C). Then the exposed photoresist was washed away and the LOR 5A layer was etched by developing in Olin OPD 4262 (90 s). The LOR 5A layer was overetched slightly, creating an undercut, which is favorable for the lift-off step. As a last step the wafer was rinsed with MQ water in a quickdump rinser.

Prior to metal deposition, the wafer was cleaned with UV-ozone (5 min, PR-100, UVP Inc.), guaranteeing a clean substrate. Immediately after this step, 5 nm Ti and 95 nm Pt was evaporated (BAK 600, Balzers), with a deposition rate between 1-3 $Å*s^{-1}$ (< 10^{-6} mbar). After the evaporation step, metal lift-off was performed by sonication in acetone (20 min) and

isopropanol (10 min). Afterwards, the wafer was rinsed with a quick dump rinser (DI water), followed by spin-drying. Then the wafer was diced (back-end dicing saw, Loadpoint Micro Ace 3) into appropriately sized samples which were cleaned prior to use, by sonicating in acetone, rinsing with ethanol and drying in a stream of N_2.

Electrochemically activated CuAAC. The procedure for the formation of azide monolayers was adopted from literature.[22] The glass substrates prepatterned with electrode arrays were activated by an oxygen plasma treatment (10 min, 50 mA, <200 mTorr). After the activation, the substrates were immersed in 0.1 vol% of 11-bromoundecyltrichlorosilane in dry toluene under argon atmosphere for 1 h at room temperature. Following monolayer formation, the electrodes were rinsed with toluene and ethanol to remove any excess of silanes, and blown dry with N_2. The bromide/azide nucleophilic substitution was carried out with a saturated NaN_3 solution in DMF for 48 h at 70 °C. The electrodes were thoroughly rinsed with MilliQ water and ethanol, and blown dry with N_2.

For performing "reactivity mapping" of the electrochemically activated CuAAC reaction on surfaces, the Cu(I) concentration was changed from high (cathode) to low (anode) by the following electrochemical reactions respectively:

$$Cu(II) + e^- \rightarrow Cu(I) \quad (3)$$

$$Cu(I) \rightarrow Cu(II) + e^- \quad (4)$$

This gradient in [Cu(I)] was generated by application of a potential difference of 1.0 V. Reactions with different reaction times were performed in silicone containers on top of the electrode array with 100 µl of a solution containing 1 mM alkyne-modified fluorescein and 1 mM $Cu(II)SO_4$ in DMSO. After the reaction, the electrodes were quickly rinsed with DMF and ethanol to avoid any further progress of the reaction, and blown dry with N_2. Prior to fluorescence characterization, all samples were dipped in a 50 mM borax solution at pH 10 for 1 min to assure the activation of the fluorescein dye.

5.5.4 Finite element modelling

The setup was modeled using the commercial Comsol Multiphysics finite element software (version 4.3). The geometry used is shown in Figure 5.7 and all values are summarized in Table 5.1. It is assumed that the reactions take place only locally and therefore only a part of the whole substrate is simulated. The gap (100 µm), with half a cathode and half an anode (25 µm, 0.1 µm thick), and 2000 µm of solution on top was modeled

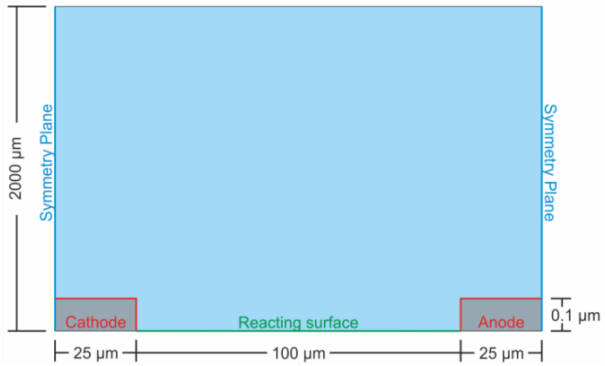

Figure 5.7. Geometry of the electrode system, reactive surface and top solution used in the finite element simulation. Assuming reaction to occur only between two local electrodes, the use of symmetry planes simplifies the calculation. The gap (100 µm), with half a cathode and anode (25 µm, 0.1 µm thick), and 2000 µm of solution on top was modeled. In between the electrodes a reacting surface (green line) is defined, where the e-click can take place.

At the cathode (Figure 5.7, two red lines), an influx of Cu(I), $N_{in,Cu}$ (in mol/(m^2*s)) is defined:

$$N_{in,Cu} = \frac{I}{A * F} \tag{5}$$

where I is the experimentally measured current (A) (Figure 5.4c), A is the electrode area (m^2) and F is the constant of Faraday (C*mol^{-1}).

At the anode (Figure 5.7, two red lines), an outflux of Cu(I), $N_{out,Cu}$ (in mol/(m^2*s)) is defined:

$$N_{out,Cu} = k_{ox} * [Cu(I)] \tag{6}$$

Where k_{ox} is the anodic rate constant (m/s) (determined from literature[35]) and [Cu(I)] is the Cu(I) concentration at the anode surface

The diffusion of the formed Cu(I) and alkyne in solution (Figure 5.7, blue area) was simulated using Fick's second law including a reaction rate term.

$$\frac{\partial c}{\partial t} = \nabla \cdot (D \nabla c) + R \tag{7}$$

The diffusion coefficients (D, in m^2/s) of Cu(I) and alkyne are adopted from similar values in water.[34-36]

Representative results of the simulation are shown in Figure 5.4A for the Cu(I) gradient at the reacting surface, which shows that the resulting gradient in between the electrodes is nearly linear and relatively stable from 30 s onwards.

At the reacting surface (Figure 5.7, green line) the surface bound azide can react with the dissolved alkyne, under the influence of Cu(I) to form triazole. The reaction is first order in azide, second order in Cu(I) and alkyne,[25,31] resulting in eq. (1).

Representative results of the simulation are shown in Figure 5.8 for the resulting e-click on the reacting surface. When comparing reaction rates (k_{obs}) of the experimental results and the simulation, as shown in Figure 5.5A, good overlap is seen, confirming that the model included the most important factors influencing the gradient formation.

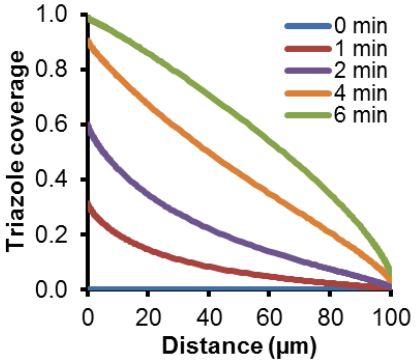

Figure 5.8 Modeling results of the click reaction. Finite element modelling results of the resulting normalized fluorescence intensities after different reaction times, at the reacting surface (Figure 5.8, green line).

Table 5.1. Summary of the values used for the finite element simulations.

Variable	Determined or estimated value / Units
Starting [alkyne]	1 mol/m^3
Bulk [alkyne]	1 mol/m^3
Starting [Cu(I)]	0 mol/m^3
Bulk [Cu(I)]	0 mol/m^3
Starting [azide]	~1*10^{-6} mol/m^2
Starting [triazole]	0 mol/m^2
Diffusion coefficients (Cu(I), alkyne)	~5*10^{-10} m^2/s
Anodic rate constant (k_{ox})	~1*10^{-4} m/s
Reaction rate constant (k)	32.69 m^{12}/(s*mol^4)
Electrode area (A)	8.225*10^{-5} m^2
Constant of Faraday (F)	96485,5 C/mol

5.5.5 Equipment

Fluorescence microscopy. Fluorescence microscopy images were taken using an Olympus inverted research microscope IX71 equipped with a mercury burner U-RFL-T as light source and a digital Olympus DR70 camera for image acquisition. Blue excitation (460 nm ≤ λ_{ex} ≤

490 nm) and green emission (λ_{em} > 520 nm) was filtered using the U-MWB2 Olympus filter. All fluorescence microscopy images acquired from the imine hydrolysis were taken with 100 µl of aqueous solution on top. The rest of the fluorescence microscopy images were acquired in air.

Mass spectra. ESI-MS mass spectra were recorded using an LCT Mass spectrometer (Waters/Micromass).

NMR. ^{1}H and ^{13}C NMR spectra were recorded on a Varian Unity (300 MHz) spectrometer. ^{1}H and ^{13}C chemical shifts values, measured at 300 MHz and 75 MHz, respectively, are reported as δ (in ppm) using the residual solvent signal as internal standard (7.26 ppm for $CDCl_3$ and 2.50 ppm for DMSO-d_6).

Electrical measurements and electrochemical reaction. The electrical current measurements were done with a Karl Süss probe station connected to a Keithley 4200 Semiconductor Characterization System.

The electrochemical reaction was performed using an ES015-10 power supply (Delta Elektronica) with voltage range from 0 to 15 V and current range from 0 to 10 A.

5.6 References

(1) N. Gupta, B. F. Lin, L. M. Campos, M. D. Dimitriou, S. T. Hikita, N. D. Treat, M. V. Tirrell, D. O. Clegg, E. J. Kramer, Craig J. Hawker, *Nat. Chem.* 2010, *2*, 138.

(2) Mrksich, M. *Acta Biomater.* 2009, *5*, 832.

(3) E. C. P. Smits, S. G. J. Mathijssen, P. A. van Hal, S. Setayesh, T. C. T. Geuns, K. A. H. A. Mutsaers, E. Cantatore, H. J. Wondergem, O. Werzer, R. Resel, M. Kemerink, S. Kirchmeyer, A. M. Muzafarov, S. A. Ponomarenko, B. de Boer, P. W. M. Blom, D. M. de Leeuw, *Nature* 2008, *455*, 956.

(4) D. W. Robbins, J. F. Hartwig, *Science* 2011, *333*, 1423.

(5) A. McNally, C. K. Prier, D. W. C. MacMillan, *Science* 2011, *334*, 1114.

(6) J. H. Clark, D. J. Macquarrie, *Chem. Soc. Rev*. 1996, *25*

(7) V. Chechik, R. M. Crooks, C. J. M. Stirling, *Adv. Mater.* 2000, *12*, 1161.

(8) X. Zhou, N. M. Andoy, G. Liu, E. Choudhary, K.-S. Han, H. Shen, P. Chen, *Nat Nanotech.* 2012, *7*, 237.

(9) S. Nunige, R. Cornut, H. Hazimeh, F. Hauquier, C. Lefrou, C. Combellas, F. Kanoufi, *Angew. Chem. Int. Ed.*, 2012, *51*, 5208.

(10) J. J. Gooding, S. Ciampi, *Chem. Soc. Rev.* 2011, *40*, 2704.

(11) T. J. Montavon, J. Li, J. R. Cabrera-Pardo, M. Mrksich, S. A. Kozmin, *Nat. Chem.* 2012, *4*, 45.

(12) M. K. Chaudhury, G. M. Whitesides, *Science* 1992, *256*, 1539.

(13) T. Gang, M.D. Yilmaz, D. Ataç, S.K. Bose, E. Strambini, A.H. Velders, M.P. de Jong, J. Huskens, and W.G. van der Wiel, *Nat. Nanotech.* 2012, *7*, 232.

(14) S. Jayaraman, A. C. Hillier, *J. Comb. Chem.* 2003, *6*, 27.
(15) S. Jayaraman, A. C. Hillier, *Meas. Sci. Technol.* 2005, *16*, 5.
(16) C. G. Simon, S. Lin-Gibson, *Adv. Mater.* 2011, *23*, 369.
(17) C. Wu, S. B. Asokan, M. E. Berginski, E. M. Haynes, N. E. Sharpless, J. D. Griffith, S. M. Gomez, J. E. Bear, *Cell* 2012, *148*, 973.
(18) A. Perl, A. Gomez-Casado, D. Thompson, H. H. Dam, P. Jonkheijm, D. N. Reinhoudt, Jurriaan Huskens, *Nat. Chem.* 2011, *3*, 317.
(19) J. Genzer, R. R. Bhat, *Langmuir* 2008, *24*, 2294.
(20) M. Mrksich, *MRS Bull*. 2005, *30*, 180.
(21) B. Meier, A. Zielinski, C. Weber, D. Arcizet, S. Youssef, T. Franosch, J. O. Rädler, D. Heinrich, *Proc. Natl. Acad. Sci.* 2011, *108*, 11417.
(22) N. Balachander, C. N. Sukenik, *Langmuir* 1990, 6, 1621.
(23) V. V. Rostovtsev, L. G. Green, V. V. Fokin, K. B. Sharpless, *Angew. Chem. Int. Ed.* 2002, *41*, 2596.
(24) C. W. Tornøe, C. Christensen, M. Meldal, *J. Org. Chem.* 2002, *67*, 3057.
(25) M. Meldal, C. W. Tornøe, *Chem. Rev.* 2008, *108*, 2952.
(26) V. D. Bock, H. Hiemstra, J. H. van Maarseveen, *Eur. J. Org. Chem.* 2006, *1*, 51.
(27) H. C. Kolb, M. G. Finn, K. B. Sharpless, *Angew. Chem. Int. Ed.* 2001, *40*, 2004.
(28) J. P. Collman, N. K. Devaraj, C. E. D. Chidsey, *Langmuir* 2004, *20*, 1051.
(29) A. J. D. Magenau, N. C. Strandwitz, A. Gennaro, K. Matyjaszewski, *Science* 2011, *332*, 81.
(30) C. A. Schneider, W. S. Rasband, K. W. Eliceiri, *Nat. Methods* 2012, *9*, 671.
(31) V. O. Rodionov, V. V. Fokin, M. G. Finn, *Angew. Chem. Int. Ed.* 2005, *44*, 2210.
(32) C. Nicosia, J. Cabanas-Danés, P. Jonkheijm, J. Huskens, *ChemBioChem* 2012, *13*, 778.
(33) D. I. Rozkiewicz, D. Janczewski, W. Verboom, B. J. Ravoo, D. N. Reinhoudt, *Angew. Chem. Int. Ed.* 2006, *45*, 5292.
(34) CRC Handbook of Chemistry and Physics, 92nd ed, internet version 2012.
(35) J. Małyszko, M. *J.* Scendo, *Electroanal. Chem. Interfac.* 1988, *250*, 61.
(36) T. S. Hansen, J. U. Lind, A. E. Daugaard, S. Hvilsted, T. L. Andresen, N. B. Larsen *Langmuir* 2010, *26*, 16171.

Chapter 6

"The true delight is in the finding out rather than in the knowing." — Isaac Asimov.

Shape-controlled fabrication of micron-scale surface chemical gradients via electrochemically activated copper(I) "click" chemistry*

We report an electrochemical method for the shape-controlled fabrication of micron-scale surface-bound chemical gradients. The approach is based on employing platinum microelectrode arrays on glass, for the establishment of a Cu(I) solution gradient via local electrochemical reduction of Cu(II) (cathodic reaction), and oxidation of the generated Cu(I) back to Cu(II) (anodic reaction), under ambient conditions. The Cu(I) solution gradient, in the presence of an alkyne in solution and an azide monolayer on the glass surface in between the platinum electrodes, is exploited for the surface-confined gradient fabrication via the Huisgen 1,3-dipolar cycloaddition (CuAAC). Owing to the high sensitivity of the CuAAC on the Cu(I) concentration, we demonstrate here the control of the shape of the micron-scale surface gradient, in terms of steepness and surface density, as a function of the reaction conditions. The surface gradients were assessed by fluorescence microscopy and time-of-flight secondary ion mass spectrometry (Tof-SIMS). Moreover, bi-component and biomolecular gradients have been fabricated and a method for the electrochemically mediated patterning of surface chemical gradients on external azide-functionalized substrates has been developed for the implementation of bi-directional 2D surface gradients.

*Part of this chapter has been published in: C. Nicosia, S. O. Krabbenborg, P. Chen, J. Huskens, *J. Mater. Chem. B*, 2013, accepted.

6.1 Introduction

Gradients of physicochemical properties, i.e. their gradual variation in space and/or time, are of great value both in solution and on surfaces. Gradients, in continuous or discrete form, have been successfully employed in materials science[1,2] and combinatorial/analytical chemistry[3-5] improving the efficiency of the design and discovery of catalysts and drugs, and providing new analytical methods.

Above all, gradients are an essential attribute of biology.[6-8] Of fundamental importance is the migration of cells in solution gradients (chemotaxis) during biological processes like angiogenesis, wound healing, metastasis, etc., underlining the impact that research in the field of cell motility has on tissue engineering and cancer research development.[9-13] Considering that most biological reactions and interactions occur at the cell membrane-surface interface, a convenient model to investigate these biological mechanisms is the directed cell migration on surface chemical gradients (haptotaxis). Since typical cell sizes are in the micrometer range (less than 10 μm for prokaryotes and more than 10 μm for eukaryotes), micron-scale surface gradients with fine tuning of the gradient length-scale and steepness are needed to allow cell edges to adhere and detach directionally.[8] With this intention, Winkler *et al.* have recently demonstrated that electron-beam irradiation on self-assembled monolayers on gold is suitable to introduce surface defects in a micron-scale gradient manner. The surface alteration was employed for the fabrication of bio-resistant micrometer-scale gradients by means of a surface exchange reaction with oligo(ethylene glycol)-terminated thiols.[14]

Moreover, surface chemical gradients are conveniently used for the investigation of the induced directional motion of materials. One example, out of many, is the macroscopic motion of liquid droplets driven by surface energy gradients that affect the interfacial tension at the front and back edges of the droplet.[15-18]

Nanoscale transport of materials, driven by micrometer-scale surface energy gradients, plays an important role on the investigation of the assembly and propulsion of nanometer-sized objects. Recently, Walder *et al.* employed micrometer-scale hydrophobic surface energy gradients to direct the motion of nanoparticles.[19] On an even smaller scale, Perl and coworkers analyzed the directional spreading of multivalent ligands subjected to self-developing gradients on a receptor platform.[20]

The ability to control the motion of molecules and nano-objects on surfaces will thus have a direct impact on single molecule science and nanotechnology, and constitute a link to natural, artificial and dynamic assembled systems.

Many techniques are available for the generation of surface chemical gradients, mainly based on the modification/deposition of monolayers on substrates. An exhaustive description of methods for the generation of surface gradients has been reported in comprehensive reviews.[21-23] Very few of these methods allow the fabrication of continuous covalently bound surface chemical gradients on the micron-scale,[14,24-27] and they usually show limited control over the shape (surface density and steepness) or require expensive equipment (e.g. electron-beam,[13,27] UV lithography[26] and scanning tunneling microscopy[28]).

In order to exert high control over the length-scale and shape of surface chemical gradients, we here describe electrochemically mediated reactions, in particular the electrochemically activated copper(I) azide-alkyne cycloaddition ("e-click"). Especially after the introduction of Cu(I) catalysis,[29,30] the Huisgen 1,3-dipolar cycloaddition reaction of organic azides and alkynes, has gained increasing attention.[31,32] A lot of effort has been focused on the optimization of the active catalyst (Cu(I)). Finn and coworkers have demonstrated the electrochemical generation of Cu(I) (from a $CuSO_4$ solution), in the presence of air, for the bio-functionalization of an azide-modified protein capsid in solution.[33] Moreover, "e-click" has been successfully exploited for the modification of surfaces, in particular for the independent functionalization of electrodes,[34-36] patterning of surfaces,[37] and morphogen-driven formation of films.[38] Furthermore, by means of stenciled[39] or bipolar[40] "e-click", shallow surface gradients of covalently bound molecules were created on azide-functionalized conductive polymers on the millimeter-centimeter length-scale. The independent functionalization of electrodes[34-36] and the fabrication of surface concentration gradients[39,40] demonstrate that the electrochemical reduction of Cu(II) to Cu(I) is a suitable method for the local modulation of the "e-click".

In our previous chapter,[41] we generated a solution gradient of a catalytic species (Cu(I)) for the investigation of the kinetics and the reaction order of the electrochemically activated copper(I)-catalyzed azide-alkyne 1,3-dipolar cycloaddition (CuAAC). This gradient was obtained by means of platinum microelectrodes arrays on glass substrate modified with an azide-terminated silane in the areas between the electrodes. In the present study, the electrochemically promoted CuAAC is employed to investigate the effect and the control of the reaction conditions on the shape of micron-scale surface chemical gradients. Furthermore, we show that this system allows the fabrication of bi-component and biomolecular gradients and the mediated patterning of surface gradients on external substrates when the active substrate is brought in close proximity to the microelectrode array.

6.2 Results and discussion

6.2.1 Investigation of the parameter space of the "e-click" gradient formation

The system used for the fabrication of surface chemical gradients via "e-click" is the same employed for the kinetic study in Chapter 5 and is illustrated in Scheme 6.1.

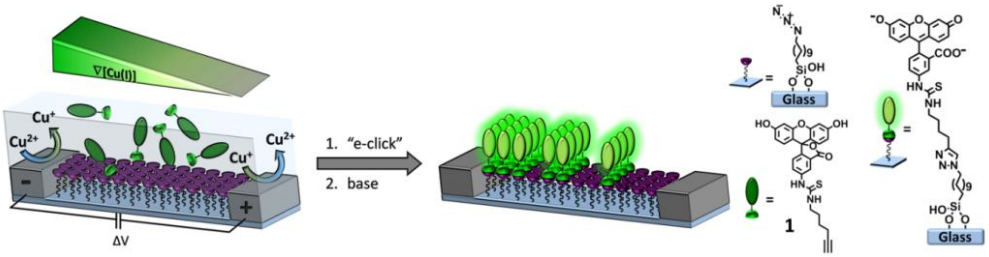

Scheme 6.1. Fabrication of surface chemical gradients via electrochemically promoted CuAAC of alkyne-modified fluorescein (**1**) on an azide monolayer on glass between a platinum microelectrode array.

Platinum microelectrode arrays on glass were fabricated using a bilayer lift-off procedure based on a standard photolithographic technique. In order to study the effect of the geometry of the microelectrodes on the surface gradient formation, arrays with different electrode sizes and spacings were fabricated. The glass surface of the platinum microelectrode array on glass was modified by using silane chemistry to prepare an azide monolayer.[45] To attest the advantage of the electrochemically activated CuAAC for the fabrication of micron-scale surface chemical gradients on azide monolayers, we employed an alkyne-modified fluorescein (**1**) for the fluorescence read-out of the reaction.

The CuAAC reaction, which takes place only in the presence of Cu(I), was carried out on top of the electrode by using a solution of $CuSO_4$ and **1** in DMSO, in the absence or presence of a Cu(I)-stabilizing ligand. A constant potential difference, ranging from 0.4 to 1.2 V, was applied between the electrodes to perform the reduction of Cu(II) to the catalytically active Cu(I) at the cathode and the re-oxidation of Cu(I) to Cu(II) at the anode. Owing to the concentration gradient of Cu(I) in solution, the CuAAC between **1** and the azide monolayer results in a faster formation of triazole molecules next to the cathode (where Cu(I) is produced) compared to next to the anode, with the consequent formation of a surface gradient of covalently bound **1**. The reaction is very sensitive to the Cu(I) concentration as was demonstrated by the second order rate dependence on the Cu(I) concentration.[41,48]

Figure 6.1A-D shows the fluorescence microscopy images of the resulting micron-scale surface gradients after different reaction times. After preparation of the azide monolayer, 50 μm wide and 100 μm spaced platinum microelectrodes on glass were incubated in a

mixture of $CuSO_4$, **1**, and Cu(I)-stabilizing ligand in DMSO. The electrochemically activated CuAAC was performed applying a potential difference of 1.0 V for different reaction times. Because gradients were prepared using compound **1** in the neutral lactone form (low quantum yield),[49] the surface gradient was barely visible (not shown). Therefore, the substrates were rinsed with a pH 10 buffered solution prior characterization to generate the highly fluorescent dianion and achieve a more pronounced visualization of the fluorescent dye gradients.[49] The CuAAC reaction between alkyne and azide reflects the concentration gradient of Cu(I) in solution with consistent formation of a surface gradient of the reaction product. In the fluorescence microscopy images of Figure 6.1, we observe the gradient of fluorescence intensity with the maximum localized next to the cathode. Furthermore, the intensity of the gradient increased with increasing reaction time.

Figure 6.1E shows the intensity vs. distance graph obtained from Figure 6.1C. The shape of the surface gradients was analyzed by means of two main parameters: the maximum intensity near the cathode (I_{max}) and the steepness (m). The direct comparison of the results required the normalization of the fluorescence intensities of the surface gradients. To obtain normalized fluorescence intensities, the background was subtracted and the resulting intensities were divided by the fluorescence intensity obtained from the full monolayer of **1** (with subtracted background, Figure 6.2). Since the electrochemical activation of Cu(II) is faster and more efficient than the chemical reduction (e.g. using sodium ascorbate as a reducing agent),[33] for some reaction conditions we observed fluorescence intensities higher than observed for the reference (full) monolayer made by chemical reduction.

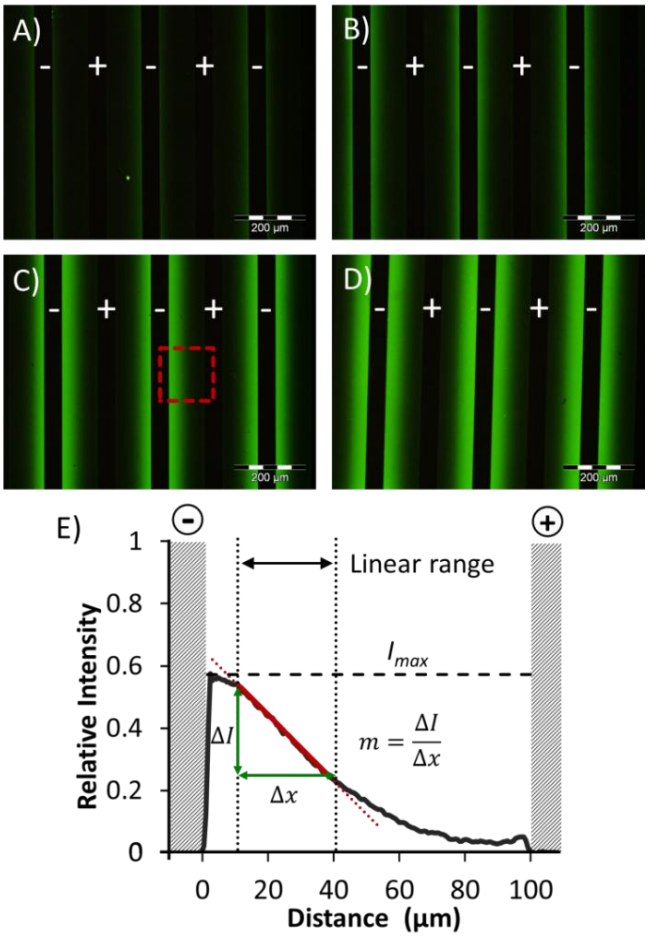

Figure 6.1. Fluorescence microscopy images of the surface chemical gradients resulting from electrochemically activated CuAAC, using 1.0 mM alkyne-modified fluorescein (**1**), 1.0 mM $CuSO_4$ salt, 100 mM 2,6-lutidine, 100 mM n-Bu_4NBF_4 in DMSO, ΔV = 1 V, after A) 2 min, B) 4 min, C) 8 min, and D) 16 min reaction time (50 µm electrodes, 100 µm gap). E) Normalized intensity vs. distance graph of the surface chemical gradient shown in C) depicting the parameters considered for the analysis of the surface gradients: steepness (m) and maximum intensity (I_{max}). Images were recorded at an excitation wavelength of 490 nm and an emission wavelength of 520 nm (exposure time: 400 ms).

The steepness of the gradient gives information about the gradual variation of the fluorescence intensity (related to the surface coverage) in space, and it was estimated as the (steepest) slope m obtained from the intensity vs. distance graph (Figure 6.1E). Consequently, the slope was calculated from the linear regression ($\Delta I/\Delta x$) of a range of data selected from the steeper region of the surface gradient that led to a correlation coefficient (R^2), higher than 0.97 (see Figure 6.1E and Table 6.1 in the Experimental section). The maximum intensity (I_{max}) was defined as the highest intensity observed in the intensity

profile (Figure 1E). as it reflects the surface density and coverage of covalently attached alkyne molecules.

Steepness and maximum intensity of the surface gradients were found to be strongly affected by several process parameters such as the concentration of Cu(II) and alkyne, use of Cu(I)-stabilizing ligands (tris[(1-benzyl-1H-1,2,3-triazol-4-yl)methyl]amine (TBTA) or 2,6-lutidine), solvent, distance between the electrodes, reaction time and electrical potential.

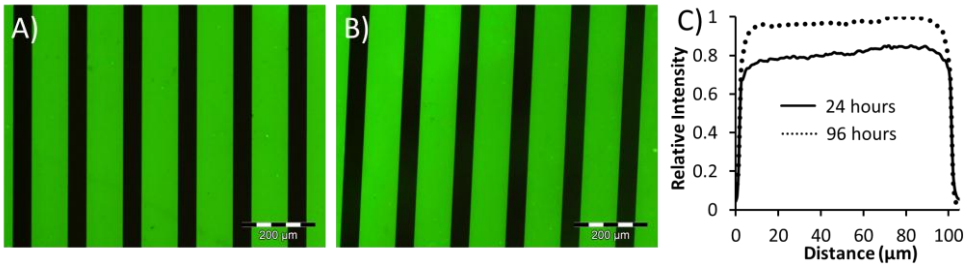

Figure 6.2. Fluorescence microscopy images after A) 24 h and B) 96 h incubation of an azide functionalized substrate in a 1 mM solution of **1**, 10 µM $CuSO_4$ and 1mM ascorbic acid in tert-butanol/water=1/2. C) Intensity profiles of the images A) and B).

Figure 6.3 shows the intensity profiles of the surface gradients obtained under varying reaction conditions using microelectrode arrays with a 100 µm gap width and 50 µm wide electrodes. When no Cu(I)-stabilizing ligand was added to the reaction mixture (Figure 6.3A) the kinetics of the "e-click" reaction was rather slow, yielding surface gradients characterized by shallow profiles (low intensity and steepness), and yielding products over the whole distance range.

Finn and coworkers described that only in the presence of suitable ligands the electrochemically activated CuAAC shows excellent yield and fast kinetics in DMSO/water in the presence of air.[33] In contrast to aqueous media, the deprotonation of the alkyne to the Cu(I) acetylide complex is very slow in pure organic solvents. Therefore the addition of a base in DMSO is needed. TBTA, the well-known accelerating ligand for CuAAC, provides protection of Cu(I) under aerobic conditions and promotes the rate of the reaction because of the presence of a basic site employed for the deprotonation of the alkyne. As shown in Figure 6.3B, we indeed observed a strong enhancement of reactivity upon addition of 1 equivalent of TBTA. After 1 min, the fluorescence intensity obtained without using TBTA was less than 0.2 (Figure 6.3A) while upon addition of TBTA it reached almost 1.0 (Figure 6.3B).

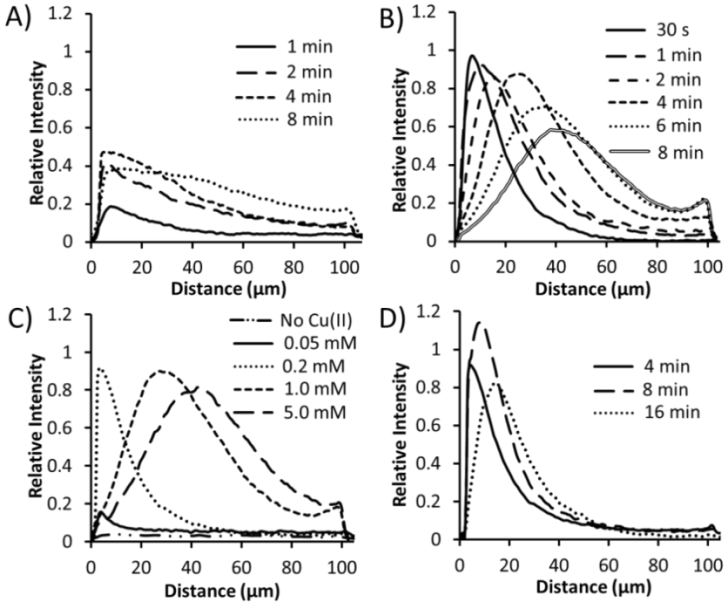

Figure 6.3. Intensity profiles of the surface chemical gradients obtained reacting 1 mM of **1** in DMSO at a potential difference of 1.0 V under varying reaction conditions: reaction time in the presence of A) 1 mM $CuSO_4$ or B) 1 mM $CuSO_4$ and 1 mM TBTA; C) $CuSO_4$ and TBTA concentration ($CuSO_4$/TBTA=1/1; in case of $CuSO_4$ concentration lower than 1 mM, Na_2SO_4 is used as supporting electrolyte to maintain the overall salt concentration at 1 mM) for 4 min reaction time; D) reaction time in the presence of 0.2 mM $CuSO_4$, 0.8 mM Na_2SO_4 and 0.2 mM TBTA. In all cases platinum interdigitated electrodes on glass with 100 µm electrode separation and 50 µm electrode width were employed.

In both cases we noticed a decrease of intensity near the cathode upon prolonged reaction times, with a more pronounced effect in the presence of the Cu(I)-stabilizing ligand, TBTA (Figures 6.3A/B and 6.4). To exclude any specific side reactions affecting the structural integrity of fluorescein derivative **1** or the monolayer, the same reaction conditions were employed using an alkyne-modified coumarin (**2**) (Figure 6.4). Also with this dye, similar results were observed regarding gradient shape and steepness, and in particular also the effect of fluorescence intensity decrease near the cathode at prolonged reaction times.

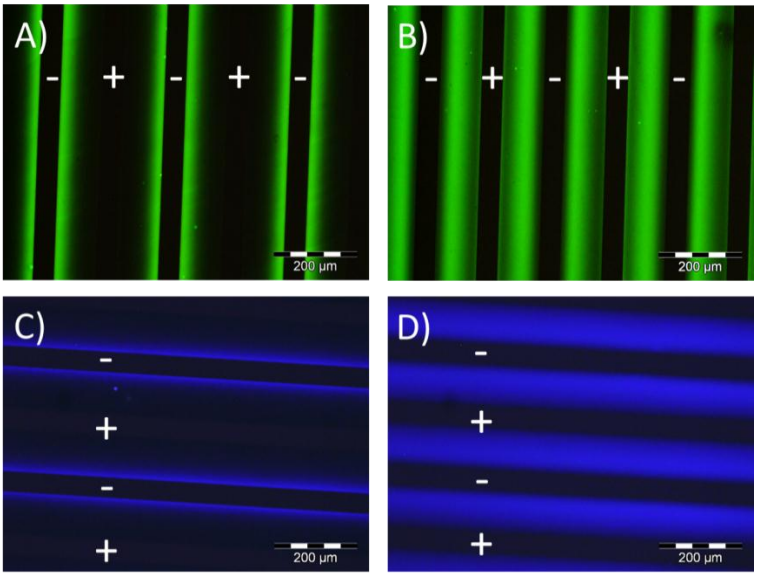

Figure 6.4. Fluorescence microscopy images of the surface chemical gradients resulting from electrochemically activated CuAAC, using 1.0 mM alkyne-modified fluorescein (**1**, A/B) or 1.0 mM alkyne-modified coumarin (**2**, C/D), 1.0 mM $CuSO_4$ salt, 1 mM TBTA in DMSO, ΔV = 1 V, after reaction times of 1 min (A/C)or 8 min (B/D). (50 µm electrodes, 100 µm gap). Images were recorded at A,B) λ_{exc} = 395 nm and $\lambda_{em} \geq$ 520 nm, C,D) λ_{exc} = 360 nm and $\lambda_{em} \geq$ 420 nm.

Tof-SIMS analysis was performed before and after 8 min reaction using **1** in the presence of TBTA (Figure 6.5). Detection of molecular fragments of the azide or product triazole was not possible on these samples because of strong interference of the metal electrodes present. This was however possible on the transfer gradients (see below). After 8 min reaction, the sample exhibited (Figure 6.5C) a surface gradient of sulfur (in negative mode), without the decrease of intensity near the cathode observed in fluorescence. This indicates that the monolayer of **1** is still intact. At the same time, a strong copper signal, attributed to Cu(0), is detected both on the cathode and, in a gradient fashion, on the monolayer areas near the cathode (Figure 6.5D). The presence of Cu(0) on the cathode is attributed to electrodeposition, while deposition on the SAM areas is ascribed to the disproportionation of Cu(I) into Cu(0) and Cu(II).[47,50] Therefore, the decrease in fluorescence intensity observed near the cathode is attributed to the presence of Cu(0) on the surface, upon prolonged reaction times, causing the quenching of the fluorescence of **1**.

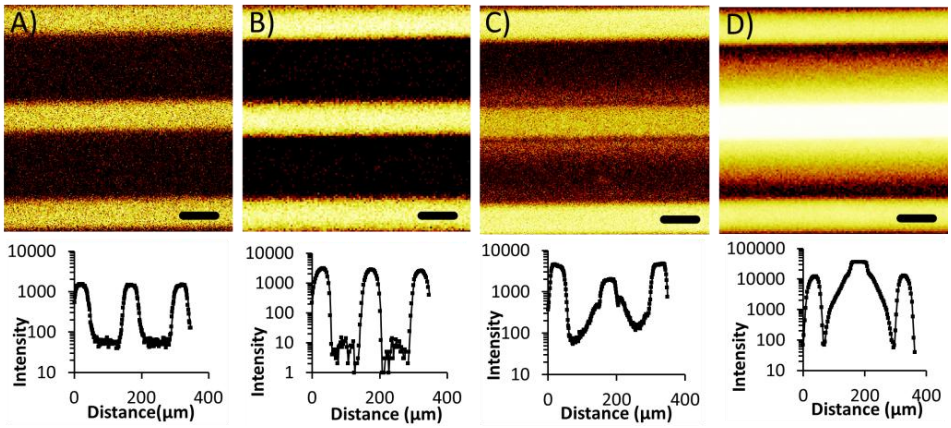

Figure 6.5. Tof-SIMS images of sulfur (A/C, in negative mode) and Cu (B/D, in positive mode) of the azide monolayer before (A and B) and after (C and D) the surface gradient formation using 1 mM of **1**, 1 mM $CuSO_4$, and 1 mM TBTA in DMSO at a potential difference of 1.0 V for 8 min using interdigitated microelectrode arrays with a 100 µm gap width (insets show the intensity profiles, scale bar = 50 µm).

The hypothesis of quenching of the fluorescence due to the formation of Cu(0) by the disproportionation of Cu(I) was further confirmed performing the "e-click" at different Cu(II) concentrations (Figure 6.3C). For instance, decreasing the Cu(II) concentration from 1 mM to 0.2 mM, using equimolar amounts of TBTA and the same conditions reported previously for 4 min reaction, showed less influence of Cu(0) deposition and a sharp surface gradient with high intensity (0.92). When the reaction was performed for a longer time (Figure 6.3D, 8 min) we observed an additional enhancement of intensity (1.14) and a high steepness, but again a decrease of intensity occurred after 16 min reaction time indicating that even at a low concentration of Cu(II) the disproportionation becomes significant at prolonged reaction times. When the concentration of Cu(II) was further reduced to 0.05 mM the amount of electrochemically produced Cu(I) was not enough to perform the "e-click" effectively. When no Cu salt was added at all, no functionalization was observed (shown in Chapter 5). On the other hand, when employing higher Cu(II) concentrations (5 mM), the effect of the disproportionation was evident, and the Cu(0) deposition compromised the characterization by fluorescence microscopy already at short reaction times (Figure 6.3C).

This series of experiments indicates that: (i) the presence of a ligand for the couple Cu(II)/Cu(I) and a base for the deprotonation of alkynes in pure organic solvents and aerobic conditions is crucial to activate the “e-click” and obtain highly dense and steep surface gradients; (ii) Cu(II) is required for the reaction to occur: low concentrations of Cu(II) give only very low surface functionalization in line with the observed second order

rate dependence on Cu(I);[41] (iii) moderate Cu(II) concentrations give less Cu(I) formation compared to high Cu(II) concentrations but still an efficient reactivity of the "e-click" reaction, while achieving an apparently more localized electrochemical production of Cu(I) allowing the fabrication of steeper gradients; (iv) long reaction times and high concentrations of Cu(II) are responsible for a stronger effect of the disproportionation of Cu(I) resulting in fast Cu(0) deposition and concomitantly strong fluorescence quenching.

In an attempt to minimize the effect of the disproportionation and to study the effect on the diffusion of the catalyst and the reactivity of the CuAAC, some other solvent mixtures were tested, in particular glycerol/DMSO 99/1 (v/v), DMSO/water 1/1 (v/v) and acetonitrile (in the last case Cu(II) acetate was used instead of $CuSO_4$). None of these reaction conditions displayed an appreciable improvement regarding disproportionation and the formation of surface gradients was unclear. Therefore DMSO was used for all subsequent experiments. In the case of DMSO, a polar aprotic solvent, the electrochemically activated CuAAC reaction results in a less extensive disproportionation of Cu(I) and more stable gradients, owing to a combination of solvation, complexation and stabilization effects of Cu(I).[47]

Smaller electrode sizes and gap widths were employed to investigate the limits of the fabrication of micron-scale surface chemical gradients making use of the same system described above (Figure 6.6). Decreasing the distance between the electrodes required a further optimization of the reaction conditions. In general the amount of Cu(II) employed was reduced (from 1.0 mM to 0.2 mM), leading to surface gradients with low I_{max} and high m values (see below). As a result of the relatively high Cu(II) concentration (1 mM) when using a small electrode gap of 10 µm, the monolayer between the electrodes was almost homogeneously functionalized even after only 1 min reaction (Figure 6.6G/H). In contrast, in particular when using a 10 µm electrode gap width and 5 µm wide electrodes (Figure 6.6D/H) and performing the reaction in the presence of 0.2 mM Cu(II) and TBTA, a very sharp gradient was obtained after 1 min.

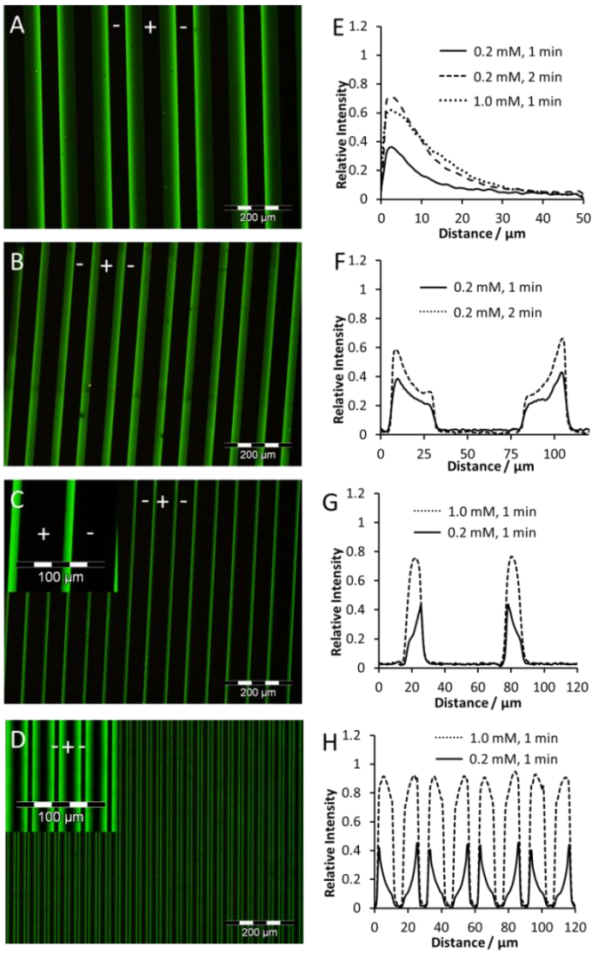

Figure 6.6. Examples of fluorescence microscopy images at different gap sizes between the electrodes: A) 50 µm; B) 25 µm; C) 10 µm (50 µm electrode width); D) 10 µm gap width (5 µm electrode width). Images were recorded at λ_{exc} = 395 nm and $\lambda_{em} \geq$ 520 nm. Intensity profiles of the surface chemical gradients obtained after reacting 1 mM of **1** in the presence of $CuSO_4$/TBTA 1/1 in DMSO at a potential difference of 1.0 V with various electrode distances and conditions: E) 50 µm gap width at different $CuSO_4$ concentrations and reaction times; F) 25 µm gap width at different reaction times; G) 10 µm gap width (50 µm electrode width) at different $CuSO_4$ concentrations; H) 10 µm gap width (5 µm electrode width) at different $CuSO_4$ concentrations.

With the purpose of finding reaction conditions for the fabrication of a Cu(I) gradient with limited effect of the disproportionation, we employed 2,6-lutidine as promoter and supporter ligand of the "e-click". Excess of an organic base (e.g. 2,6-lutidine) is particularly beneficent in promoting the formation of the copper acetylide complex, to achieve high yields of CuAAC, and to prevent degradation of Cu(I) by oxidation in air or disproportionation, minimizing side-products.[29,51] Therefore, we used similar conditions as described before, replacing TBTA with an excess of 2,6-lutidine (Cu(II)/2,6-lutidine = 1/100).

Figure 6.7A shows the intensity profiles of the surface chemical gradients of **1**, obtained performing the "e-click" using 1 mM Cu(II), 100 mM 2,6-lutidine and 1 mM **1** in DMSO at varying applied potential differences for 4 min reaction time.

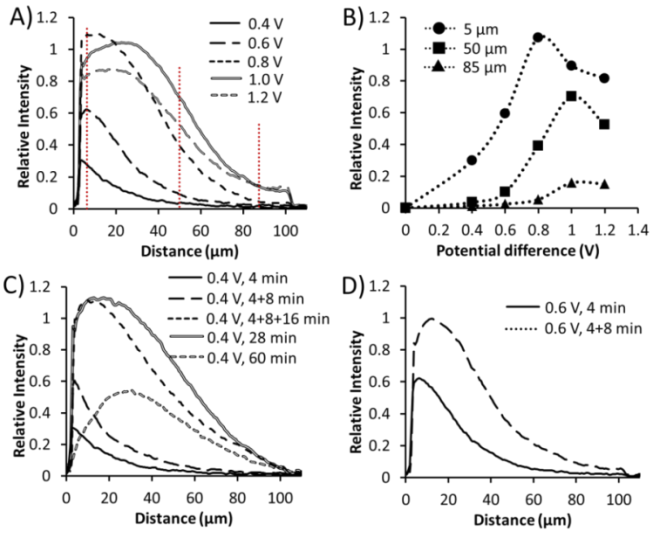

Figure 6.7. Intensity profiles of the surface chemical gradients obtained reacting 1 mM of **1** in the presence of 1 mM $CuSO_4$, 100 mM 2,6-lutidine in DMSO: A) at various potential differences for 4 min reaction; B) as a function of the potential difference at 5, 50 and 85 µm distance from the cathode for 4 min reaction (dotted lines are guidelines); C) at 0.4 V for different reaction times; D) at 0.6 V for different reaction times. In all cases platinum microelectrode arrays on glass with 100 µm electrode separation and 50 µm electrode width were employed.

When we plotted the intensity profiles as a function of the potential difference at three different positions (5, 50 and 85 µm) from the cathode (Figure 6.7B), we observed that the reactivity increased with the potential, presumably owing to the higher concentration of Cu(I) locally produced, but potential differences higher than 1.0 V induced faster side reactions (e.g. disproportionation) giving decreasing intensities as a result of quenching. Surface gradients, made using different potentials, displayed a strong influence of the potential on the fluorescence intensity ($0.30 \leq I_{max} \leq 1.13$) but a weak effect on the steepness ($0.013 \leq m \leq 0.023$ µm^{-1}, see Table 6.1 in the Experimental section).

The "e-click" as a function of electrochemical potential difference was also performed for different reaction times (Figure 6.7C and D). Working at 0.4 V (Figure 6.7C) the "e-click" appeared slow enough to provide a better control of the reaction in time. In particular a slow but effective enhancement of I_{max} from 0.30 (4 min) to 1.10 (28 min) was observed, but when the reaction time was pushed to 60 min, the intensity decreased everywhere and most strongly near the cathode, showing a limitation of the system at prolonged reaction times.

Notably, the configuration of the system and the reaction conditions allowed the fabrication of multi-step surface gradients on one microelectrode array (Figure 6.7C). After 4 min reaction at 0.4 V the substrate was rinsed with DMF and ethanol to arrest the reaction and to remove any unspecifically adsorbed compounds, followed by characterization via fluorescence microscopy. The same substrate was employed for a subsequent functionalization for 8 min reaction (followed by rinsing and visualization of the gradient) and another 16 min, observing an increase of intensity and negligible influence of Cu(I) disproportionation. The surface gradient obtained after 28 min of continuous reaction yielded a gradient similar to the one obtained after three sequential steps of 4, 8 and 16 min. Figure 6.7D shows that a similar multi-step fabrication scheme is also possible using a potential difference of 0.6 V. This approach can potentially be employed for the immobilization, in a gradient fashion, of different alkynes, introducing the gradual variation of more than a single physicochemical property in one or different (see below) directions along the substrate.

Once the influence of the applied potential on the shape (I_{max} and m) of the surface gradient was established, we proceeded with a comprehensive study of other parameters (e.g. the Cu(II)/2,6-lutidine ratio, the concentration of **1**, and the addition of a supporting electrolyte) employing 1.0 V for generally short reaction times (Figure 6.8).

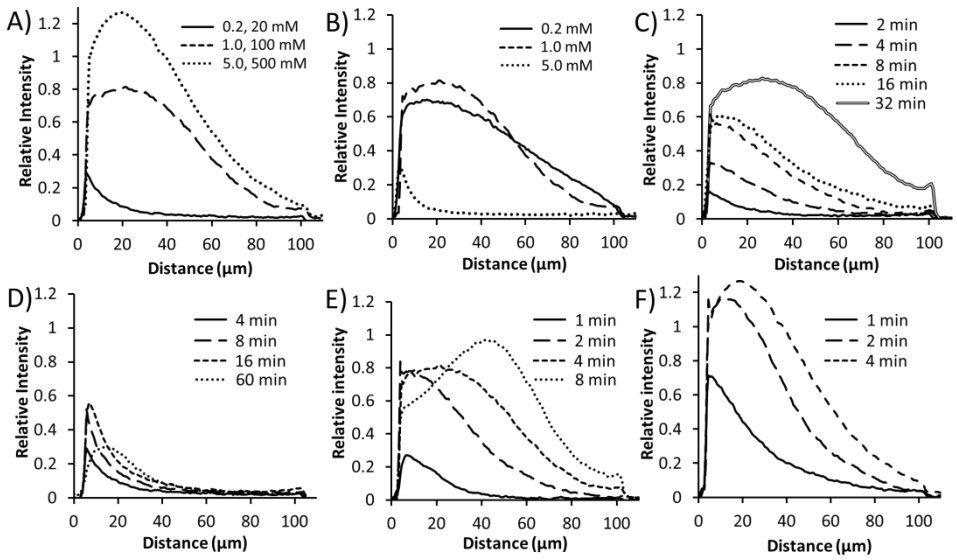

Figure 6.8. Fluorescence intensity profiles of the surface chemical gradients obtained reacting **1** in DMSO at a potential difference of 1.0 V in the presence of A) different $CuSO_4$/2,6-lutidine concentrations for 4 min reaction; B) $CuSO_4$/2,6-lutidine at 1.0/100 mM for different concentrations of **1** for 4 min reaction. C) 1.0/100 mM and 100 mM of n-Bu_4NBF_4 at different reaction times; and for different reaction times in the presence of different $CuSO_4$/2,6-lutidine concentrations D) 0.2/20 mM; E) 1/100 mM; F) 5/500 mM.

The results of the screening of reaction conditions are summarized as follows: i) a high concentration of Cu(II) (5 mM), in combination with an excess of 2,6-lutidine (100 equiv), yielded high density gradients across the whole inter-electrode spacing while sharp and low density surface gradients were obtained using a low concentration of Cu(II) (0.2 mM) reflecting the small and localized amount of electrochemically produced Cu(I) (Figure 6.8A); ii) the "e-click" demonstrated to be more stable towards the Cu(I) disproportionation in the presence of an excess of 2,6-lutidine, in comparison with for the use of TBTA (Figure 6.3C) ; iii) a severe drop of intensity was detected at a high concentration of alkyne (5.0 mM) (Figure 6.8B). This counterintuitive behavior is explained by the mechanism of the CuAAC reaction:[48] the reduced reactivity in the presence of an excess of alkyne is attributed to the saturation of the Cu(I) coordination sites by alkyne molecules preventing the azide groups from binding, and consequently reducing the overall rate;[32,48] iv) the addition of a supporting electrolyte (100 mM of n-Bu_4NBF_4) led to surface gradients with a lower intensity and steepness due to the contribution of the electrolyte to a significant change of the solvent conductivity and therefore to a different Cu(I) concentration gradient in solution (Figure 6.8C); v) surface chemical gradients fabricated in the presence of the supporting electrolyte were less affected by the deposition of Cu(0). This behavior is most likely related to the stabilizing effect of tetraalkylammonium salts on copper metal clusters and colloids;[52,53] vi) reactions at different Cu(II) concentrations were performed also for different reaction times highlighting again a higher activity but lower stability at higher Cu(II) concentrations (Figure 6.8D-F).

Figure 6.9 shows the correlation between steepness, m, and density, I_{max}, for the surface gradients described in our work. Figure 6.9A gives information about the effects of the different reaction conditions employed on steepness, m, and density, I_{max}, of the surface gradients. Overall, tuning the reaction conditions allowed the preparation of micron-scale surface chemical gradients with a wide range of intensities and steepnesses. In general we observed that longer reaction times (depicted with arrows in Figure 6.9A) led to higher I_{max} and the formation of steeper gradients.

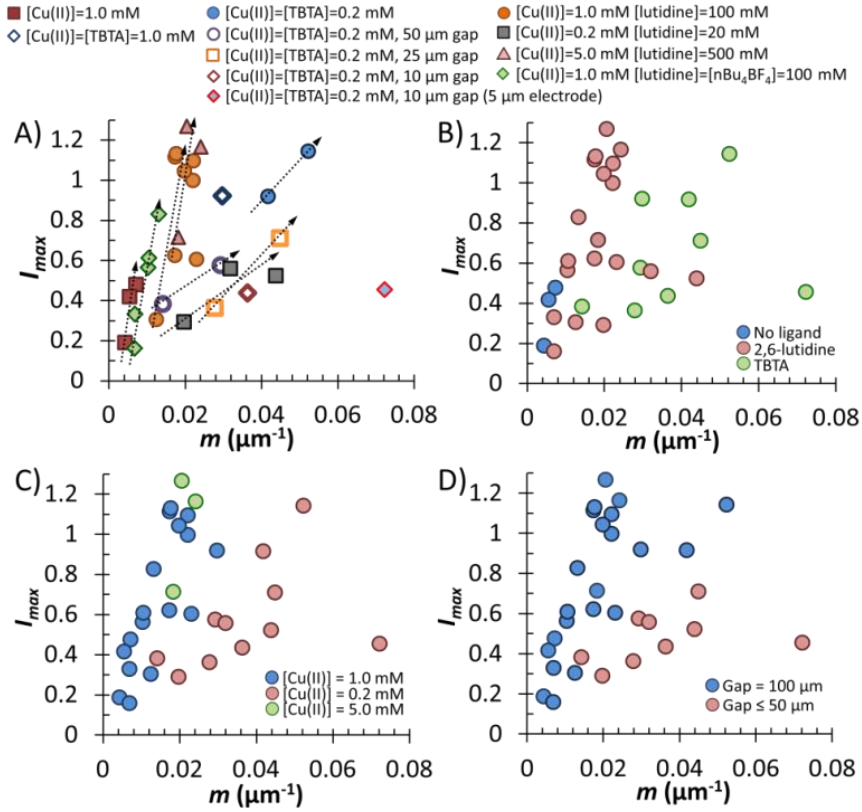

Figure 6.9. A) Graph of the maximum fluorescence intensity, I_{max}, near the cathode and the steepness, m, under different working conditions. Graphs I_{max} vs. m highlighting the effects of B) Cu(I)-stabilizing ligand; C) Cu(II) concentration; and D) electrode gap under different reaction conditions.

Figure 6.9B highlights the effect of the Cu(I)-stabilizing ligand. The addition of TBTA, or 2,6-lutidine, clearly promoted the "e-click", allowing the fabrication of higher density surface gradients. Without any addition of ligand, shallow (m < 0.007 µm^{-1}) and low intensity (I_{max} < 0.48) gradients were prepared, while using TBTA the reaction usually yielded steep and highly dense surface gradients (Figure 6.9B). High concentrations of Cu(II) (e.g. 1 mM and 5 mM) led to shallow to moderately steep surface gradients (m < 0.03 µm^{-1}) with a wide intensity range (I_{max} extends from 0.19 to 1.14 using 1 mM and 0.71 to 1.27 using 5 mM of Cu(II)) based on different reaction conditions (Figure 6.9C).

The most common inter-electrode gap employed in this report was 100 µm (Figure 6.9D). However, we observed that using smaller microelectrode arrays allowed the fabrication of steep gradients, with the extreme case of a steepness of 0.072 µm^{-1} (i.e. going from 0 – 1 monolayer over 14 µm) when using a 10 µm gap and 5 µm electrode width.

6.2.2 Biomolecular surface gradients

The electrochemically activated CuAAC allows the fabrication of micron-scale bio-molecular surface gradients. As depicted in Scheme 6.2, an alkyne-modified biotin **3** was immobilized via microcontact printing (μCP) or via "e-click". Upon incubation with Alexa-SAv, which is expected to interact with the biotin units by noncovalent interactions, the maximum intensity of the fluorescent gradient obtained by "e-click" (Figure 6.10C/D) reached a value similar to the one obtained via microcontact printing (Figure 6.10A/B), indicating a similar surface density. This result shows that this method allows the facile fabrication of micron-scale biomolecular gradients.

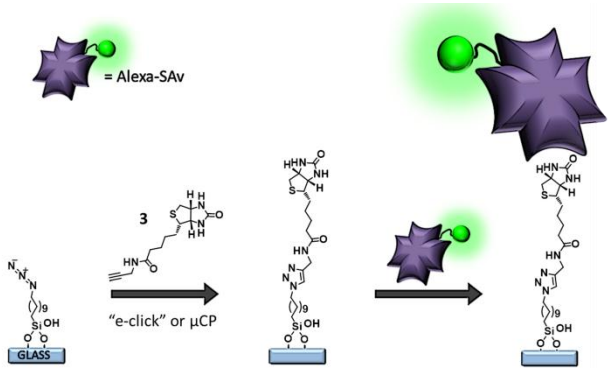

Scheme 6.2. Immobilization of alkyne-modified biotin (**3**)/Alexa-SAv on an azide monolayer on glass, performed by means of either reactive microcontact printing or "e-click" gradient formation.

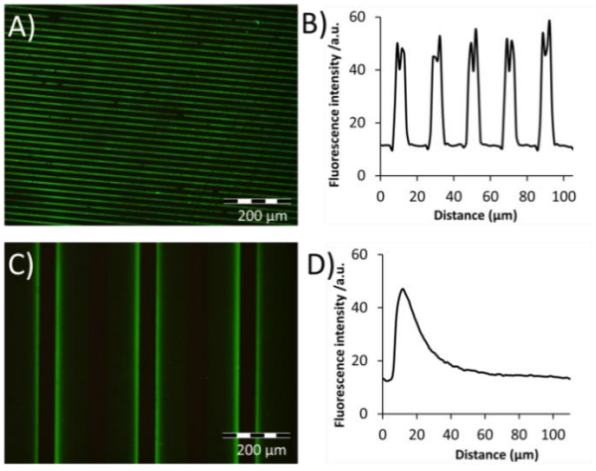

Figure 6.10. Fluorescence microscopy images and intensity profiles: A), B) after microcontact printing of **3** (5x15 μm lines) (1.5 mM **3** in CH_3CN, 0.5 mM Cu(I)$(CH_3CN)_4PF_6$ and 0.5 mM TBTA (CH_3CN/EtOH 2/1), 4 min inking, 1 h μCP) or C), D) after reaction of 1 mM of **3** in the presence of 1.0 mM $CuSO_4$ and 1.0 mM TBTA in DMSO at the potential difference of 1.0 V for 2 min, in both cases followed by incubation in 300 nM Alexa Fluor® 488-labeled streptavidin in PBS (with 0.005% Tween20) for 5 min followed by rinsing in PBS (with 0.01% Tween20) for 30 min. Images were recorded at λ_{exc} = 395 nm and $\lambda_{em} \geq$ 520 nm.

6.2.3 Dual gradients and transfer gradient fabrication

The step-by-step surface gradient fabrication and the configuration of the system allowed the controlled immobilization of different alkynes in different positions on the same substrate. As a proof of principle, here we demonstrate the development of bi-component surface chemical gradients via a two-step procedure based on the immobilization of two different alkyne-modified dyes. As depicted in Scheme 6.3, the surface gradient of the first dye (**1**) was obtained upon "e-click" followed by switching of the polarity of the electrodes and further gradient formation via immobilization of the other alkyne (**2**). Figure 6.11A and B shows the fluorescence microscopy image and the intensity profile, respectively, obtained after overlay of the two fluorescence images upon immobilization of **1** (λ_{exc} = 460-490 nm, $\lambda_{em} \geq$ 520 nm) and **2** (λ_{exc} = 350 nm, $\lambda_{em} \geq$ 420 nm). The two reversed surface gradients were obtained via selective and localized covalent bonding of the alkyne-modified dyes next to the respective cathode. In a similar way, mono-component bi-directional surface chemical gradients were fabricated by immobilization of **2** in a two-step method via switching of the polarity of the electrodes (Figure 6.11C/D).

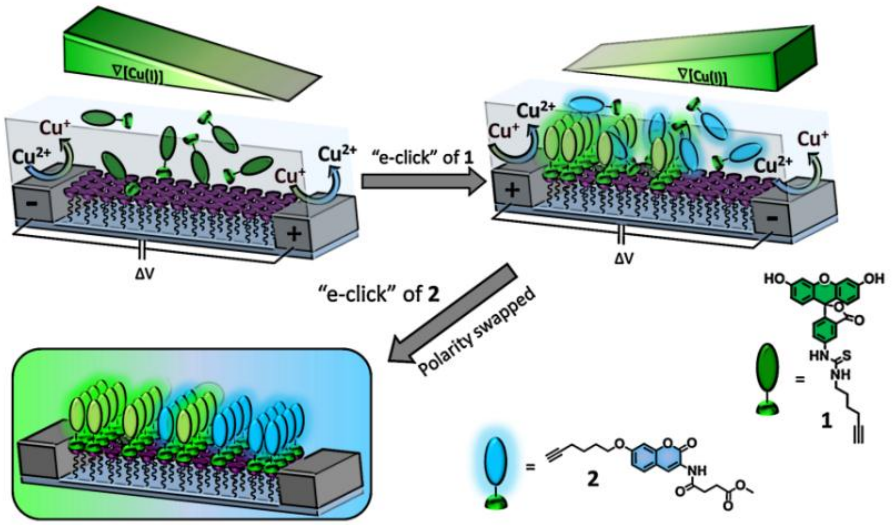

Scheme 6.3. Fabrication of a bi-component surface chemical gradient by means of the "e-click" of **1**, followed by switching of the polarity of the electrodes and subsequent"e-click" of **2**.

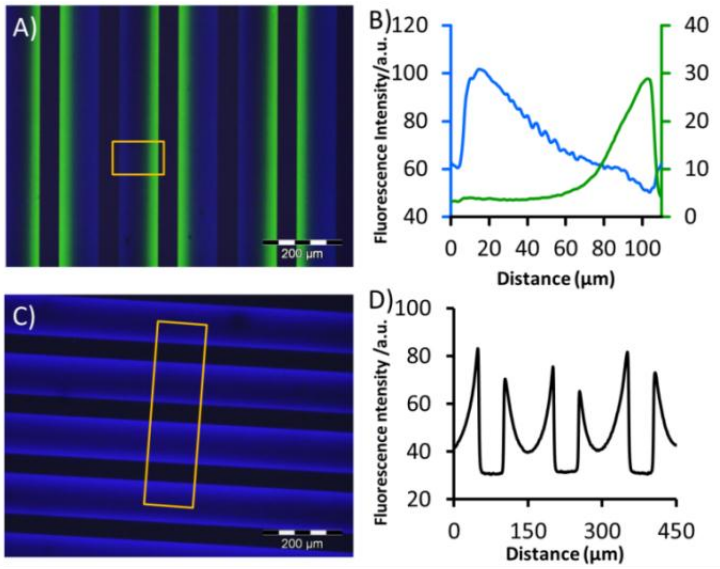

Figure 6.11. A) Fluorescence microscopy image and B) corresponding fluorescence intensity profiles after overlay of the green (**1**, λ_{exc} = 460-490 nm, $\lambda_{em} \geq$ 520 nm) and blue (**2**, λ_{exc} = 350 nm, $\lambda_{em} \geq$ 420 nm) filters. C) Fluorescence microscopy image and D) corresponding fluorescence intensity profile obtained reacting 1 mM of **2** in the presence of 1.0 mM $CuSO_4$ and 1.0 mM TBTA in DMSO at a potential difference of 1.0 V for 2 min and two consecutive times upon switching of anode and cathode. In both cases 100 µm electrode separation and 50 µm electrode width were employed.

Platinum microelectrode arrays on glass were used in a stacked configuration to transfer the triazole gradient onto an azide-functionalized external substrate (Scheme 6.4). A drop of a solution containing **1**, Cu(I)-stabilizing ligand and $CuSO_4$ in DMSO was spotted on the microelectrode array, and a glass slide (1.5x1.5 cm^2) was placed on top of it resulting in the formation of a thin layer of solution. A potential difference of 1.0 V was applied to generate a solution gradient of Cu(I) employed for the surface immobilization via CuAAC (Scheme 6.4).

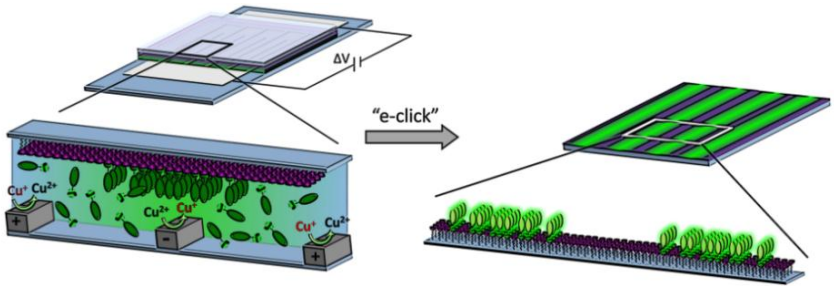

Scheme 6.4. Schematic procedure of the "e-click"-mediated transfer patterning of surface chemical gradients on an azide monolayer on glass.

Also in this case the reaction was observed to be slow when it was performed without any ligand (only $CuSO_4$ and **1** in DMSO, Figure 6.12A) but a higher density was observed when adding a Cu(I)-stabilizing ligand (Figure 6.12B).

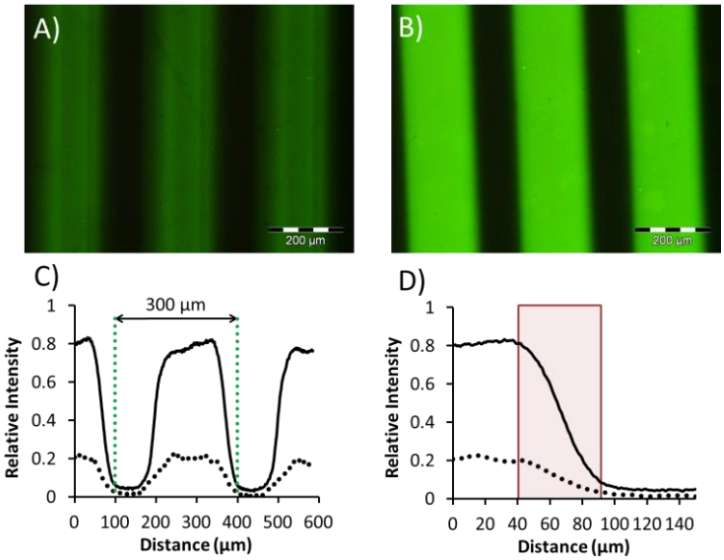

Figure 6.12. Fluorescence microscopy images of the surface chemical gradients obtained by transfer patterning from a platinum microelectrode array onto a glass slide functionalized with an azide monolayer using 1 mM **1** and A) 1.0 mM $CuSO_4$ or B) 1.0 mM $CuSO_4$ and 100 mM 2,6-lutidine, in DMSO at 1.0 V for 2 min reaction time. C) Intensity profiles and D) zoom-in of the profile at the gradient sections of A (•••) and B (—) illustrating the periodicity and the length-scale of the surface gradients (pink box, approximately 50 µm).

As a result of the geometry of the electrode arrays (50 µm electrode width and 100 µm electrode gap), a periodicity of the fluorescence intensity of 300 µm was expected and observed (Figure 6.12C), while the gradient was observed over a length-scale of approximately 50 µm (Figure 6.12D).

To support the fluorescence results, Tof-SIMS characterization of the transfer gradient was carried out. Full monolayers before and after CuAAC of **1** were analyzed to detect typical fragments associated with the covalent attachment of **1** on the surface. While a full azide monolayer on glass shows only typical fragments coming from the aliphatic chain of the monolayer (Figure 6.16, Experimental section), organic fragments at higher molecular weight and containing N, O, and S characteristic of **1**, were detected after the reaction with the alkyne-modified fluorescein (**1**) (Figure 6.17, Experimental section). Accordingly, the Tof-SIMS surface mappings in positive (Figure 6.13A/B) and negative (Figure 6.13C/D) mode illustrate the formation of gradients, very similar to the observation made by fluorescence microscopy, confirming the selective attachment of **1** in a gradient fashion.

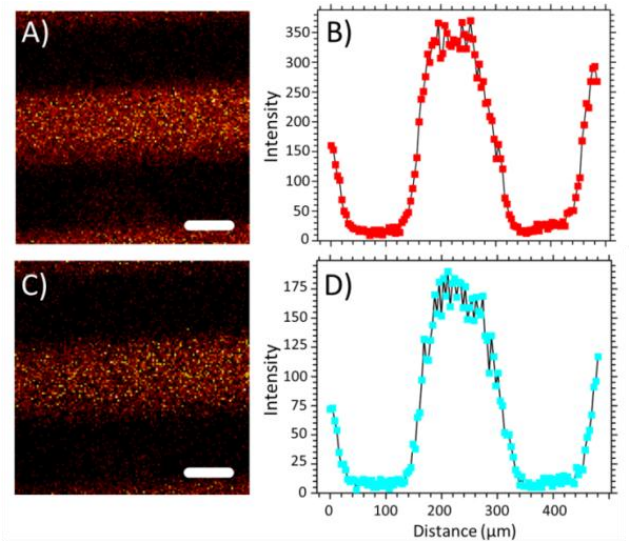

Figure 6.13. Tof-SIMS images of organic fragments detected after transfer gradient fabrication: (A/C) surface mappings (scale bar = 100 µm) and (B/D) intensity profiles obtained in positive mode for *m/z* = 332, 374 and 390 u (A/B), and in negative mode for *m/z* 300, 310 and 325 u (C/D). The transfer gradient was prepared from a platinum microelectrode array onto a glass slide functionalized with an azide monolayer using 1 mM **1**, 1.0 mM $CuSO_4$ and 100 mM 2,6-lutidine in DMSO at 1.0 V for 2 min.

Gradients are, by definition, directional but the most common structure is unidirectional, i.e. with variation of physicochemical properties in one direction along the substrate. Here we show that, by means of the transfer patterned "e-click" method, more complex orthogonal surface gradients can be obtained in a two-step process. Upon gradient-wise immobilization of **1** in a first step, the substrate was rinsed and employed for a second functionalization after 90° rotation of the substrate. Figure 6.14 shows two different 2D orthogonal gradients, obtained using different reaction conditions. This result highlights the flexibility of the system towards the patterning of bi-directional surface gradients on external substrates.

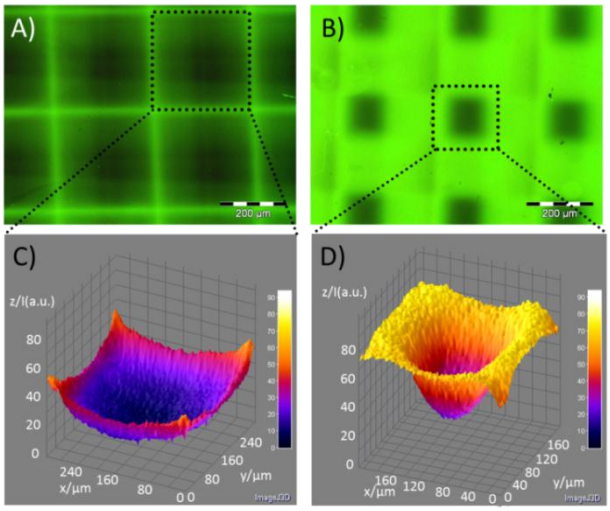

Figure 6.14. Fluorescence microscopy images (A/B) and corresponding intensity profiles (C/D) of the 2D surface chemical gradients obtained by transfer patterning from a platinum microelectrode array onto a glass slide functionalized with an azide monolayer using 1 mM **1** and A/C) 0.2 mM $CuSO_4$ and TBTA or B/D) 1.0 mM $CuSO_4$ and 100 mM 2,6-lutidine, in DMSO at 1.0 V for 2 min.

6.3 Conclusions

In summary we have demonstrated that platinum microelectrode arrays on glass, with the glass surface in between functionalized with an azide monolayer, were successfully employed for the fabrication of micron-scale surface chemical gradients via electrochemically activated CuAAC ("e-click"). The detection of the surface gradients was performed mainly using fluorescence microscopy, but the method is in principle open to other surface characterization techniques (e.g. SIMS, as also employed here, and Raman spectroscopy) to remove the constraint of a fluorescent dye present.

The shape of the gradient (surface density and steepness) can be tuned, when selecting the proper reaction conditions, ranging from shallow and low density gradients (e.g. using a reaction mixture without Cu(I)-stabilizing ligand) to steep and high density gradients (e.g. using low concentration of Cu(II) in the presence of TBTA).

Furthermore, after optimization of the technique directed to diminish the effect of the disproportionation of Cu(I), we proved the efficacy of the "e-click" to fabricate bio-active surface gradients (here using biotin/streptavidin as a test case). Using the same process, we also attested a readily accessible method for the fabrication of bi-component surface chemical gradients, by means of a facile two-step gradient fabrication. A stacked configuration of electrode array and target substrate appeared useful to create surface gradients on external substrates without electrodes.

This method is an important achievement on the way towards establishing micrometer-scale surface chemical gradients with control over steepness, composition and surface density, of great interest for applications, among others, in biomedicine to investigate physiological processes such as polarization and migration of cells, and in nanotechnology to explore, for example, the induced motion of nano-objects on surfaces.

6.4 Acknowledgments

Sven O. Krabbenborg is gratefully acknowledged for the fabrication of the electrode arrays, for his help and fruitful discussions.

6.5 Experimental section

6.5.1 Materials

The following materials and chemicals were used as received without further purification: 11-bromoundecyltrichlorosilane (ABCR), sodium azide (Sigma-Aldrich), copper sulfate pentahydrate (Aldrich), sodium sulfate anh. (Sigma-Aldrich), L-ascorbic acid (Sigma), 2,6-lutidine (Sigma-Aldrich), tetrabutylammonium tetrafluoroborate (Aldrich), Alexa Fluor® 488 streptavidin (Invitrogen), tetrakis(acetonitrile)copper(I) hexafluorophosphate (Aldrich), poly(dimethylsiloxane) and curing agent (Sylgard 184, Dow Corning), HMDS (BASF), LOR 5A (MicroChem), Olin OiR 907-17 photoresist, Olin OPD 4262 developer (FujiFilm). Ultrapure water with a resistivity below 18.2 MΩ·cm at 25 °C was employed (MilliQ water).
Tris[(1-benzyl-1H-1,2,3-triazol-4-yl)methyl]amine (TBTA),[42] alkyne-modified fluorescein (**1**),[41] coumarin (**2**),[43] and biotin (**3**)[44] were prepared as described before.

6.5.2 Methods

Electrode fabrication. A bilayer lift-off recipe was used for fabricating the Pt electrode arrays on borofloat glass wafers. The detailed fabrication protocol is described in Chapter 5.

Substrate and monolayer preparation. Platinum microelectrode arrays on glass and microscope glass slides were functionalized with azide monolayers.[45] The preparation methods for the two different substrates differ only for the activation step. In the case of microelectrode arrays on glass, the substrates were activated by oxygen plasma treatment prior monolayer formation (10 min, 50 mA, <200 mTorr). In contrast, microscope glass slides were oxidized with piranha solution for 45 min (concentrated H_2SO_4 and 33 % aqueous H_2O_2 in a 3:1 ratio), rinsed with copious amount of MilliQ water, and dried in a nitrogen stream. The activated substrates were used immediately to form a silanized monolayer. The substrates were immersed in 0.1 vol% of 11-bromoundecyltrichlorosilane in dry toluene under argon for 1 h at room temperature. Following monolayer formation,

the substrates were rinsed with toluene to remove any excess of silanes, with ethanol and subsequently dried in a nitrogen flow. The bromide/azide nucleophilic substitution was carried out by reaction with a saturated NaN_3 solution in DMF for 48 h at 70 ^oC. The substrates were thoroughly rinsed with MilliQ water and ethanol and dried in a nitrogen flow.

Electrochemically activated CuAAC. Platinum microelectrode arrays on glass, with the glass substrate areas functionalized with the azide monolayer, were subsequently used for the surface gradient fabrication via electrochemically activated CuAAC reaction. The electrochemical experiments were conducted using a voltage source without a reference electrode. Aware that the exact potential applied on the working electrode is unknown, we first performed a basic electrochemical characterization of the system. The current vs. time and current vs. potential difference graphs (Figure 6.15) illustrate that the reduction reactions of Cu(II) occurred for an applied potential difference higher than 0.4 V, and that the current became constant within 30 s. By leaving out a reference electrode we made sure that the current generated at the anode and cathode are of the same magnitude but of opposite sign, which made sure that the two electrochemical reactions occurring are equal when no side reactions are occurring.[46] This should ensure a stable solution gradient in between the interdigitated electrode array.

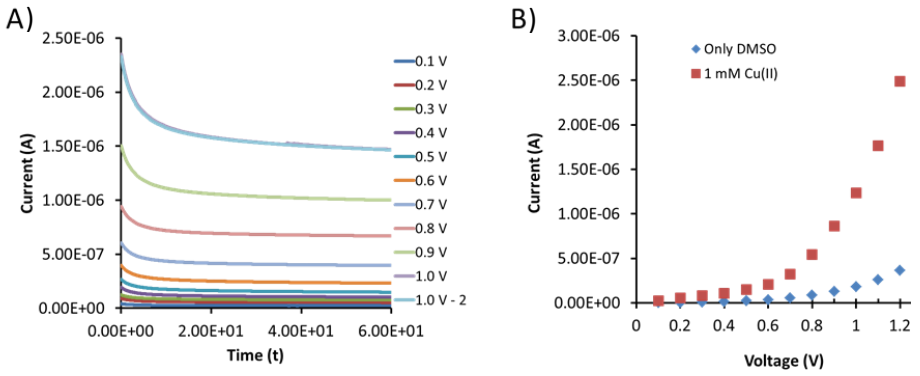

Figure 6.15. Graphs of A) Current vs. Time for a solution of 1 mM $CuSO_4$ in DMSO and B) current vs. potential for a solution with or without 1 mM $CuSO_4$ in DMSO.

Owing to the enhancement of Cu(I) stability in non-aqueous solvents and to ensure the solubility of all the components of the reaction mixture, the reaction was conducted in dry dimethylsulfoxide (DMSO).[47] The reaction was performed under ambient conditions.

Reactions with different experimental conditions were performed in silicone containers on top of the electrode array. In a typical electrochemical experiment, 100 µL of

a solution containing alkyne-modified fluorescein (**1**) (or alkyne-modified coumarin (**2**) or biotin (**3**)), $CuSO_4$ and Cu(I)-stabilizing ligand (TBTA or 2,6-lutidine) in DMSO were subjected to a potential difference for a few min to perform the reduction of Cu(II) to Cu(I) at the cathode (source) and the oxidation of Cu(I) to Cu(II) at the anode (sink). Adopting this protocol, surface gradients of **1**, of a second alkyne modified dye **2** and of biotin (**3**)/streptavidin (SAv) were achieved. After the reaction, the electrodes were quickly rinsed with DMF and ethanol to avoid any further progress of the reaction and to remove any physisorbed material, then they were dried in a stream of N_2.

For preparing a bi-component gradient, after development of the first surface gradient of **1** as described above, the cathode and anode were swapped and a second surface gradient of **2** was formed using the same method and conditions. Using similar conditions also a mono-component bi-directional surface chemical gradient of **2** was fabricated.

A full monolayer of **1** was prepared by incubation of an azide monolayer on glass in a 1 mM solution of **1**, 10 µM $CuSO_4$ and 150 µM ascorbic acid in t-BuOH/H_2O (2/1 v/v) for 24 and 96 h. The substrates were rinsed with methanol, water, sonicated in methanol and dried with N_2.

Prior to fluorescence characterization all the samples were dipped in a 50 mM borax solution at pH 10 to assure the activation of **1**.

Micro-contact printing of alkyne-modified biotin and immobilization of Alexa Fluor 488-labeled streptavidin. Stamps were prepared by casting a 10:1 (v/v) mixture of poly(dimethylsiloxane) and curing agent (Sylgard 184, Dow Corning) against a silicon master. After overnight curing at 60°C, the stamps were oxidized by oxygen plasma for 10 s (current tuned at 50 mA) and subsequently inked by dropcasting the inking solution onto the stamp (1.5 mM alkyne-modified biotin (**3**), 0.5 mM Cu(I)$(CH_3CN)_4PF_6$ and 0.5 mM TBTA (CH_3CN/EtOH 2/1, v/v) (catalyst mixture), prepared by mixing 75 µL of a 2 mM solution of **3** in CH_3CN and 25 µL of 2 mM of catalyst mixture). After 4 min incubation the stamps were blown dry in a stream of nitrogen and brought into conformal contact with the substrate for 60 min. The stamps were changed for each new printing, and the same inking procedure was used. After stamp removal, the printed substrates were rinsed with ethanol, sonicated in acetonitrile for 2 min, rinsed again with ethanol, blown dry with nitrogen and imaged by fluorescence microscopy.

The substrates functionalized with biotin were incubated with 300 nM Alexa Fluor® 488 streptavidin (Alexa-SAv) in phosphate buffered saline (PBS) with 0.005%Tween20 for 5 min, rinsed with PBS with 0.01% Tween20 for 30 min and with MilliQ water, and dried with

nitrogen. The same incubation/rinsing protocol was employed for substrates with patterns and surface gradients of biotin.

Transfer of gradients onto external substrates via electrochemically activated CuAAC. Glass slides (1.5 × 1.5 cm) functionalized with azide monolayers were employed as external substrates for the fabrication of surface chemical gradients transferred from platinum microelectrode arrays (which are not modified with azide monolayers). In a typical electrochemical experiment, 5 µL of a solution containing **1**, $CuSO_4$ and Cu(I)-stabilizing ligand (TBTA or 2,6-lutidine) in DMSO was put on top of the microelectrode array, and the azide-functionalized glass slide was gently placed on top, with consequent spreading and formation of a thin layer of solution. The maximum distance between glass slide and microelectrode array, considering the volume of solution used and the contact area between the two surfaces, was estimated to be approximately 28 µm. The electrochemically activated CuAAC reaction was performed using similar conditions described above for the fabrication of surface chemical gradients. Following the gradient fabrication, both glass slide and microelectrode array were rinsed with DMF and ethanol to avoid any further proceeding of the reaction and to remove any physisorbed material, after which they were blown dry with N_2. In addition, more complex surface chemical gradients were prepared on existing surface gradients performing a second transfer of gradient upon perpendicular rotation of the previously functionalized substrate.

Data fitting. All fluorescence images were analyzed with ImageJ, by extracting cross sections with averaging over 100 µm, resulting in fluorescence intensity vs. distance graphs. A different substrate was used for every different set of reaction conditions.
To compare the results of different samples, the fluorescence intensity profiles were normalized. To obtain normalized fluorescence intensities, the background was subtracted and the resulting intensities were divided by the intensity obtained from the full monolayer (with subtracted background, Figure 6.2).

The steepness (m) of the gradient was estimated as the slope obtained from the linear fitting of the intensity vs. distance graph. Consequently, the slope was calculated from the linear regression of a range of data selected from the steeper region of the surface gradient (defined as the linear range) that led to a correlation coefficient (R^2) higher than 0.97. The maximum intensity (I_{max}) was extracted directly as the highest value of the intensity profile. Calculation of m and I_{max} was performed only on samples that experienced negligible effect of the Cu(I) disproportionation.

Table 6.1. Table of the slope (*m*), correlation coefficient (R^2), linear range and maximum of intensity near the cathode (I_{max}) as function of the reaction conditions. All the results refer to 1 mM of compound **1** in the reaction mixture, with the exception of 33. and 34. where **1** was used in a concentration of 5.0 mM and 0.2 mM, respectively.

[Cu(II)] (mM)	Ligand / [ligand] (mM)	Supporting electrolyte (mM)	Potential (V)	Reaction time (min)	Gap size (µm)	*m* (μm^{-1})	R^2	Linear range [µm]	I_{max}
1. 0.2	TBTA/0.2	Na_2SO_4 0.8	1.0	4	100	0.042	0.995	13.7	0.917
2. 0.2	TBTA/0.2	Na_2SO_4 0.8	1.0	8	100	0.052	0.998	16.3	1.142
3. 1.0	TBTA/1.0	/	1.0	1	100	0.030	0.998	22.8	0.920
4. 1.0	/	/	1.0	4	100	0.007	0.993	42.3	0.477
5. 1.0	/	/	1.0	2	100	0.006	0.983	34.5	0.416
6. 1.0	/	/	1.0	1	100	0.004	0.975	24.7	0.188
7. 0.2	TBTA/0.2	Na_2SO_4 0.8	1.0	2	50	0.045	0.999	9.8	0.710
8. 0.2	TBTA/0.2	Na_2SO_4 0.8	1.0	1	50	0.028	0.993	8.5	0.363
9. 1.0	TBTA/1.0	/	1.0	1	50	0.026	0.984	16.3	0.620
10. 0.2	TBTA/0.2	Na_2SO_4 0.8	1.0	1	25	0.014	0.984	10.4	0.382
11. 0.2	TBTA/0.2	Na_2SO_4 0.8	1.0	2	25	0.029	0.991	8.5	0.575
12. 0.2	TBTA/0.2	Na_2SO_4 0.8	1.0	1	10/50	0.036	0.987	6.5	0.436
13. 0.2	TBTA/0.2	Na_2SO_4 0.8	1.0	1	10/5	0.072	0.968	3.2	0.455
14. 1.0	2,6-lut./100	/	0.4	4	100	0.013	0.996	13.0	0.304
15. 1.0	2,6-lut./100	/	0.6	4	100	0.023	0.991	14.3	0.604
16. 1.0	2,6-lut./100	/	0.8	4	100	0.017	0.997	40.3	1.114
17. 1.0	2,6-lut./100	/	1.0	4	100	0.018	0.998	47.5	1.130
18. 1.0	2,6-lut./100	/	0.4	4+8	100	0.017	0.997	22.8	0.622
19. 1.0	2,6-lut./100	/	0.4	4+8+16	100	0.022	0.998	26.0	0.997
20. 1.0	2,6-lut./100	/	0.4	28	100	0.022	0.998	32.5	1.095
21. 1.0	2,6-lut./100	/	0.6	4+8	100	0.020	0.996	32.5	1.043
22. 0.2	2,6-lut./20	Na_2SO_4 0.8	1.0	4	100	0.020	0.972	7.8	0.291
23. 0.2	2,6-lut./20	Na_2SO_4 0.8	1.0	8	100	0.044	0.967	4.6	0.522
24. 0.2	2,6-lut./20	Na_2SO_4 0.8	1.0	16	100	0.032	0.995	9.8	0.558
25. 5.0	2,6-lut./500	/	1.0	1	100	0.018	0.998	20.8	0.713
26. 5.0	2,6-lut./500	/	1.0	2	100	0.024	0.997	34.5	1.163
27. 5.0	2,6-lut./500	/	1.0	4	100	0.021	0.998	47.5	1.267
28. 1.0	2,6-lut./100	nBu_4NBF_4 100	1.0	2	100	0.007	0.997	12.4	0.160
29. 1.0	2,6-lut./100	nBu_4NBF_4 100	1.0	4	100	0.007	0.994	29.9	0.329
30. 1.0	2,6-lut./100	nBu_4NBF_4 100	1.0	8	100	0.010	0.998	39.7	0.563

31. 1.0	2,6-lut./100	nBu_4NBF_4 100	1.0	16	100	0.011	0.996	31.9	0.610
32. 1.0	2,6-lut./100	nBu_4NBF_4 100	1.0	32	100	0.013	0.997	37.1	0.828
33. 1.0	2,6-lut./100	/	1.0	4	100	0.034	0.997	5.9	0.318
34. 1.0	2,6-lut./100	/	1.0	4	100	0.008	0.998	65.1	0.702

6.5.3 Equipment

Fluorescence microscopy. Fluorescence microscopy images were taken using an Olympus inverted research microscope IX71 equipped with a mercury burner U-RFL-T as light source and a digital Olympus DR70 camera for image acquisition. For the visualization of the coumarin gradient (**2**), UV excitation ($350 \leq \lambda_{ex} \leq 370$ nm) and blue emission ($\lambda_{em} \geq 420$ nm) was employed using a Dapi Olympus filter cube. For the visualization of **1** and Alexa-SAv gradient, blue excitation ($460 \leq \lambda_{ex} \leq 490$ nm) and green emission ($\lambda_{em} \geq 520$ nm) was employed using the U-MWB2 Olympus filter. All fluorescence microscopy images were acquired in air.

Mass spectra. ESI-MS mass spectra were recorded using an LCT Mass spectrometer (Waters/Micromass).

NMR. ^{1}H and ^{13}C NMR spectra were recorded on a Varian Unity (300 MHz) spectrometer. ^{1}H and ^{13}C chemical shifts values, measured at 300 MHz and 75 MHz, respectively, are reported as δ (in ppm) using the residual solvent signal as internal standard (7.26 ppm for $CDCl_3$ and 2.50 ppm for DMSO-d_6).

Electrical measurements and electrochemical reaction. The electrical current measurements were done with a Karl Süss probe station connected to a Keithley 4200 Semiconductor Characterization System.
The electrochemical reaction was performed using an ES015-10 power supply (Delta Elektronica) with voltage range from 0 to 15 V and current range from 0 to 10 A.

Time-of-flight secondary ion mass spectrometry (ToF-SIMS). ToF-SIMS experiments were performed with ToF-SIMS IV and ToF-SIMS5-300 (tascon GmbH, Münster, Germany). For all measurements, a 25 keV Bi^{3+} cluster primary ion beam was employed (target current of 1 pA). The lateral resolution is 3-5 µm for routine analysis at full mass resolution. A pulsed, low energy electron flood was used to neutralize sample charging. For each sample, spectra were collected from 128 × 128 pixels over an area of 500 × 500 μm^2. The positive and negative secondary ions were extracted from the sample surface, mass separated and

detected via a reflectron-type of time-of-flight analyzer, allowing parallel detection of ion fragments having a mass/charge ratio up to 900 within each cycle (100 µs).

The most intense signals for the azide monolayer were recorded in the region with mass below 60 u, belonging to $(CH2)_xN_x$ fragments, typical of the azide monolayer ($Si(CH_2)11N_3$).

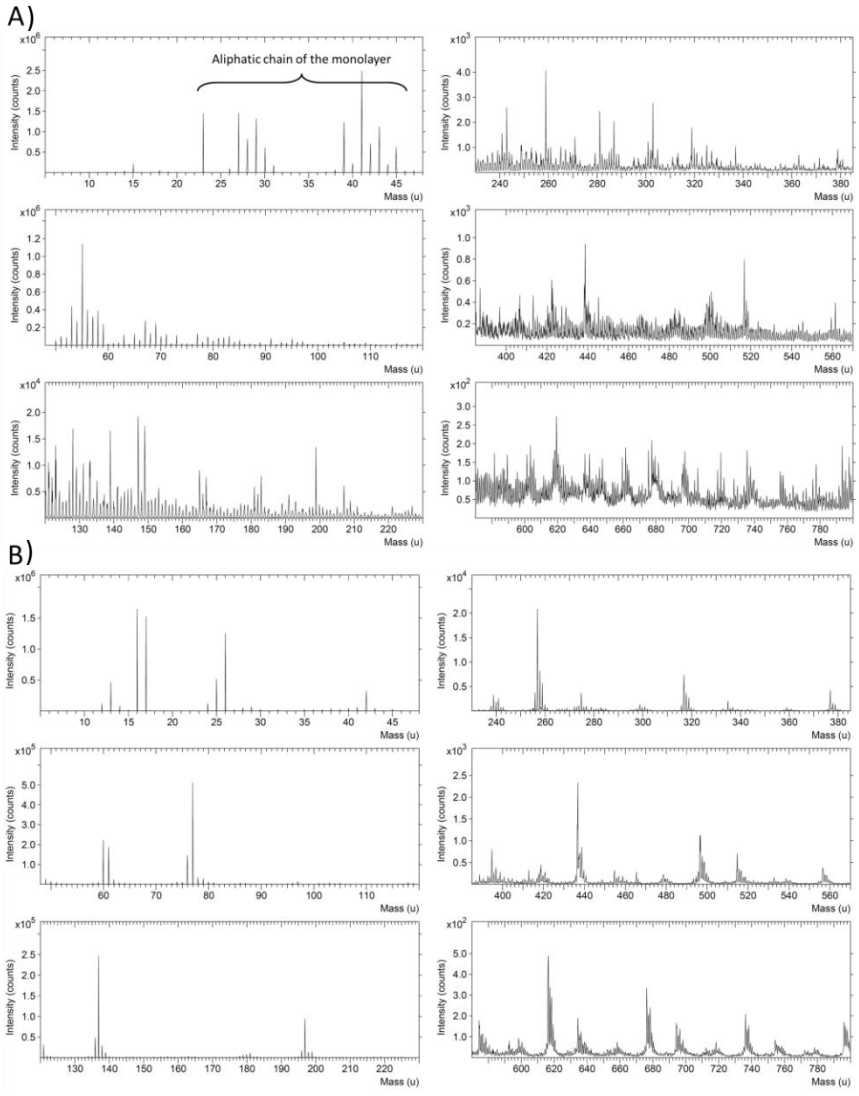

Figure 6.16. Surface analysis by means of Tof-SIMS of an azide monolayer on glass, in A) positive and B) negative mode.

The typical peaks for the monolayer of **1** in positive mode are: 332 ($C_{20}H_{12}O_5^+$), 374 ($C_{21}H_{12}O_4NS^+$) and 390 ($C_{21}H_{12}O_5NS^+$) u; and in negative mode are 300, 310 and 325 u.

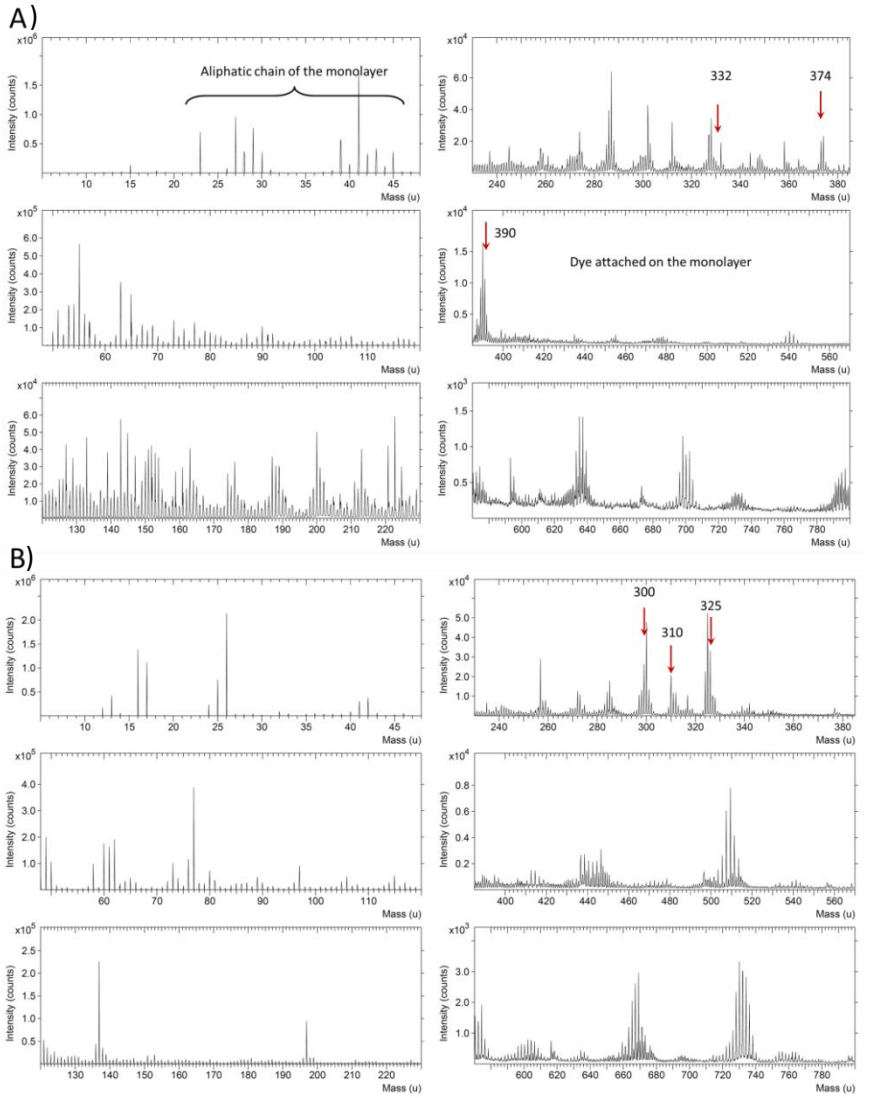

Figure 6.17. Surface analysis by means of Tof-SIMS of an azide monolayer on glass after functionalization with **1** (1 mM **1**, 10µM $CuSO_4$ and 1mM ascorbic acid in tert-butanol/water=1/2 for 24 h), in A) positive and B) negative mode.

6.6 References

(1) van Dover, R. B.; Schneemeyer, L. F.; Fleming, R. M. *Nature* **1998**, *392*, 162.
(2) Suresh, S. *Science* **2001**, 292, 2447.
(3) Genzer, J.; Fischer, D. A.; Efimenko, K. *Appl. Phys. Lett.* **2003**, *82*, 266.

(4) Stafford, C. M.; Harrison, C.; Beers, K. L.; Karim, A.; Amis, E. J.; Vanlandingham, M. R.; Kim, H.-C.; Volksen, W.; Miller, R. D.; Simonyi, E. E. *Nat. Mater.* **2004**, *3*, 545.
(5) Julthongpiput, D.; Fasolka, M. J.; Zhang, W.; Nguyen, T.; Amis, E. J. *Nano Lett.* **2005**, *5*, 1535.
(6) Kholodenko, B. N. *Nat. Rev. Mol. Cell Biol.* **2006**, *7*, 165.
(7) Gurdon, J. B.; Bourillot, P. Y. *Nature* **2001**, *413*, 797.
(8) Weber, M.; Hauschild, R.; Schwarz, J.; Moussion, C.; de Vries, I.; Legler, D. F.; Luther, S. A.; Bollenbach, T.; Sixt, M. *Science* **2013**, *339*, 328.
(9) Coussens, L. M.; Werb, Z. *Nature* **2002**, *420*, 860.
(10) Smith, J. T.; Elkin, J. T.; Reichert, W. M. *Exp. Cell Res.* **2006**, *312*, 2424.
(11) Smith, J. T.; Tomfohr, J. K.; Wells, M. C.; Beebe, T. P.; Kepler, T. B.; Reichert, W. M. *Langmuir* **2004**, *20*, 8279.
(12) Liu, L. Y.; Ratner, B. D.; Sage, E. H.; Jiang, S. Y. *Langmuir* **2007**, *23*, 11168.
(13) Wu, J. D.; Mao, Z. W.; Tan, H. P.; Han, L. L.; Ren, T. C.; Gao, C. Y. *Interface Focus* **2012**, *2*, 337.
(14) Winkler, T.; Ballav, N.; Thomas, H.; Zharnikov, M.; Terfort, A. *Angew. Chem. Int. Ed.* **2008**, *47*, 7238.
(15) Chaudhury, M. K.; Whitesides, G. M. *Science* **1992**, *256*, 1539.
(16) Daniel, S.; Chaudhury, M. K.; Chen, J. C. *Science* **2001**, *291*, 633.
(17) Ichimura, K.; Oh, S. K.; Nakagawa, M. *Science* **2000**, *288*, 1624.
(18) Berna, J.; Leigh, D. A.; Lubomska, M.; Mendoza, S. M.; Perez, E. M.; Rudolf, P.; Teobaldi, G.; Zerbetto, F. *Nat. Mater.* **2005**, *4*, 704.
(19) Walder, R.; Honciuc, A.; Schwartz, D. K. *Langmuir* **2010**, *26*, 1501.
(20) Perl, A.; Gomez-Casado, A.; Thompson, D.; Dam, H. H.; Jonkheijm, P.; Reinhoudt, D. N.; Huskens, J. *Nat. Chem.* **2011**, *3*, 317.
(21) Simon, C. G.; Lin-Gibson, S. *Adv. Mater*. **2011**, *23*, 369.
(22) Genzer, J.; Bhat, R. R. *Langmuir* **2008**, *24*, 2294.
(23) Morgenthaler, S.; Zink, C.; Spencer, N. D. *Soft Matter* **2008**, *4*, 419.
(24) Lamb, B. M.; Park, S.; Yousaf, M. N. *Langmuir* **2010**, *26*, 12817.
(25) Geissler, M.; Chalsani, P.; Cameron, N. S.; Veres, T. *Small* **2006**, 2, 760.
(26) Burgos, P.; Geoghegan, M.; Leggett, G. J. *Nano Lett.* **2007**, *7*, 3747.
(27) Ballav, N.; Schilp, S.; Zharnikov, M. *Angew. Chem. Int. Ed.* **2008**, *47*, 1421.
(28) Fuierer, R. R.; Carroll, R. L.; Feldheim, D. L.; Gorman, C. B. *Adv. Mater*. **2002**, *14*, 154.
(29) Rostovtsev, V. V.; Green, L. G.; Fokin, V. V.; Sharpless, K. B. *Angew. Chem. Int. Ed.* **2002**, *41*, 2596.
(30) Tornøe, C. W.; Christensen, C.; Meldal, M. *J. Org. Chem.* **2002**, *67*, 3057.
(31) Meldal, M.; Tornøe, C. W. *Chem. Rev.* **2008**, *108*, 2952.
(32) Bock, V. D.; Hiemstra, H.; van Maarseveen, J. H. *Eur. J. Org. Chem.* **2006**, *1*, 51.
(33) Hong, V.; Udit, A. K.; Evans, R. A.; Finn, M. G. *ChemBioChem* **2008**, *9*, 1481.
(34) Hansen, T. S.; Daugaard, A. E.; Hvilsted, S.; Larsen, N. B. *Adv. Mater.* **2009**, *21*, 4483.
(35) Devaraj, N. K.; Dinolfo, P. H.; Chidsey, C. E. D.; Collman, J. P. *J. Am. Chem. Soc.* **2006**, *128*, 1794.
(36) Bartels, J.; Lu, P.; Maurer, K.; Walker, A. V.; Moeller, K. D. *Langmuir* **2011**, *27*, 11199.
(37) Ku, S. Y.; Wong, K. T.; Bard, A. J. *J. Am. Chem. Soc.* **2008**, *130*, 2392.

(38) Rydzek, G.; Jierry, L.; Parat, A.; Thomann, J.-S.; Voegel, J.-C.; Senger, B.; Hemmerlé, J.; Ponche, A.; Frisch, B.; Schaaf, P.; Boulmedais, F. *Angew. Chem. Int. Ed.* 2011, *50*, 4374.
(39) Hansen, T. S.; Lind, J. U.; Daugaard, A. E.; Hvilsted, S.; Andresen, T. L.; Larsen, N. B. *Langmuir* 2010, *26*, 16171.
(40) Shida, N.; Ishiguro, Y.; Atobe, M.; Fuchigami, T.; Inagi, S. *ACS Macro Lett.* 2012, *1*, 656.
(41) Krabbenborg, O. S.; Nicosia, C.; Chen, P.; Huskens, J. *Nat. Commun.* 2013, *4*:1667 doi: 10.1038/ncomms2688.
(42) Chan, T. R.; Hilgraf, R.; Sharpless, K. B.; Fokin, V. V. *Org. Lett.* 2004, *6*, 2853.
(43) Nicosia, C.; Cabanas-Danes, J.; Jonkheijm, P.; Huskens, J. *ChemBioChem* 2012, *13*, 778 .
(44) He, B.; Velaparthi, S.; Pieffet, G.; Pennington, C.; Mahesh, A.; Holzle, D. L.; Brunsteiner, M.; van Breemen, R.; Blond, S. Y.; Petukhov, P. A. *J. Med. Chem.* 2009, *52*, 7003.
(45) Balachander, N.; Sukenik, C. N. *Langmuir* 1990, 6, 1621.
(46) Bard, A. J.; Faulkner, L. R. Electrochemical Methods: Fundamentals and Applications, 2nd Ed., Wiley: New York, 2001.
(47) Malyszko, J.; Scendo, M. *Monatsh. Chem*. 1987, *118*, 435.
(48) Rodionov, V. O.; Fokin, V. V.; Finn, M. G. *Angew. Chem. Int. Ed.* 2005, *44*, 2210.
(49) Klonis, N.; Sawyer, W. H. *J. Fluoresc.* 1996, *6*, 147.
(50) Malyszko, J.; Scendo, M. J. *Electroanal. Chem.* 1988, *250*, 61.
(51) Horne, W. S.; Stout, C. D.; Ghadiri, M. R *J. Am. Chem. Soc.* 2003, *125*, 9372.
(52) Reetz, M. T.; Quaiser, S. A. *Angew. Chem. Int. Ed.* 1995, *34*, 2240.
(53) Reetz, M. T.; Westermann, E. *Angew. Chem. Int. Ed.* 2000, *39*, 165.

Chapter 7

"I don't know anything, but I do know that everything is interesting if you go into it deeply enough." — Richard P. Feynman, The Pleasure of Finding Things Out.

In-situ fluorimetric detection of micrometer-scale pH gradients at the solid/liquid interface*

This chapter describes the development of a sensing system for the real-time analysis of the pH of solutions and pH gradients in solution at the solid/liquid interface. A pH-sensitive fluorescent platform has been developed by "clicking" an alkyne-modified N-methylpiperazine naphthalimide on an azide monolayer on glass. The surface immobilization of the molecular probe was assessed by X-ray photoelectron spectroscopy while sensitivity and reversibility were demonstrated by fluorescence microscopy and contact angle goniometry. The pH titration of the platform allowed for the determination of the pK_a value of the pH-sensitive probe at the solid/liquid interface. The effect of the surface density of the pH-sensitive probe on the acid/base equilibrium was investigated using a micron-scale surface chemical gradient of the dye fabricated by means of the electrochemically activated "click" reaction. The platform was employed for the real-time interfacial analysis of micron-scale pH gradients at the solid/liquid interface induced by the electrolysis of water as exerted by an interdigitated microelectrode array.

*Part of this chapter has been published in: C. Nicosia, S. O. Krabbenborg, D. N. Reinhoudt, J. Huskens, *Supramol. Chem.*, **2013**, accepted

7.1 Introduction

Reactions on surfaces are of key importance to control the chemical and physical properties of surfaces for the implementation of microarray-, sensor-, and catalyst-based technologies. Self-assembled monolayers (SAMs), highly ordered molecular assemblies formed by the adsorption of a one-molecule-thick layer on the surface of a variety of solids,[1, 2] are excellent systems to study interfacial reactions owing to the fine-tuning of the surface chemistry obtained upon assembly of functional molecules.[3-6]

The development of molecular sensing systems on surfaces is of paramount importance for the development of optical and biomedical applications. SAMs can be designed to function as optical sensors for example when functionalized with fluorescent groups. Fluorogenic molecules were employed as reactive monolayers for the fabrication of microarrays[7, 8] and for the simultaneous immobilization and detection of bio- and macro-molecules.[9-13] In particular, the need for monitoring pH in many chemical and biological processes at interfaces has driven the development of pH-sensitive fluorescent monolayers. SAMs have been modified with pH sensing units and employed for the fabrication of pH-sensitive multicolor fluorescent platforms,[14] arrays[15, 16] and microflluidic devices.[17]

Reversible fluorescent switches are commonly used for the preparation of pH-sensitive materials. Naphthalimide-based dyes have exceptional photophysical properties due to their high photostability and quantum yield, and their large Stokes shift. Furthermore, their easy synthesis and structural modification allow for the straightforward insertion of a suitable anchoring group for the covalent immobilization in polymer networks or on reactive surfaces. The “off-on” fluorescent behavior of amino-functionalized naphthalimides is based on the well-known protonation-mediated photo-induced electron transfer (PET) process.[18-21] Previous studies have shown the fabrication of naphthalimide-based pH-sensitive sensors upon covalent immobilization via photo-copolymerization of an allyl- or acrylate-modified dye with other acrylates as diluents to prepare pH-sensing membranes[22] or via amide formation between the *N*-hydroxysuccinimide ester-activated dye and hydrogels.[23]

Proton gradients play a pivotal role in nature, in particular in a process called aerobic respiration in which the concentration difference of protons across a membrane is responsible for powering the synthesis of ATP, the energy building block of life. Electrochemical methods based on the electrolysis of water for the generation of pH gradients in solution have been described.[24, 25] Macounovà and coworkers quantified the gradients via optical microscopy using acid-base indicators in solution and employed them

to investigate the isoelectric focusing of proteins in microfluidic channels formed by two parallel gold electrodes.[24] Similar pH gradients were obtained by Fuhr *et al.* and these were characterized by fluorescence microscopy using a fluorescein-based dye in solution.[26] Moreover, a microelectrochemical pH-stat was fabricated and employed for the determination of the bioactivity of enzymes and resulted useful also for the fabrication of pH gradients in solution.[27]

Here we describe the fabrication of a pH-sensitive platform upon immobilization of an alkyne-modified *N*-methylpiperazine naphthalimide on an azide monolayer on glass. After calibration of the platform for the determination of the pK_a value of the pH-sensitive probe at the solid/liquid interface, the platform was employed for the real-time interfacial analysis and quantification of pH gradients prepared by the electrolysis of water. The effect of the surface density of the pH-sensitive probe on the acid/base equilibrium was investigated using a micron-scale surface chemical gradient of the dye.

7.2 Results and discussion

7.2.1 Synthesis

The synthesis of the 1,8-naphthalimide-based pH probe **2** functionalized with alkyne and *N*-methylpiperazine groups was performed in two steps as described in Scheme 7.1. The alkyne moiety is introduced for the surface immobilization of **2** on azide monolayers on glass via the copper(I)-catalyzed azide-alkyne cycloaddition (CuAAC) while the *N*-methylpiperazine unit allows for the "off-on" photoinduced electron transfer (PET)-mediated switching upon modulation of the pH of the solution.

4-Bromo-1,8-naphthalic acid anhydride in ethanol was reacted overnight at reflux with 6-amino-1-hexyne to give the condensation product **1**. In order to obtain the target 1,8-naphthalimide **2**, a nucleophilic substitution of the bromide of the intermediate compound **1** was accomplished in the presence of *N*-methylpiperazine via overnight reaction at reflux in 2-methoxyethanol. The water-soluble compound **3** was synthesized by means of the Cu(I)-catalyzed alkyne-azide cycloaddition between compound **2** and azido-tri(ethylene glycol). The pH-insensitive and water-soluble compound **4** was prepared via methylation of **2** with methyl iodide by overnight reaction at reflux in methanol. While compounds **2** and **4** were used for surface immobilization, compounds **3** and **4** were employed for the characterization in solution.

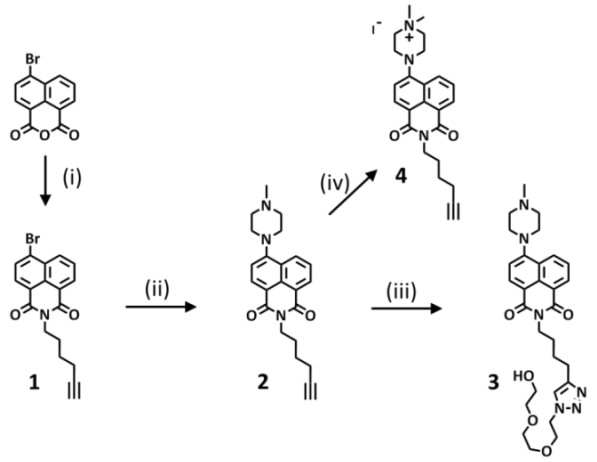

Scheme 7.1 i) 6-amino-1-hexyne, ethanol, reflux, o.n.; ii) *N*-methylpiperazine, 2-methoxyethanol, reflux, o.n.; iii) azido-tri(ethylene glycol), $Cu(CN)_4PF_6$, TBTA, MeOH, r.t., o.n.; iv) methyl iodide, methanol, reflux.

7.2.2 Photophysical characterization in solution

Prior to investigation of the properties of the, poorly water-soluble, compound **2** at the solid/liquid interface, the fluorescence properties of the water-soluble derivative **3** were studied in solution. The pH dependence of its properties result from the protonation/deprotonation of the *N*-methylpiperazine unit. As already demonstrated by others, the fluorescence quenching of the naphthalimide fluorophore of *N*-methylpiperazinyl-modified naphthalimides is governed by the PET process between the electron-donating aliphatic amine in the basic form of the piperazine moiety and the naphthalimide fluorophore.[18] Therefore, the basic form represents the "off" state. Upon protonation of the aliphatic amine, PET is no longer possible and the fluorescence quenching is suppressed. In other words, the fluorescence intensity is enhanced upon protonation, and the protonated form represents the "on" state. To study the pH dependence of **3**, absorbance and fluorescence spectra of compound **3** were measured in buffer solutions at pH values ranging from 4 to 10 (Figure 7.1A and B). While the absorbance of **3** experienced a blue-shift of a few nm upon protonation (Figure 7.1A), a strong, 125-fold increase of fluorescence intensity at 520 nm was observed when the pH was lowered from 10 to 4 (Figure 7.1B and D). Compound **3** showed a strong fluorescence at a pH lower than 5 with a large Stokes shift of about 125 nm (with excitation and emission peaks at 395 nm and 520 nm, respectively). The pK_a value of compound **3** in solution was determined from the fluorescence spectra (Figure 7.1B) and found to be 6.76 ± 0.03 with a sensitivity range of three pH units (approximately from pH 5.3 to 8.3) using either the Henderson-Hasselbalch equation or the Boltzmann equation for sigmoidal curves (Figure

7.1D).[28] The fact that both equations give comparably good fits indicates that the dye moieties do not influence each other's protonation behavior. All properties indicate that the dye has good qualities to function as a pH-sensitive dye.

As predicted by the PET process, the fluorescence emission of compound 4, which is water-soluble over the whole pH range applied here owing to its permanent positive charge, obtained by quaternization of the aliphatic amine of the piperazine unit of compound **2**, is independent on pH showing a high fluorescence intensity over the whole pH window employed (Figure 7.1C and D).

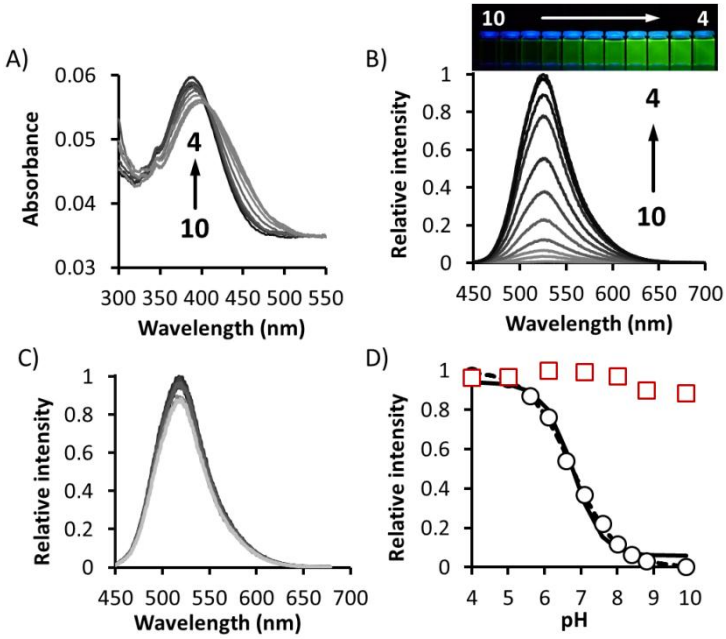

Figure 7.1. A) Absorbance and B) fluorescence spectra of 2 µM of compound **3** at different pHs. The insert shows a fluorescence image of 10 µM solutions of compound **3** at different pHs. C) Fluorescence spectra of 2 µM of compound **4** at different pHs. D) Titration results derived from **3** (B; circles) and **4** (C; squares) selecting the emission intensity at 520 nm at different pHs. The fitting of the data of **3** was performed using the Henderson-Hasselbalch equation (solid line) and the Boltzmann equation for sigmoidal curves (dashed line); both cases gave $pK_a = 6.76 \pm 0.03$ (λ_{exc} = 405 nm, 50 mM buffer solutions).

7.2.3 Fabrication and characterization of the platform

Scheme 7.2 illustrates the procedure employed for the surface immobilization of compound **2** (or **4**) by means of CuAAC. The surface reaction between the azide-terminated monolayer on glass and the alkyne-modified naphthalimide **2** (or **4**) was accomplished via reactive microcontact printing (µCP) using flat or patterned PDMS stamps for the preparation of full monolayers or surface patterns, respectively. During reactive µCP, an oxidized polydimethylsiloxane (PDMS) stamp was inked with a solution of **2** or **4**,

Cu(I)$(CH_3CN)_4PF_6$ and tris[(1-benzyl-1*H*-1,2,3-triazol-4-yl)methyl]amine (TBTA), dried under nitrogen flow and brought into conformal contact for 1 h with a glass slide which was functionalized beforehand with an azide monolayer. After stamp removal, the substrates were rinsed with acetonitrile, blown dry with nitrogen and imaged by fluorescence microscopy.

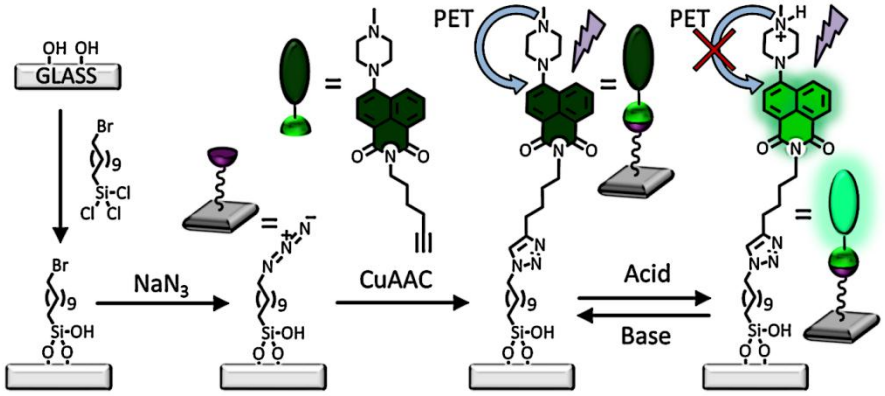

Scheme 7.2. Schematic procedure of the surface functionalization by immobilization of **2** (or **4**) via CuAAC. The fluorescence emission of **2** is switched "on" or "off" by the pH of a solution on top of the monolayer or by pH gradients induced by the electrolysis of water.

When surface patterns of **4** were incubated at either pH 4 (Figure 7.2A) or pH 10 (Figure 7.2B), a negligible effect on the fluorescence intensity was observed. However, when the pH-sensitive platform obtained upon immobilization of **2** was incubated at pH 4 (Figure 7.2C), a 4-fold fluorescence enhancement was observed compared with the intensity obtained at pH 10 (Figure 7.2D). The fluorescence enhancement observed upon switching the pH on the surface is significantly lower than that observed in solution mainly due to the residual fluorescence at high pH (Figure 7.2C and D). Yet this does not preclude the use of the platform for the targeted pH-sensing.

A full monolayer was obtained after printing compound **2** using the above protocol on azide-terminated substrates using a flat PDMS stamp. Water contact angles (Table 7.1) on these substrates were performed using freshly prepared 1 mM hydrochloric acid (pH 3, Figure 7.2E) and 1 mM sodium hydroxide (pH 11, Figure 7.2F) solutions. It is clear that the protonation of the monolayer occurring at low pH increases the hydrophilicity and wettability of the surface as witnessed by a concomitant change of the contact angle (Figure 7.2E-F and Table 7.1).

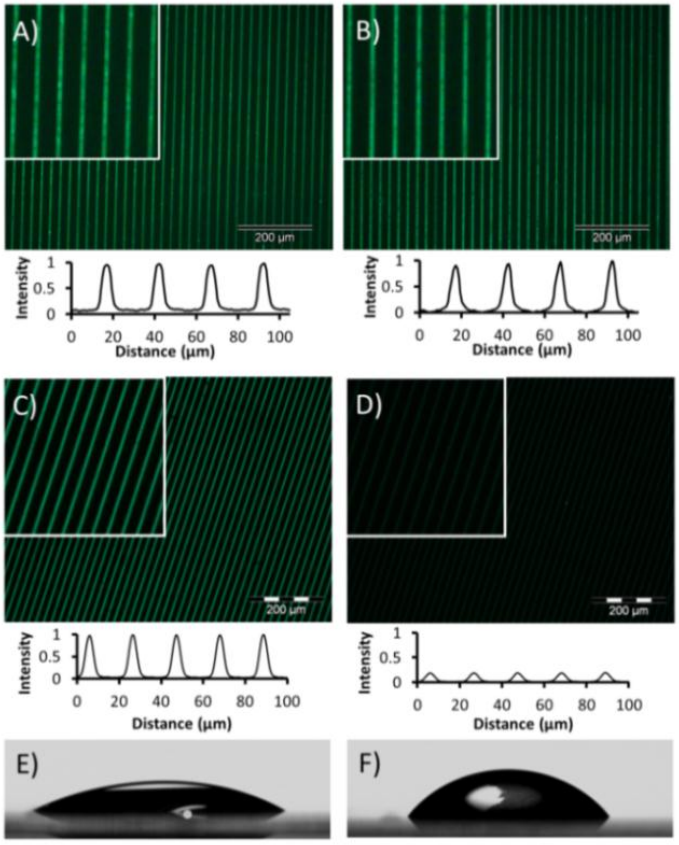

Figure 7.2. Fluorescence microscopy images and corresponding intensity profiles of 5 µm lines prepared by printing **4** (A, B) and **2** (C, D) on an azide-terminated monolayer followed by incubation with pH 4 (A, C) and pH 10 (B, D) solutions (400 nm ≤ λ_{ex} ≤ 420 nm, 490 nm ≤ λ_{em} ≤ 540 nm, 50 mM buffer solution). Contact angle goniometry of a full monolayer of **2** treated with E) pH 3 (1 mM HCl) and F) pH 11 (1 mM NaOH) aqueous solutions.

X-ray photoelectron spectroscopy (XPS) characterization of full monolayers of **2** and its precursor bromide and azide SAMs (see Scheme 7.2) on silicon substrates was performed to provide information on the efficiency of the chemical reactions adopted for the fabrication of the pH-sensitive platform. The XP spectrum of the bromide-terminated SAM shows a pronounced Br_{3d} peak at 70 eV (Figure 7.3A). The nucleophilic substitution of the bromide-terminated SAM with sodium azide resulted in the quantitative disappearance of the Br_{3d} peak and the formation of two N_{1s} peaks at 401 eV (2N) and 405 eV (1N) belonging to the azide-terminated SAM (Figure 7.3B), and the observed C/N ratio (4.0) is in good agreement with the predicted value (3.7). When **2** was immobilized via CuAAC reactive contact printing using a flat PDMS stamp, we observed a drastic change of the N_{1s} spectrum owing to the formation of the triazole unit and the introduction of three new

nitrogens from compound **2**. Further evidence for the formation of the naphthalimide monolayer is the increased C/N ratio (observed 6.5, predicted 5.8) and the appearance of a new peak at 289 eV in the C_{1s} region attributed to the presence of C=O bonds from the naphthalimide group (Figure 7.3C).

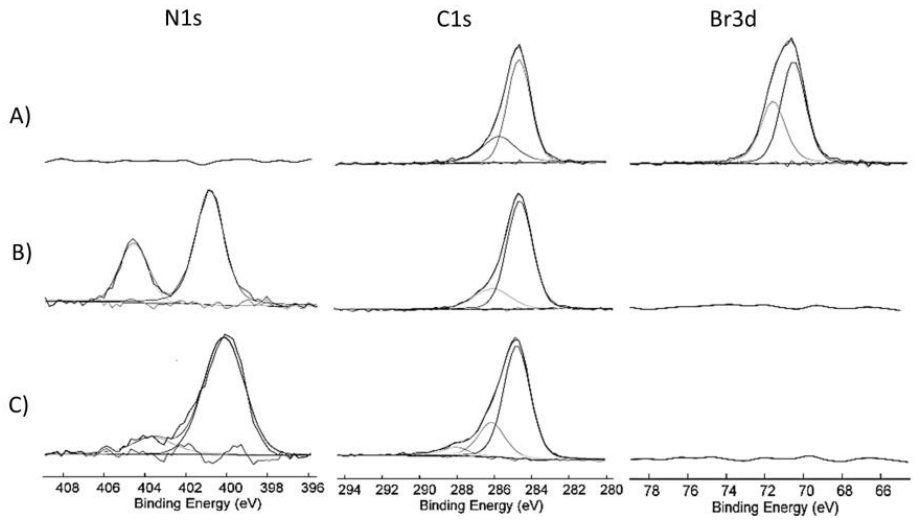

Figure 7.3. X-ray photoelectron spectra of the C_{1s}, N_{1s}, and Br_{3d} regions for monolayers terminated by A) bromide, B) azide, and C) **2**.

Table 7.1. Contact angles and experimental and theoretical atomic C/N ratios by XPS of monolayers of **2** and its precursors.

Monolayer	Static contact angle (θ)	$C/N_{(exp)}$	$C/N_{(th)}$
Br	81±2	---	---
N_3	76±2	4.0	3.7
2	54±2 (pH=11) 30±1 (pH=3)	6.5	5.8

The pH sensitivity of **2** immobilized on azide-terminated monolayers on glass substrates was evaluated by incubating the platform with different buffer solutions ranging from pH 10 to 4 and recording the fluorescence intensity by fluorescence microscopy (Figure 7.4A). The pK_a value of the immobilized compound **2** was found to be similar using either the Henderson-Hasselbalch equation (6.42 ± 0.11) or the Boltzmann equation for sigmoidal curves (6.33 ± 0.14).[28] However, the trend obtained for the pH titration of surface-bound **2** was more gradual than that observed in solution (Figure 7.1D). Clearly, the best fitting was obtained using the Boltzmann equation. Furthermore, the titration of surface-bound **2** resulted in a lower pK_a value (indicating more difficult protonation) in

comparison with the titration of **3** in solution. Numerous studies on carboxylic acid-terminated SAMs on gold have been carried out to determine the pK_a of the carboxylic acid moieties in the monolayer.[29-33] Common results demonstrated that the pK_a of such monolayers is shifted to higher values (indicating more difficult deprotonation) compared to the same molecules in solution owing to a possible combination of effects including steric hindrance, electrostatic repulsion between charged groups, ion solvation, and hydrogen bonding. Thus, we take both the lower pK_a and the more gradual intensity change as evidence of the effect of the surface immobilization of **2** and of the likely interactions between adjacent functional groups.

The fluorescence intensity of platforms patterned with **2** was monitored while switching the pH of the solutions on top between 4 and 10. For several cycles the fluorescent patterns appeared to be reversible and reproducible (Figure 7.4B). Moreover, the reversibility was tested by water contact angle measurements on a full monolayer of **2** on glass. The water contact angle was switched from low to high values, using 1 mM hydrochloric acid and 1 mM sodium hydroxide solutions, respectively (Figure 7.4B) highlighting the effect of the surface protonation/deprotonation on the wettability.

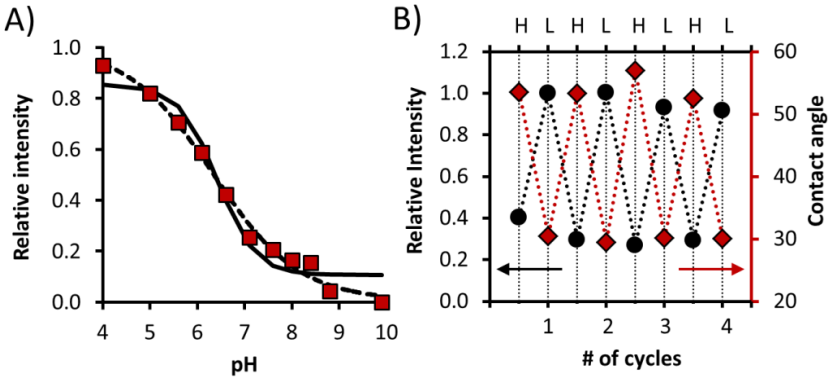

Figure 7.4 A) Titration curve obtained from the fluorescence microscopy images of **2** printed on an azide monolayer on glass and incubated at different pHs (50 mM buffer solutions). The fitting was performed using the Henderson-Hasselbalch equation (solid line) and the Boltzmann equation for sigmoidal curves (dashed line) resulting in a pK_a of 6.42 ± 0.11 or 6.33 ± 0.14, respectively. B) Reversibility of the fluorescence intensity (black dots) and the surface wettability (red diamonds) as a function of the pH of the solution employed (H for high corresponds to pH 10 for the fluorescence and pH 11 for the wettability experiments; L for low corresponds to pH 4 for the fluorescence and pH 3 for the wettability experiments).

The above series of experiments proved that: i) compound **2** is covalently immobilized on azide-terminated monolayers on glass; ii) the PET process responsible for the fluorescent "off-on" switching of immobilized probe **2** is reversibly modulated at the solid/liquid interface; iii) protonation/deprotonation events are also witnessed by surface wettability changes; iv) the pH dependence of surface-bound **2** is slightly affected by the

surface immobilization. At the same time, the calibration curve obtained above will allow us to use the surface-bound pH probe to quantitatively assess pH measurements of solutions positioned on top of it.

7.2.4 Surface chemical gradients via electrochemically activated CuAAC

In order to investigate the effect of the neighboring chargeable groups on the pK_a further, we aimed for varying the density of the pH-sensitive dye on the surface. We envisaged that making a gradient of the dye would allow us to investigate the effect of the density in one go using a single fluorescent substrate.

Recently, we have demonstrated the fabrication of platinum microelectrode arrays on glass to generate micron-scale solution gradients of Cu(I) used to investigate the kinetics of the electrochemically promoted CuAAC, "e-click", on top of azide-terminated monolayers attached to the glass substrate areas between the electrodes (Chapter 5). Furthermore, tuning the reaction conditions (e.g. Cu(II) and alkyne concentration, Cu(I)-stabilizing ligand, reaction time, *etc.*) allowed to control the shape of the micron-scale surface chemical gradients (Chapter 6).

Scheme 7.3 illustrates the system used for the fabrication of surface chemical gradients of **2** via "e-click". Platinum microelectrode arrays on glass, with the glass surface modified with an azide-terminated monolayer, were employed as a reactive platform for the surface gradient immobilization of **2**. The CuAAC reaction, which takes place only in the presence of Cu(I), was carried out by using a solution of Cu(II) ($CuSO_4$) and **2** in DMSO, in the presence of a Cu(I)-stabilizing ligand (TBTA). A constant potential difference of 1.0 V was applied between the electrodes to perform the reduction of Cu(II) to the catalytically active Cu(I) at the cathode and the re-oxidation of Cu(I) to Cu(II) at the anode. Owing to the concentration gradient of Cu(I) in solution, the CuAAC between **2** and the azide monolayer resulted in a faster formation of triazole bonds next to the cathode (where Cu(I) is produced) compared to next to the anode, with the consequent formation of a surface gradient of covalently bound **2**.

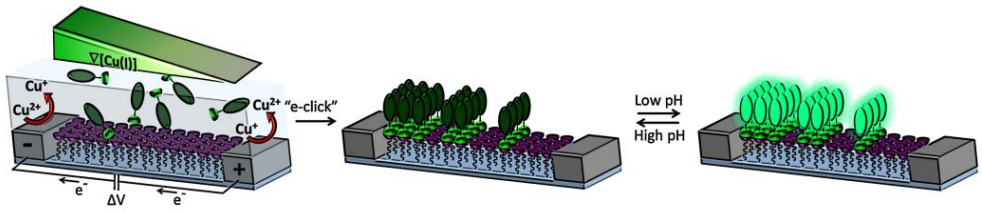

Scheme 7.3. Schematic representation of the fabrication of surface chemical gradients via electrochemically promoted CuAAC of compound **2** on an azide-terminated monolayer on glass between a platinum microelectrode array followed by pH modulation.

Figure 7.5A and B show the fluorescence microscopy images of the resulting micron-scale surface gradients after 2 min reaction of 1 mM $CuSO_4$, 1 mM TBTA and 1 mM **2** in DMSO at a potential difference of 1.0 V upon incubation with buffer solutions at pH 4 and 10, respectively.

Figure 7.5C shows the pH titration of the surface chemical gradient of **2**. The fluorescence intensity vs. distance profiles were extracted from the fluorescence microscopy images upon incubation of the surface gradient of **2** at various pH values ranging from 4 to 10 and plotted on a relative scale assuming the intensity value obtained with the contact printing method to represent full coverage. The intensity profiles were obtained by extracting cross sections with averaging over 100 µm parallel to the electrode. The surface chemical gradient exhibited an approximate 3-fold fluorescence enhancement switching from pH 10 to 4 with the maximum intensity localized next to the cathode. The intensity profiles in Figure 7.5C show a maximum fluorescence intensity, at pH values below 5, at about 70 % of that observed for the microcontact printed sample.

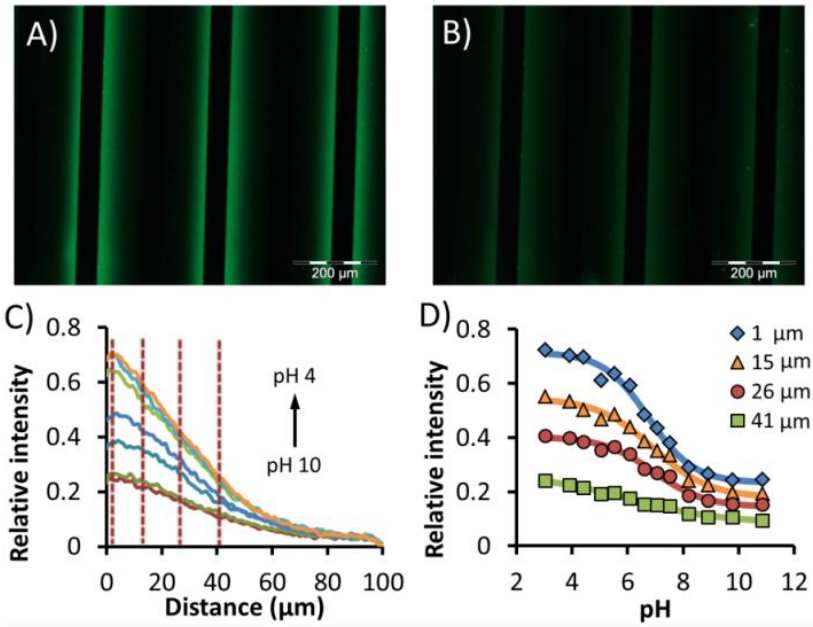

Figure 7.5. Fluorescence microscopy images of the surface chemical gradients resulting from electrochemically activated CuAAC, using 1.0 mM **2**, 1.0 mM $CuSO_4$, 1.0 mM TBTA in DMSO, ΔV = 1 V, after 2 min reaction time incubated with 50 mM buffer solutions at A) pH 4 and B) pH 10. C) Normalized intensity vs. distance graph of the surface chemical gradient of **2** upon incubation at different pHs. D) Normalized intensity vs. pH graph of the surface chemical gradient of **2** at different distances from the cathode (markers) and Boltzmann sigmoidal fits (lines).

In Figure 7.5D the fluorescence vs. distance profiles were plotted vs. pH, each at a specific distance from the negative electrode. At a distance greater than 40 µm from the cathode, the surface density of **2** is too low to allow any fitting of the experimental data. The Boltzmann fitting of the data at the representative distances of 1, 15 and 26 µm from the cathode resulted in pK_a values of 6.75 ± 0.12, 6.92 ± 0.17, and 6.95 ± 0.16, respectively. The pK_a value near the cathode, where the surface density of compound **2** is higher, appeared to be slightly lower than at 15 and 26 µm in agreement with the results obtained for the high density pattern obtained with the microcontact printing method (Figure 7.4A). This indicates that i) pK_a changes only occur at fairly high densities of dyes (> 60 % of dense coverage), and ii) that the changes are small so that the pH sensing properties are not seriously compromised when having samples with slightly varying dye densities.

7.2.5 Analysis of a pH gradient at the solid/liquid interface

We recently demonstrated that micron-scale pH gradients in solution can be obtained via electrolysis of water using platinum microelectrode arrays on glass and that these can be used to perform local pH-dependent surface reactions, such as the acid-catalyzed imine hydrolysis.[34] Here we employed such gradients to investigate the performance of the pH-sensitive dye platform in monitoring and quantifying pH gradients.

Compound **2** was employed for the visualization of a micron-scale pH gradient at the solid/liquid interface (Scheme 7.4). The pH gradient in solution was induced by means of electrolysis of water using a platinum microelectrode array on glass (50 µm electrode size and 100 µm gap width), generating protons at the anode and hydroxide ions at the cathode. In the electrolysis of water, the following reactions occur:

$$H_2O \rightarrow \tfrac{1}{2}O_2 + 2H^+ + 2e^- \quad \text{(anode)} \qquad (1)$$

$$2H_2O + 2e^- \rightarrow H_2 + 2OH^- \quad \text{(cathode)} \qquad (2)$$

The glass surface between the electrodes was first functionalized with an azide-terminated monolayer and then the pH-sensitive probe **2** was immobilized via CuAAC, as shown in Scheme 7.2, yet now using a solution procedure for performing the click step since µCP between the electrodes was not feasible. An electrochemically produced pH gradient was applied on top of the full monolayer in the presence of a supporting electrolyte (100 mM Na_2SO_4). A phosphate buffer (1 mM at pH 7.0) was added to stabilize the pH gradient.[24]

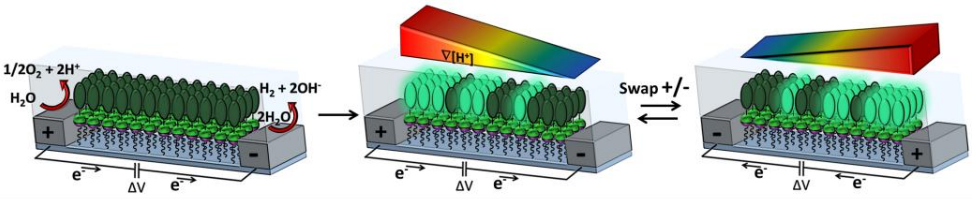

Scheme 7.4. Schematic representation of the *in-situ* visualization of the interfacial pH gradient produced via electrolysis of water between a platinum microelectrode array.

The pH gradient was generated by application of a potential difference over the interdigitated microelectrode array which generated a constant current of 50 µA using a potentiostat. Immobilized compound **2** allowed the *in-situ* visualization of the micron-scale pH gradient generated at the interface between the solution and the monolayer (Figure 7.6A). Figure 7.6B shows the normalized fluorescence intensity profile between anode and cathode at 2 min of electrolysis and the corresponding pH value as a function of the distance from the anode. The position-dependent pH curve (red line in Figure 7.6B) was calculated using the pK_a value and sigmoidal curve determined from the Boltzmann sigmoidal fit of the surface titration of **2** immobilized via microcontact printing (Figure 7.4A). Due to the presence of the pH 7.0 buffer during electrolysis, the pH gradient spanned roughly 2.5 pH unit around the 7.0 central value (Figure 7.6B) falling in the sensitivity range of the surface bound probe **2** (Figure 7.4A).

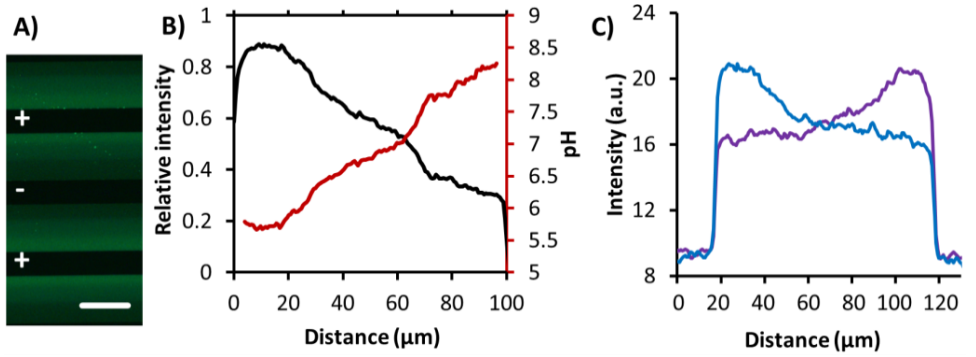

Figure 7.6. A) Fluorescence microscopy image of the micron-scale pH gradient at the solid/liquid interface between a platinum microelectrode array after 2 min at a potential difference which generated a constant current of 50 µA (400 nm ≤ λ_{ex} ≤ 420 nm, 490 nm ≤ λ_{em} ≤ 540 nm; scale bar, 100 µm). B) Fluorescence intensity profile (black) and calculated pH (red) of the surface pH gradient *vs.* distance from the anode. C) Fluorescence intensity profiles upon switching the polarity of anode and cathode.

Figure 7.6C shows the fluorescence intensity profile of the pH-sensitive platform obtained during electrolysis of water after switching the polarity of anode and cathode. Overall, upon switching the polarity of the electrodes, the pH-sensitive platform

demonstrated to be a robust and reversible method for the real-time monitoring of the pH gradient change at the interface.

7.3 Conclusions

In summary, a pH-sensitive fluorescent platform was fabricated via covalent immobilization of an alkyne-modified naphthalimide dye on an azide-terminated monolayer through copper(I) azide-alkyne cycloaddition. The covalent attachment of the pH-sensitive dye was assessed by XPS, while sensitivity, reproducibility and reversibility of the platform upon protonation/deprotonation were demonstrated by water contact angle and fluorescence microscopy. Analysis of the acid/base equilibrium of the pH-sensitive platform resulted in a pK_a value lower than that observed for the same dye free in solution, probably due to increased electrostatic repulsion between neighboring groups upon protonation.

A micron-scale surface gradient of the pH-sensitive probe was prepared to study the effect of the surface density on the pK_a of the immobilized dye in an efficient manner. The results indicated that significant changes of pK_a, in comparison with the solution case, only occur at high surface density (>60%) of the immobilized pH-sensitive probe while at lower density the pH sensing properties are not compromised when having samples with slightly varying dye densities.

The immobilization of the pH-sensitive probe on the glass surface between platinum microelectrode arrays allowed the monitoring of a micron-scale pH gradient at the interface. The pK_a obtained with the calibration of the pH sensitive platform allowed for the *in-situ* quantification of the pH gradient generated by the electrolysis of water. The real-time monitoring of interfacial pH effects is a promising method for the investigation of (bio)chemical processes at interfaces.

7.4 Acknowledgments

Sven O. Krabbenborg is gratefully acknowledged for the pH gradient investigation, for his help and fruitful discussions.

7.5 Experimental section

7.5.1 Materials

The following materials and chemicals were used as received without further purification: 11-bromoundecyltrichlorosilane (ABCR), sodium azide (Acros), 4-bromo-1,8-naphthalic acid anhydride (Aldrich), 1-methyl-piperazine (Fluka), methyl iodide (Sigma-Aldrich), dimethylformamide (Fluka), copper(II) sulfate pentahydrate (Sigma-Aldrich), L-ascorbic acid (Sigma), tetrakis(acetonitrile)copper(I) hexafluorophosphate (Aldrich), 2-

methoxy-ethanol (Aldrich), sodium dihydrogen phosphate monohydrate (Fluka), disodium hydrogen phosphate dehydrate (Fluka), sodium tetraborate decahydrate (Sigma-Aldrich), sodium carbonate (Sigma-Aldrich).

Azido-tri(ethylene glycol)[35] and tris(benzyltriazolylmethyl)amine (TBTA)[36] were prepared as described in the literature.

7.5.2 Synthetic procedures

N-6-Hexynyl-4-bromo-1,8-naphthalimide, 1

A suspension of 4-bromo-1,8-naphthalic acid anhydride (1.0 g, 3.6 mmol) in 100 ml of ethanol, was warmed to obtain a clear solution and then 6-amino-1-hexyne (0.35 g, 4.4 mmol) was added to the solution. The resulting mixture was stirred at reflux for 16 h. The crude product that precipitated on cooling was recrystallized from ethanol as a pale yellow powder (1.13 g, 3.2 mmol, 89%).

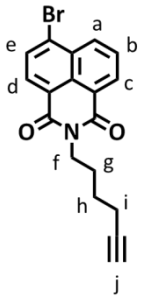

^{1}H NMR (300 MHz, $CDCl_3$): δ (ppm) = 8.7 (d, 1 H, H_a), 8.6 (d, 1 H, H_c), 8.4 (d, 1 H, H_d), 8.1 (d, 1 H, H_e), 7.8 (t, 1 H, H_b), 4.2 (t, 2 H, H_f), 2.2 (dt, 2H, H_i), 1.9 (t, 1H, H_j), 1.8 (m, 2H, H_g), 1.6 (m, 2H, H_h).

^{13}C NMR (75 MHz, $CDCl_3$): δ (ppm) = 163.74, 163.71, 133.40, 132.19, 131.38, 131.23, 130.75, 130.40, 129.12, 128.21, 123.19, 122.32, 84.16, 68.76, 40.10, 27.40, 26.12, 18.36.

ESI-MS: measured 356.1 [M+H$^+$], calculated 356.0 [M+H$^+$].

N-6-Hexynyl-4-(4'-methyl-piperazinyl)-1,8-naphthalimide, 2

A suspension of *N*-6-hexynyl-4-bromo-1,8-naphthalimide (500 mg, 1.4 mmol) in 50 ml of 2-methoxyethanol was refluxed for 16 h with 2.5 equiv of 1-methyl-piperazine (0.39 ml, 3.5 mmol). This product was purified on silica gel using a gradient elution with dichloromethane/ethanol from 95:5 to 9:1 to give **2** as a yellow solid. (410 mg, 0.66 mmol, 78%).

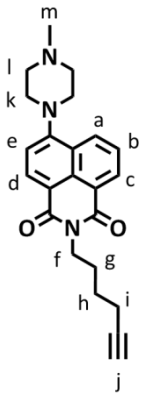

UV absorption: $\lambda_{max}(H_2O)$ = 395 nm

^{1}H NMR (300 MHz, $CDCl_3$): δ (ppm) = 8.58 (d, 1H, H_a), 8.52 (d, 1H, H_d), 8.40 (d, 1H, H_c), 7.69 (t, 1H, H_b), 7.22 (d, 1H, H_e), 4.22 (t, 2H, H_f), 3.32 (bt, 4H, H_k), 2.77 (bt, 4H, H_l), 2.46 (s, 3H, H_m), 2.27 (dt, 2H, H_i), 1.93 (t, 1H, H_j), 1.85 (m, 2H, H_g), 1.65 (m, 2H, H_h).

^{13}C NMR (75 MHz, $CDCl_3$): δ (ppm) = 164.49, 164.00, 132.59, 131.12, 130.24, 129.88, 126.16, 125.66, 123.25, 116.75, 115.04, 84.18, 68.51, 55.13, 52.88, 46.07, 39.67, 27.38, 26.05, 18.26.

ESI-MS: measured 376.3 [M+H$^+$], calculated 376.2 [M+H$^+$].

2-(4-(1-(2-(2-(2-Hydroxyethoxy)ethoxy)ethyl)-1H-1,2,3-triazol-4-yl)butyl)-6-(4 methylpiperazin-1-yl)-1,8-naphthalimide, 3

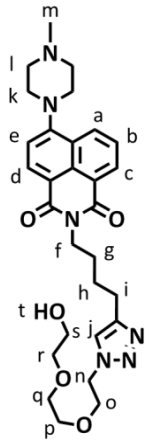

Under nitrogen, **2** (50 mg, 0.13 mmol) was dissolved in dichloromethane (10 mL) and a solution of azido-tri(ethylene glycol) (28 mg, 0.16 mmol) in methanol (5 mL) was added. A solution of TBTA (10.6 mg, 20 µmol) and $Cu(CH_3CN)_4PF_6$ (7.5 mg, 20 µmol) in methanol (10 mL) was added to the reaction mixture, which was allowed to stir overnight at room temperature. Evaporation of the solvent under reduced pressure and flash column chromatography (SiO_2, CH_2Cl_2/MeOH = 95/5) gave **3** as a yellow solid (Yield: 66 mg, 0.11 mmol, 85%).

^{1}H NMR (300 MHz, $CDCl_3$): δ (ppm) = 8.49 (d, 1H, H_a), 8.41 (d, 1H, H_d), 8.33 (d, 1H, H_c), 7.60 (t, 1H, H_b), 7.51 (s, 1H, H_j), 7.15 (d, 1H, H_e), 4.46 (t, 2H, H_f), 4.13 (t, 2H, H_n), 3.82 (t, 2H), 3.70-3.50 (m, 10H, $H_{o\text{-}s}$), 3.25 (bt, 4H, H_k), 2.71 (m, 6H, H_l, H_i), 2.39 (s, 3H, H_m), 1.74 (m, 4H, H_g, H_h).

^{13}C NMR (75 MHz, $CDCl_3$): δ (ppm) = 164.46, 163.99, 155.95, 132.57, 131.07, 130.33, 129.79, 126.06, 125.61, 123.08, 116.49, 114.94, 72.45, 70.49, 70.17, 69.52, 61.52, 55.08, 52.88, 50.07, 46.07, 39.83, 27.63, 26.91, 25.32.

ESI-MS: measured 551.3 [M+H$^+$], calculated 551.3 [M+H$^+$].

N-6-Hexynyl-4-(4'4'-dimethyl-piperazinyl)-1,8-naphthalimide iodide, 4

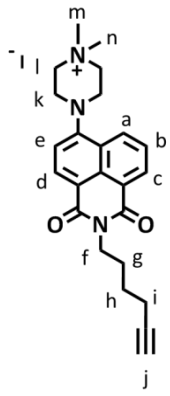

Methyl iodide (0.83 ml, 13.3 mmol) was added to a solution of *N*-6-hexynyl-4-(4'-methyl-piperazinyl)-1,8-naphthalimide (0.20 g, 0.53 mmol) in 25 ml of methanol while stirring at room temperature. The resulting mixture was stirred at reflux for 16h. Yellow solid was precipitated by adding 10 ml aqueous sodium carbonate (20 %).

^{1}H NMR (300 MHz, DMSO-d_6): δ (ppm) = 8.50 (m, 3H, $H_{a,c,d}$), 7.87 (t, 1H, H_b), 7.51 (d, 1H, H_e), 4.06 (t, 2H, H_f), 3.77 (br t, 4H, H_k), 3.61 (br t, 4H, H_l), 3.30 (s, 6H, $H_{m,\,n}$), 2.76 (t, 1H, H_j), 2.22 (dt, 2H, H_i), 1.85 (m, 2H, H_g), 1.65 (m, 2H, H_h).

^{13}C NMR (75 MHz, DMSO-d_6): δ (ppm) = 163.50, 163.00, 153.65, 131.90, 130.83, 130.30, 128.95, 126.50, 125.38, 122.66, 116.93, 116.32, 84.25, 71.35, 60.77, 46.03, 26.80, 25.60, 17.46.

ESI-MS: measured 390.3 [M+H$^+$], calculated 390.2 [M+H$^+$].

7.5.3 Methods

Substrate and precursor monolayer preparation. Microscope glass slides and interdigitated platinum electrodes on glass were used for monolayer preparation.[37] When using glass slides, the substrates were oxidized in a piranha solution for 45 min (concentrated H_2SO_4 and 33 % aqueous H_2O_2 in a 3:1 ratio; Warning: piranha should be handled carefully: it has been reported to detonate unexpectedly) and rinsed with water (MilliQ). After drying in a nitrogen stream, the substrates were used immediately to form a silanized monolayer. The substrates were immersed in 0.1 vol% 11-bromoundecyltrichlorosilane in dry toluene for 45 min at room temperature. Following monolayer formation, the substrates were rinsed with toluene to remove any excess of silanes, with ethanol and subsequently dried in a nitrogen flow. The bromide/azide nucleophilic substitution was carried out by the reaction with a saturated solution of NaN_3 in DMF for 48 h at 70 ^oC. The substrates were thoroughly rinsed with MilliQ water and ethanol and dried in a nitrogen flow.

For the gradient experiments, glass slides with interdigitated microelectrodes were prepared as described before (Chapter 5). When using interdigitated microelectrodes on glass, the substrates were activated by oxygen plasma treatment (10 min, 50 mA, <200 mTorr). The formation of bromide- and azide-terminated monolayers followed the same protocol described above for microscope glass slides.

Dye monolayer formation. When using glass substrates without electrodes, a reactive µCP procedure was used to immobilize **2** or **4**. Stamps were prepared by casting a 10:1 (v/v) mixture of poly(dimethylsiloxane) and curing agent (Sylgard 184, Dow Corning) against a silicon master. After overnight curing at 60^oC, the stamps were oxidized by oxygen plasma for 10 s (power tuned at 50 mA) and subsequently inked by dropping the inking solution onto the stamp (1.5 mM **2** or **4** (in CH_3CN), 0.5 mM $Cu(I)(CH_3CN)_4PF_6$ and 0.5 mM TBTA (CH_3CN/EtOH=2/1) (catalyst mixture), prepared by mixing 75 µL of 2 mM solution of **2** or **4** in CH_3CN and 25 µL of 2 mM of catalyst mixture). After 4 min incubation the stamps were blown dry in a stream of nitrogen and brought into conformal contact with the substrate for 60 min. The stamps were changed for each new printing, and the same inking procedure was used. After stamp removal, the printed substrates were rinsed with ethanol, sonicated in acetonitrile for 2 min, rinsed again with ethanol, blown dry with nitrogen and imaged by fluorescence microscopy.

When using interdigitated microelectrodes on glass, the fabrication of micron-scale surface chemical gradients was accomplished by means of electrochemically activated CuAAC in a similar way as described in Chapter 6. The reaction was performed in a silicone container on top of the electrode array. In the electrochemical experiment, 100 µL of a

solution containing 1 mM alkyne-modified *N*-methylpiperazine naphthalimide (**2**) 1 mM $CuSO_4$ and 1 mM Cu(I)-stabilizing ligand (TBTA) in DMSO were subjected to a potential difference of 1.0 V for 2 min to perform the reduction of Cu(II) to Cu(I) at the cathode (source) and the oxidation of Cu(I) to Cu(II) at the anode (sink). After the reaction, the electrodes were quickly rinsed with DMF and ethanol to avoid any further progress of the reaction and to remove any physisorbed material, then they were dried in a stream of N_2.

When using interdigitated microelectrodes on glass, for the investigation of the micron-scale pH gradient induced by electrolysis of water, a solution process was employed to immobilize **2** on azide-terminate monolayers. The substrates were incubated with a 3 mM **2** and a 0.3 mM $Cu(I)(CH_3CN)_4PF_6$/TBTA in DMF for 4 h at room temperature. After the reaction, the substrate were rinsed with DMF and ethanol and dried in a stream of N_2.

Surface pH titration. After immobilization of **2**, or **4**, via micro-contact printing on azide-terminated monolayers, the platforms were incubated with 200 μL of buffered solutions at various pHs and fluorescence images were recorded with the solution on top of the monolayer. Upon changing pH solution, substrates were always rinsed with the new solution prior to fluorescence microscopy characterization.

pH gradient generation. A pH gradient was generated in between the interdigitated electrodes by driving 50 μA in chronopotentiometry mode, with the counter and reference electrode shorted. Because the current generated at the working and counter electrode are of the same magnitude but with opposite sign,[38] the two electrochemical reactions occurring can be assumed equal when no side reactions are occurring. By using a constant current, it is ensured that the same amounts of H^+ and OH^- were generated in time by changing the voltage gradually. The current of 50 μA resulted in an applied voltage of the working electrode of roughly 1.45 V. To switch the pH gradient, the current polarity was switched from +50 to -50 μA, which resulted in an applied voltage of the working electrode of roughly -0.27 V, which means that a potential difference of roughly 1.7 V was applied while generating the pH gradient.

7.5.4 Equipment

UV/Vis spectroscopy. UV/Vis absorption spectra were recorded using a Perkin Elmer Lambda 850 UV-Vis spectrometer.

Fluorescence spectroscopy. Fluorescence spectra were recorded using a Perkin Elmer LS 55 fluorescence spectrometer equipped with a high energy pulsed Xenon source for excitation. Emission and excitation slits were kept constant at 2.5 nm.

Fluorescence microscopy. Fluorescence microscopy images were taken using an Olympus inverted research microscope IX71 equipped with a mercury burner U-RFL-T as light source and a digital Olympus DR70 camera for image acquisition. Blue excitation (400 nm ≤ λ_{ex} ≤ 420 nm) and green emission (490 nm ≤ λ_{em} ≤ 540 nm) was filtered using a Saphira Olympus filter cube. All fluorescence microscopy images were acquired in solution upon incubation with a specific buffered solution or while applying the pH gradient.

Potentiostat. Electrochemical reactions were performed with a CHInstruments 760D potentiostat, having the counter and reference connections shorted. The working and counter electrodes consisted of planar, 100 nm thick, Pt electrodes.

Contact angle measurements. Contact angles were measured on a Krüss G10 goniometer, equipped with a CCD camera. Contact angles were determined automatically by a drop shape analysis software. Milli-Q water (18.4 MΩ·cm), 1 mM NaOH or 1 mM HCl, were employed as probe liquids.

XPS. XPS spectra were obtained on a Physical Electronics Quantera Scanning X-ray Multiprobe instrument, equipped with a monochromatic AlKα X-ray source operated at 1486.6 eV and 26.18 W. Spectra were referenced to the main C_{1s} peak set at 284.0 eV. The X-ray beam size was 100 µm and the data were collected from surface areas of 100 µm × 300 µm with a pass energy of 224 eV and a step energy of 0.8 eV for survey scans and 0.4 eV for high resolution scans. For quantitative analysis, the sensitivity factors used to correct the number of counts under each peak were: C_{1s}, 1.00; N_{1s}, 1.59. The measurement was collected after 25 scanning cycles.

Mass spectra. ESI-TOF-MS mass spectra were recorded using a LCT Mass spectrometer (Waters/Micromass).

NMR. ^{1}H and ^{13}C NMR spectra were recorded on a Varian Unity (300 MHz) spectrometer. ^{1}H and ^{13}C chemical shifts values, measured at 300 MHz and 75 MHz, respectively, are reported as δ (in ppm) using the residual solvent signal as internal standard.

7.6 References

(1) J. C. Love, L. A. Estroff, J. K. Kriebel, R. G. Nuzzo, G. M. Whitesides, *Chem. Rev.* **2005**, *105*, 1103.
(2) S. Onclin, B. J. Ravoo, D. N. Reinhoudt, *Angew. Chem. Int. Ed.* **2005**, *44*, 6282.
(3) C. Haensch, S. Hoeppener, U. S. Schubert, *Chem. Soc. Rev.* **2010**, *39*, 2323.
(4) T. P. Sullivan, W. T. S. Huck, *Eur. J. Org. Chem.* **2003**, *1*, 17.
(5) V. Chechik, R. M. Crooks, C. J. M. Stirling, *Adv. Mater.* **2000**, *12*, 1161.

(6) P. Jonkheijm, D. Weinrich, H. Schroeder, C. M. Niemeyer, H. Waldmann, *Angew. Chem. Int. Ed.* 2008, *47*, 9618.
(7) C. M. Salisbury, D. J. Maly, J. A. Ellman, *J. Am. Chem. Soc.* 2002, *124*, 14868.
(8) Q. Zhu, M. Uttamchandani, D. B. Li, M. L. Lesaicherre, S. Q. Yao, *Org. Lett.* 2003, *5*, 1257.
(9) F. A. Scaramuzzo, A. Gonzalez-Campo, C.-C. Wu, A. H. Velders, V. Subramaniam, G. Doddi, P. Mencarelli, M. Barteri, P. Jonkheijm, J. Huskens, *Chem. Commun.* 2010, *46*, 4193.
(10) A. Gonzalez-Campo, S.-H. Hsu, L. Puig, J. Huskens, D. N. Reinhoudt, A. H. Velders, *J. Am. Chem. Soc.* 2010, *132*, 11434.
(11) C. Nicosia, J. Cabanas-Danes, P. Jonkheijm, J. Huskens, *ChemBioChem* 2012, *13*, 778.
(12) D. Wasserberg, C. Nicosia, E. E. Tromp, V. Subramaniam, J. Huskens, P. Jonkheijm, *J. Am. Chem. Soc.* 2013, *135*, 3104.
(13) J. Cabanas-Danes, C. Nicosia, E. Landman, M. Karperien, J. Huskens, P. Jonkheijm, *J. Mater. Chem. B* 2013, *1*, 1903.
(14) M. Melucci, M. Zambianchi, L. Favaretto, V. Palermo, E. Treossi, M. Montalti, S. Bonacchi, M. Cavallini, *Chem. Commun.* 2011, *47*, 1689.
(15) A. Martinez-Otero, P. Gonzalez-Monje, D. Maspoch, J. Hernando, D. Ruiz-Molina, *Chem. Commun.* 2011, *47*, 6864.
(16) A. Martinez-Otero, J. Hernando, D. Ruiz-Molina, D. Maspoch, *Small* 2008, *4*, 2131.
(17) P. Mela, S. Onclin, M. H. Goedbloed, S. Levi, M. F. Garcia-Parajo, N. F. van Hulst, B. J. Ravoo, D. N. Reinhoudt, A. van den Berg, *Lab on a Chip* 2005, *5*, 163.
(18) J. Gan, K. Chen, C.-P. Chang, H. Tian, Dyes Pigments, 2003, *57*, 21.
(19) A. P. de Silva, H. Q. N. Gunaratne, T. Gunnlaugsson, A. J. M. Huxley, C. P. McCoy, J. T. Rademacher, T. E. Rice, *Chem. Rev.*, 1997, *97*, 1515.
(20) A. P. de Silva, H. Q. N. Gunaratne, C. P. McCoy, *Chem. Commun.*, 1996, 2399.
(21) A. P. de Silva, S. S. K. de Silva, N. C. W. Goonesekera, H. Q. N. Gunaratne, P. L. M. Lynch, K. R. Nesbitt, S. T. Patuwathavithana, N. Ramyalal, *J. Am. Chem. Soc.* 2007, *129*, 3050.
(22) C.-G. Niu, G.-M. Zeng, L.-X. Chen, G.-L. Shen, R.-Q. Yu, *Analyst* 2004, *129*, 20.
(23) S. Trupp, P. Hoffmann, T. Henkel, G. J. Mohr, *Org. Biomol. Chem*. 2008, *6*, 4319.
(24) K. Macounová, C. R. Cabrera, M. R. Holl, P. Yager, *Anal. Chem.* 2000, *72*, 3745.
(25) C. R. Cabrera, B. Finlayson, P. Yager, *Anal. Chem.* 2000, *73*, 658.
(26) S. Fiedler, R. Hagedom, T. Schnelle, E. Richter, B. Wagner, G. Fuhr, *Anal. Chem.* 1995, *67*, 820.
(27) K. Morimoto, M. Toya, J. Fukuda, H. Suzuki, *Anal. Chem.* 2008, *80*, 905.
(28) The curves were fitted by using the Boltzmann sigmoidal equation: $I_{rel} = (I-I_0)/(I_{max}-I_0)= 1/(1+exp[(pH-pK_a)/s])$ where I_{max} and I_0 are the (fitted) maximum and minimum intensity values, respectively, and s is the slope factor. When fixing s = 1/ln(10) = 0.434, this equation corresponds to the Henderson-Hasselbalch equation.
(29) S. Y. Hu, A. J. Bard, *Langmuir* 1997, *13*, 5114.
(30) S. E. Creager, J. Clarke, *Langmuir* 1994, *10*, 3675.
(31) C. D. Bain, G. M. Whitesides, *Langmuir* 1989, *5*, 1370.
(32) T. Kakiuchi, M. Iida, S.-i. Imabayashi, K. Niki, *Langmuir* 2000, *16*, 5397.
(33) K. Aoki, T. Kakiuchi, *J. Electroanal. Chem.* 1999, *478*, 101.
(34) S. O. Krabbenborg, C. Nicosia, P. Chen, J. Huskens, *Nat. Commun*. 2013, *4*, 1667.

(35) A. R. Schneekloth, M. Pucheault, H. S. Tae, C. M. Crews, *Bioorg. Med. Chem. Lett.* 2008, *18*, 5904.
(36) T. R. Chan, R. Hilgraf, K. B. Sharpless, V. V. Fokin, *Org. Lett*. 2004, *6*, 2853.
(37) N. Balachander, C. N. Sukenik, *Langmuir* 1990, *6*, 1621.
(38) Bard, A. J.; Faulkner, L. R. Electrochemical Methods: Fundamentals and Applications, 2nd Ed., Wiley: New York, 2001.

Chapter 8

"It doesn't matter how beautiful your theory is, it doesn't matter how smart you are. If it doesn't agree with experiment, it's wrong." — Richard P. Feynman, The Pleasure of Finding Things Out.

Superselectivity in multivalent ligand-receptor binding*

This chapter describes the first experimental demonstration of superselectivity in multivalent ligand-receptor binding. A thiol-reactive fluorogenic platform was employed for the anchoring of thiol-modified ligands and the visualization of their surface density. The adamantyl-β-cyclodextrin supramolecular system was employed as a model ligand-receptor couple. The effect of the surface density of the ligand on the selective multivalent assembly of the receptor-functionalized nanoparticles was investigated using micron-scale surface chemical gradients allowing the variation of ligand density in space. The self-assembly resulted in a nonlinear dependence of particle density with ligand density. This behavior is an experimental demonstration of superselective systems in which efficient multivalent binding is achieved at a threshold surface ligand concentration that is characteristic for the multivalent nature of the system.

*Manuscript in preparation.

8.1 Introduction

Multivalent interactions are characterized by the simultaneous, specific association of two or more ligands and receptors within a molecular assembly.[1] Multivalency plays a pivotal role in many biological processes. Typical examples are the adhesion of viruses or bacteria to the surface of a cell, the binding of cells to antibodies, cell-cell interactions, the binding of transcription factors to multiple sites at DNA, *etc*.[1] A better understanding of these processes is of paramount importance for the design and implementation of pharmaceutical agents, such as polyvalent molecules that are able to inhibit undesired biological processes. To this end, Kiessling *et al.* have developed a low-affinity, multivalent system capable of distinguishing between cells with different concentrations of surface receptors.[2] In particular they used a bifunctional conjugate that binds tightly to cell-surface receptors and presents a carbohydrate molecule for the interaction with antibodies that trigger cell complement-mediated lysis. Antibodies bind tightly only upon multivalent interactions allowing to selectively target and kill tumor cells, characterized by high levels of surface receptors.

Nanoparticles (NPs) can be engineered to carry different kinds of bioactive ligands with well-defined biological functions on their surfaces, capable of forming specific interactions with cell membrane receptors.[3,4] This approach has been used to systematically investigate the specificity of multivalent interactions for cell targeting.[5-7] The density of ligands, for example, is a critical parameter that has to be optimized to control the specificity of the binding of nanoparticles to target cells.[8]

Numerical models have contributed to the systematic design of multivalent ligand-coated nanoparticles for the superselective binding on receptor-decorated surfaces.[9,10] Superselectivity is the property of multivalent systems to bind specifically to surfaces that display a concentration of receptors above a certain threshold.[9] A hallmark of this behavior is that the fraction of bound particles increases faster than linearly with the surface concentration of receptors. One of the main applications of superselectivity is in nano-medicine for predicting the specific targeting of cells based on differences in surface receptor density. The numerical models have demonstrated that three requirements need to be met in order to observe superselective binding: i) multivalent ligand-receptor interactions, ii) a weak individual ligand-receptor binding energy, and iii) a concentration of surface-bound receptors (or ligands) greater than a critical (threshold) value.

In this chapter, we show an experimental demonstration of superselectivity for the first time. To this end, we fabricate micron-scale surface chemical gradients of a ligand (see Chapters 5 and 6),[11] bound to a fluorescent reporter monolayer (see Chapter 3),[12] to

investigate the effect of its surface density on the superselective multivalent assembly of receptor-functionalized NPs. The gradient-wise exposure of the ligand provides a spatial variation of density of ligands, while the reporter monolayer allows the direct and combined (co-localized) visualization of both the immobilized ligand and the multivalently bound NPs (Scheme 8.1). The supramolecular system employed here uses the well-known β-cyclodextrin/adamantane hydrophobic interaction. It has a binding energy of the same order of magnitude as those used for multivalent selective targeting.[2] This makes this system directly relevant to processes happening in biological systems where superselectivity might be a decisive criterium of binding.

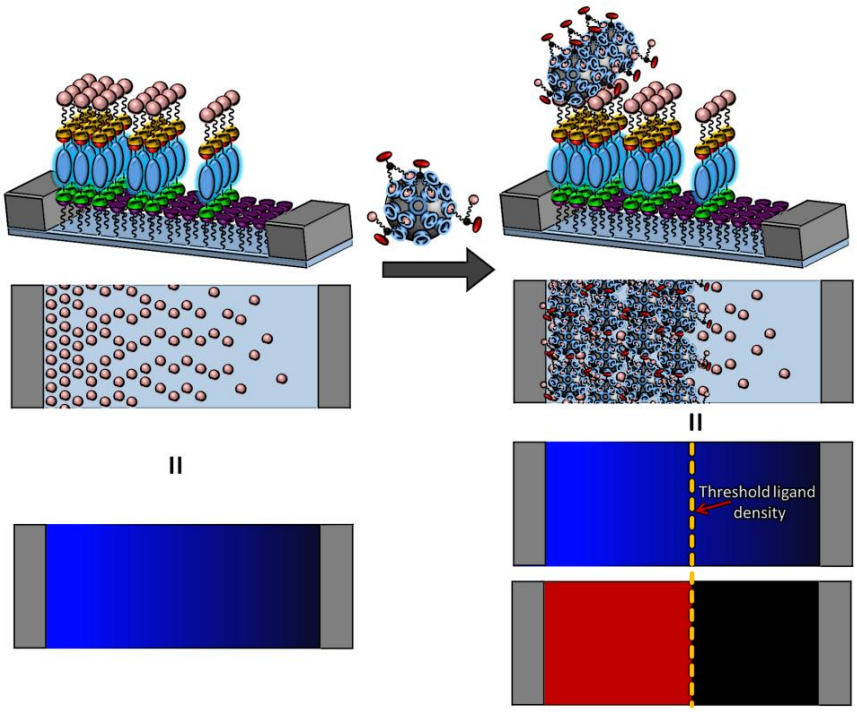

Scheme 8.1. Schematic representation of the superselective assembly of red fluorescently labeled CD-functionalized silica NPs on a micron-scale adamantyl-terminated surface chemical gradient. Fluorescence microscopy is used to compare the surface gradient of the bound ligand (blue fluorescent monolayer) and the co-localized assembly of the NPs (red fluorescent particle layer).

8.2 Results and discussion

8.2.1 Synthesis of cyclodextrin-functionalized silica nanoparticles and their non-covalent fluorescent labeling by dye-functionalized guests

As illustrated in Scheme 8.1, β-cyclodextrin (CD)-functionalized NPs are to be assembled on a ligand-functionalized surface exploiting multivalent host-guest interactions. We aim to investigate the co-localization between the functionalized surface and the NPs

by fluorescence microscopy. First we describe the preparation of the CD-functionalized NPs **5** and their non-covalent fluorescent labeling using a divalent adamantyl-functionalized fluorescent dye **6** (Scheme 8.2) to yield the labeled NPs **7**.

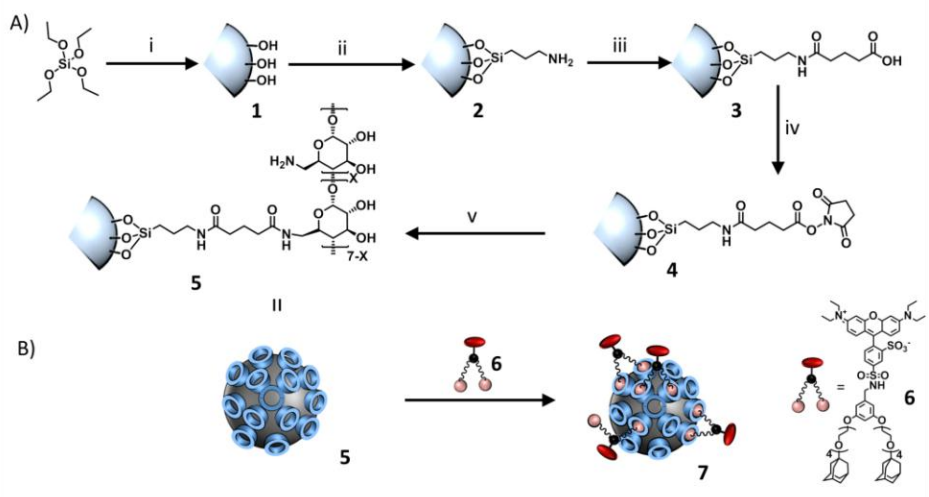

Scheme 8.2. A) Preparation of CD-functionalized silica NPs **5**): i) tetraethyl orthosilicate, ammonium hydroxide, EtOH, r.t., o.n.; ii) (3-aminopropyl)triethoxysilane (APTES), EtOH, r.t., o.n.; iii) glutaric anhydride, DMF, r.t., o.n.; iv) *N*-(3-dimethylaminopropyl)-*N'*-ethylcarbodiimide hydrochloride (EDC), *N*-hydroxysuccinimide (NHS), 2-(*N*-morpholino)ethanesulfonic acid (MES) buffer (pH 5), r.t., 1 h; v) CD heptamine, carbonate buffer (pH 9), r.t., 3 h. B) Non-covalent fluorescent labeling of **5** with bis-adamantyl-functionalized rhodamine dye **6** in carbonate buffer (pH 9.5).

CD-functionalized silica NPs **5** were prepared using a procedure described before as illustrated in Scheme 8.2A.[13,14] Briefly, silica NPs **1** were generated by the hydrolysis and condensation of tetraethyl orthosilicate in the presence of ammonia as the catalyst. Silica NPs **1** were not isolated but converted directly into amino-terminated silica NPs **2** by the addition of 3-aminopropyl triethoxysilane (APTES) to the reaction mixture. The presence of amino groups was confirmed by addition of salicylaldehyde to a small amount of purified amino-terminated silica NPs **2** leading to the formation of a yellow solution. Characterization by dynamic light scattering (DLS) of **2** in ethanol showed relatively monodisperse NPs with an average number diameter of 68 ± 16 nm. In the next step terminal carboxylic acid groups were introduced by the reaction of **2** with glutaric anhydride. The addition of salicylaldehyde to a suspension of a small aliquot of purified carboxylic-terminated silica nanoparticles **3** did not show any change of color, indicating a quantitative conversion of the amino groups to carboxylic acid groups. The carboxylic acid-terminated silica NPs **3** were subsequently activated with *N*-(3-dimethylaminopropyl)-*N'*-ethylcarbodiimide hydrochloride (EDC) and *N*-hydroxysuccinimide (NHS) in 2-(*N*-

morpholino)ethanesulfonic acid (MES) buffer at pH 5 to give **4**. NHS-activated silica NPs **4** were reacted with CD heptamine in carbonate buffer at pH 9.5 to yield CD-terminated silica NPs **5**. The DLS characterization of **5** in carbonate buffer showed a relatively narrow distribution of NPs with an average number diameter of 72 ± 20 nm.

A 0.2 wt % suspension of **5** in carbonate buffer was prepared, corresponding to 5.2×10^{12} particles per mL (8.6×10^{-9} M). When assuming a similar surface density of CD molecules on the NP surface as on the CD printboards on glass (about 2.5×10^{-11} mol cm^{-2}),[15] the number of CD molecules per nanoparticle can be estimated to be about 2500, and the concentration of particle-bound CD in the 0.2 wt % suspension is about 21 μM.

Huskens, Reinhoudt and coworkers have demonstrated that the addition of multivalent guest molecules to CD-functionalized silica NPs in solution led to a strong aggregation due to specific host-guest interactions.[13] In another study they investigated the effect of the ligand valency and structure of adamantyl-terminated guest molecules on the aggregation of CD-functionalized gold NPs in solution.[16] They observed that, while multivalent adamantyl-terminated dendrimers led to the formation of strong aggregates, negligible aggregation resulted from the addition of a flexible bis-adamantyl molecule. In the latter case, intramolecular interactions were favored over intermolecular ones, thus inhibiting the aggregation process. We employed this strategy to bind a flexible bis-adamantyl molecule equipped with a fluorescent unit (bis-adamantyl-rhodamine dye) **6** onto the surface of **5** (Scheme 8.2B). The supramolecular fluorescent complex **7** was obtained upon mixing a solution of bis-adamantyl-rhodamine dye and **5** in a 1:1 ratio. The resulting fluorescent supramolecular complex **7** was purified by repeated centrifugation and redispersion in a carbonate buffer. The DLS characterization of **7** showed NPs with an average number diameter of 77 ± 25 nm, while SEM gave 73 ± 18 nm (Figure 8.1). These results confirm that the labeling by **6** does not lead to any detectable aggregation of the CD NPs.

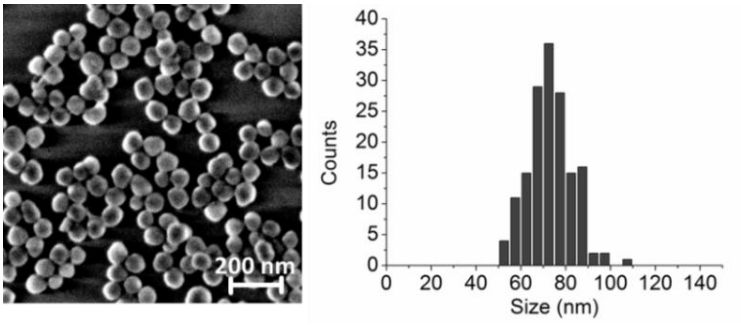

Figure 8.1. SEM image (left) and size distribution histogram (right) of the non-covalently, fluorescently labeled CD NPs **7**.

8.2.2 Fabrication and host-guest binding of the guest-functionalized supramolecular platform

Two different thiol-terminated ligands were synthesized (Scheme 8.3) and immobilized on the fluorogenic platform to investigate the multivalent binding of **7** (see Scheme 8.4 below). The ligands bear an adamantyl or a methyl terminal group to fabricate two distinct platforms that allow the discrimination of specific and nonspecific host-guest binding, respectively. Thiol-terminated tetra(ethylene glycol) linkers were synthesized via an alcohol-tosylate-thiol route as described in Scheme 8.3A.[17] The tosylate derivatives (**10** and **11**) were obtained upon reaction of adamantyl-[18] (**8**) and methyl- (**9**) terminated tetra(ethylene glycol) with p-toluenesulfonyl chloride and NaOH in a water/THF mixture. **10** and **11** were converted into the corresponding thiol-terminated tetra(ethylene glycol) linkers (**12** and **13**) by means of a reaction with thiourea followed by the hydrolysis of the thiourea-glycol adduct by addition of a NaOH solution.

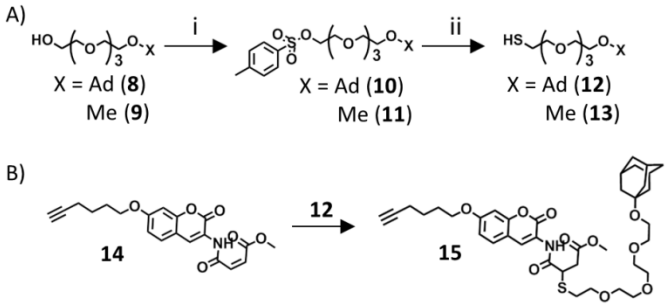

Scheme 8.3. A) i) *p*-Toluenesulfonyl chloride, NaOH, water, THF, r.t., o.n.; ii) a) thiourea, EtOH, water, reflux, 3 h, b) NaOH, EtOH, water, reflux, 4 h; B) Synthesis of the fluorescent compound **15** obtained upon conjugation of **14** and **12** with triethylamine as catalyst in methanol.

Prior to investigation of the immobilization of **12** and **13** on the thiol-reactive fluorogenic monolayer, we demonstrated that the fluorogenic coumarin **14** is reactive toward the synthesized thiol **12** in solution (Scheme 8.3B). The reaction between **14** and **12** occurred quantitatively with formation of the strongly fluorescent conjugation product **15**, with maximum absorption and emission at wavelengths of 345 nm and 405 nm, respectively (Figure 8.2). ^{1}H-NMR characterization showed the formation of a second compound (about 20%) as a result of the 1,4-addition of **12** to the methyl-4-oxo-2-butenoate group from the amide side. Since the fluorescence of **15** is caused by the inhibition of the photo-induced electron transfer pathway that exists in case of **14** by the presence of the C-C double bond adjacent to the coumarin unit,[19] we do not expect any difference between the photophysical properties of the two isomers of **15**.

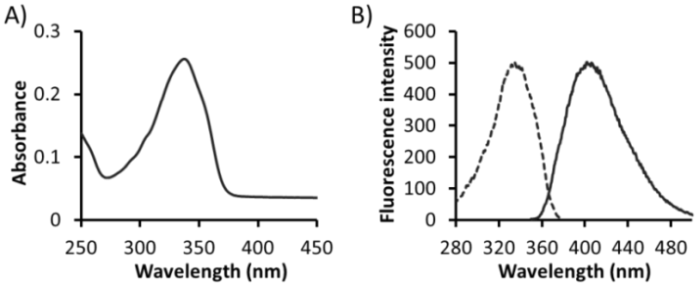

Figure 8.2. A) Absorption spectrum of 10 µM of **15** in acetonitrile. B) Emission (solid; λ_{exc} = 345 nm) and excitation (dashed; λ_{em} = 405 nm) spectra of 0.1 µM of **15** in acetonitrile.

Hereafter, we used the fluorogenic platform (see Chapter 3) for the efficient immobilization and visualization of the adamantyl- (**12**) and methyl-terminated (**13**) thiols to form the guest-functionalized supramolecular platform. Scheme 8.4 illustrates the strategy for the surface immobilization of compound **14** by means of copper(I) azide-alkyne cycloaddition (CuAAC) followed by the interfacial reaction in the presence of **12** or **13**.

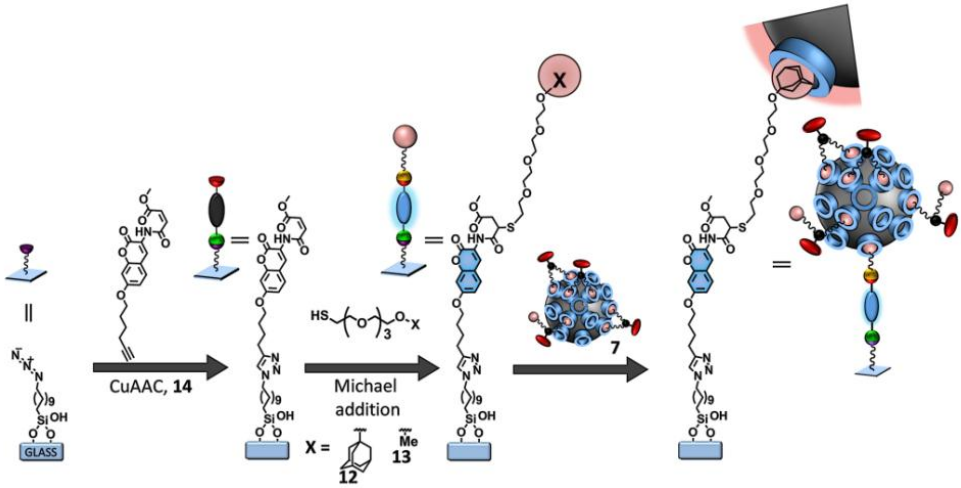

Scheme 8.4. Schematic procedure of the surface functionalization with the supramolecular (adamantyl) ligand, starting from the immobilization of the pro-dye **14** via CuAAC onto an azide monolayer, followed by the covalent immobilization of the thiols **12** or **13** (10 mM thiol and 0.5 v % triethylamine solution in methanol for 30 min) by means of the fluorogenic Michael addition to the methyl-4-oxo-2-butenoate moiety. Subsequently, cyclodextrin receptor-functionalized silica NPs **7** are self-assembled onto the ligand monolayer.

Initially, the CuAAC surface reaction between the azide-terminated monolayer on glass and the alkyne-modified coumarin **14** was accomplished by reactive microcontact printing (µCP) using patterned PDMS stamps in order to form surface patterns.[12] When surface patterns of **14** were subsequently incubated with **12** (or **13**, not shown here), a strong enhancement of the blue fluorescence intensity was observed (Figure 8.3A). This

result is consistent with our previous work (see Chapter 3) in which was demonstrated that both the CuAAC reaction of the alkyne-functionalized coumarin to the azide monolayer and the thiol-Michael addition proceed with very high conversions resulting in fully covered surfaces.[12] The average height of the 10 µm dots pattern obtained after interfacial reaction of **14** with **12** was measured by AFM in air resulting in about 1.6 nm, in good agreement with the length of the conjugation product between **14** and **12** (Figure 8.3B).

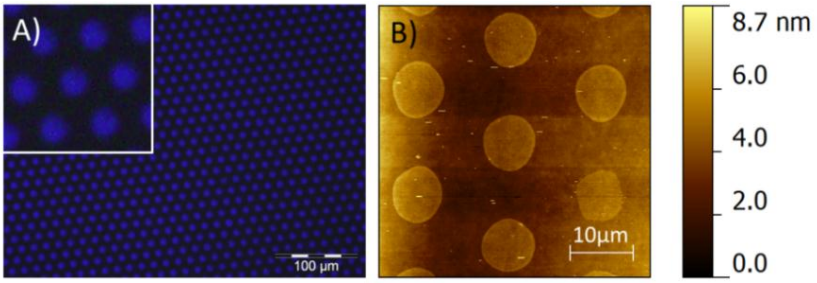

Figure 8.3. A) Fluorescence microscopy and B) AFM height images of the substrate after reactive contact printing (10 µm dots) of **14** followed by incubation with a solution of 10 mM **12** and 0.5 v/v % of triethylamine in methanol. λ_{exc} = 350 nm, λ_{em} > 420 nm.

After the successful immobilization of **12** and **13** on the surface patterns (now in 10 × 5 µm lines) of **14**, we investigated the host-guest self-assembly of the fluorescently labeled CD-functionalized silica NPs (**7**) (Scheme 8.4). The incubation of a suspension of **7** on the adamantyl-terminated patterns, obtained upon reaction of surface patterns of **14** with **12**, led to the perfect co-localization of the fluorescently labeled CD-functionalized silica NPs **7** on the adamantyl-terminated areas (Figure 8.4A and B). In contrast, when methyl-terminated surface patterns, obtained via reaction of the surface-immobilized **14** with **13**, were incubated with a 0.2 wt % suspension of **7** in carbonate buffer, a negligible assembly of the CD-functionalized silica nanoparticles was observed (Figure 8.4C and D). These results indicate that the binding of the CD NPs to the adamantyl ligand monolayer is specific, and strong at the given ligand density. These results also confirm that the noncovalently bound divalent red fluorescent dye of **7** remains on the NPs and does not bind non-specifically to the areas in between the patterns of **12**, nor to the methyl-terminated areas in the case of **13**. As a consequence, this system allows the visualization of the co-localization of the surface-bound ligands and the receptor NPs.

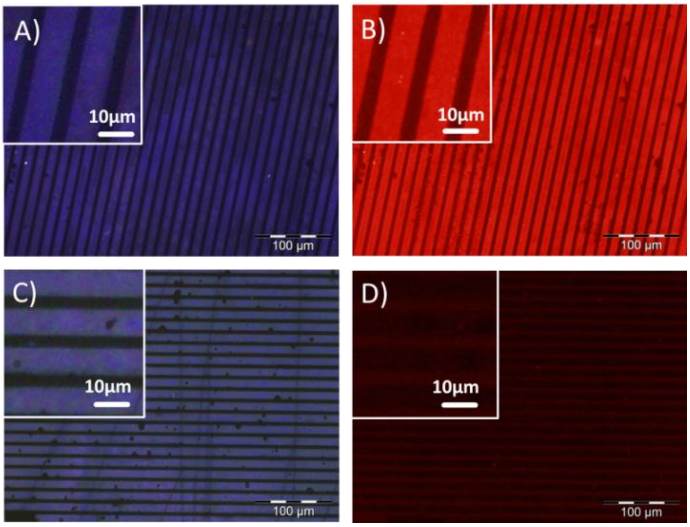

Figure 8.4. Fluorescence microscopy images after reactive microcontact printing of **14,** followed by reaction with A,B) adamantyl-terminated **12** or C,D) methyl-terminated **13**, and subsequent incubation with a 0.2 wt % suspension of **7** in carbonate buffer, imaged using A,C) the blue (λ_{exc} = 350 nm, λ_{em} > 420 nm) and B,D) red filters (λ_{exc} = 510-550 nm, λ_{em} = 590 nm) to visualize the coumarin fluorescence of **14** and the rhodamine fluorescence of the CD NPs, respectively.

AFM imaging (Figure 8.5A) demonstrated the surface assembly of the NPs **7** on the adamantyl-terminated monolayer **12** with formation of patterns with a thickness of 70 to 80 nm, in agreement with the size distribution obtained by DLS and SEM (Figure 8.1) and indicating the assembly of a monolayer of particles. Moreover, high-resolution SEM imaging allowed the visualization of individual NPs confirming the formation of a dense monolayer of **7** on the micron-scale pattern of **12**.

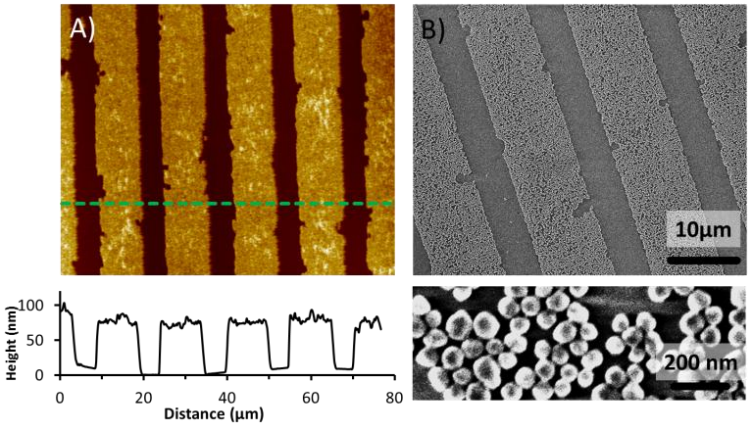

Figure 8.5. A) Tapping mode AFM (below: height profile) and B) high resolution SEM (below: zoom-in) images after incubation of the substrate patterned with **12** with 0.2 wt % suspension of **7** in carbonate buffer.

8.2.3 Superselectivity in the multivalent binding of CD nanoparticles to surface chemical ligand gradients

In order to investigate the effect of the surface density of the ligand on the multivalent host-guest interactions with receptor-decorated NPs **7** we prepared micron-scale gradients of the coumarin reporter **14** for the anchoring of ligand **12** and the subsequent assembly of NPs **7**. Scheme 8.5 illustrates the system used for the fabrication of micron-scale surface chemical gradients of **14** via electrochemically promoted CuAAC (see Chapters 5 and 6).[11] Platinum microelectrode arrays on glass, with the glass surface in between modified with an azide-terminated monolayer, were employed as a reactive platform for the surface gradient immobilization of the alkyne-terminated coumarin **14**. The CuAAC reaction, which takes place only in the presence of Cu(I), was carried out by using a solution of Cu(II) ($CuSO_4$) and **14** in DMSO, in the presence of a Cu(I)-stabilizing ligand (TBTA). A constant potential difference of 1.0 V was applied between the electrodes to perform the reduction of Cu(II) to the catalytically active Cu(I) at the cathode and the re-oxidation of Cu(I) to Cu(II) at the anode. Owing to the concentration gradient of Cu(I) in solution, the CuAAC between **14** and the azide monolayer resulted in a faster formation of triazole bonds next to the cathode (where Cu(I) is produced) compared to next to the anode, with the consequent formation of a surface gradient of covalently bound **14**.

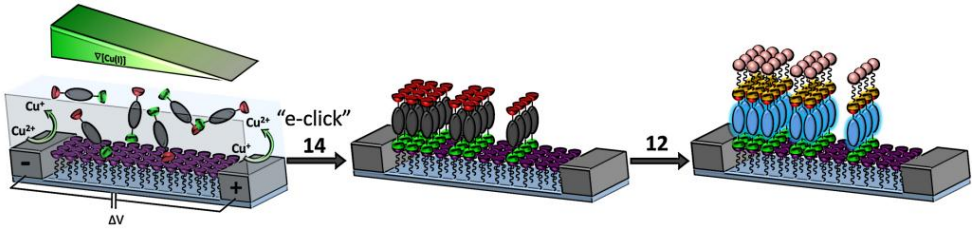

Scheme 8.5. Schematic representation of the fabrication of micron-scale surface chemical gradients of the alkyne-functionalized thiol-sensitive probe **14** via electrochemically promoted CuAAC on an azide-terminated monolayer on glass between a platinum microelectrode array followed by covalent immobilization of the adamantyl-terminated ligand **12** which is visualized by the fluorogenic reaction with surface-bound **14**.

The surface gradients of the thiol-sensitive probe **14** were incubated with a solution of the adamantyl-terminated ligand **12**, and a strong enhancement of fluorescence was observed in a gradient fashion (Figure 8.6A). The fluorescence intensity of the micron-scale surface gradient was compared with the fluorescence intensity obtained by μCP (Figure 8.3A). Similar maximum intensities were obtained indicating that the reaction conditions employed for the "e-click" led to a surface gradient with a high ligand density near the cathode (Figure 8.6B).

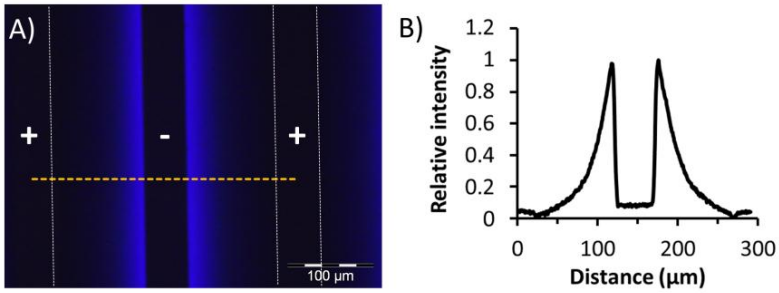

Figure 8.6. A) Fluorescence microscopy images and B) intensity profile of the surface chemical gradient of adamantyl ligands resulting from electrochemically activated CuAAC, using 1.0 mM **14**, 2.0 mM $CuSO_4$, 2.0 mM TBTA in DMSO, ΔV = 1 V, after 2 min reaction time, and subsequent reaction with **12**. λ_{exc} = 350 nm, λ_{em} > 420 nm.

The surface density of azide groups of the azide-terminated monolayers (assuming a well-packed fully extended monolayer) was estimated to be about 10^{-10} mol/cm^2.[20] Since from previous X-ray photoelectron spectroscopy (XPS) and fluorescence microscopy analyses (Chapter 3), the reactive contact printing of the alkyne-functionalized coumarin **14** on the azide-terminated monolayer and the following fluorogenic Michael addition of thiols showed quantitative conversions, we expect the highest surface density of adamantyl moieties of **12** to be about 10^{-10} mol/cm^2. This density corresponds to an average ligand-ligand spacing of 1.4 nm which sterically should allow efficient interaction with the CD receptors of the CD NPs.

The next step involved the self-assembly of the receptor-coated NPs **7** on the micron-scale surface-bound ligand gradient (Scheme 8.1). Figure 8.7A and B show the fluorescence microscopy results obtained upon drop-casting a 0.2 wt % suspension of **7** in carbonate buffer on the surface gradient of **12**. The CD-functionalized silica nanoparticles coated with bis-adamantyl-rhodamine dye (**7**) assembled selectively on the surface areas onto which the adamantyl ligand was immobilized with the formation of a dense layer of NPs on the dense ligand areas with fractal-like edges towards the less dense ligand areas (Figure 8.7B).

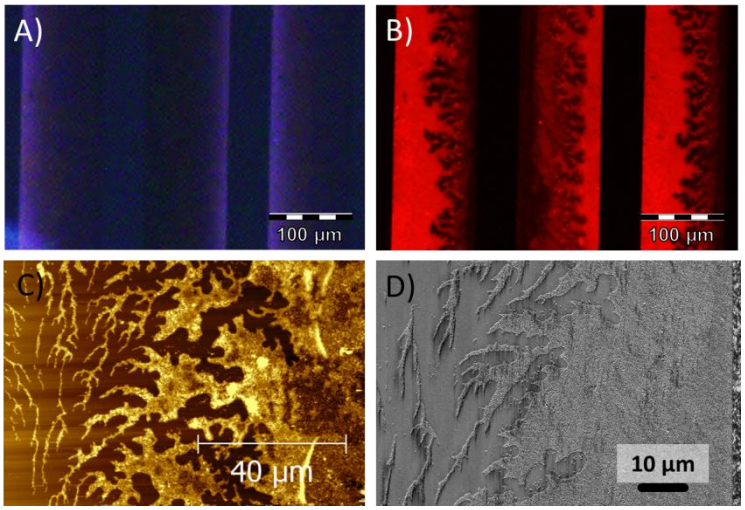

Figure 8.7. A,B) Fluorescence microscopy, C) tapping mode AFM height, and D) high resolution SEM images obtained upon incubation of the surface chemical gradients of **12** with a 0.2 wt % suspension of **7** in carbonate buffer. Fluorescence microscopy images were visualized with A) blue (λ_{exc} = 350 nm, λ_{em} > 420 nm) and B) red filters (λ_{exc} = 510-550 nm, λ_{em} = 590 nm).

Atomic force and high resolution scanning electron microscopies (Figure 8.7C and D) confirmed the results obtained by fluorescence microscopy: Both techniques showed the assembly of CD-coated NPs **7** on the surface gradient of **12** with a dense particle layer at the high ligand density side of the gradient and the formation of the fractal-like edges toward to lower ligand densities. However, these techniques do not allow to compare the NP density with the ligand density.

The blue and red fluorescence images shown in Figure 8.7A and B clearly indicate differences in the steepness of the intensities. While the blue fluorescence intensity profiles of the surface-bound gradient of ligand **12** showed a gradual change of surface density in space (Figure 8.8A), the red fluorescence intensity profiles displayed a steeper change of surface density of the receptor-coated NPs **7** in space (Figure 8.8B). Noteworthy is the strong correlation between the position of the edge of the dense NP monolayer and the density of the surface bound gradient of ligand **12**. This is visualized by plotting the red NP fluorescence as a function of the blue ligand density fluorescence (Figure 8.8C). Although the gradient densities slightly differed on different areas of a sample (Figure 8.8A), leading to concomitantly enhanced differences in NP densities vs. distance (Figure 8.8B), the NP and ligand densities are well correlated as indicated by the good overlap of the red vs. blue fluorescence intensity plots (Figure 8.8C) obtained at the different surface areas of the gradient. This correlation demonstrates that the coverage of CD-coated NPs **7** increases faster than linearly with the ligand density of the surface gradient of **12**. This is a

clear signature of superselectivity, attributed to a minimum number of receptor-ligand bonds needed to obtain stable binding. Below a threshold (relative) ligand density of approx. 0.2, a negligible assembly of NPs was observed, while above 0.2 a steep increase in particle coverage was recorded with dense packing observed for ligand coverages above 0.5.

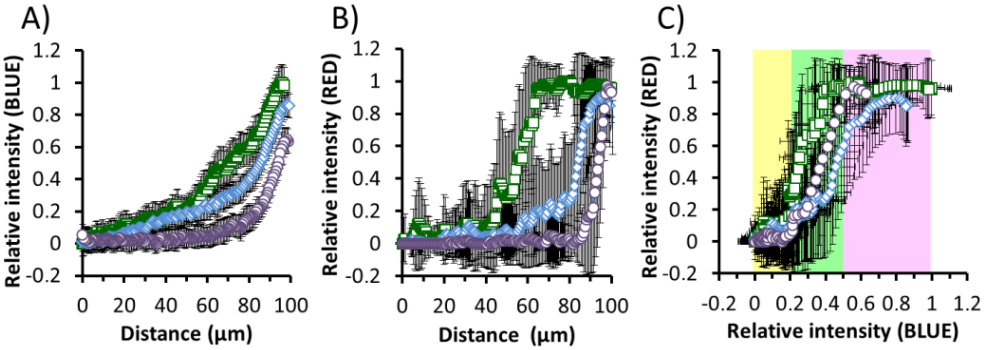

Figure 8.8. Intensity profiles of A) the surface chemical gradient of **12** of three different representative areas of the sample, B) the assembly of **7** at the same areas illustrated in A). C) Graph of the fluorescence intensity profiles of **7** assembled on the substrate (B), RED) as a function of the surface chemical gradient of **12** (A), BLUE).

Scheme 8.6 illustrates the idealized geometry of the interaction between a CD-functionalized silica NP and an adamantyl-terminated monolayer. Previous results have shown that a stable, kinetically inert NP assembly is obtained upon the formation of 4 to 5 Ad-CD bonds.[20,21] It is therefore logical to assume that the observed strong particle binding at about 0.5 relative intensity corresponds to the formation of such a number of bonds in the contact area between the particle and the substrate. This implies that the threshold value of 0.2 results from divalent binding, again in agreement with data[21,22] on small molecule binding that has indicated that divalent Ad-CD interactions are strong enough to be observable at low concentrations yet at the same time still dynamic and reversible. The latter would be an explanation for the observed fractal-like structures at the intermediate (0.2-0.5) intensities to be a result of interfacial motion by Ad-CD dissociation and reassociation during drying.

In absolute values, the threshold ligand density, at a relative intensity of 0.2, corresponds to a value of 2×10^{-11} mol/cm^2. This is surprisingly similar to the estimated CD density on the NP (2.5×10^{-11} mol/cm^2). In order to form two bonds between surface and particle, the contact area between particle and substrate should thus be about 15 nm^2. A model calculation, assuming the height *h* in Scheme 8.6to be 1 nm (based on the average length of the surface-bound **12**, 1.6 nm from the AFM result, Figure 8.3B, minus the length of the Ad group) and a radius r of the CD-functionalized NP of 36 nm, gives an estimated

contact area of 230 nm^2. The large discrepancy between experimentally estimated and modeled contact areas may be attributed to the rigidity of the system (short surface-bound ligand and receptor), a potentially lower receptor coverage on the particles than expected, roughness of the particle and substrate surface leading to a smaller contact area than expected, and competition between the ligand and the divalent dye used for fluorescent NP visualization. Therefore, future improvements of the system may involve silica NPs with a core-embedded dye and longer linkers for attachment of the ligand. All-in-all, however, the results clearly show the superselectivity of the binding of the multivalent host-guest system, and the validity and high potential of the gradient-wise ligand exposure, combined with the co-localized visualization offered by the platform, for studying such binding events.

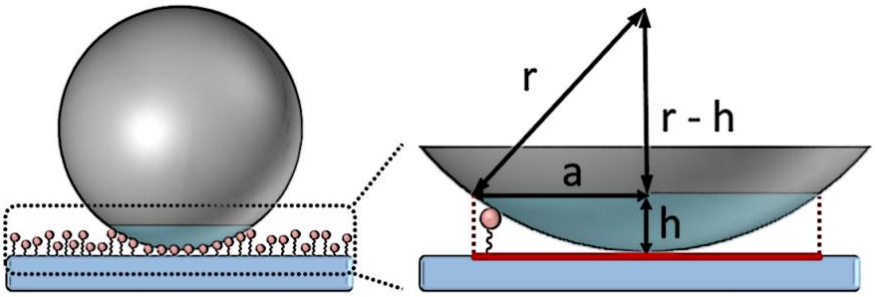

Scheme 8.6. Schematic representation of the geometry of the interaction between CD-functionalized silica NPs and the adamantyl-terminated monolayer (*r* is the radius of the nanoparticle, *h* is the average extension of the ligand, and *a* is the radius of the contact area).

8.3 Conclusions

In summary, in this chapter we have demonstrated the superselective multivalent binding of receptor-functionalized NPs on ligand-terminated monolayers. This was achieved combining a thiol-reactive fluorogenic platform, for the simultaneous immobilization and visualization of thiol-modified ligands, with a method to generate micron-scale gradients of surface bound ligands.

The β-cyclodextrin/adamantane supramolecular interaction was selected as a model receptor/ligand couple. The specific self-assembly of CD-functionalized NPs on the adamantyl micron-scale surface gradient resulted in a nonlinear dependence of particle density *vs* ligand density. In particular, the efficient multivalent binding occurred at a specific surface concentration threshold of ligands typical of a superselective system.

Using the approach presented in this chapter we envisage potential applications for biological studies of the effects of ligand/receptor surface density variation. In particular this kind of surface gradients could have striking effects for the efficient and systematic

investigation of multivalency in biological processes in which the density of ligands/receptors is a critical parameter, such as the detection and inhibition of viruses and bacteria, cell adhesion, differentiation and migration, and the detection and discrimination of cancer cells from healthy cells.

8.4 Acknowledgments

Carmen Stoffelen, Dr. Alejandro Méndez Ardoy and Sven O. Krabbenborg are gratefully acknowledged for the DLS measurements, the synthesis of β–cyclodextrin heptamine and for the fabrication of the platinum microelectrode arrays, respectively.

8.5 Experimental section

8.5.1 Materials

The following materials and chemicals were used as received without further purification: 11-bromoundecyltrichlorosilane (ABCR), sodium azide (Acros), copper(II) sulfate pentahydrate (Sigma-Aldrich), tetrakis(acetonitrile)copper(I) hexafluorophosphate (Aldrich), (3-aminopropyl)triethoxysilane (Aldrich), glutaric anhydride (Fluka), *N*-(3-dimethylaminopropyl)-*N'*-ethylcarbodiimide hydrochloride (Sigma-Aldrich), *N*-hydroxysuccinimide (Sigma-Aldrich), tetraethyl orthosilicate (Acros), ammonium hydroxide (Fluka), 2-(*N*-morpholino)ethanesulfonic acid (Sigma-Aldrich), *p*-toluenesulfonyl chloride (Acros), NaOH (Sigma-Aldrich), thiourea (Sigma-Aldrich), triethylamine (Sigma-Aldrich).

β-Cyclodextrin (CD) heptamine,[23] CD-functionalized silica nanoparticles,[13] adamantyl-terminated tetra(ethylene glycol) p-toluenesulfonate **10**,[24] methyl-terminated tri(ethylene glycol)ethanethiol **13**,[17] fluorogenic coumarin **14**,[12] bis-adamantyl-functionalized rhodamine dye **6**[25] and tris-(benzyltriazolylmethyl)amine (TBTA),[26] were prepared according to literature procedures.

8.5.2 Synthetic procedures

Synthesis of adamantyl-terminated tri(ethylene glycol)ethanethiol (12)

A mixture of **10** (1.15 g, 2.31 mmol) and thiourea (0.18 g, 2.31 mmol) in ethanol (5 mL) and distilled water (3.5 mL) was refluxed for 3 h under nitrogen. A solution of NaOH (0.11 g, 2.77 mmol) in distilled water (2 mL) was added, and the mixture was refluxed for 4 h. The reaction mixture was concentrated to 2 mL, diluted with distilled water (4 mL), neutralized with concentrated HCl, extracted with dichloromethane (2 × 10 mL), dried over Na_2SO_4, evaporated to dryness and purified by column chromatography (dichloromethane/methanol = 99/1) obtaining 0.55 g (70%) of a colorless liquid.

^{1}H NMR (300 MHz, $CDCl_3$): δ (ppm) = 3.75-3.50 (m, 14H), 2.63 (q, 2H), 2.07 (m, 3H), 1.67 (m, 6H), 1.53 (m, 7H).

^{13}C NMR (75 MHz, $CDCl_3$): δ (ppm) = 73.04, 72.38, 71.43, 70.81, 70.77, 70.69, 70.40, 59.39, 41.61, 36.60, 30.64, 24.43.

HRMS (ESI): m/z = 345.198 $[M+H]^+$ (calcd. 345.210 for $C_{18}H_{33}O_4S$).

Synthesis of 15

A mixture of **14** (8 mg, 0.022 mmol), NEt_3 (6 µl), and **12** (9 mg, 0.026 mmol) in 5 ml of methanol was stirred overnight at room temperature. After evaporation of the solvent, a colorless product was obtained via LC (silica, CH_2Cl_2/MeOH, 95/5 v/v). Yield: 16 mg, 100%. ^{1}H NMR showed the presence of two isomers owing to the addition of the thiol on the two possible positions of the C-C double bond. The 1,4-addition of the methyl-ester group was estimated to be 80%.

HRMS (ESI): m/z = 714.329 $[M+H]^+$ (calcd. 714.331 for $C_{38}H_{52}NO_{10}S$).

8.5.3 Methods

Substrate and monolayer preparation. Microscope glass slides were used for monolayer preparation.[12] The substrates were oxidized in a piranha solution for 45 min (concentrated H_2SO_4 and 33 % aqueous H_2O_2 in a 3:1 ratio; Warning: piranha should be handled carefully: it has been reported to detonate unexpectedly) and rinsed with water (MilliQ). After drying in a nitrogen stream, the substrates were used immediately to form a silanized monolayer. The substrates were immersed in 0.1 vol% 11-bromoundecyltrichlorosilane in dry toluene for 45 min at room temperature. Following monolayer formation, the substrates were rinsed with toluene to remove any excess of silanes, with ethanol and subsequently dried in a nitrogen flow. The bromide/azide nucleophilic substitution was carried out by the reaction with a saturated solution of NaN_3 in DMF for 48 h at 70 ^{o}C. The substrates were thoroughly rinsed with MilliQ water and ethanol and dried in a nitrogen flow.

For the gradient experiments, glass slides with interdigitated microelectrodes were prepared as described before (Chapter 5). When using interdigitated microelectrodes on glass, the substrates were activated by oxygen plasma treatment (10 min, 50 mA, <200 mTorr). The formation of bromide- and azide-terminated monolayers followed the same protocol described above for microscope glass slides.

Fluorogenic platform formation. When using glass substrates without electrodes, the reactive µCP procedure described in Chapter 3 was used to immobilize **14** on azide-

terminated monolayers. Stamps were prepared by casting a 10:1 (v/v) mixture of poly(dimethylsiloxane) and curing agent (Sylgard 184, Dow Corning) against a silicon master. After overnight curing at 60°C, the stamps were oxidized by oxygen plasma for 10 s (power tuned at 50 mA) and subsequently inked by dropping the inking solution onto the stamp (1.5 mM **14** (in CH_3CN), 0.5 mM $Cu(I)(CH_3CN)_4PF_6$ and 0.5 mM TBTA (CH_3CN/EtOH=2/1) (catalyst mixture), prepared by mixing 75 µL of 2 mM solution of **14** in CH_3CN and 25 µL of 2 mM of catalyst mixture). After 4 min incubation the stamps were blown dry in a stream of nitrogen and brought into conformal contact with the substrate for 60 min. After stamp removal, the printed substrates were rinsed with ethanol, sonicated in acetonitrile for 2 min, rinsed again with ethanol, blown dry with nitrogen and imaged by fluorescence microscopy.

When using interdigitated microelectrodes on glass, the fabrication of micron-scale surface chemical gradients was accomplished by means of electrochemically activated CuAAC in a similar way as described in Chapter 6. The reaction was performed in a silicone container on top of the electrode array. In the electrochemical experiment, 100 µL of a solution containing 1 mM alkyne-modified coumarin (**14**), 1 mM $CuSO_4$ and 1 mM Cu(I)-stabilizing ligand (TBTA) in DMSO were subjected to a potential difference of 1.0 V for 2 min to perform the reduction of Cu(II) to Cu(I) at the cathode (source) and the oxidation of Cu(I) to Cu(II) at the anode (sink). After the reaction, the electrodes were quickly rinsed with DMF and ethanol to avoid any further progress of the reaction and to remove any physisorbed material, followed by drying in a stream of N_2.

Interfacial reaction with thiols. After immobilization of **14** (in surface patterns or gradients), the platform was further reacted via incubation with thiols. The substrates were incubated in 10 mM adamantyl- (**12**) or methyl-terminated (**13**) tri(ethylene glycol)ethanethiol and 0.5 vol% triethylamine solution in methanol for 30 min. The substrates were cleaned by sonication in methanol, rinsed and blown dry with nitrogen.

Non-covalent fluorescent labeling of CD-functionalized silica nanoparticles. The supramolecular fluorescent complex **7** was obtained upon mixing a 10 µM solution of bis-adamantyl-rhodamine dye **6** and 0.2 wt% suspension of **5** (about 21 µM in particle-bound CD) in a 1:1 ratio. The resulting fluorescent supramolecular complex **7** was purified by repeated centrifugation and redispersion in a carbonate buffer. The final concentration of the suspension was about 0.2 wt%.

Assembly of fluorescently labeled CD-functionalized silica nanoparticles. After the immobilization of **12** (or **13**) on the surface patterns or gradients of **14**, the substrates were incubated with 200 µL of a 0.2 wt% suspension of the fluorescently labeled CD-functionalized silica nanoparticles (**7**). The assembly was performed in a humidified chamber to reduce evaporation of the solvent. After 10 min incubation, the suspension was removed and the substrates were washed with 0.1 M carbonate buffer at pH 9.4, MilliQ water and dried with nitrogen.

8.5.4 Equipment

UV/Vis spectroscopy. UV/Vis absorption spectra were recorded using a Perkin Elmer Lambda 850 UV-Vis spectrophotometer.

Fluorescence spectroscopy. Fluorescence spectra were recorded using a Perkin Elmer LS 55 fluorescence spectrophotometer equipped with a high energy pulsed Xenon source for excitation. Emission and excitation slits were kept constant at 2.5 nm.

Fluorescence microscopy. Fluorescence microscopy images were taken using an Olympus inverted research microscope IX71 equipped with a mercury burner U-RFL-T as light source and a digital Olympus DR70 camera for image acquisition. UV excitation (300 nm ≤ λ_{ex} ≤ 400 nm) and blue emission (λ_{em} ≥ 420 nm) was filtered using a Dapi Olympus filter cube. Green excitation (510 nm ≤ λ_{ex} ≤ 550 nm) and red emission (λ_{em} ≥ 580 nm) was filtered using an Olympus filter cube. All fluorescence microscopy images were acquired in air.

Dynamic light scattering (DLS). DLS experiments were performed with a Nanotrac Wave (Microtrac) at 25 ^{o}C using a laser wavelength of 780 nm at a scattering angle of 90^{o}.

Atomic force microscopy (AFM). AFM experiments were carried out with a NanoScope IIIa Multimode AFM (Digital Instruments, Veeco Metrology Group, USA) in tapping mode with a J-scanner. AFM imaging was performed under ambient conditions.

Scanning electron microscopy (SEM). All SEM images were taken with a HR-LEO 1550 FEF SEM.

Potentiostat. The electrochemical reaction was performed using an ES015-10 power supply (Delta Elektronica) with voltage range from 0 to 15 V and current range from 0 to 10 A.

Mass spectra. ESI-TOF-MS mass spectra were recorded using a LCT Mass spectrometer (Waters/Micromass).

NMR. ^{1}H and ^{13}C NMR spectra were recorded on Varian Unity (300 MHz) spectrometer. ^{1}H and ^{13}C chemical shifts values, recorded at 300 MHz and 75 MHz, respectively, are reported as δ (in ppm) using the residual solvent signal as internal standard.

8.6 References

(1) Mammen, M.; Choi, S.-K.; Whitesides, G. M. *Angew. Chem. Int. Ed*. **1998**, *37*, 2754.
(2) Carlson, C. B.; Mowery, P.; Owen, R. M.; Dykhuizen, E. C.; Kiessling, L. L. *ACS Chem. Biol.* **2007**, *2*, 119.
(3) Peer, D.; Karp, J. M.; Hong, S.; Farokhzad, O. C.; Margalit, R.; Langer, R. *Nat. Nanotechnol.* **2007**, *2*, 751.
(4) Loomis, K.; McNeeley, K.; Bellamkonda, R. V. *Soft Matter* **2011**, *7*, 839.
(5) Weissleder, R.; Kelly, K.; Sun, E. Y.; Shtatland, T.; Josephson, L. *Nat. Biotechnol*. **2005**, *23*, 1418.
(6) Hong, S.; Leroueil, P. R.; Majoros, I. J.; Orr, B. G.; Baker, J. R.; Holl, M. M. B. *Chem. Biol*. **2007**, *14*, 107.
(7) Davis, M. E.; Zuckerman, J. E.; Choi, C. H. J.; Seligson, D.; Tolcher, A.; Alabi, C. A.; Yen, Y.; Heidel, J. D.; Ribas, A. *Nature* **2010**, *464*, 1067.
(8) Zern, B. J.; Chacko, A. M.; Liu, J.; Greineder, C. F.; Blankemeyer, E. R.; Radhakrishnan, R.; Muzykantov, V. *ACS Nano* **2013**, *7*, 2461.
(9) Martinez-Veracoechea, F. J.; Frenkel, D. *Proc. Natl. Acad. Sci. USA* **2011**, *108*, 10963.
(10) Wang, S.; Dormidontova, E. E. *Phys. Rev. Lett.* **2012**, *109*, 238102.
(11) Krabbenborg, S. O.; Nicosia, C.; Chen, P.; Huskens, J. *Nat. Commun.* **2013**, *4*, 1667.
(12) Nicosia, C.; Cabanas-Danes, J.; Jonkheijm, P.; Huskens, J. *ChemBioChem* **2012**, *13*, 778.
(13) Mahalingam, V.; Onclin, S.; Péter, M.; Ravoo, B. J.; Huskens, J.; Reinhoudt, D. N. *Langmuir* **2004**, *20*, 11756.
(14) Stöber, W.; Fink, A.; Bohn, E. *J. Colloid Interf. Sci.* **1968**, *26*, 62.
(15) Onclin, S.; Mulder, A.; Huskens, J.; Ravoo, B. J.; Reinhoudt, D. N. *Langmuir* **2004**, *20*, 5460.
(16) Crespo-Biel, O.; Jukovic, A.; Karlsson, M.; Reinhoudt, D. N.; Huskens, J. *Israel J. Chem.* **2005**, *45*, 353.
(17) Snow, A. W.; Foos, E. E. *Synthesis-Stuttgart* **2003**, 509.
(18) Auletta, T.; Dordi, B.; Mulder, A.; Sartori, A.; Onclin, S.; Bruinink, C. M.; Peter, M.; Nijhuis, C. A.; Beijleveld, H.; Schonherr, H.; Vancso, G. J.; Casnati, A.; Ungaro, R.; Ravoo, B. J.; Huskens, J.; Reinhoudt, D. N. *Angew. Chem. Int. Ed*. **2004**, *43*, 369.
(19) Yi, L.; Li, H.; Sun, L.; Liu, L.; Zhang, C.; Xi, Z. *Angew. Chem. Int. Ed*. **2009**, *48*, 4034.
(20) Zhang, S.; Koberstem, J. T. *Langmuir* **2012**, *28*, 486.
(21) Huskens, J.; Mulder, A.; Auletta, T.; Nijhuis, C. A.; Ludden, M. J. W.; Reinhoudt, D. N. *J. Am. Chem. Soc.* **2004**, *126*, 6784.
(22) Perl, A.; Gomez-Casado, A.; Thompson, D.; Dam, H. H.; Jonkheijm, P.; Reinhoudt, D. N.; Huskens, J. *Nat. Chem.* **2011**, *3*, 317.
(23) Ashton, P. R.; Königer, R.; Stoddart, J. F.; Alker, D.; Harding, V. D. . *J. Org. Chem.* **1996**, *61*, 903.
(24) Mulder, A.; Auletta, T.; Sartori, A.; Del Ciotto, S.; Casnati, A.; Ungaro, R.; Huskens, J.; Reinhoudt, D. N. *J. Am. Chem. Soc.* **2004**, *126*, 6627.

(25) Mulder, A.; Onclin, S.; Péter, M.; Hoogenboom, J. P.; Beijleveld, H.; ter Maat, J.; García-Parajó, M. F.; Ravoo, B. J.; Huskens, J.; van Hulst, N. F.; Reinhoudt, D. N. *Small* 2005, *1*, 242.
(26) Chan, T. R.; Hilgraf, R.; Sharpless, K. B.; Fokin, V. V. *Org. Lett.* 2004, *6*, 2853.

Summary

Self-assembled monolayers (SAMs) are an excellent platform to implement and develop interfacial reactions for the preparation of versatile materials of pivotal importance for the fabrication of, among others, biochips, sensors, catalysts, smart surfaces and electronic devices. The development of methods for selective, efficient, simple and rapid surface transformations with control over the surface composition is still a fundamental challenge in surface science. The research described in this thesis is aimed at the fabrication and investigation of functional and reactive SAM-based platforms for the development of bioactive monolayers and surface chemical gradients.

In the first part (Chapters 3-4), a thiol-reactive fluorogenic platform has been employed for the simultaneous immobilization and detection of bioactive ligands and proteins. In particular, this system allowed the selective and sensitive signaled immobilization of active peptides for cell adhesion and cell differentiation studies. Moreover, this method has been used to fabricate patterned protein arrays with control over the protein orientation *via* covalent and non-covalent immobilization strategies. In the second part (Chapters 5-8), electrochemically derived concentration gradients of a catalyst (Cu(I)) in solution have been employed to make micron-scale surface gradients by means of the surface-confined copper(I)-catalyzed azide-alkyne 1,3-dipolar cycloaddition. The system allowed mapping of the reaction kinetics in space and direct visualization of the reaction order. Additionally, the shape of the surface chemical gradients was tuned by the reaction conditions. The fabrication of a pH-sensitive platform allowed the in-situ visualization and quantification of micron-scale pH gradients induced by the electrolysis of water. Combination of the thiol-reactive fluorogenic platform and the micron-scale surface gradient fabrication method provided a supramolecular platform that allowed the first experimental evidence of superselectivity in a multivalent host-guest system.

In summary, the results described in this thesis demonstrate the power of reactive monolayers to provide valuable tools for biological applications and to control the local surface composition by the fabrication of surface gradients. In both cases, the reactive SAMs allow the systematic investigation of micron-scale physicochemical phenomena at interfaces. Reactive monolayers thus constitute a valuable tool for the modification of surfaces leading to new functionalities and novel materials. We expect that future developments will show new functionalization schemes in particular by the integration of dynamic systems in the fabrication processes, thus providing spatiotemporal control over

the surface composition and properties and allowing to tackle unique challenges in surface science and biology.

Samenvatting

Zelf-assemblerende monolagen (SAM) zijn een zeer geschikt platform voor het implementeren en ontwikkelen van grensvlak reacties, welke gebruikt kunnen worden voor de preparatie een verscheidenheid aan materialen, voor het gebruik in biochips, sensoren, katalyse, “slimme” oppervlakken en elektrische apparaten. Het ontwikkelen van methoden om selectief, efficiënt, simpel en snel oppervlakken te modificeren, met controle over de oppervlakte compositie, is nog steeds een onderwerp van fundamenteel onderzoek in de oppervlakte wetenschap. Het doel van het onderzoek, beschreven in dit proefschrift, is het fabriceren en onderzoeken van functionele en reactieve SAM-gebaseerde platformen voor de ontwikkeling van bioactieve monolagen en chemische oppervlakte gradiënten.

In het eerste gedeelte (hoofdstukken 3-4), is een thiol-reactief fluorescerend platform gebruikt voor het gelijktijdig immobiliseren en detecteren van bioactieve liganden en eiwitten. Dit systeem maakte het vooral mogelijk om selectief en sensitief actieve peptides meetbaar te immobiliseren om cel adhesie en differentiëring te onderzoeken. Verder is deze methode gebruikt voor het fabriceren van gepatroneerde eiwit matrices, met controle over de oriëntatie via covalente en niet-covalente immobilisatie strategieën. In het tweede gedeelte (hoofdstukken 5-8), zijn elektrochemische concentratie gradiënten in oplossing van een katalysator (Cu(I)) gebruikt voor het fabriceren van oppervlakte gradiënten op de micrometer schaal met behulp van de oppervlakte-gebonden koper(I)-gekatalyseerde azide-alkyn 1,3-dipolaire cycloadditie. Dit systeem maakte het mogelijk om de reactie kinetiek op het oppervlak te mappen en om de reactie orde direct te visualiseren. Verder kon de vorm van het chemische oppervlakte gradiënt worden aangepast door de reactie condities. Het fabriceren van een pH-sensitief platform maakte de in-situ visualisatie en kwantificatie mogelijk van een pH gradiënt op de micron schaal, welke veroorzaakt werd door elektrolyse van water. Door het combineren van het thiol-reactief fluorescerend platform en de methode voor het fabriceren van oppervlakte gradiënten op de micrometer schaal, werd voor het eerst experimenteel bewijs geleverd voor super-selectiviteit in een multivalente gastheer-gast systeem.

De resultaten beschreven in dit proefschrift demonstreren de kracht van reactieve monolagen als waardevolle hulpmiddelen voor biologische applicaties en om de lokale oppervlakte compositie te controleren door middel van het fabriceren van oppervlakte gradiënten. In beide gevallen maken de reactieve SAMs het mogelijk om fysisch-chemische fenomenen op de micron-schaal te bestuderen op een grensvlak. Reactieve monolagen

vertegenwoordigen dus een waardevol hulpmiddel voor het modificeren van oppervlaktes, welke lijden tot nieuwe functionaliteit en materialen. We verwachten dat verdere ontwikkelingen nieuwe functionaliserings schema's opleveren, specifiek door het integreren van dynamische systemen in het fabricerings proces, wat controle moet geven over de oppervlakte compositie in plaats en tijd. Dit zou het mogelijk maken om unieke uitdagingen in de oppervlakte wetenschap en biologie aan te pakken.

List of publications

1. Carlo Nicosia and Jurriaan Huskens, Reactive self-assembled monolayers: from surface functionalization to gradient formation, *Mater. Horiz.*, 2013, accepted.

2. Carlo Nicosia, Sven O. Krabbenborg, Pengkun Chen, Jurriaan Huskens, Shape-controlled fabrication of micron-scale surface chemical gradients via electrochemically activated copper(I) "click" chemistry, *J. Mater. Chem. B,* 2013*,* accepted.

3. Carlo Nicosia, Sven O. Krabbenborg, David N. Reinhoudt, Jurriaan Huskens, *In-situ* fluorimetric detection of micrometer-scale pH gradients at the solid/liquid interface, *Supramol. Chem.*, 2013, in press.

4. Sven O. Krabbenborg, Carlo Nicosia, Pengkun Chen, Jurriaan Huskens, Reactivity mapping with electrochemical gradients for monitoring reactivity at surfaces in space and time, *Nat. Commun.*, 2013, *4*, 1667.

5. Jordi Cabanas-Danés, Carlo Nicosia, Ellie Landman, Marcel Karperien, Jurriaan Huskens, Pascal Jonkheijm, A fluorogenic monolayer to detect the co-immobilization of peptides that combine cartilage targeting and regeneration, *J. Mater. Chem. B*, 2013, *1*, 1903-1908.

6. Dorothee Wasserberg,* Carlo Nicosia,* Eldrich Tromp, Vinod Subramaniam, Jurriaan Huskens, Pascal Jonkheijm, Oriented protein immobilization using covalent and non-covalent chemistry on a thiol-reactive self-reporting surface, *J. Am. Chem. Soc*., 2013, *135*, 3104-3111 (* equal autorship).

7. Carlo Nicosia, Jordi Cabanas-Danés, Pascal Jonkheijm, Jurriaan Huskens, A fluorogenic reactive monolayer platform for the signaled immobilization of thiols, *ChemBioChem*, 2012, *13*, 778-782 (with inside cover of the journal).

Publications in preparation

- Carlo Nicosia and Jurriaan Huskens, Superselectivity in multivalent receptor-ligand binding.

Acknowledgements

Finally the time is come to acknowledge all the people that have shared with me these unforgettable four years of PhD. I am proud of the results described in my thesis but it would not have been possible without the support of my family and all the fantastic people I met along the way. I had a great time together, gained new technical skills and established preciousness friendships.

Jurriaan, I am grateful to have had a great supervisor and promoter like you, I could have not asked for anyone better, thank you for giving me the opportunity to work in your group on exciting projects. You are the most rational and efficient person I have ever met, with a genuine enchantment for science and teaching, instilling everyone with passion and motivation for research. I have enjoyed talking and discussing with you and I thank you for the freedom you gave me to work on challenging projects. I have appreciated your competence and respect, you have always been there with tips and suggestions for many problems I encountered along the way. I enjoyed and learned a lot from your interactive way of writing manuscripts in particular during your sabbatical period at the Northwestern University; I was not surprised anymore to find in my inbox the corrections of the draft I sent you the day before.

I would like to acknowledge some fantastic people that are somehow related with my decision to come to Twente for my memorable PhD in Jurriaan's group: Prof. Enrico Dalcanale, Prof. David Reinhoudt and Prof. Alessandro Casnati. Dear Enrico, I enjoyed to work in your group for my master's thesis, you are an inspiring and super active person and I want to thank you to have introduced me to the exciting world of supramolecular chemistry with your amazing and multifunctional phosphonate cavitands. Thank you to have accepted to partecipate for my promotion. During that time (2007) Prof. Reinhoudt got the honorary doctorate in Chemistry of the Faculty of Science of the University of Parma and he gave a fascinating talk about the work that was carried out in the chemistry laboratories of the University of Twente and I got intrigued by his legendary molecular printboards (for the record, I am proud to have published a paper together dedicated to Prof. Rocco Ungaro). I had to wait for the encouragement of Alessandro to apply for a PhD position in Jurriaan's group and begin my Dutch adventure.

Many people have contributed to improve the quality of my thesis and to make the everyday work enjoyable and exciting. Pascal, thank you for all your great suggestions and encouragement. Your office was (almost) always open for a quick chat providing

confidence and optimism, even though I realized that during these four years you got busier and busier. Dodo, I enjoyed and learned a lot working with you, and I have been lucky meeting such a pragmatic, efficient and systematic person. Sven, I for sure got some more confidence working with you, I enjoyed a lot our chats in- and outside the lab, even though I must say I preferred when we were discussing with a beer in our hands ☺; thanks for the support, your critical and constructive comments, the constant help and tens (if not hundreds) of electrodes you made during all these years. When I look back I see a good friend and enjoyable and fruitful collaborations. I wish you a great future with Maaike. Jordi, thanks for all the nice words and the infusion of positivity, for the nights and weekends spent on our collaboration and for the good time shared outside the office. I wish you a happy future with Danny. Tibor, thanks for proof-reading my thesis and for all the constructive comments you gave me to improve it.

I would like to thank all the staff members of the MnF/SMCT/BNT cluster, Wim, Jeroen, Nathalie and Melissa, for their support, and all the technicians, Tieme, Regine, Marcel, Richard and Bianca, for their contribution and help any time I approached them. I would like to spend few more words to thank Richard for the wise tips and suggestions in the lab and for all the technical problems he solved. Thank you also for the fascinating stories and the curious anecdotes about the Dutch culture during daily chats at lunch break. I would like to thank Gerard for all the XPS and SEM analysis. Thanks also to Izabel and Nicole for their help with all the bureaucracy from the first till the last day of my PhD.

Of course a special thanks goes to my dear paranimfen (or "Charlie´s Angels" ☺) Raquel and Emanuela. First of all thanks to both of you for your help and support. Raquel, thanks for the fun we had in the lab/office and outside, for all the chats, for giving me a bit of your Colombian energy, and for your noisy laughs, I have really enjoyed to be your lab mate. Thank you for all the dinners and parties you have arranged at your place in the last three years even though all of them end up with all the guests dancing salsa music ☺. Thank you to have invited me to your and Thomas´ fantastic wedding. Sorry for the misadventure in the adventure at the Oktoberfest. I wish you and Thomas a future filled with happiness and success. Emanuela, you are a strong, efficient, clever, amiable and calm girl that make you a great person to talk and spend time with. I remember when we met in the corridor for your first day of Erasmus in the MnF group, I was very happy to meet another Italian, in particular from Parma and I was glad when you came back for the PhD with Pascal. Thank you for the careful proofreading of the concept thesis, you really did a great job, you have for sure contributed for a better final version. Thank you for your kindness and your help, I wish you a bright and happy future.

When I arrived in Enschede four years ago the group was not in the brand new building where I write today but in the old fashion Langezijds. Nevertheless there I met the first fantastic people that welcomed me in the group. Xuexin, we shared the office while I was writing my first literature report. I would like to thank you for the optimism and the support you gave me when I was just arrived, good luck with your academic career. Shu-Han, you are one of the sweetest and most positive girls I have ever met. I would like to thank you to have introduced me to the world of microcontact printing including all the necessary tips and tricks. Was nice to be housemates (and not roommates ☺), meet your family and see how you cook practically anything with your rice cooker! Thank you for inviting me to your great and memorable wedding celebration in Thailand, was a fantastic day and holiday!

My very first days in The Netherlands were very exciting. Chaitanya, my first housemate in Holland, you are a great person, very friendly and sensitive. I thank you for your hospitality but after just one month, bugs and butterflies helped me to move to a more comfortable place. In Javastraat I had two wonderful housemates: Raluca and Arancha. Ralu, you are my "oldest" friend here in Enschede and member of the Thailand expedition, I want to thank you for the many evenings we cooked together sharing recipes in particular my famous risotto with pumpkin and the best cheese of the world (Parmigiano Reggiano, of course) and your tortilla de patata, lasagne and tiramisu'. I cannot forget all the Saturday lunch in the city centre, the only moment I saw Arancha outside the lab.

Thanks to the Italian community in Enschede. Emanuele, è stato divertente lavorare assieme e non sarà facile dimenticare tutte quelle pizze così squisite. Albert, grazie per tutte le conversazioni di chimica, di spettroscopia, e di vita, sei un grande. Ricordo con piacere la gita Enschede-Zutphen-Deventer-Enschede con tappa intermedia a casa di Aldrik, i viaggi a Cologna per comprare prodotti italiani alla Standa, il pranzo con lo stinco di maiale (indimenticabile la disavventura della marmitta in autostrada ☺), ed il trasloco di casa tua riempiendo tutti i bidoni della spazzatura del vicinato. Sono sicuro che diventerai un grande professore, buona fortuna con la tua carriera accademica a Fribourg. Roberto, grazie per tutte le belle serate (le famose ´boys nights´), per tutte le piacevoli ed interessanti discussioni di sport, politica, scienza, chimica, economia, cultura ... e vita dentro e fuori il laboratorio. Grazie anche per tutte le indimenticabili avventure e ricordo con piacere e con un sorriso il viaggio in Thailandia e la festa all´Oktoberfest. In bocca al lupo con il tuo PhD, ti auguro un futuro pieno di felicità. Jealemy (Venezuelana/Olandese in Italia ☺), grazie per tutte le serate e le cene trascorse insieme, per avermi insegnato a preparare i Maki e per le fantastiche gite fuori porta che hai organizzato in questi anni (indimenticabili Verona e

Dolomiti). Sono sicuro che avrai una vita felice e piena di successi con Cristian. Francesco, ti conoscevo per fama a Parma, il mitico "Sean" della mensa, e sono contento di averti incontrato ad Enschede. Sei una persona fantastica, spontanea, e sincera; grazie per rallegrare sempre l´atmosfera, per tutte le cenette, le partite a biliardo e le serate in compagnia. Se diventerai un famoso attore di Holliwood sarà anche merito mio. ☺ Ti auguro un futuro felice assieme a Veronica.

Pengkun, was nice working together and I am sure that with a bit more initiative you will have a great future. Kim, thanks buddy for all the evenings spent together that made life in Enschede more active and happy; I really had a great time together. The holiday in Budapest was fantastic and memorable. I wish you all the best in Singapore and wherever you will end up. Carmen, thanks for being a great and supportive lab/office friend, the lab would not be so tidy and organized without you. Thanks for the everyday chats, for your contagious laughs and for sharing part of the Holiday in Thailand! ☺ Thank you for inviting me to your wedding, was an amazing day and a great party. I wish you and Jan all the best in life. Sarah, I have always been surprised about the amount of energy you burst out! I would say that you are a supergirl and I felt a bit astonished the first time I saw a little girl drinking so much beer ☺. You are a nice and kind girl that will get very far. I wish you all the happiness for your future. Guzman, thanks for the nice time spent together, I enjoyed hanging out with you. It was funny to see you at the gym with your long tight pants and I was really surprised when I heard you playing a simply beautiful melody with the piano, it was a bit like seeing a hard-core metal guy playing Beethoven. I wish you all the best mate. Nicolai, sometimes I was afraid to approach you because of your manners but I was always interested to your stories of life. You are a great chemist and I am sure you will find the way for happiness too. Mudassir, you are a very kind person, I have always seen you smiling, I wish you all the best back in Pakistan. Alejandro, thanks for your support and unconditioned help in the lab, for the time spent together inside and outside the lab. I wish you a very happy future. Benjamin, it is a pity we met only on my last year of PhD, you are a very open, amiable and kind person and I really enjoyed all the conversations we had and the time spent together in New Orleans. I wish you and Ben a happy life together. Derya, thanks for all the time spent together for our collaboration even though we did not manage to get good results. I wish you all the best for your PhD and life. Thanks to the Indian fellows, Rajesh, Tushar and Shirish for their contribution in teaching me about the amazing and fascinating Indian culture, the spicy food and the Diwali celebration among others. Rajesh, thanks for the optimism you instilled to me and for all the beautiful words of peace and wisdom you always spread around. I wish you a happy future. Tushar, your calm and

friendly spirit will take you far. Shirish, thanks for your support and kindness, I wish you and the sweet Jenny all the best in life.

I would like to thank Rik and Melanie that shared with me the office during the final part of the PhD for the writing up of the thesis. Thank you for the mutual support and help; it would have been more difficult without you guys. Thank you Melanie (and Alberto) to have invited me for many pleasant dinners at yours place, and for the tips to get through the bureaucracy at the end of the PhD. I wish you all the best in Austria.

I would like to thank all the people of the MnF and BNT groups that shared with me nice moments and helped me during the PhD: Angel, Chien-Ching, Vijay, Denis, Bala, Francesca, Anna, Pieter, Erhan, Deniz, Peter, Janneke, Timon, Rick, Anne, Rianne, Maarten, Piotr, Supitchaya, Martijn, Laura, Ye, Bettina, Tom, Jasper, Jens, Wies, Jiguang, Marloes, Nicole, Miguel, Eugenio, Andrea.

Un ringraziamento speciale è doveroso a tutti gli amici in Italia, in particolare Andrea, Marcello, Roberto, Paolo, e Matteo. Anche se non ci vediamo spesso, ogni volta è come se ci fossimo visti il giorno prima.

A tutta la mia famiglia, mamma, papà, Irene, Susanna, Francesco, Riccardo, nonni, zii e cugini, grazie per avermi sempre aiutato sin dall´inizio di questa indimenticabile avventura. Senza il vostro appoggio e conforto sarebbe stato molto più difficile. Grazie Susanna per aver disegnato la copertina di questa tesi. In particolare voglio ringraziare nonna Severina e nonno Carmelo che avrei voluto potessero essere qui oggi a festeggiare con noi. To all my Dutch family, Yvonne, Hennie, Nathalie, Martin, Pascalle, Thijmen, Raymond and Shahla, BEDANKT to have accepted me in your family to have supported and helped me and for the Dutch “gezelligheid” ☺.

Last but not least I want to thank my sweetheart Mariska. Every day I am grateful for the day we met. I am very happy to be with you and I want to thank you to be as you are and for all the special and beautiful moments we spent together since we met two years ago. Without any doubt being with you made difficulties easier to overcome. I am looking forward and I feel excited to start a new period of our life together. Ik hou van jou.

Carlo

Enschede, August, 2013

About the Author

Carlo Nicosia was born in Guastalla (Italy) on June 26th 1983. He studied industrial chemistry at the University of Parma, where he received his master´s degree (cum laude) on November 2007. During his undergraduate period he worked under the supervision of Professor Enrico Dalcanale on a project focused on the molecular recognition of chiral alcohols using phosphonate cavitands. After two years spent at the University of Parma and at a private laboratory working as research scientist, in September 2009, he started his PhD research under the supervision of Professor Jurriaan Huskens at the Molecular Nanofabrication group (MnF), University of Twente (The Netherlands), on a project focused on the investigation of the reactivity of chemical reactions at the liquid/solid interface for the fabrication of surface gradients and biomolecular patterned surfaces. The results of this research are described in this thesis.